Structural and Functional Remodelling of the Atrioventricular node with Ageing

A Thesis submitted to the University of Manchester for the degree of Doctor of Philosophy in the Faculty of Medical and Human Sciences

2015

Dr Yawer Saeed

Institute of Cardiovascular Sciences
School of Medicine

Table of Contents

List of Tables

Chapter 1

Chapter 2

Chapter 3

Chapter 4

Chapter 5

List of Figures

Chapter 1

Chapter 2

Chapter 3

Chapter 4

Chapter 5

Abstract

Submission for the degree of Doctor of Philosophy, The University of Manchester
Dr Yawer Saeed

Structural and functional remodelling of the atrioventricular node with ageing
September 2015

Introduction: Factors that influence atrioventricular (AV) nodal conduction are complex and not well understood. Multiple studies have been performed to explain the mechanisms responsible for AV nodal conduction but the AV node (AVN) remains a "riddle". With ageing there is an increase in the incidence of AV nodal dysfunction leading to AV block.

Methodology: I have performed electrophysiological (EP) and immunohistochemistry experiments on male Wistar-Hanover rats aged 3 months (equivalent to 20 year old humans; n=24) and 2 years (equivalent to 70 year old humans; n=15). AH interval, Wenkebach cycle length (WCL) and AV node effective refractory period (AVNERP) were measured. I used cesium (Cs^+ = 2 mM) to block HCN channels responsible for the funny current "$\boldsymbol{I_f}$" (and therefore the membrane clock), and ryanodine (2 μM) to block RyR2 channels responsible for Ca^{2+} release from the sarcoplasmic reticulum (and therefore the Ca^{2+} clock) in the two age groups. Protein expression in each group (from n=9 young and n=8 old rats) from different regions of the AV conduction axis: inferior nodal extension (INE), compact node (CN), proximal penetrating bundle (PPB) and distal penetrating or His bundle (His) were studied using immunofluorescence and confocal microscopy. The expression of the gap junction channels Cx43 and Cx40 and ion channel's including HCN4 (responsible for I_f current), $Na_v1.5$ (major cardiac Na^+ channel responsible for I_{Na}) and $Ca_v1.3$ (L-type Ca^{2+} channel), and calcium handling proteins, RyR2 and SERCA 2a (involved in Ca^{2+} release and reuptake from cardiac sarcoplasmic reticulum, SR) were studied. Semi-quantitative signal intensity of these channels was measured using Volocity software. Structural characteristics of the tissue were studied using histology (Masson's trichome stain and picrosirius red stain for collagen). Statistical analysis was performed with Prism 6.0. Electrophysiological measurements were performed using Spike2.

Results: Without drugs to block the $\boldsymbol{I_f}$ current and Ca^{2+} release from the SR, there was a significant prolongation of the AH interval ($P<0.005$), WCL ($P<0.005$) and AVNERP ($P<0.001$) with ageing. In young rats (but not old rats), Cs^+ prolonged the AH interval ($P<0.001$), WCL ($P<0.01$) and AVNERP ($P<0.01$). Ryanodine prolonged the AH interval ($P<0.01$) and WCL ($P<0.01$) in young and old rats. Immunofluorescence revealed that with ageing: Cx43 is downregulated in the PPB and His ($P<0.05$); Cx40 is upregulated in the INE and CN ($P<0.05$); HCN4 is downregulated in the His bundle ($P=0.05$); $Na_v1.5$ is downregulated in the CN and PB ($P<0.05$); RyR2 is downregulated in the CN and PPB ($P<0.05$); SERCA2a and $Ca_v1.3$ is upregulated in the PPB ($P<0.05$). Histology confirmed that with ageing that the cells of CN, PPB and His are more loosely packed and irregularly arranged. There is cellular hypertrophy, decrease in the number of nuclei and increase in the collagen content with ageing. The clinical study has shown that elderly patients with syncope and cardiac conduction system disease are at risk of high mortality and recurrent transient loss of consciousness.

Conclusion: For the first time, we have shown that both HCN and RyR2 channels play an important role in AV nodal conduction. With ageing the expression of HCN4 and the role of $\boldsymbol{I_f}$ in AV nodal conduction decreases, whereas the role of Ca^{2+} clock in AV nodal conduction was unchanged, although the expression of RyR2 and SERCA2a changes. The clinical study suggests that AV nodal disease is associated with significant morbidity and higher mortality among elderly patients who present with transient loss of consciousness.

Declaration

No portion of this work referred to in the thesis has been submitted in support of an application for another degree or qualification of this or any other university or other institute of learning.

Copyright statement

Acknowledgements

This PhD thesis has only become a reality because of my several colleagues' immense contribution. I am obliged to every member of the Cardiovascular Research Group and Manchester Heart Centre.
Especially, I extend my gratitude to my supervisors Dr Halina Dobrzynski, Professor Clifford Garratt and my advisor Professor Mark Boyett for their guidance and support throughout my PhD.
I am really thankful to Professor Clifford Garrat and Manchester Heart Centre for providing me the opportunity of the research fellowship and financial support during the PhD, which made it possible for me to concentrate on research with minimal clinical activities.
I am in debt to Dr Halina Dobrzynski, she is an extremely patient and knowledgeable supervisor. She is always accessible if I have any questions or queries. She has supported me throughout my PhD especially with my initial inexperience in laboratory work. I am really pleased to have her as my supervisor.
I am also grateful to Professor Mark Boyett for his help during the electrophysiology experiments and his continued support in the preparation of this thesis.
I would also like to thank Dr Adam Fitzpatrick and Dr Amir Anwar for their unrelenting support during my clinical study.
I would also like to thank Dr Joseph Yanni, Mr Andrew Atkinson, Dr Zoltan Borbas, Mr Sunil Logantha and Dr Ian Temple for the training in histology, immunohistochemistry, electrophysiology and laboratory techniques. Without their help it would have been impossible to meet the deadlines and complete the experiments.
I acknowledge Ms Mariam Aly, Mr Ahad Aly and Dr Rebecca Dobson for the proof reading of this thesis.
I would specially like to thank my parents Mr Syed Saeed Akhtar Zaidi and Mrs Aale Fatima for their encouragement and prayers. Without them it would be impossible to reach the stage I am at present.
My children's Shayan and Anoushey have been a source of relief and motivation that kept me going during the writing of this thesis despite my busy schedule.
And finally I dedicate this PhD thesis to my wife Dr Nawazish Zehra. She has taken care of the house, kids and especially me. It would not have been possible if she had not supported me during difficult times.
I have made several friends during my PhD years and I hope that my relationship with them last forever. This is my way of saying a little thankyou for their help, support, encouragement and guidance that has enabled me to complete my goal.

Abbreviations

AERP	Atrial effective refractory period
AF	Atrial fibrillation
AN cell	Atrio-nodal cell
Ach	Acetylcholine
APD	Action potential duration
ATP	Adenosine triphosphate
AV	Atrioventricular
AVERP	Atrioventricular effective refractory period
AVFRP	Atrioventricular functional refractory period
AVN	Atrioventricular node
AVNRT	Atrioventricular nodal reentry tachycardia
AVJ	Atrioventicular junction
BSA	Bovine serum albumin
cAMP	Cyclic adenosine monophosphate
CCS	Cardiac conduction system
cDNA	Complementary deoxyribonucleic acid
CL	Cycle length
Cs^+	Cesium
Cx	Connexin
Cy	Cyanine
DPB	Distal penetrating bundle or His bundle
ECG	Electrocardiogram
ECG-CTA	Electrocardiogram in patients with conduction tissue abnormalities
EDTA	Ethylenediaminetetraacetic acid
FITC	Flourescein isothiocyanate
I_{CaL}	L-Type Ca^{2+} current
I_{CaT}	T-Type Ca^{2+} current
I_f	Funny current
IFT	Inflow tract
I_{K1}	Inward rectifying K^+ current
I_{KAch}	Ach-activated K^+ current
I_{KATP}	ATP-sensitive K^+
I_{Kr}	Rapidly activating K^+ current

I_{Ks}	Slowly activation K^+ current
I_{Kur}	Ultra-rapid delayed rectifier K^+ current
I_{Na}	Na^+ current
I_{NCX}	Na^+/Ca^{2+} exchange current
I_{to}	Transient outward K^+ current
INE	Inferior nodal extension
IVC	Inferior vena cava
LA	Left atrium
LV	Left ventricle
mRNA	Messenger ribonucleic acid
MT	Masson's trichome
N cell	Nodal cell
OFT	Outflow tract
PBS	Phosphate buffered saline
PR	Picrosirius red stain
PPB	Proximal penetrating bundle
qPCR	Quantitative Polymerase chain reaction
RA	Right atrium
RV	Right ventricle
RNase	Ribonuclease
RyR	Ryanodine receptor
SA	Sinoatrial
SAN	Sinoatrial node
SEM	Standard error of mean
SSS	Sick sinus syndrome
SR	Sarcoplasmic reticulum
SVC	Superior vena cava
TGFβ1	Transforming growth factor β1
Tbx-3	T-Box transcription factor 3
Tbx-5	T-Box transcription factor 5
Tbx-18	T-Box transcription factor 18
TTX	Teterodoxin

The Author

Qualifications

MBBS (Honours) University of Karachi, August 2002

MRCP (UK) Member of Royal College of Physicians, London, United Kingdom, July 2008

ECFMG Certified United States of America, 2007

KBA Knowledge Based Assessment (Exit exam in Cardiology), British Cardiac Society, June 2011

BHRS Accreditation British Heart Rhythm Society Accreditation Electrophysiology, May 2014

BSE Accredited British Society of Echocardiography Accreditation, 2011

PLAB Licence to Practice GMC, PLAB, Professional Linguistic and Assessment Board exam, General Medical Council, UK, 2004

Oral Presentations at National/International Conferences

Yawer Saeed, Amir Anwar, Adam Fitzpatrick: Effectiveness of ECG-based triage in older patients with TLOC attending a rapid access blackouts triage clinic: conduction tissue abnormalities predict a higher mortality, recurrent TLOC and a good response to cardiac pacing. Birmingham, UK. British Heart Rhythm Society Congress, **HRC 2014**

Amir Anwar, **Yawer Saeed,** Adam Fitzpatrick: Use of Midodrine in patients with reflex syncope, single center experience in 178 patients. Barcelona, Spain, European Society of Cardiology, **ESC 2014**

Peer Reviewed Abstract Publications

Yawer Saeed, Ian Temple, Zoltan Borbas, Andrew Atkinson, Joseph Yanni, Mark Boyett, Clifford Garratt, Halina Dobrzynski. Are membrane clock and calcium clock involved in atrioventricular nodal conduction in young and aged rats? Milan, Italy. European Heart Rhythm Association Conference 2015, **EHRA 2015**

Yawer Saeed, Ian Temple, Zoltan Borbas, Andrew Atkinson, Joseph Yanni, Mark Boyett, Clifford Garratt, Halina Dobrzynski: Do major ion channels of pacemaker clock play a role in AV nodal conduction in young and aged rats? London, UK. European Society of Cardiology, **ESC 2015.**

Yawer Saeed, Ian Temple, Zoltan Borbas, Andrew Atkinson, Joseph Yanni, Mark Boyett, Clifford Garratt, Halina Dobrzynski: Ageing is associated with myocardial disarray, changes in the expression of ion channels, gap junction proteins and calcium handling proteins with in the atrioventricular conduction axis. Birmingham, UK, British Heart Rhythm Society Congress, **HRC 2014.**

Yawer Saeed, Amir Anwar, Andrea Donald, Adam Fitzpatrick: Effectiveness of ECG based traige in older patients with TLOC attending a rapid access blackout triage clinic: Conduction tissue abnormalities predict a higher mortality recurrent TLOC and a good response to cardiac pacing." San Francisco, United States, Heart Rhythm Society

Conference, **HRS 2014**.

Yawer Saeed, Z Borbas, Ian Temple, A Atkinson, J Yanni, M R Boyett, C J Garrat, H Dobrzynski**:** Ageing is associated with changes in the structure and ion channel expression within the atrioventricular conduction axis. Birmingham UK, International Union of Physiological Society conference, **IUPS 2013.**

Yawer Saeed, Daniel Lythgoe, Som Chuah**.** Osteoporosis or Bisphosphonate use associated with decreased progression of calcific aortic stenosis. Reterospective case control study in a single centre. Manchester, UK, British Cardiology Society, **BCS 2012.**

Yawer Saeed, A Innasimuthu, G Rao, D Robinson, Peter Wong. Prongnostic factors affecting 1- year survival in hospitalised patients with a raised Troponin T. European Society of Cardiology 2010, Annual Meeting, Stockholm, **ESC 2010.**

Peter Wong, G Rao, A Innasimuthu, **Yawer Saeed**, D Robinson. Validation of a prediction score to distinguish patients with acute myocardial infarction from other causes of raised troponin T, European Society of Cardiology, Annual Meeting, Stockholm, **ESC 2010.**

Peer Reviewed Journal Publications

Yawer Saeed, Ian Temple, Zoltan Borbas, Andrew Atkinson, Joseph Yanni, Mark Boyett, Clifford Garratt and Halina Dobrzynski. Are membrane clock and calcium clock involved in atrioventricular conduction in young and aged rats? submitted for Young investigator award. HRS 2015.

Clifford Garratt, **Yawer Saeed.** A Year in Cardiology 2012. Arrhythmia and pacing: European Heart Journal 2013: Feb; 34 (5): 33-7. doi: 10.1093/eurheartj/ehs451. Epub 2013: Jan 2. Review (PMID: 23284092 [PubMed - indexed for MEDLINE]

PS Wong, GK Rao, AL Innasimuthu, **Yawer Saeed**, C van Heyningen, DR Robinson.Validation of a prediction score model to distinguish acute coronary syndromes from other conditions causing raised cardiac troponin T levels. Coronary Artery Diesease, 2010 Sep; 21(6): 363-8. (Pub Med Indexed PMID: 20661138)

SF Hussain, **Yawer Saeed**, M Irfan. Clinical characteristics of patients with obstructive sleep apnoea. Journal of College of Physicians and Surgeons Pakistan: Jan 2005, Vol 15(1) 37,38 (PMID: 15670523 [PubMed - indexed for MEDLINE]

SF Hussain, M Irfan, N **Yawer Saeed**, W Akthar. Acute respiratory failure in Pakistani patients: risk factors associated with mortality. Journal of College of Physicians and Surgeons Pakistan, JCPSP 2006, Vol. 16 (4): 287-290 (PMID: 16624195 [PubMed - indexed for MEDLINE]

Chapter 1

1. General Introduction

The Atrioventricular node (AVN), since its discovery, has held scientists and clinicians interested in its structure and function for at least the last century. The functions of the AVN are not only to serve as a connection between atria and ventricles but also includes providing adequate time for the filling of the ventricles for optimal cardiac output and protecting the ventricles from atrial fibrillation by delaying the cardiac impulse transmission. The AVN also operate as a backup pacemaker in patients with Sinus node (SN) dysfunction.

AVN is the only connection that exists in normal individuals between atria and ventricles; if it becomes diseased it can lead to heart blocks, which may have the consequence of heart failure and ultimately death. This necessitates permanent pacemaker implantation in patients with the AVN dysfunction. Furthermore, Atrioventricular nodal reentry tachycardia (AVNRT) is a form of arrhythmia that has been credited to dual AVN physiology, which will be explained later in the text.

Ageing, certainly has a part to play in the pathophysiology of heart blocks and AVNRT. Incidence of heart blocks, especially third-degree atrio-ventricluar (AV) block is more common in the elderly population. AVNRT, though, is more common in adolescent as compared to infants and elderly.

Although ageing studies on the cardiac conduction system have been performed, the explanation of the AVN dysfunction with ageing has not been clearly established in terms of ion channel expression. At a cellular level, immunohistochemical techniques have opened avenues of ion channel research. Use of ion channel blockers to assess the AVN functional properties in the young and with ageing is also not fully established. It is therefore prudent to fill the knowledge gap that exists at a cellular level with ageing AVN.

1.1 History of atrioventricular node and cardiac conduction system

The structure and function of the atrioventricular node (AVN) started to unravel very early in the 20th century when in 1906 Sunao Tawara discovered "the Knoten" that we now know as the AVN. The discovery of the AVN has changed the manner in which the cardiac conduction system (CCS) had been perceived by scientists and clinicians. It paved the way for future generations of researchers to build on this discovery, which solved the important puzzle in interpretation of electrocardiogram (ECG) and also improved the understanding about the CCS function and morphology.[1]

Sunao Tawara, started his work with Professor Ludwig Aschoff in Marburg, Germany in 1903.[2] After two and half years of considerable work on mammalian hearts, he was able to explain the theory that stands the test of time. Interestingly, he started his work on the myocardium to find the cause of heart failure in patients with valvular heart disease but did not find a correlation between histological changes and clinical findings of heart failure. Then, as suggested by Profosser Aschoff, he started working on the AV bundle.

Tawara together with Prof. Aschoff, later made an important discovery related to rheumatic valvular heart disease, but the discovery that gave him immortality is the theory that links the individual components of the CCS. Although, the His bundle and Purkinje fibers were discovered years before the discovery of the AVN but a clear explanation of their role in the CCS were missing. As early as 1839 in the Czech Republic, Jan Evangelista Purkinje discovered the fibers in the ventricle wall now known as the Purkinje fibers.[3] In 1893 Wilhelm His Jr. discovered the His bundle[3] but he was not certain about its function. Therefore, the discovery made by Tawara assumes greater significance in that it provided the missing link of the conduction of cardiac impulse between atria and ventricles. Tawara not only discovered the AVN, he was also able to present the theory of conduction of cardiac impulse through the AVN, His bundle, right

and left bundle branches and Purkinje fibers down to ventricular muscle.[4] He called it *"The Stimulus Conducting System or The atrioventricular connecting system"*. In his landmark article, he wrote:

> *"I intend, for the first time in medical History, to propose an integral and consistent explanation concerning the atrioventricular bundle and the Purkinje fibers."* [4]

He described "The Stimulus conducting system" as having a tree like configuration, which he believed, was quite similar to other "parenchymal or ductal systems" including the respiratory, nervous and circulatory systems. He wrote as follows:

> *" The connecting bundle is a closed system like a tree. This tree is rooted in the atrial septum, the stem and the main branches penetrate the fibrocartilaginous septum and ventricular septum, the peripheral branches reach the parietal wall and the papillary muscles through the false tendinous fibers, and finally the thinnest twigs spread as the terminal ramifications of the connencting bundle……..From the structural standpoint, the connecting system also represents a transporting or conducting pathway. Because the pathway is not a ductal but continuously related protoplasmic cord, conduction of excitation impulses surely must take place here."*

Tawara first discovered the correlation between ventricular muscles & Purkinje fibers in sheep hearts as Purkinje fibers are clearly visible in sheep hearts. Then he traced them back to the bundle branches and AV or His bundle in human hearts. With the help of serial histological section towards atria he then discovered the AVN.

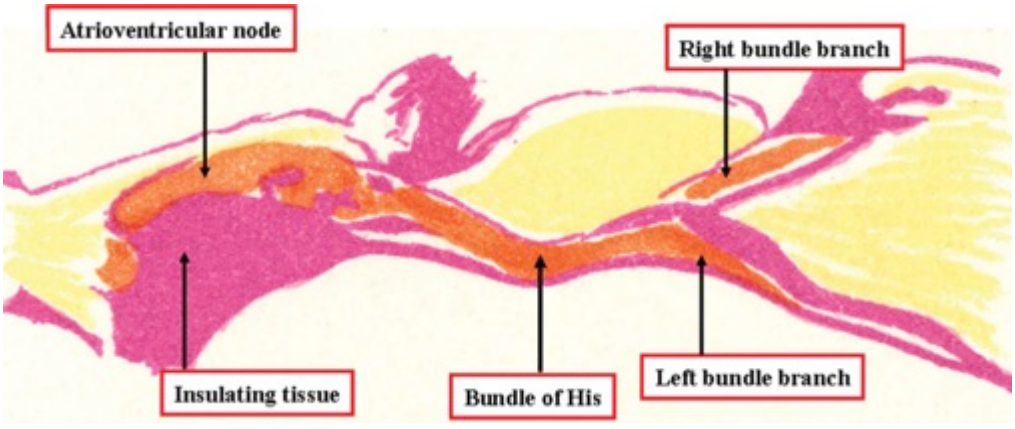

Figure 1.1: A closer view of figure in Tawara's monograph highlighting individual components of the atrioventricular junction. Adapted from, The anatomy of cardiac conduction system, from Anderson et al 2009.[5]

Figure 1.1 is an adaptation of Tawara's original figures; demonstrating a closer view of the stimulus conduction system. Figure 1.2 showed the tree like pattern of the cardiac conduction system described in Tawara's monograph.

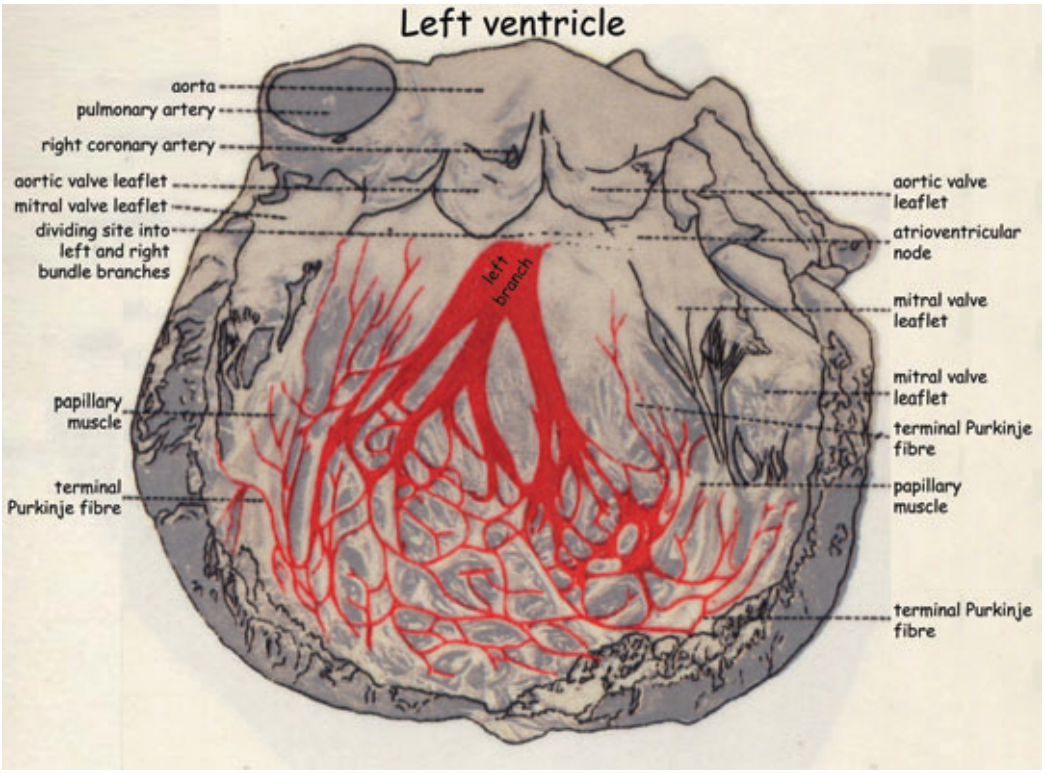

Figure 1.2: The tree like configuration of the stimulus conducting system. Adapted from Tawara[4] and Boyett.[6]

Just after Tawara discovered the AVN, Sir Arthur Keith and Martin Flack, from Kent, England, published their discovery of the Sinus node (SN) in 1907.[7] Their work on several mammalian hearts including moles, rats, mice, hedgehogs and humans, confirmed Tawara's discovery of the AVN and also made the unexpected discovery of the SN in the right atrium, close to the entrance of the superior vena cava.

Edward Hering's experiments are also worth mentioning, whose findings were published in 1910 in relation with the AVN conduction.[8,9] Hering was a distinguished physiologist in Prague, known for his work on cardiac arrhythmias. Hering, in close association with Tawara, was conducting experiments on the AV conduction delay after severing the AV bundle in dogs. He sent Tawara four samples of dog's heart to confirm that the AV bundle was correctly severed. After performing several experiments on dogs interrupting their AV bundle, he showed that the delay in the conduction of impulse at the AV junction (AVJ) was secondary to the AVN.[2]

The anatomic findings of the SN by Keith and Flack, the discovery of the AVN and the theory of "The stimulus conducting system" by Tawara were all important discoveries in the history of CCS. Building on these pieces of evidence, in 1910, Thomas Lewis, recorded electrical activity from the heart using the string galvanometer invented by William Einthoven. The string galvanometer device made it possible to record electrical activity from the heart for the first time and still remains the cornerstone of modern electrocardiography.[2,10]

1.2 Development of the atrioventricular node

It is fascinating to observe the fact that the electrocardiogram (ECG) with individual PQRS components can be seen as early as the first few days of vertebrate embryos development. Figure 1.3 showed the ECG seen early in vertebrate embryos.

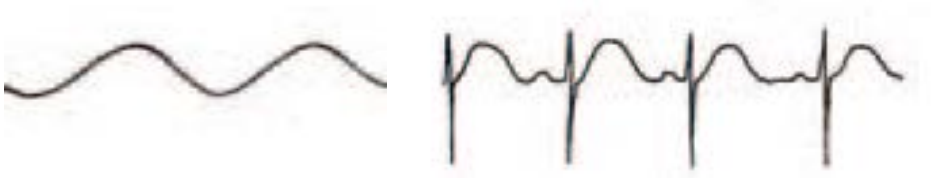

Figure 1.3: **The sinusoidal looking ECG pattern becomes distinct to resemble that of mature heart as early as 10.5-12.5 days in vertebrate embryos.** Adapted from Christoffels et al 2010.[11]

The Figure 1.3 shows that the CCS is one of the foremost components during early heart development. The origin of these individual components of electrical impulse sweeping through the heart at the start of these primitive lives are found in human embryos and also seen in the simple hearts of lower vertebrates and hearts of vertebrate embryos. It is worth reviewing developmental changes in the AVN at a cellular and molecular level as it can be hypothesized that they are preserved through evolution. As Christoffels et al., put it[11]

" The cellular and molecular mechanisms that derive the formation of pacemaker tissues are evolutionary conserved."

1.3 Atrioventricular node through evolution

Amongst "evolutionary conserved" components of CCS, atrio-ventricular junction (AVJ) has been established as a region which reduced the speed of conduction of the depolarization wave. In fish hearts, pacemaker tissue that was found at the AVJ delays the deplorization wave propagation. Amphibians display similar characteristics as the AVJ diminished the speed of depolarization. The AVJ in amphibians exhibits scarcity of

gap junctions, which provide the molecular basis of the slow depolarization wave.[11,12] Similarly, in the embryonic chicken's heart, Lieberman et al.,[13] showed that slow action potential propagation is due to delay in the AV canal.

1.4 Embryology of the atrioventricular node and cardiac conduction system

Development of the AVN and CCS is a challenging concept, to fully comprehend this I have reviewed the basic concepts of embryogenesis, as without this, a sound understanding of the CCS development in general and the AVN in particular would be difficult.

Embryogenesis (the formation of embryo) starts with fertilization but it is the stage of gastrulation (gastrula formation), which marks the formation of three germinal layers (i.e ectoderm, mesoderm and endoderm) that are the precursors of various organ systems. These three germ layers together form the embryonic discs. The heart originates as a tubular structure that develops from the mesoderm. The cardiac tube forms during the process of folding of the embryonic disc when bilateral cardiac plates (parts of the embryonic disc or heart forming areas located on either side of midline) fuse to form cardiac tube (Figure 1.4).[14]

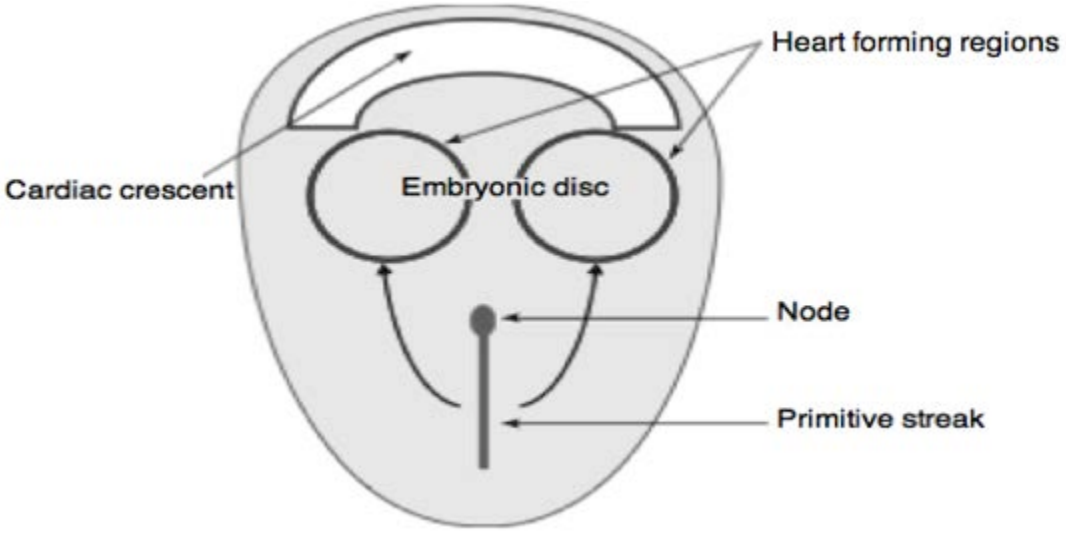

Figure 1.4: The cartoon showing an idealized view of the embryonic disc. It indicates how migrations of cells from the primitive streak between the ectodermal and endodermal layers form initially the heart-forming areas (cardiac plates), and then coalesce to form the cardiac crescent. These heart forming areas then fold to form the heart tube. Adapted from Moorman et al., 2003.[14]

The atria & ventricles formed as a result of budding or ballooning of the linear primary heart tube. Figure 1.5 explains the orientation of the primary heart tube and the relationship of the various heart chambers to each other during development.

The formation of the primary heart tube marks the beginning of a series of important steps that ultimately result in the formation of a mature heart. The next step in this process is the addition of cells to the primary tube from the heart-forming areas at both the venous (inflow tract) and arterial poles (outflow tract) (Figure 1.5A). The walls of the primary heart tube at this stage consist of **"primary myocardium"**.[13,14]

With this addition of new cells the primary heart tube undergoes looping resulting in the formation of atria and ventricles by the budding or ballooning process as mentioned before and shown in Figure 1.5B and C. The cardiomyocytes making up these new parts together make up the "**working chamber myocardium"**.[14]

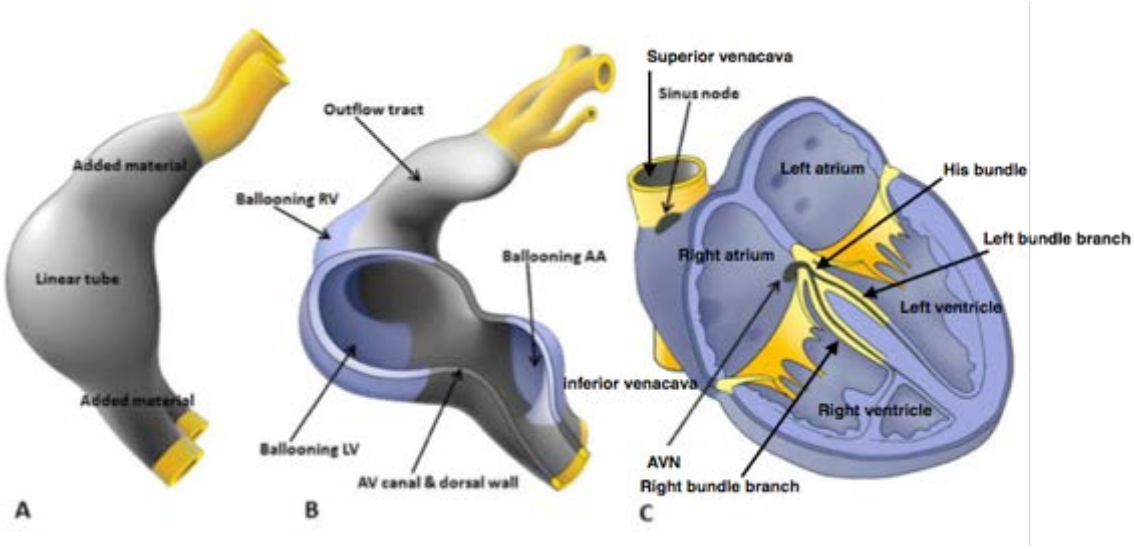

Figure 1.5: The cartoons show the changes involved in the formation of definitive conduction tissues. A. Shows a lateral view of the developing heart tube subsequent to the addition of new material from the inflow and outflow tracts. Heart-forming areas at both the arterial and venous poles. The central component, the intrapericardial components (shown in grey) are all formed of primary myocardium at this stage. The extrapericardial parts are shown in yellow. B. Shows how the chamber components balloon from the primary tube, with the atrial appendages ballooning from the newly formed atrial component of the heart tube, and the left and right ventricles ballooning from the inlet and outlet parts of the ventricular loop. Note that, during this intermediate stage, the persisting primary myocardium forms the AV canal, the developing outflow tract is formed at this stage by primary myocardium. Eventually, as shown in C, the primary myocardium persists only as the sinus node and the atrioventricular conduction axis.[14,15]

The cardiomyocytes of the working chamber myocardium differ from the primary myocardium. Primary myocardial cell characteristics include slow growth, slow conduction and pacemaking (spontaneous depolarization). Conversely, working chamber myocardial cells are connected with each other through gap junctions made up of connexin 40 (Cx40) and connexin 43 (Cx43), which permit rapid conduction, along with rapid rates of cell division. Cx40 and Cx43 are intercellular gap junctions and members of connexins family of ion channels, which aids in the electrical coupling of heart cells

(details of these can be found later in the text).[14] Figure 1.6 and 1.7 explain the role of transcription factors during the CCS development.

Another important concept to understand is that of the **primary myocardial cells,** only a few retain their primary phenotype to form parts of the CCS. Most of the primary myocardial cells differentiate in to the **working chamber myocardium** that loses its primary phenotype. The CCS retains the primary phenotype of primary myocardium under the influence of the transcription factor, Tbx3. However, the working chamber myocardium of atria and ventricle seems to lose their primary phenotype. Tbx family of transcription factors plays an important role in the development of CCS. It is now well established that the expression of the Tbx3 is responsible for this process. Ectopic expression of Tbx3 in the atrial chambers was shown to result in the formation of functional ectopic nodes exhibiting pacemaking activity.[15,16]

The AVN region functional match in the primary heart tube is the AV canal. It is known that the primary heart tube lacks Cx43 and Cx40 when compared with working chamber myocardium and the primary heart tube consists of the AV canal, inner curvature and outflow tract (Figure 1.6).[12, 15,16,17]

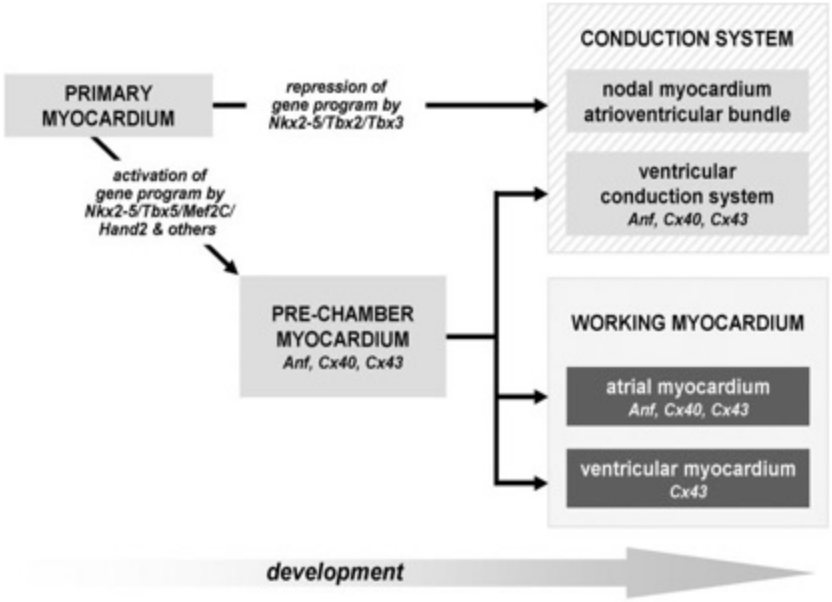

Figure 1.6: Schematic diagram showing various steps in the formation of the cardiac chambers and conduction system components. The primary myocardial tube cells differentiate into pre-chamber myocardium that subsequently will form the trabecules, the bundle branches and peripheral ventricular conduction system, and compact ventricular and atrial working myocardium. Part of the primary myocardium is set aside from differentiation and will form the nodal components of the conduction system, the SN, AVN, and AVB. Anf, Nkx2.5, Tbx 2, Tbx3, Tbx5, Mef2C, Hand 2 are transcription factors that helps in differentiating of various components of CCS and myocardium, Cx40 and 43 are gap junctions protein involved in cell to cell coupling.[17]

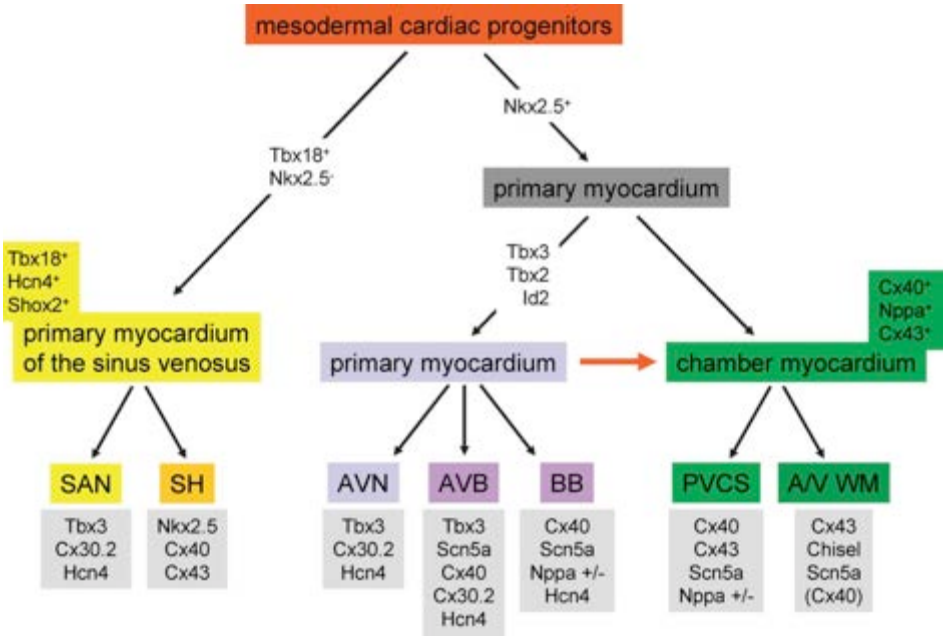

Figure 1.7: Model for cardiomyocyte differentiation into all myocardial components of the vertebrate heart. The red arrow between primary and chamber myocardium indicates continuous differentiation of primary cardiomyocytes into chamber myocardium. A/V WM, atrial/ventricular working myocardium; AVB, AV bundle; AVN, AV node; BB, bundle braches; SAN, sinus node; SH, sinus horns.[16,17]

Figure 1.7 showed that the mesodermal cardiac progenitors differentiate under the influence of transcription factors Tbx18 and Nkx 2.5 into primary myocardium which either retains its primary phenotype to form the SN, AVN, AV bundle and BB, under the influence of Tbx3, Tbx2 and Id2 or loses its primary phenotype to form chamber myocardium. The grey boxes showed the final phenotype expression of primary myocardium and chamber myocardium. The SN, AVN and AV bundle continue to express Tbx3. Cx30.2, Cx40, Cx43 are gap junctions whereas HCN4 is the ion channel primarily responsible for I_f current, SCN5A is the gene that encodes Na^+ channel $Na_v1.5$. $Na_v1.5$ is primarily responsible for I_{Na}. These ion channels details can be found later in the text. As shown HCN4 expression is consistent throughout the CCS.

1.5 Anatomy and morphology of atrioventricular node

The AVN is located at the base of the triangle of Koch, where the tendon of Todaro, the coronary sinus and the septal leaflet of the tricuspid valve, form the boundaries of the Koch's triangle. (Figure 1.8 and Figure 1.9)

Controversies exist in literature regarding the nomenclature to define the various components of the AVJ.[5,16] But more recently consensus has been reached in defining these components as described by Tawara.[5,18]

Morphologically the AVN can then be further divided into the lower nodal bundle (LNB) and compact node (CN).[18,19] In the LNB, cells are longer and arranged more parallel to one another, whereas in the CN cells are small and spindle-shaped with no clear orientation. Extending proximally from the LNB towards the coronary sinus (CS) is the inferior nodal extension or posterior nodal extension (INE/PNE), also known as the rightward nodal extension (RE) in humans.[19, 20] We will mention this area of AVN as INE throughout the text. The second nodal extension or leftward nodal extension (LE), found in humans, extends from the CN towards the CS, and is usually shorter than the rightward extension.[20,21] This LE has also been found in other mammalian hearts studied including mouse, rat and rabbit hearts.

Out of these different areas of the AVN special mention should be made of the INE. The location of INE corresponds to the location of the slow pathway, which is ablated to interrupt the reentry circuit in the treatment of AV nodal reentry tachycardia (AVNRT). This area could potentially act as ectopic focus. Further more HCN4 Channel that are primarily responsible for I_f current is abundantly found in the INE and this area is the site of AV junctional rhythm as found by Dobrzynski et al., in rabbit AVN. The I_f current is the hyperpolarization activated current involved in generating phase 4 depolarization in the SN and AVN.[21-23]

Figure 1.8 explains various components of the AVJ described above in the human heart. Figure 1.9 showed the AVJ components in rabbit and their cross section at 3 levels. These figures described the fast and slow component of the AVN conduction axis, explanation of which can be found later in the text. Figure 1.9 also highlights the penetrating bundle, which starts when the AVN penetrates the central fibrous body. The terms of penetrating bundle or His bundle have been used interchangeably in the text. This fact has also been endorsed by Anderson[18] who when referring to Tawara's original monograph states;

"*Significantly, he showed that the pathway became insulated as it crossed from atrial to ventricular musculatures, and suggested that the point at which the muscle became engulfed in fibrous tissue should be taken as the boundary between the "knoten," or atrioventricular node, and the penetrating bundle described earlier by Wilhelm His."*

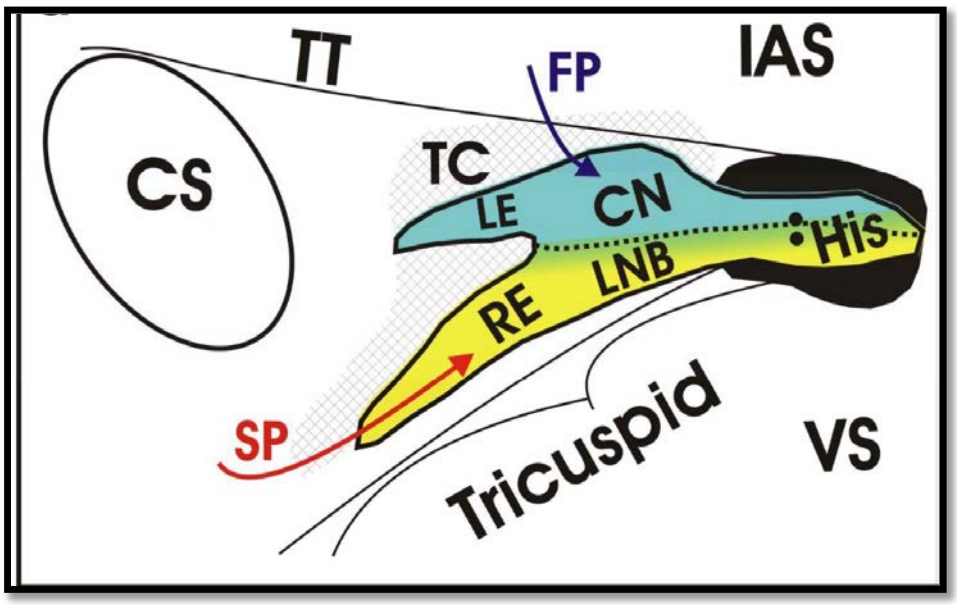

Figure 1.8: AVJ anatomy and morphology illustrating the location of the AVN and different AVJ regions of human heart: CN (compact node), LE (left ward extension), RE (right ward extension), His (His bundle), CS (coronary sinus), IAS (interatrial septum), VS (ventricular septum), TT (tendon of todaro), FP (fast pathway), SP (slow pathway). Adapted from Kurian et al 2010. Yellow colour indicates the Cx43 positive area and blue indicates Cx43 negative area.[18,21]

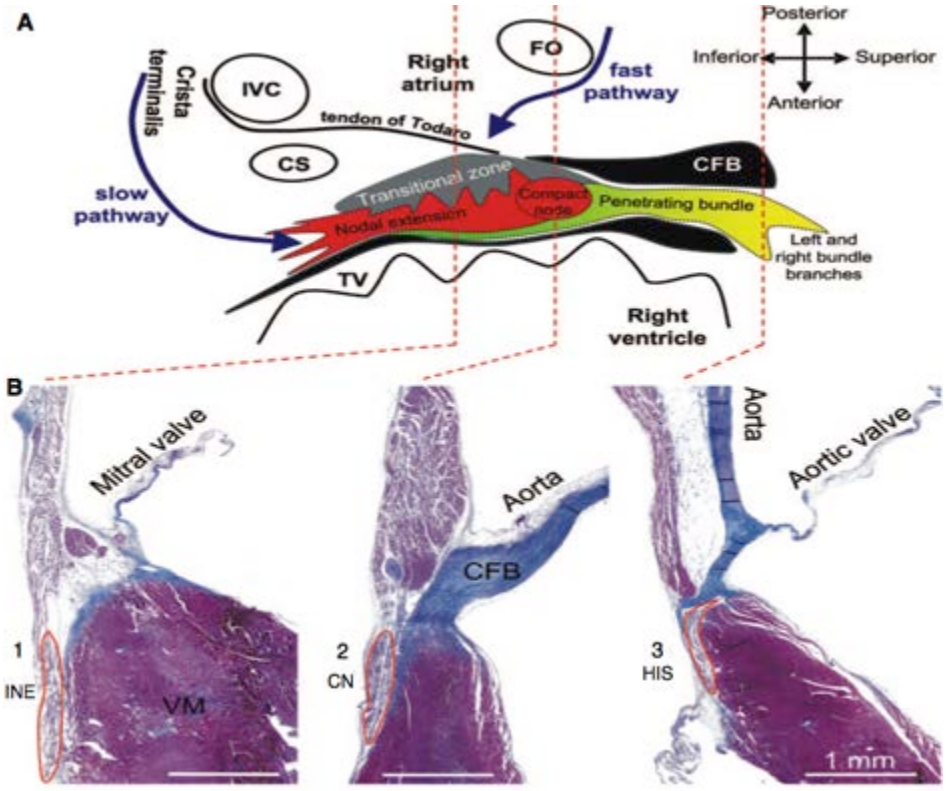

Figure 1.9: (A) Schematic diagram of rabbit AV junction and (B) 1-3 Masson trichrome stained sections through AVJ at levels shown. Masson trichrome stains myocytes red and connective tissue blue. Three regions ringed in red show nodal extension or INE (1), compact node or CN (2), and distal penetrating bundle or His (3). Adapted from Mazgalev et al., and Greener et al.[24,25] FO (foramen ovale), IVC (inferior venacava), CS (coronary sinus), CFB (central fibrous body), TV (tricuspid valve).

1.6 Cellular electrophysiology of the atrioventricular node

The complex structural nature of the AVN makes it challenging for scientists to completely understand its electrophysiology. Different electrophysiological responses are observed in the AVN and the dual AVN physiology is apparent in functional experiments.[25-28] This chapter summarizes the electrophysiological responses, ion channel expression, cell coupling proteins and the multilayer conduction pattern in the AVN, together with a discussion about dual AVN physiology.

1.6.1 Electrophysiological responses, action potential characterstics and multilayer conduction pattern in the atrioventricular node

Carvalho et al., in 1960, showed that three different electrophysiological responses are recorded in the AVJ with microelectrodes.[29] Based on their electrophysiological properties, the myocytes in the AVN can further subdivided in 3 different groups, the atrio-nodal (AN), true nodal or compact nodal (N) and nodo-His (NH). Moreover, Billete et al.,[30] in 1987 documented action potential recordings from 9 different regions of the rabbit AVJ and categorized them into 6 types N-type, 3 AN-types (AN, ANCO, and ANL), NH-type, and H-type (His-type). On the basis of this study the AVN myocytes can be classified as 6 types similar to their action potential morphology (Figure 1.10).[31]

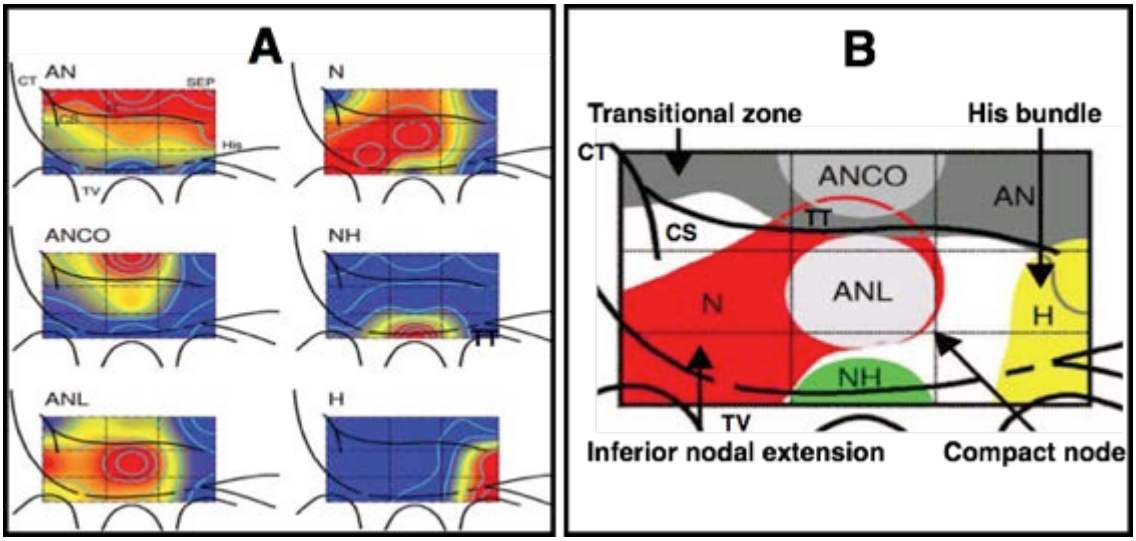

Figure 1.10: Schematic drawings of the AVJ showing different types of myocytes. (A) Frequency of occurrence of AN, ANCO, ANL, N, NH, and H myocytes in different parts of the AVJ of rabbit. (Red indicates frequent and blue, infrequent). (B) Regions in which AN (dark grey), ANCO (middle gray), ANL (light grey), N (red), NH (green), and H (yellow) myocytes are most frequent based on data from Billette et al., (Adapted from Greener et al).[24,30] CT (crista terminalis), SEP, (interatrial septum), TV (tricuspid valve), His (His bundle), CS (coronary sinus), TT (tendon of Todaro).

The electrophysiological response from N myocytes was characterized by a relatively slow rate of rise during upstroke of action potential, small amplitude of the action potential and relatively positive resting membrane potential.[29,30] (Figure 1.11) The AN action potential showed an intermediate morphology between the N cells and the atrial muscle and NH action potential between the N region and His bundle (Figure 1.11). Both of these cells have a faster rate of rise during upstroke and more negative resting membrane potential.

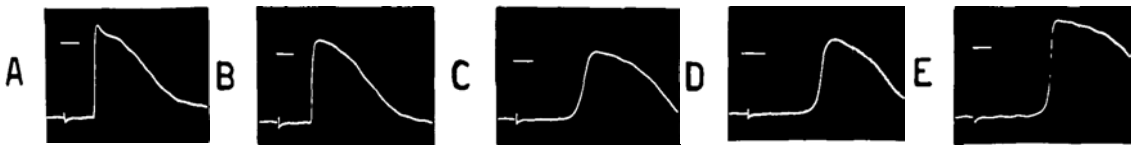

Figure 1.11: Transmembrane records of the excitation of 5 cells in the AVJ region during normal propagation of the action potential. A, atrial muscle. B, AN region of the AVN. C, N from N region. D, NH region closer to N layer. E, NH cells. Adapted from Carvalho et al 1960.[29]

The action potential characterstics of the AVN cells differ significantly from the atrial and ventricular myocardium. The reason for this difference in action potential is the different ionic currents. The phase 0 or the upstroke of the action potential is characterized by slow depolarization in N cells. The resting membrane potential of N cells is relatively more positive (i.e -50 to -65mV) than the atrial and ventricular myocardium (i.e -85 to -90mV) because of the absence of I_{K1}. I_{K1} is an outward K^+ current responsible for maintaining the resting membrane potential in atrial and ventricular myocardium. Because of this difference in the resting membrane potential the Na^+ channel are inactivated and unavailable for phase 0 thus I_{CaL} is primarily responsible for the action potential upstroke resulting in slow rate of deplorization and low amplitude of the action potential.[32.33] The rapid early replorization that marks the phase 1 of action potential in atrial and ventricular muscle are partly due to inactivation of I_{Na} (Na^+ channels) but principally due to I_{to} (transient outward K^+ current). Munk et al.,[32] and Ren et al.,[33] have shown that the majority of N myocytes do not have Na^+ current (I_{Na}) and lacks I_{to} and they are dependent on Ca^{2+} channels for their action potential. The AN myocytes on the other hand have I_{Na}.[32] The rapid early reploriazation phase is not clearly seen in N cells, they have a much smother plateau phase that's mark their dependency of Ca^{2+} channels or I_{CaL}. The I_{CaL} is activated at membrane deplorization (potential positive to -40mV) and are responsible of plateau phase or phase 2 of the action potential. The other ionic current those are responsible for phase 2 and phase 3 (final rapid reploraziation) of the action potential are I_{Kr} (delayed rectifier K^+ current) and I_{Ks} (slow delayed rectifier K^+ current). The I_{Ks} play a major role in determining phase 3 of action

potential. The phase 4 of the action potential in the N cells is characterized by slow diastolic deplorization, which is slow progressive change in the resting membrane potential. This characterstics is the hallmark of excitable pacemaker cells in the Sinus node and Atrioventricular node. Once this reaches the threshold of -40mV the action potential is generated. The channels responsible for phase 4 is subject of much debate in the recent past and the I_f current together with the calcium clock involving Ryanodine channels (RyR2), Na^+- Ca^{2+} exchanger and L-type Ca^{2+} channels were involved in this mechanism. The N cells expresses HCN channels responsible for I_f current.[32,33] These ionic currents and channels will be explained later in the text.

Further to these different electrophysiological responses, conduction pattern in the AVN is also multilayer. This multilayer conduction pattern in the AVN has been found with the use of optical imaging techniques and microelectrode recording.[24,34] Figure 1.14 shows the multilayer conduction pattern with optical recording at AVN (discussed in more detail in section 1.9).

Histologically, in the AVN histologically at least 3 layers have been identified as superficial, intermediate, and the deep.[35] The superficial layer is composed of the transitional AN cells, which express Na^+ channels and Cx43, while the intermediate compact node layer does not express Na^+ channels and relies on low-conductance Cx45 for cell to cell coupling. As a result, these two layers have markedly dissimilar action potential morphologies, which correspond to AN and N cells, respectively. Conduction velocity also differs in between these two layers.[31,35] It will be interesting to see how these different cells, layers and regions of the AVN undergo structural change with ageing and whether these structural changes have any impact on AVN conduction.

Recent work by Li et al., on the rabbit AVN further establishes the multilayer structure of the AVN.[36] Neurofilament and Cx43 have been used to differentiate between various layers found in the AVJ. Neurofilament in a neuronal cytoskeletal protein that has been found in the rabbit CCS whilst absent in the working myocardium. The tissues found in the AVJ include neurofilament positive nodal tissue (densely packed Cx43 positive tissues of the penetrating bundle, loosely packed Cx43 negative nodal tissues of the INE), neurofilament negative transitional tissue, (loosely packed Cx43 positive), neurofilament-negative atrial and ventricular muscle (densely packed, Cx43 positive).

These studies have demonstrated a multilayer conduction pattern in the AVN and also helpful in explaining electrophysiological and anatomical concepts regarding dual AVN physiology.

1.6.2 Dual atrioventricular physiology

Functional electrophysiological experiments have proven the existence of dual conduction pattern within the AVN. However, the anatomical substrate to explain dual AVN conduction was recently studied.

Dual AVN physiology is a representation of dual inputs that travel through the AVN down to the His bundle. These dual inputs are known as fast and slow pathways (as shown in Figure 1.8 and 1.9). Morphologically, the slow pathway proceeds parallel to the tricuspid valve annulus from beneath the coronary sinus to the penetrating AV bundle near the apex of the triangle of Koch. Whereas the fast pathway enters the penetrating AV bundle superiorly from the direction of the atrial septum.[26,27,36,37] This process of transmission of impulses through the AVN down to the His bundle permitted electrophysiologists to devise experiments to prove the dual pathways existence via atrial extrastimulus (AES) technique. Extrastimulus (A2) is a second stimulus that is produced soon after the first stimulus (A1) in the atria. The impulse then travels down the AVN into the His bundle where it is recorded as H1 and H2 respectively, as they reached the His bundle. The time interval between the two stimulus i.e A1H1 or A2H2 interval is the time taken for the impulse to travel from the atria to the His bundle. H1-H2 is time difference between two His responses as the result of atrial stimulus.

The presence of dual AVN pathways is indicated by the evidence of an atrial-His bundle (AH) jump—a jump in the A2H2 or H1H2 interval of more than 50 milliseconds in response to a 10-millisecond shortening of the AES coupling interval (i.e., A1-A2) or pacing cycle length (CL) (i.e., A1-A1). Similarly, a 1:2 response (i.e., a single atrial stimulus results in two ventricular complexes, the first one because of conduction over the fast AVN pathway, and the second one because of conduction over the slow AVN pathway also indicates the presence of dual AVN physiology (Figure 1.12). [38,39]

The anatomic substrate that can explain these functional experiments are lacking but recently evidence is now emerging that can partially explain this dual AVN physiology.[21,31,38,23,39] The Figure 1.8 shows the slow pathway as being Cx43 positive region consisting of LNB and INE as compared to fast pathway being Cx43 negative region consisting of CN & LE area of the AVN. Although it can partially explain the fast and slow pathway theory, it is a bit puzzling to find fast pathway as being Cx43 negative region and slow pathway being Cx43 positive. Cx43 is less resistant than Cx45 in cell-to-cell coupling, whereas Cx45 is the major Cx isoform found in the AVN and SN. Although it is possible that other components may act in the transmission of action

potential in the fast and slow pathway, it makes one wonder about the structural components responsible for communication in the AVJ.

Dual AVN physiology with this partial anatomic explanation also put forth a fundamental question; why is the dual AVN physiology being found in humans and higher mammals? Is its development the result of evolution to protect the AVN from the ageing phenomenon? What are the changes that happen during ageing that results in decreased incidence of AVNRT and also increased incidence of heart blocks in the elderly?

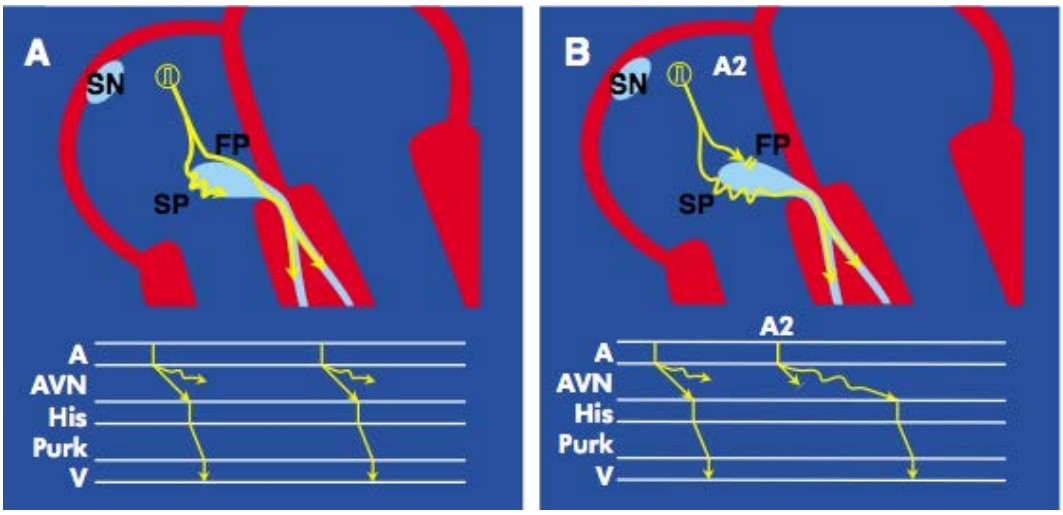

Figure 1.12: Schematic diagram to show dual AV nodal physiology. (A) Usually the conduction through the AVN is down the fast pathway. The conduction down the slow pathway is usually blocked at the point where the two pathways join as the tissue is still recovering from the depolarization via the fast pathway. (B) An earliear extrastimulus A2 may be blocked down the fast pathway yet still conduct down the slow pathway. The slow pathway has a shorter effective refractory period thus recovers quicker than the fast pathway allowing the A2 to conduct but because the conduction down the slow pathway is slower, AH interval is consequently prolonged. SN, sinus node, A, Atrium, AVN, atrioventricular node, His, His bundle, Purk, Purkinje fibers, V ventricle. The bottom ladder diagram in each figure shows the time intervals in relation with the conduction of impulse. Adapted from Handbook of cardiac electrophysiology.[40]

1.7 Ion channel expression in the atrioventricular node

Ion channel expression in the AVN is heterogeneous correlating with the complex anatomy and electrophysiology of AVN described earlier. Table 1.1 lists the important ionic currents.

Table 1.1: Important ionic currents, the ion channels responsible for these current and the functional properties of these ionic currents. ATP = adenosine triphosphate; cAMP = cyclic adenosine monophosphate; GTP = guanosine triphosphate; SR = sarcoplasmic reticulum. (Adapted from Braunwald's Heart Disease, 8th Edition. Saunders 2008)

Current	Ion Channel Subunit	Functional Properties
I_{Na}	$Na_v1.5$ (alpha subunit)	Tetrodotoxin-insensitive voltage-gated Na^+ current. Responsible for Phase 0 (upstroke) of cardiac action potential in the working myocardium, also in the transitional cell layer of the AVN.
$I_{Ca.L}$	$Ca_v1.2$,(alpha subunit), Ca_v 1.3 (alpha subunit)	L-type (*l*ong lasting, *l*arge conductance) Ca^{2+} current through voltage-gated Ca^{2+} responsible for phase 0 and propagation in the SN and AVN cells. Also implicated in pacemaker function of these cells and to the plateau of atrial, His-Purkinje, and ventricular cells; main trigger of Ca^{2+} release from the sarcoplasmic reticulum
$I_{Ca.T}$	$Ca_v3.1$, 3.3/alpha$_1$ G (alpha subunit)	T-type (*t*ransient current, *t*iny conductance) Ca^{2+} current through Ca^{2+} channels, contribute inward current to the early phase 1 and later phase of phase 4 depolarization in pacemaker cells and action potential propagation in the AVN cells.
I_f	HCN4 (alpha subunit)	Hyperpolarization-activated current carried by Na^+ and K^+ in the SN, AVN and His-Purkinje cells, involved in generating phase 4 depolarization; increases rate of impulse initiation in pacemaker cells.
I_{K1}	$K_{ir}2.1$ (alpha subunit)	K^+ current through inwardly rectifying K^+ (K_{ir}) channels, responsible for maintaining resting membrane potential in atrial, His-Purkinje, and ventricular cells; channel activity is function of both membrane potential and $[K^+]_o$; inward rectification appears to result from depolarization-induced internal block by Mg^{2+}.
$I_{K.Ach}$	$K_{ir}3.1/K_{ir}$ 3.4 (alpha subunit)	Inwardly rectifying K^+ current activated by muscarinic (M_2) and purinergic (type 1) receptor stimulation via GTP regulatory (G) protein signal transduction; expressed in the SN, AVN and atrial cells, where it causes hyperpolarization and action potential shortening; activation causes negative chronotropic and dromotropic effects.
I_{Ks}	K_vLQT1 (alpha subunit)/minK (beta subunit)	K^+ current carried by a voltage-gated K^+ (Kv) channel (slow delayed rectifier K^+ channel); plays a major role in determining phase 3 of the cardiac action potential.
I_{Kr}	hERG (alpha subunit)/MiRP 1(beta subunit)	Rapidly activating component of delayed rectifier K^+ current; I_{Kr} inward rectification of I_{Kr} results from depolarization-induced fast inactivation; plays a major role in determining cardiac action potential duration.
I_{Kur}	$K_v1.5$ (alpha subunit)	K^+ current through a Kv channel with ultrarapid activation but ultraslow inactivation kinetics; expressed in atrial and nodal myocytes; determines action potential duration and initiates repolarization in phase 2 of action potential.
I_{to}	$K_v4.3$, $K_v4.2$, KChIP2, $K_v1.4$	Transient outward K^+ current through voltage-gated (K_v) channels; exhibits fast activation and inactivation, and recovery kinetics; contributes to time course of phase 1 repolarization.

1.7.1 Na^+ current

I_{Na} is primarily carried by the $Na_v1.5$ ion channel and encoded by the SCN5A gene. The inward sodium current (I_{Na}) is responsible for the first phase of the action potential, resulting in a rapid depolarization of the myocardium. In the AVJ lower expression of Na^+ channels in the compact AVN region was reported.[24,31,41,42] These lower levels of expression of Na^+ channels have been linked with ovoid type isolated cells which exhibit an N-Type electrophysiological response.[43] Transitional cells of AN and NH types, on the other hand, have more abundant expression of I_{Na} which explains their fast upstroke velocity and speed of conduction.[42] However, another study showed the presence of both TTX (Tetrodoxin) sensitive and TTX resistant I_{Na} recorded in mouse AVN cells. Block of I_{Na} abolishes the pacemaker activity of the AVN cells.[44]

Furthermore, a more comprehensive study of the localization of Na^+ Channels isoforms in the AVN has been performed by Yoo et al., in the rat heart[45] which confirmed that $Na_v1.1$ and $Na_v1.5$ were abundant in the atrial, ventricular myocardium, left bundle, present at a reduced level in the INE, transitional layer and absent in the CN and penetrating bundle. $Na_v1.3$ was present in neuronal tissue of AVN (but not myocytes) and it was abundant in the penetrating bundle but was reduced in other regions of AVN.

1.7.2 Ca^{2+} current

Ca^{2+} channels played an important role in the AVN conduction. Both L-type, and T-type calcium channels responsible for I_{CaL} and I_{CaT}, respectively, have been found in the AVN, especially L-type Ca^{2+} channels which have been responsible for the upstroke of action potential (AP) in N type nodal cells.[32,45-47] In a study by Mangoni and colleagues, I_{CaL} inhibition by Isradapine (L-type calcium channel blocker) completely abolishes the pacemaker activity of the mouse AVN cells. The study also shows that in the AVN the density of I_{CaT} is higher as compared to I_{CaL}.

Greener et al., study on messenger RNA (mRNA) expression measured via qPCR technique showed that the expression of $Ca_v1.3$ is more abundant in the nodal tissues including the CN, INE and distal penetrating bundle as compared to atrial and ventricular muscle in which $Ca_v1.2$ is more abundant.[24]

Mice lacking $Ca_v3.1$/ alpha 1G, T type Ca^{2+} channels responsible for I_{CaT} showed a prolonged PQ interval, suggesting a role for T type Ca^{2+} channels in the AVN conduction.[32,46,48] In another study, Mangoni and colleagues showed that the mice lacking $Ca_v1.3$ (homozygous loss of CACNA1d) showed a prolonged PR interval and intermittent AV block. Similar findings are seen in mice lacking $Ca_v3.1$. The mice

lacking both these channels ($Ca_v1.3$ and $Ca_v3.1$) showed additive effects of these channels resulting in more pronounced AV block.[49] The homozygous loss of $Ca_v1.3$ (CACNA1d) in human's results in bradycardia, AV nodal disease with intermittent AV block and deafness.[50]

1.7.3 Funny current (I_f)

HCN channels or hyperpolarization activated cyclic nucleotide gated channels are responsible for I_f current. Four isoforms of HCN channels have been identified.[51] Specific to the CCS, HCN channels are poorly expressed by atrial and ventricular myocytes. The presence and the important role of a pacemaker "funny" current, I_f was firmly established by different investigators[52-54] and it has been demonstrated that predominant isoform of genes encoding I_f current is HCN4 which is expressed in the INE of the rabbit heart.[9,22,51] This was confirmed by Greener et al., which showed abundant expression of HCN4 in the INE but much less in other nodal cells.[24] HCN1 on the other hand is uniformly expressed throughout the AVN and penetrating bundle. In a recent study on HCN4 knockout mice with the use of daily tamoxifen, it was shown that HCN4 knockout mice not only led to the development of severe bradycardia but also associated with higher degrees of AV block (2:1 and 4:1 2nd degree AV block) as the heart rate progressively decreased.[54] Another independent group yielded similar results that showed the destruction of HCN positive myocytes resulted in profound bradycardia and AV block.[53]

1.7.4 K^+ Current

Expression of K^+ channels is also nonuniform in the AVN. Transient outward current I_{to}, similar to I_{Na}, appears to reside primarily in the transitional layer of the AVN, while being more scarcely expressed in N cells.[32] However, Marger et al., study showed presence of I_{to} in mouse AVN cells. K^+ channels mRNA that contributes for I_{to}, i.e $K_v4.3$, $K_v1.4$ were shown by Greener et al., to be significantly less abundant or absent in the INE. However, $K_v4.2$ mRNA tended to be more abundant in the nodal tissues. There was a distinct decrease in the abundance of KChIP2 mRNA from the atrial and ventricular muscle compared to the nodal tissues and is absent from CN.[24]

On the other hand, a well-documented vagal control[55,56] of the AVN suggests a role for I_{KAch}. I_{KAch} is a large inwardly rectifying outward K^+ current that is acetylcholine regulated. I_{Kr} plays an important role in the repolarization of the action potential in the rabbit AVN and it also recorded in the mouse AVN cells by Marger et al.[44,57] I_{Ks} does not contribute to the repolarization and was not observed in AVN cells.[44] Furthermore,

Greener et al., study showed that hERG mRNA (responsible for I_{Kr}) was more abundant in the CN than K_vLQT1 and minK mRNA (responsible for I_{Ks}). K_v1.5 mRNA (responsible for I_{Kur}) however has been abundantly found in the nodal tissues.[24]

1.7.5 Electrical coupling and the connexins

Electrical coupling between myocardial cells is imperative for the transmission and propagation of the action potential. Without the appropriate electrical coupling fast conduction between myocardial cells would be difficult and also transmission of impulse between various components of the CCS would suffer. Myocardial cells have a unique way of electrical coupling via gap junctions (low resistance, non-selective ion channels) known as connexins (Cx).

These connexins appear to play an especially prominent role in the AV conduction. Three major isoforms of these gap junctional channel proteins, Cx40, Cx43 and Cx45, have been mapped to specific regions of the mammalian heart.

The main connexins isoform in the AVN is Cx45 followed by Cx43 and Cx40.[58-60] The compact node (N region) has been shown to have low level of expression of the major cardiac isoform, Cx43, which is responsible for cell-to-cell communication throughout most of the myocardium, specifically in the atrial and ventricular myocardium. The transitional layer of the AV node, including both AN and NH, exhibit greater levels of expression of Cx43. Discussion regarding role of Cx43 expression in dual AVN physiology can been found earlier in section 1.6.2. Cx43 expression in the AVJ appears to be higher in the His bundle, the lower part of the CN or LNB, and its rightward inferior extension in the human compared to the leftward extension and the upper part of the CN.[41,58,59]

The Cx isoforms have been reported to play a role in the conduction through the compact node (Cx45) and NH region (both Cx40 and Cx45). Cx45 is high resistance Cx, not only it is the major isoform in the AVN causing impulse delay but also found in the SN.[58-60] Other Cx isoform, Cx30.2 have been found in the CCS of mice, its human counterpart Cx 31.9 has not been found in the human AVN.[61,62] Cx30.2/Cx31.9 role in cardiac conduction is still debatable.

1.8 Autonomic innervation of the atrioventricular node

The autonomic nervous system (ANS) has a well-documented effect on the CCS. Tachycardia during exercise and bradycardia during sleep is an example of the everyday effect of the ANS on the CCS. The two components of the ANS namely the parasympathetic and the sympathetic nervous system act in an opposing way to modulate the activity of the SN and AVN. The parasympathetic activity is shown to be present in the AVN by nerve endings exhibiting acetylcholinestrase (AChE) activity and the sympathetic activity via tyrosine hydroxylase or dopamine hydroxylase enzymes.

In the AV nodal cells sympathetic stimulation via B-adrenergic receptor activates adenylate cyclase with converts ATP to cAMP which in turn phosphorylate protein kinase A. Elevated cAMP levels activate protein kinase A (PKA), which phosphorylates L-type calcium channels, leading to an influx of Ca^{2+} into myocytes. This influx releases stores of intracellular Ca^{2+} from the sarcoplasmic reticulum resulting in increased intracellular Ca^{2+} and thus early deplorization. (Fig:1.13) The effect of parasympathetic stimulation on AVN cells is applied via acetylcholine, which acts via muscurainic receptor to decrease cAMP via inhibitory G protein. The G protein are also linked to I_{KAch} which is an outward K^+ current in resulting in efflux of K^+ upon parasympathetic stimulation. The effects of parasympathetic stimulation thus is decreased intracellular Ca^{2+} via decreased cAMP and hyperpolarization of cells due to K^+ efflux both of these results in delayed deplorization.

The structural study by Petrecca et al., demonstrated the sympathetic, parasympathetic nerve endings and β receptors distribution in the rat AVJ.[63] They have shown that in the mid nodal cell region or the CN region relatively few AChE reactive nerve endings were found while the transitional cell layer exhibits an abundance of these nerve endings. On the other hand tyosine hydroxylase (TH) immunoreactivity is present throughout the transitional, lower nodal, midnodal and CN regions in a spatially uniform manner. It is, therefore, possible that the parasympathetic branch of the ANS preferentially exerts its effect on the transitional cell layer as compared to the CN region. The study by Prystowsky et al., showed that the effect of the parasympathetic and sympathetic nervous systems on AVN conduction is balanced or equal. They have performed electrophysiological measurements of AVNERP (AV nodal effective refractory period) and AVN conduction time on human subjects after application of atropine (acetylcholine receptor blocker) and propranolol (non selective β blocker). No effect on the AVN conduction were observed with simultaneous administration of atropine and propranolol but when applied separately confirmed negative dromotropic

(conduction/speed across the AVN) effect of propranolol and positive dromotropic effect of atropine.[64] This effect is also well documented in other studies.[65,66] This balanced effect of the ANS on the AVN contrasts with the marked effect of the parasympathetic nervous system on the sinus nodal automaticity.

The modulation of the AVJ pacemaker via autonomic stimulation has been studied using subthreshold stimulation and optical mapping technique by Hucker et al.,[41] in the rabbit AVJ preparation. The sub threshold stimulation excites the intra-cardiac neuron without causing myocyte contraction. They have shown that the sub threshold stimulation applied adjacent to the conduction system in the triangle of Koch autonomically modulates the junctional rate, which increases to almost 145±16 beats/min when subthreshold stimulation was applied in combination with atropine and decreases by 13% when applied together with nadolol (β-receptor blocker). The anatomic location of the AVJ pacemaker remains stationary in response to autonomic stimulation (most often in the INE).

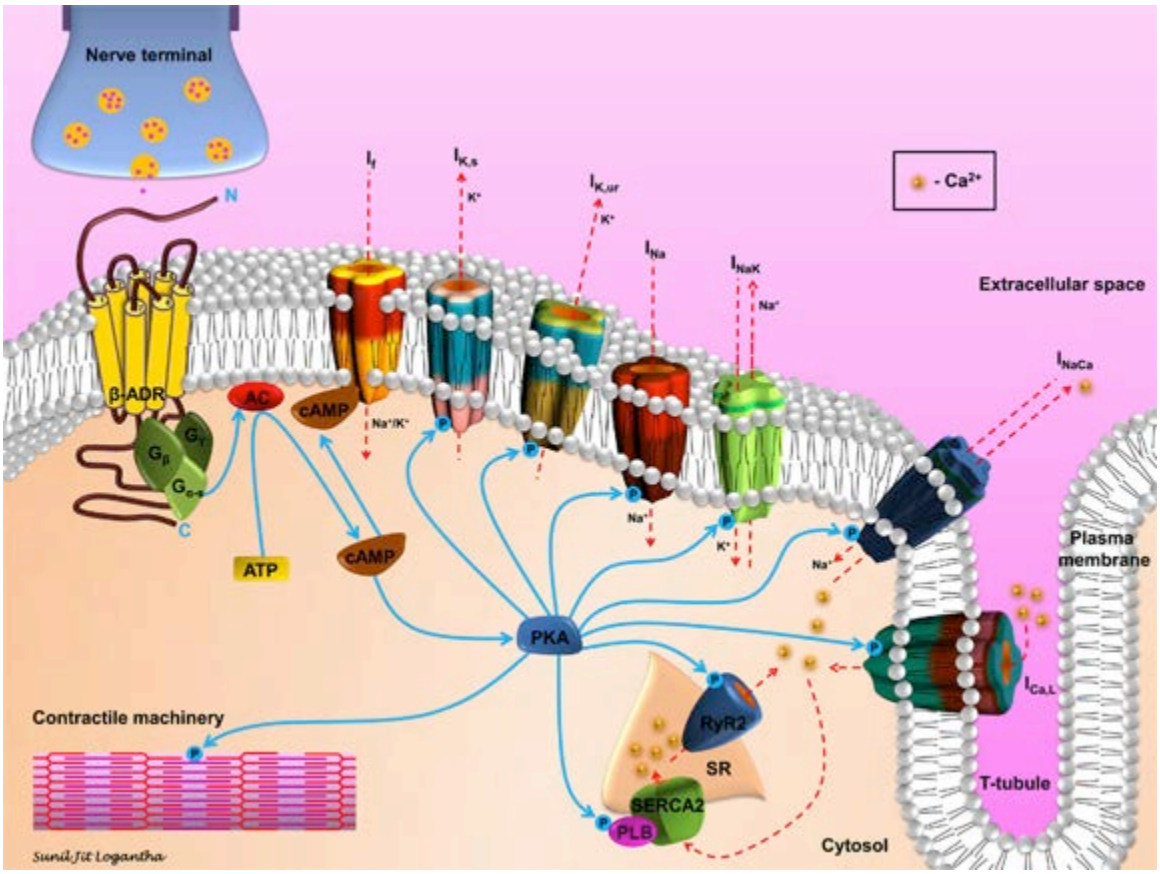

Figure 1.13: Schematic diagram to show different ionic currents that contribute towards action potential in a cardiomyocyte and their relation ship with sympathetic nervous system. Also shown is the calcium handling proteins and their relationship with T-tubule. β-adrenergic receptor (β-ADR) can modulates the effect of these ionic currents by activating adenylate cyclase (AC), which converts ATP to cAMP. cAMP activates I_f and protein kinase A (PKA). PKA then modulates via phosphorylation a number of cellular substrate as shown. cAMP (cyclic adenosine monophosphate), ATP (adenosine triphosphate), PLB (phospholamban), SR (sarcoplasmic reticulum). Adapted from Taggart et al.[67]

1.9 Summary of action potential propagation through the atrioventricular node and ion channels expression

The cardiac action potential is generated in the SN and transmitted through the atrial myocardium to the AVN. Conduction through the AVN is slow and as shown via optical recordings in Figure 1.14 transmitted as a dual wave front. The action potential travels through the transitional cell layer rich in AN cells and AVN (compact node and INE, abundant in N Cells) to reach the His bundle. The proximal part of the His bundle consist largely of NH and H cells. Conduction through the AVN is being regulated by autonomic nervous system. Then action potential propagates from the His bundle to the bundle branches, Purkinje fibers and finally to the ventricular muscle to initiate ventricular contraction.

Figure 1.14 shows the transmission of the AP through the AVN during AVN block to increase understanding of dual wave front involved in the action potential propagation. The figure show recordings from the superficial transitional cell layer and second from the deeper CN layer during 3:2 Wenkebach AVN block. The bottom left panel shows recordings from the CN. The action potential in this CN cell preceded or coincided with the His bundle signal and absent when the His bundle signal is missing in case of AVN block. It further shows that the action potential in the CN is associated with the second component of the optical signal that is also missing with AVN block. The bottom right panel shows recordings from the superficial transitional cell layer, which has a faster upstroke and coincided with the first of the two components in the optical signal. As demonstrated both the first optical signal and the action potential in the superficial transitional cell are present even with AVN block and is depolarized earlier after atrial signal as compared to action potential in the CN layer.[34]

The I_{Na} is principally responsible for action potential upstroke in the transitional layer of the AVN comprising primarily of AN cells. The I_{CaL} is primarily responsible for the action potential upstroke in the CN. N cells primarily found in in CN and INE, also exhibit pacemaker current, I_f. In keeping with these findings at the molecular level, Greener et al., showed that mRNA for $Na_v1.5$ is less abundant in all components of the AVJ in the human and rabbit compared to working myocardium, while $Ca_v1.3$ is increased. HCN4 is more abundant in all areas of the AVJ.[24] Table 1.2 shows the summary of ion channel expression in various regions of the AVJ and their contribution to the different action potential phases. In terms of the resting membrane potential, N cells exhibit a more positive diastolic membrane potential compared to the atrial,

ventricular myocardium, AN and NH cells. This is due to lower density of I_{K1}. mRNA for $K_{ir}2.1$ (one of the principal channels responsible for I_{K1}) is reduced in the AVJ compared to working myocardium in rabbit.[24]

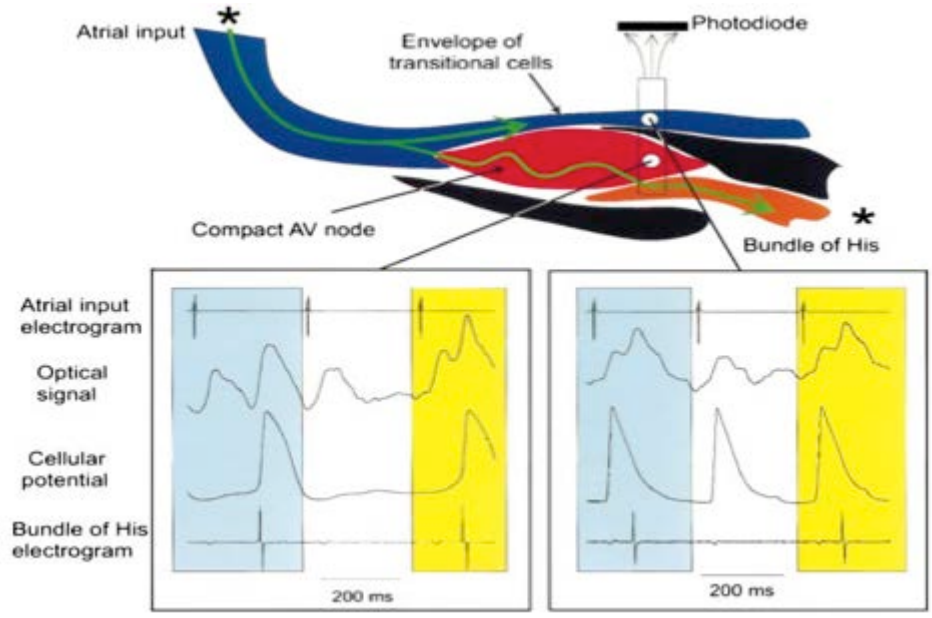

Figure 1.14: A multilayer structure is schematically drawn (top panel) to represent a cross section of the atrioventricular node (AVN) perpendicular to the endocardial atrial surface. The compact node (red) covered with a superficial layer of transitional cells (blue) providing a connection between the atrial tissue and the compact node. The compact node, in turn, connects to the bundle of His (orange). Connective tissue protrusions are shown in black. Arrows show hypothetical wave fronts in the transitional and compact nodal fibers. Optical recordings obtained by a 16 photodiode array were accompanied by bipolar electrograms from the atrial input to the AVN (*) and from the bundle of His. (*). In addition, a roving glass microelectrode was utilized to impale cells in different AVN layers (black and white circles). Each of the lower panels illustrates three consecutive heartbeats with simultaneously acquired atrial input and His electrograms, along with optical and microelectrode signals.[34]

Table 1.2: Ion channel expression at mRNA level in rabbit INE, CN, PB compared to atrial muscle (AM), & Ventricular muscle (VM). +*, significantly up-regulated; -*, significantly down-regulated; +, trend to up-regulation; -, trend to down-regulation; =, no difference. Based on the study by Greener et al.[24]

Ion Channel	Ionic Current	Action Potential Phase	Region				
		4 0 1 2 3	AM	INE	CN	PB/His	VM
HCN1	I_f		-	+*	+*	+*	-*
HCN4	I_f		-	+*	+	+	-*
$K_v2.1$	I_{K1}		-*	-*	-*	-	+*
$Na_v1.5$	I_{Na}		+*	-*	+	+	+*
$K_v1.4$	I_{to}		+	-	-	-	+*
$K_v4.2$	I_{to}		-	+	+	+*	+
KChIP2	I_{to}		+	-	-	-	+
$Ca_v1.3$	I_{CaL}		+	+*	+*	+*	-
$Ca_v1.2$	I_{CaL}		+	-*	-*	-*	+*
$K_v1.5$	I_{Kur}		+*	+*	=	=	+
ERG	I_{Kr}		+	=	=	+	+*
K_vLQT1	I_{Ks}		+	-	-	-	+*

1.10 Channelopathies associated with atrioventricular conduction disease

The etiology of AVN conduction disease is varied, ageing is implicated and it is common in patients with inherited neuromuscular diseases and congenital cardiac malformation. Genetic mutations have also been recognized in association with AVN block. Table 1.3 present a summary of various ion channel diseases associated with AVN dysfunction.

The genetic mutations in SCN5A (which codes for $Na_v1.5$) are the most studied mutations causing AVN dysfunction. SCN5A is well known for its involvement in Brugada syndrome (BrS)[68] and Long QT syndromes type 3 (LQT3).[69] However, multiple SCN5A mutation has also been reported with AVN conduction disturbances.[70-73] These mutations can lead to isolated cardiac conduction defects, which can result in AVN block as well as reduced action potential propagation throughout the CCS. Together with isolated conduction defects, mutation in the SCN5A has also been reported to be associated with the clinical syndrome causing dilated cardiomyopathy, SN dysfunction, and ventricular arrhythmias.[74] Overlapping syndromes of conduction system defects with BrS and LQT3 have also been reported.[69,75]

CACNA1C gene that codes for $Ca_v1.2$ has been associated with antibody mediated congenital AV block.[76,77] The other important mutation with regards to the Ca^{2+} channels causing AV block involves CACNB2b gene (codes for Ca_vB2b) responsible for I_{CaL} was actually identified in patients with one of SCN5A mutations. Combination of these two mutations results in CCS disease without development of BrS.[78] As already mentioned in section 1.7.2 CACNA1D ($Ca_v1.3$) mutation results in intermittent AV block.[50]

Mutation in KCNH2 (codes for KvLQT1) has been associated with AV Block. This mutation can manifest as AV block inducing Torsades de pointes (TdP) in patients together with clinical manifestations of congenital long QT syndrome.[79] HCN4 reduced expression can result in bradycardia and AV block.[54]

Table 1.3: Genetic mutations in patients with cardiac conduction system disease in particular AV conduction causing AV Block. Cases of AVN dysfunction leading to AV block with inherited or acquired mutations.

Gene	Protein name	Disorder	Reference
SCN5A	$Na_v1.5$	Atrioventricular conduction block	Wang et al., 2002
SCN5A	$Na_v1.5$	Tachycardia, atrial & ventricular conduction delay, Sudden cardiac death	Bezzina et al., 2003; Makiyama et al. 2005
SCN5A	$Na_v1.5$	Sick sinus syndrome, Atrioventricular conduction block	Lei et al, 2008
KCNQ1 or KCNH2	K_VLQT1 ERG	Atrioventricular conduction block, Torsades de pointes, QT prolongation	Oka et al., 2010
SCNA5	$Na_v1.5$	First-degree atrioventricular block, Brugada syndrome, sinus arrhythmia, bradycardia, and PR prolongation	Hu et al., 2010
CACNA 1C	$Ca_v1.2$	Congenital heart block	Qu et al., 2001; Boutjdir et al., 1998
CACNA 1D	$Ca_v1.3$	Alteration of atrioventricular nodal conduction, bradycardia, deafness	Shahid et. al 2011
HCN4	HCN4	Familial sinus bradycardia, sick sinus syndrome, AV block	Milanesi et al., 2006; Schulze-Bahr et al., 2003 Barbuti & DiFrancesco, 2008 Baruscotti et al., 2010b, Mesirca et al 2014
Cx43	Cx43	Dispersed conduction, susceptibility to ventricular arrhythmias	Boulaksil et al., 2010

1.11 Structural and electrophysiological changes in the atrioventricular node with ageing

Ageing phenomenon of the CCS is equally interesting for clinicians and scientists. The anatomical, morphological and cellular changes that occur with ageing leads to a challenging subsets of patient groups that make clinicians searching for new modalities of treatment and scientists searching for the answers that can provide better understanding of the disease process. As mentioned before, ageing affects the AVN in a peculiar way leading to an increased incidence of the heart blocks and a decreased incidence of AVNRT.

1.11.1 Structural changes

Waki et al., in a study on normal human hearts showed that the morphology of the AVN changes during postnatal development during 1-20 years.[80] The AVN shape in a newborn human, in its central part is oval shape. It lies between the transitional cell layer and central fibrous body. This shape of the AVN then changes with development into a spindle shape or a J shaped structure. These changes happen because of significant

development of muscular AV septum. As a consequence, the AVN is positioned more into the slope of the septum. Figure 1.15 shows the histological images detailing these changes. These images also show that the tightly packed transitional cell zone appears more loosely packed with an increase in the amount of the fibrofatty tissues with increasing age as shown from images A, B, C.

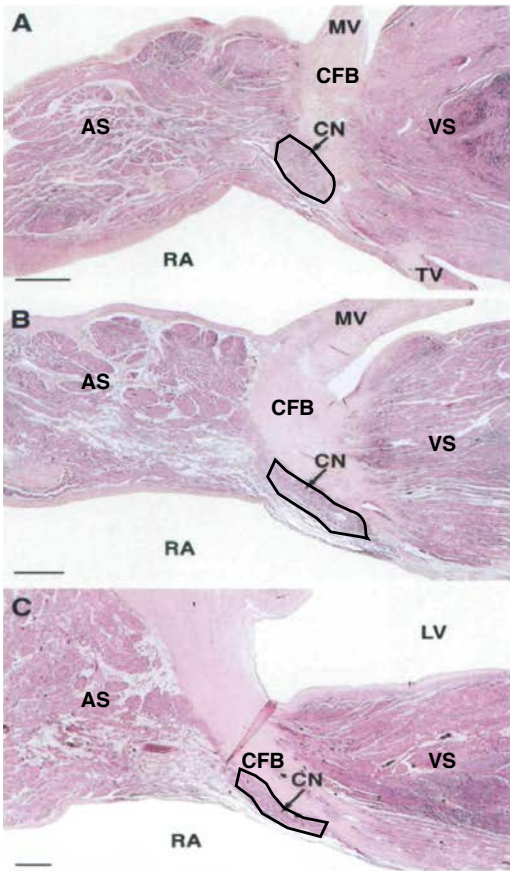

Figure 1.15: Changes in position of the compact node (CN) with ageing. The muscular AV septum is the area between the mitral valve (MV) and tricuspid valve (TV). (A) Section from 1-month-old infant. The CN is oval shaped and is in almost "horizontal" position, resting on the central fibrous body. (B) Section from 5-year-old child. The CN has changed from oval to a spindle shape. Fibrofatty tissues have already produced a looser texture of the transitional cell zone. (C) Section from 17-year-old adolescent. The CN shows an elongated spindle shape and is in a much more upright position due to the increased slope of the muscular AV septum. Note that the connections between transitional cells and CN have loosened further, due to the deposition of fibrofatty tissues in the transitional cell zone LV, left ventricle, RA, right atrium, MV, mitral Valve, TV, tricuspid valve, VS, ventricular septum, AS, atrial septum, CFB, central fibrous body. Hematoxlin and eosin stain. Bar = 1 mm. Adapted from Waki et al.[80]

The other important aspect about this study is the growth of nodal extensions i.e., INE (rightward nodal extension) and LE (leftward nodal extension) with increasing age. In the youngest age group the two extensions are relatively close to each other. However, in the older age group and with an increasing slope of the AV septum, these two extensions ran further apart from each other (Figure 1.16). The INE increases in size to such an extent that the length of INE is comparable to the CN in an adolescent heart.

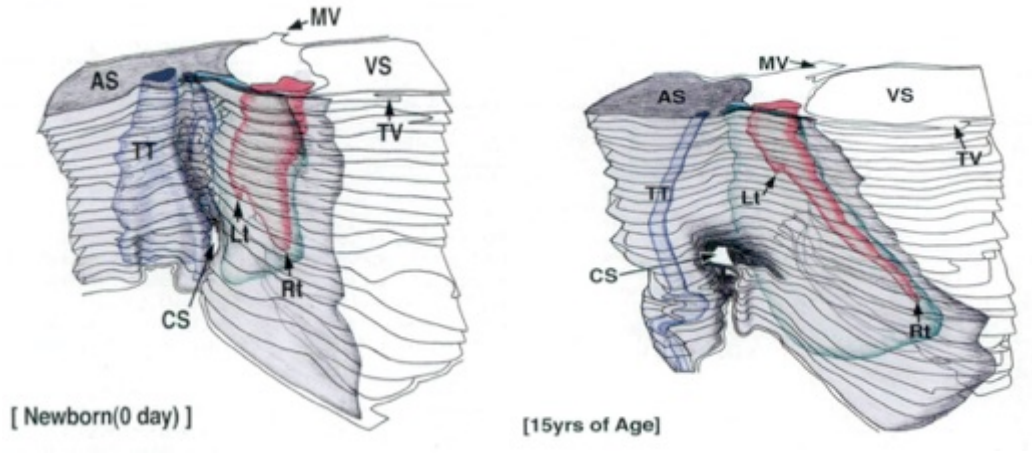

Figure 1.16: A 3D reconstruction of the human AVN showing nodal extensions. As compared to the newborn, the INE or right nodal extension growth is significant at 15 years of age. Right nodal extension (Rt), left nodal extension (Lt), tendon of Todaro (TT), atrial septum (AS), ventricular septum (VS), mitral valve (MV), tricuspid Valve (TV), coronary sinus (CS). Adapted from Waki et al.[80]

This study by Waki et al., was performed on 40 structurally normal hearts aged 1-20 years old. The age in this study is only limited to 20 years thus it is difficult to establish whether the morphology of the AVN changes in adult life after 20 years. This question still unsolved.

Multiple studies examining histological changes in the CCS and AVN with ageing confirmed that the amount of connective tissue and intercellular collagen in the AVN increases with age.[81-83] It is not known whether these changes are generalized i.e. present in all regions of AVJ. This increase in collagen in the AVN is in contrast with the ventricular muscle, which actually decrease with ageing.[83,84] In a study on ageing rabbit heart, increased fat cell deposition in the AVN and His bundle together with increased collagen deposition was found.[84]

A forensic study of the CCS by Song et al., has also suggested the above popular notion of fibrofatty infiltration of the AVN with ageing. They also noted a few interesting observations. First, as shown in previous studies, beyond 40 years there is an increase of fibrous and fatty tissue. Secondly, they have noted that the ageing process of the fatty tissue infiltration in the CCS was mild, in patients over 70 years of age, only 7.5% in the AVN and 15.2% in the SN showed fatty infiltration. Thirdly, the ageing process in the SN began from the tail and the process was usually more severe in the tail than in the head of the SN. Last but not least is the observation of deposition of calcium in about half of the persons in the central fibrous body and the top of the interventricular septum. This process began from 36 years of age and is without gender difference. [85]

These studies are important in elucidating different structural and histological changes in the AVN with ageing. To date we have not been able to locate any study, which looked at changes in ion channel expression in the AVN with ageing. In the ageing studies on ion channel expression of the SN by Tellez et al., and Yanni et al., have shown that the gene expression in the SN changed considerably with age, i.e., there was an age-dependent increase in $Na_v1.5$, $Na_v\beta1$, $Ca_v1.2$ and decrease in $K_v1.5$ and HCN1.[86,87]

1.11.2 Autonomic innervation of cardiac conduction system with ageing

The autonomic nervous system plays a significant role in modulating AVN conduction. Effects of the parasympathetic system or vagal nerve stimulation via carotid sinus massage or valsalva manouver causing transient AV block has been well established in the clinical practice during emergency treatment of AVNRT and supraventricular tachycardia.[88]

According to the study by Chow et al., the CCS has increased density of autonomic innervation as compared to atrial and ventricular myocardium in humans.[89] 24 human hearts aged from 1-80 years were used in the study. Activity of sympathetic supply was determined by immunostaining with dopamine β-hydroxylase (DβH) and tyrosine hydroxylase (TH) enzymes and the parasympathetic activity were ascertained by immunostaining for cholinesterase enzyme and acetylcholinestrase (AChE) nerve terminals. DβH, TH, and AChE innervation of the CCS follow a similar pattern of distribution during ageing. Chow et al., showed changes in the autonomic nervous system from infancy to senility and showed that the innervation is highest in the SN, and exhibits a decreasing gradient through the AVN, penetrating bundle down to the bundle branches. DβH, TH and cholinesterase activity were abundantly found in infant hearts but AChE positive nerve terminals were rarely found in the SN, AVN and bundle branches. Cholinesterase activity diminished as adulthood is reached but AChE positive nerve terminals density increased and reached similar to that of DβH and TH nerves. This co-dominance remained during senility, however the density of DβH, TH and AChE decreased.

Furthermore, with ageing, autonomic innervation of the AVN declines in humans[89] and there is a decrease in the density of β-adrenergic receptors as well as a decrease in the sensitivity to β-agonists in the AVN (but not in the ventricular myocardium) in the rat.[90] In the study on Fischer 344 rats, Kusumoto et al., used immunostaining with β-adrenergic antagonist, 125 Iodocyanopindolol, to identify β-adrenergic receptors in the AVN. They first identified the AVN by staining with

acetylcholinestrase (it readily identifies CN as shown by Figure 1.17) and then digitized this imaged section over an incubated section with 125 iodocyanopindolol to locate β-adrenergic receptors in the AVN.

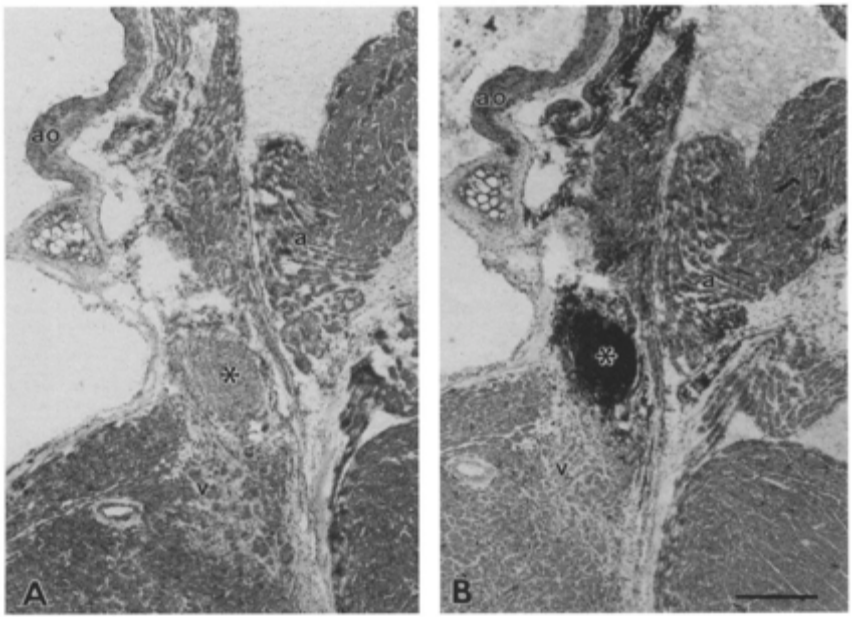

Figure 1.17: Sections stained with (A) Haematoxylin and eosin and (B) Acetylcholinestrase staining. Asterisk indicates the AVN. a (atria), v (ventricle). Ao (aortic valve) Acetylcholinesterase staining readily identifies the AVN.

1.11.3 Changes in electrophysiological measurements with ageing

Multiple studies have been performed in humans[81,91-95], rabbits[84] and rats[86,90,96] to elucidate changes in standard electrophysiological measurements with ageing. These measurements includes AV conduction time (spontaneous and paced) shown as PR/PQ interval, AH interval (time taken by the cardiac impulse to travel across the AVN), HV interval (time taken by cardiac impulse to travel across His-purkinje system), AV nodal effective refractory period (AVNERP), effective refractory period of slow and fast pathway and AV Wenkebach cycle length.

In humans, a study by Taneja et al., showed that ageing significantly prolonged the PR, AH interval, AVNERP, and the AV Wenckebach cycle length. Ageing has been associated with the prolonged PR, AH and HV interval but predominantly the prolongation of the PR interval is due to a prolonged AH interval, HV interval is only partly responsible.[94] This study was performed to identify the effects of gender and age on all electrophysiological measurement but the effects of ageing on the measurements mentioned above were independent of gender difference. The study includes 354 patients

without structural heart disease or pre-excitation. The electrophysiological testing was performed in the drug-free state and was clinically indicated. There were 124 men and 230 women with a mean age of 45±19 and 47±18 years, respectively. Figure 1.18 shows graphs with different age groups to illustrate the effects of ageing. The study includes those patients referred for electrophysiological investigations, therefore it is difficult to establish whether this group can be accepted as representative of the normal adult population.

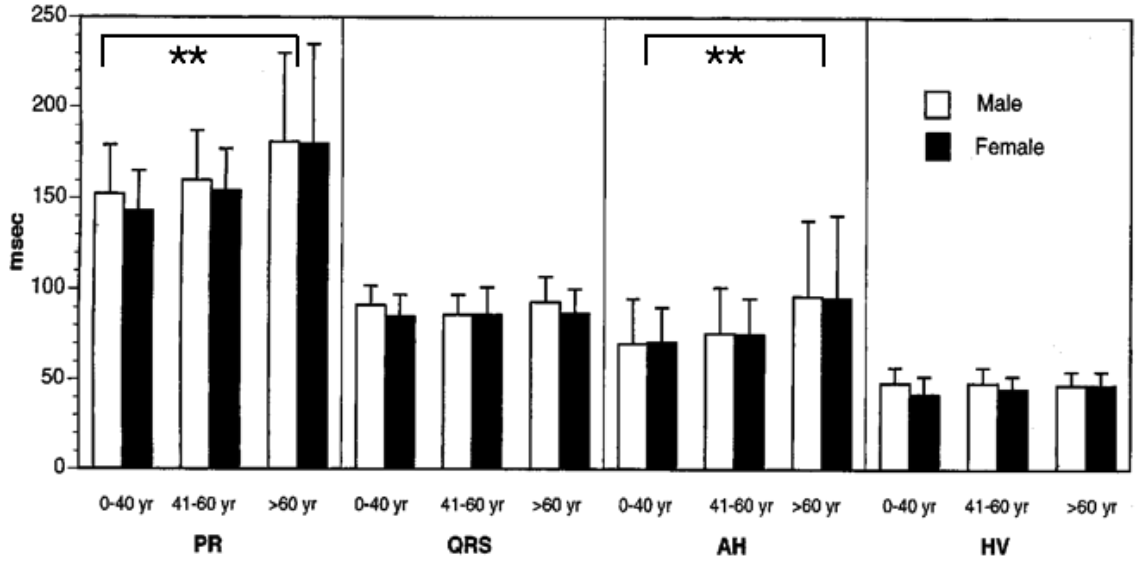

Figure 1.18: Influence of age on gender differences in PR interval, QRS duration, AH interval, and HV interval. Ageing, independent of gender difference, significantly prolonged the PR interval and AH interval as shown. Adapted from Taneja et al.[94]

Schwartz et al., performed PR interval and paced AV interval after autonomic blockade in the healthy human population. This study confirmed that the prolonged PR and paced AV interval with ageing are independent of the autonomic nervous system. Heart rate, heart rate variability, and AV conduction were studied in 20 young (30±5 years) and 19 older (69±7 years) healthy people at baseline, after single and double autonomic blockade. The older subjects showed increased PR intervals (177±24 vs. 149±17 ms, $P < 0.001$) before autonomic blockade. Atropine (muscuranic-M receptor blocker) had no effect on the PR interval. Propranolol (non selective β-receptor blocker) prolonged the PR interval equally in old and young ($P < 0.0008$). After double autonomic blockade, PR, and paced AV intervals were significantly prolonged in older subjects. Mean values from the study are statistically significant: PR intervals, 179±23 vs 149±17 ms, $P = 0.0002$; paced PR intervals (BCL 500 ms), 251±39 vs. 215±47 ms; and AV block cycle length, 413±5 vs. 385±69 ms (multivariate analysis of variance, p value < 0.03).[97]

Experimental electrophysiological studies on the ageing model of rats AVN have also been performed. Schmildin et al., study on the ageing model of rats measures heart rate and AV conduction time in Langerhorff perfused hearts from 18 mature (4-6 months), 12 middle-aged (12-14 months), and 18 senescent (24-26 months) Fischer 344 rats. Heart rate decreased with increasing age from 218±18 in mature to 196±27 (means and SD) beats/min in middle-aged rats to 183±22 beats/min in senescent rats (analysis of variance, $P < 0.001$). Spontaneous AV conduction time increased from 43±7 to 49±5 to 62±9ms with ageing ($P < 0.0001$) respectively. Paced AV conduction time also lengthened with aging, and AV Wenckebach block cycle length increased. The results of these studies are also consistent with the effects observed in humans. Spontaneous and paced AV conduction time lengthenend and AV Wenkebach cycle length increased. Also, ageing rat hearts were less sensitive to isoporternol (β-Agonist) treatment but reach similar maximal effect with increased dose. Isoproternol treatment significantly shortened AV conduction time.[96]

Tellez et al., in their study on ageing rats have shown that PQ interval prolonged significantly in anesthetized and also in Langerhoff-perfused older rats, as compared to young rats (Figure 1.19).[86] In a study on ageing rabbit hearts, Gottwald et al., showed similar findings of prolonged AV conduction time and significantly prolonged PQ/PR interval in Langerhoff-perfused rabbit hearts.[84]

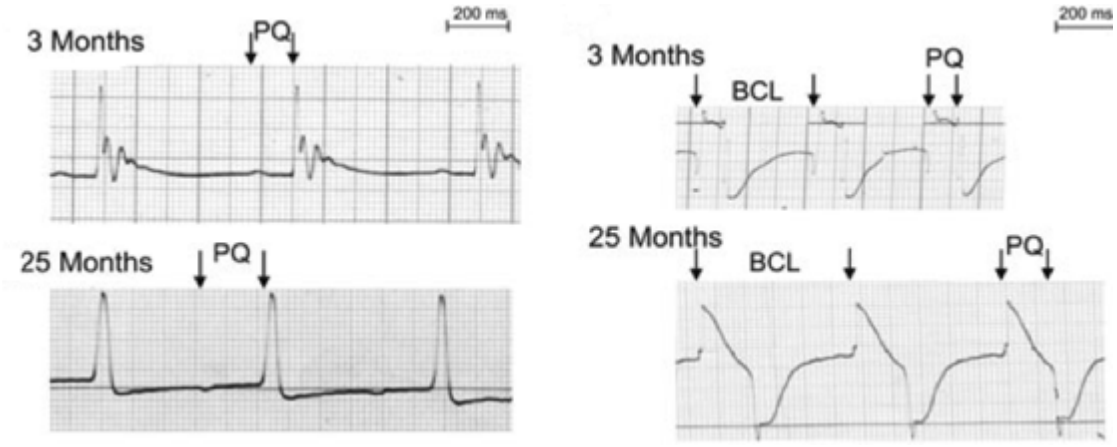

Figure 1.19: ECG recordings from young and old rats (anaesthetized rats on the Right) and ECG-like recordings from Langendorff-perfused hearts from young and old rats (Left). Measurement of basic cycle length (BCL) and PQ interval are shown. PQ interval significantly prolonged in old rats. Adapted from Tellez et al.[86]

The other important electrophysiological parameter of (AV) nodal recovery properties is AVNERP. It is related to the slow recovery of nodal cell excitability that follows nodal activation and causes nodal conduction time to increase with prematurity of the incoming impulse. They are best manifested by delivering a periodic premature atrial

extra stimulus-AES (A2) coupled with first atrial beats (A1) and measuring the shortest time in between the two His responses (H1-H2) caused by the first atrial beat (A1) and AES (A2) respectively, i.e. AVNERP is the shortest H1-H2 in response to any A1-A2. It is the time required for the atrial extrastimulus (AES) to conduct through the AVN after the first atrial beat and that can be measured at His. This time indicates the repolarization time required by the AV nodal cells.

A study on humans by Kavanagh et al., showed that recovery properties of the AVN also decline with ageing and AVNERP has a linear progression with age. The study was conducted on 30 subjects aged 18-73 years. Structural and occult heart diseases were excluded by an echocardiogram, a treadmill exercise tolerance test, a rest and exercise radionuclide angiogram, and/or a cardiac catheterization. Together with AVNERP, effective and functional refractory periods of the right atrium and the right ventricle were also showed a linear progression with ageing.[91]

AVNERP prolongation was also seen with increasing age in another study. They compared children and young adults between 1-20 years. This study by Lin et al., was conducted over a 3 year period and included 43 patients referred for electrophysiological investigation. Almost half of these patients exhibit evidence of pre-excitation (accessory pathway) and had successful ablation before the measurements were performed. The rest of the patients had other diagnoses as an indication for electrophysiological study including junctional tachycardia, atrial flutter and ventricular tachycardia though arrhythmogenic focus was ablated before measurement. This could potentially affect the results especially if the accessory pathway located close to the AVN. Furthermore the sedative procedure varied among patients as the study was conducted over 3 years. The above reasons could potentially contribute towards AVNERP prolongation.[93]

The study by Kuo et al., was conducted on 92 subjects (aged 16-92 years) without AVN disease or dual AVN physiology. They have divided patients in 3 groups based on their age and showed that AVNERP had a positive correlation with increasing age, which supports the findings by Lin et al. Their results also suggest that the AVNERP remains unchanged once it reaches adulthood, however it is slightly longer in patients over 60 years of age.[92]

Another important aspect in the electrophysiology of the AVN is dual AV nodal physiology, which is of particular importance in the genesis of AVNRT. A study group from Venice, Italy has demonstrated decreased incidence of dual AV nodal physiology with ageing. In the group of patients, older than 60 years of age, dual AVN pathways was only found in 10.8% of the patients as compared to 32% of patient in the younger age

group (11-30 years). All patients in this study had ventricular prexcitation, supraventricular tachycardia and AV block excluded with previous transoesophageal electrophysiological study. It also demonstrate prolonged AH interval, Wenkebach cycle length and AVNERP with ageing. The patients included in the study were referred for investigation of syncope, suspected sinus node disease, ventricular preexcitation and palpitaton. Interestingly sinus node dysfunction was seen in 32% of the patient >60 years of age.[98]

In conclusion, these studies confirmed functional changes associated with ageing of the AVN. Whether these functional changes have structural counterparts, specifically ion channel expression, is not known.

1.12 Research Hypothesis

Ageing is definitely involved in the AVN dysfunction, however we do not have adequate evidence of role of ion channels with AVN disease. A possible avenue for research, building on what it is found in literature, is to establish if ion channel expression in the AVN in healthy young rats is remodelled during ageing. This will greatly increase our understanding of this specialized system in the heart, which could potentially help in the development of new treatment strategies for AV block.

An ageing model of the AVN and its comparison with adult AVN model is required to fill the knowledge gap existed with regards to ion channel expression. Furthermore, even though the studies have extensively looked at electrophysiological parameters with development and ageing, application of specific ion channel blockers and their effect on electrophysiological measurements with ageing is not fully known.

Tellez et al., study on ageing SN is consistent with changes in ion channel expression. It is therefore reasonable to predict that, the structural and functional changes in the AVN described above, ion channels remodelling in the AVN is likely to occur with ageing.

I hypothesize that structurally: the myocardial cells in the AVN undergo remodelling with ageing possibly secondary to fibro-fatty deposition and/or apoptosis. In terms of ion channels expression, I also believe that potential changes that can impair the AVN conduction velocity is due to decreased expression of Cx isoforms (Cx40, 43, 45), HCN (1,4), I_{Na} (Na_v 1.5), I_{CaT} (Ca_v 3.1) and I_{CaL} (Ca_v 1.3) and changes in the calcium handling proteins (RyR2, SERCA2a). Potentially, ion channel expression change that results in increase AVNERP can include changes in I_{CaL} (Ca_v 1.3), I_{KAch} ($K_{ir}3.1/K_{ir}3.4$), I_{Kr} (hERG), I_{Ks} (K_vLQT1) and I_{to} ($K_v4.3$). I expect that the above structural changes can

lead to prolonged action potential duration, increase in effective refractory periods resulting in prolonged PQ/PR interval and ultimately heart blocks.

1.13 Aims of the project

The aims of the project include:

1. To study functional characteristics of the AVJ by performing electrophysiological experiment in the young AVN in the presence of Cesium (Cs^+) (I_f blocker) and Ryanodine (RyR2 blocker);
2. To study changes in the functional characteristics of the AVN with ageing in the Cs^+ (I_f blocker) and Ryanodine (RyR2 blocker);
3. To study the morphological characteristics of the AVJ with ageing by performing histological analysis including Masson's trichome and Picrosirius red stain;
4. To characterize changes in the ion channel, gap junction, calcium handling proteins and structural protein expression with ageing by performing immunohistochemistry;
5. To understand how the structural changes could lead to the functional changes seen with ageing;
6. To study the clinical effects of AV nodal disease (predominantly 1^{st} degree AV block) in elderly patients.

Chapter 2

2. Electrophsysiology

2.1 Introduction

We have discussed in section 1.11.3 the functional changes seen in AV nodal conduction with ageing. The atrio-hisian (AH) interval, Wenekebach cycle length (WB) and AV nodal effective refractory period (AVNERP) prolong with ageing. It is not known whether these functional changes have structural counterparts, especially the changes in ion channel expression. Furthermore, the understanding of cellular mechanisms responsible for AV nodal conduction is lacking. A few studies have used ion channel blockers to study the cellular mechanisms controlling the automaticity of the AV node. Whether these same cellular mechanisms also control AV nodal conduction and whether they change with ageing is not known.

The study by Nikmaram et al., characterized the effect of inhibition of the ryanodine receptor (RyR2) and the TTX-sensitive neuronal Na^+ current (I_{Na}) on the pacemaker activity of the sinoatrial node (SN) and the atrioventricular node (AVN) in mouse. RyR2 block and inhibition of I_{Na} resulted in decreased automaticity of the AV node thus prolonging AV nodal cycle length. Ryanodine (2 μM) increased AV nodal cycle length by 70% and TTX by 53%.[99] A study by Marger et al., showed that blocking

I_{Na} and L-type Ca^{2+} current (I_{CaL}) resulted in decreased automaticity in the mouse AVN cells. Blocking I_{Na} with 0.1 μM of TTX resulted in 20% decrease in total peak I_{Na}. However block of I_{CaL} with Isradipine (L-type Ca^{2+} channel blocker) resulted in block of the action potential suggesting the important role of $\boldsymbol{I_{CaL}}$ in AVN cells.[44]

The study by Liu et al., measure the effect of I_f block in the mouse SN and AV node by Cs^+ and ZD7288. They showed ZD7288 (1 μM) increase the cycle length by 73% in the AV node and Cs^+ (0.5 mM) increase the AV nodal cycle length by 122%. The effect of these agents is more pronounced in the SN as compared to AVN.[100]

The study by Kim et al., further examined the cellular mechanisms involved in the automaticity of the AV node in dog. Isoproterenol and caffeine caused an acceleration of the AV nodal rhythm by decreasing the cycle length. Ryanodine (3 μM) increased the cycle length by 83% and ZD7288 (3 μM) by 35%. The effect of isoproterenol was suppressed by Ryanodine but not by ZD7288. This suggests a role for Ca^{2+} release from the sarcoplasmic reticulum in the automaticity of the AV node.[101]

A recent study by Verrier et al., in the anesthetised pig model of atrial fibrillation has shown the ventricular rate during atrial fibrillation can be reduced by combined administration of Ivabradine (I_f blocking agent) and Ranolazine (membrane stabiliser, which reduces peak and late I_{Na} and delayed rectifier K^+ current). The combination of these agents (i.e combined administration of 0.25 mg/kg Ivabradine with Ranolazine) increased PR ($p=0.0002$, $p=0.0007$) and AH ($p=0.047$, $p=0.002$) intervals during pacing at 130 and 180 beats/min, respectively, to a greater degree than additive effects of single agents. It also reduced ventricular rate during AF by 51.9 ± 9.7 beats/min (23%, $\rho=0.017$) and the dominant frequency of AF by 2.8±0.5 Hz (32%, $\rho=0.005$). These experiments suggest a role for I_f and I_{Na} in AV nodal conduction.[102]

The above studies explain the role of pacemaking channels in the automaticity of the AVN, identifying the RyR2 mediated Ca^{2+} release from the sarcoplasmic reticulum (with the exception of Verrier et al., study) and I_f as important mechanisms. However these studies didnot document the effect of these pacemaking channels on AV nodal conduction. Evidence about the effect of ageing on remodelling of these pacemaker channels on AV nodal conduction is also lacking.

2.2 Preparation used for electrophysiological experiments

2.2.2 Materials and Method

The dissection method and perfusion system has been used by our group before and is described by Temple.[103] I have used the same established system in my experiments.

2.2.3 Animals

Male Wistar-Hanover rats were used in this study (Charles River UK Ltd, Kent, UK). In total, 24 young rats (3 months old) and 15 old (24 months old) rats were used in the study. All animal procedures were performed in accordance with UK Animals Scientific Procedures Act 1986.

2.2.4 Solutions

For electrophysiological experiments, Tyrode's solution (NaCl 120 mM, CaCl 1.2 mM, KCl 4mM, $MgS0_4.7H_20$ 1.3 mM, $NaH_2P0_4.2H_2O$ 1.2 mM, $NaHC0_3$ 25.2 mM, glucose 5.8 mM) was prepared on the day of the experiment and bubbled with 95% O_2/5% CO_2.

2.2.5 Dissection of the AV nodal preparation for electrophysiological experiments

Experiments were carried out on AV nodal preparations from young and old rats (see Figure 2.1). 14 young rats and 6 old rats were used in electrophysiology experiments. Animals were given 1000 I.U. of heparin 10-15 min before the procedure to prevent coagulation during dissection. Humane euthanasia was performed on these animals via carbon dioxide inhalation followed by swift dislocation of the neck. The chest was rapidly opened, the heart removed, placed and dissected in oxygenated ice-cold Tyrode's solution at 4°C. The lung, trachea and excessive connective tissue were removed. The lower part of the ventricles and the superior portion of the left atrium were then removed. The lateral wall of the left ventricle was then cut across until the left atrium and the whole preparation was then opened up. The RV free wall was then dissected into the right atrium just to the right of the ridge in the right atrial appendage. I then dissected up to the superior vena cava. The right atrium was then opened and pinned out. Finally the RVOT was opened to expose the AVN. The whole preparation was pinned on black silicon and transferred to a tray with the Tyrode's solution at room temperature and then transferred on to a tissue bath for the electrophysiological recordings. The preparation was then allowed to recover after the trauma of dissection for a period of 30 min. The tissue bath

was perfused with oxygenated Tyrode's solution at a rate of 20-25 ml/min; the temperature was maintained at 36-37°C and pH was 7.35-7.45.

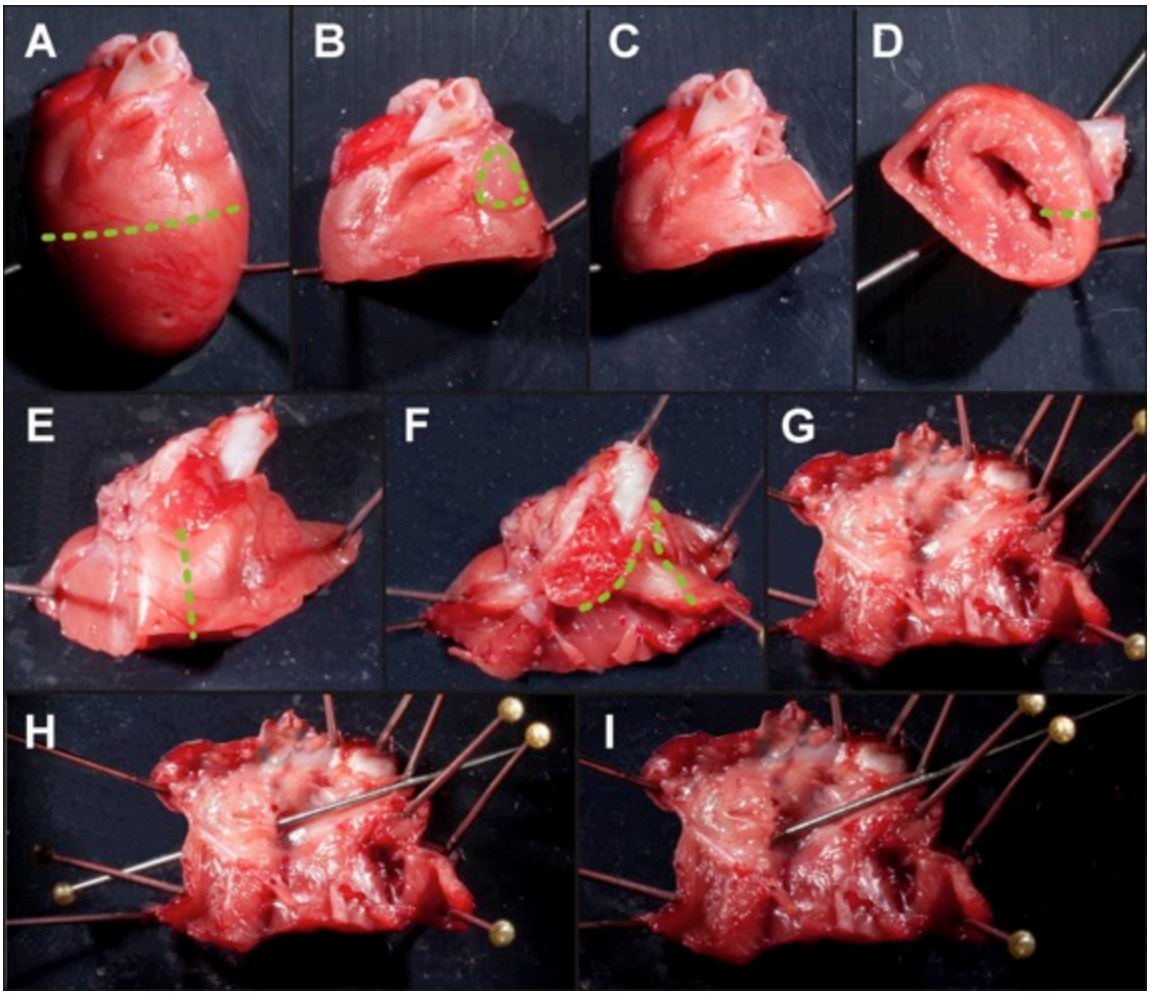

Figure 2.1: Description of dissection for the AV node preparation. The lines of dissection are shown with dashed green lines (the dissection for all experiments was performed in oxygenated Tyrode's solution but this dissection was performed a formalin fixed heart without perfusing solution for clarity of the images). A-G are described in the text. H) Demonstration of the inferior vena cava. The blunt end of the dissecting pin was pushed through the inferior vena cava from the endocardial surface with no resistance demonstrating the wide lumen of the inferior vena cava, which was severed during excision of the heart from the thorax. I) Demonstration of the coronary sinus. The blunt end of the dissecting pin was advanced into the ostium of the coronary sinus but could not pass further without resistance due to the narrow lumen of the coronary sinus, which was not severed during removal of the heart from the thorax. Modified from Temple 2014.[103]

2.2.6 Electrical recordings

After dissection the tissue preparation was allowed to recover for 30 min before functional measurements. I measured the spontaneous sinus node (SN) cycle length (SCL), paced AH interval, WB cycle length, AVERP and AVFRP using bipolar electrodes. Extracellular signals were measured with 4 modified bipolar electrodes; they were made using 0.25 mm silver wire coated with 0.04 mm Teflon (Advent Research

Materials, Oxford). The bipolar electrodes were positioned at the site of earliest activation (SN), the atrial septum, at the His bundle and between the coronary sinus and the tricuspid valve annulus.

The bipolar electrodes were connected via a headstage (NL100AK, Digitimer, UK) to an amplifier (NL104A, Digitimer, UK) with a gain of 5000 and filtered between 50–500 Hz (NL125/6, Digitimer, UK). The amplified and filtered signal was then converted to a digital signal using an analogue to digital converter (Micro 1401, Cambridge Electronic Design, UK).

Extracellular potentials were recorded and analysed using Spike2 software (Cambridge Electronic Design, UK). The preparation was then stimulated at the right atrium with a bipolar pacing electrode connected to a DS2A Isolated Constant Voltage Stimulator (Digitimer, UK). The voltage stimulator was connected to the computer via the data acquisition unit, which allowed pacing protocols programmed in Spike2 to be executed.

The spontaneous SN cycle length was measured. Stimulus threshold was determined using a fixed S1-S1 protocol with an interval of 180 ms. A square pulse of 2ms duration was gradually increased from 0 to 99 V. The minimum voltage required to capture the atrium was determined. This minimum voltage was then doubled and the output was kept constant for all subsequent pacing protocols. Wenckebach cycle length was determined using a S1-S1 protocol. The atrium was paced with a fixed cycle length of 200 ms for 30 s. If 1:1 atrial to ventricular conduction occurred the S1-S1 protocol was repeated with a 10 ms reduction in coupling interval until Wenckebach conduction was seen. A further set of 30 s S1-S1 pacing protocols was undertaken starting at 11 ms longer than the cycle length at which Wenckebach conduction had occurred. If 1:1 atrial to ventricular conduction occurred, the protocol was repeated with a 1 ms reduction in the cycle length of the S1-S1 protocol. The cycle length at which 1:1 atrial to ventricular conduction failed and Wenckebach conduction occurred using 1 ms reductions in cycle length was recorded as the Wenckebach cycle length. AV node effective refractory period (AVNERP) was determined using an S1-S2 protocol. There was an initial drive train of S1 beats (S1-S1, 180 ms) for 8 beats. The initial S1-S2 coupling interval was 170 ms. If the extrastimuli captured the atrium and was conducted to the ventricle, the protocol was repeated with a 10 ms reduction in the S1-S2 coupling interval. This was repeated until AV conduction was lost. A new set of protocols was run again with the S1-S2 coupling interval starting at 10 ms greater than the S1-S2 coupling interval at which AV node conduction had failed. If this extrastimulus was conducted successfully from the atrium to

the ventricle, the protocol was repeated with the S1-S2 coupling interval reduced by 1 ms until AV conduction was lost. The greatest S1-S2 coupling interval that did not conduct after a 1 ms decrement was defined as the AVNERP (figure 2.2).

Atrial effective refractory period (AERP) was determined using the same S1-S2 protocol as described above for AVERP. For AERP the protocol was continued until atrial capture was lost.

Atrioventricular node functional refractory period (AVFRP) was determined using the protocol described for AVNERP. The RR interval between the QRS of the last of the paced beats in the drive train and the QRS elicited by the S2 stimulus, i.e. the R1-R2 interval, was measured and plotted as an AV node conduction curve (Figure 2.2). The lowest R-R interval represents the fastest conduction across the AV node and was defined as the AVFRP.

Cesium (Cs^+) (2 mM diluted in oxygenated Tyrode's solution) was infused for a period of 20 min to reach steady-state concentration before repeating the measurements. Cs^+ is then washed off with fresh oxygenated Tyrode's solution until the all the recordings reach the pre-Cs^+ level. Ryanodine (2 μM diluted in oxygenated Tyrode's solution) then infused for 20 min before performing the final measurements.

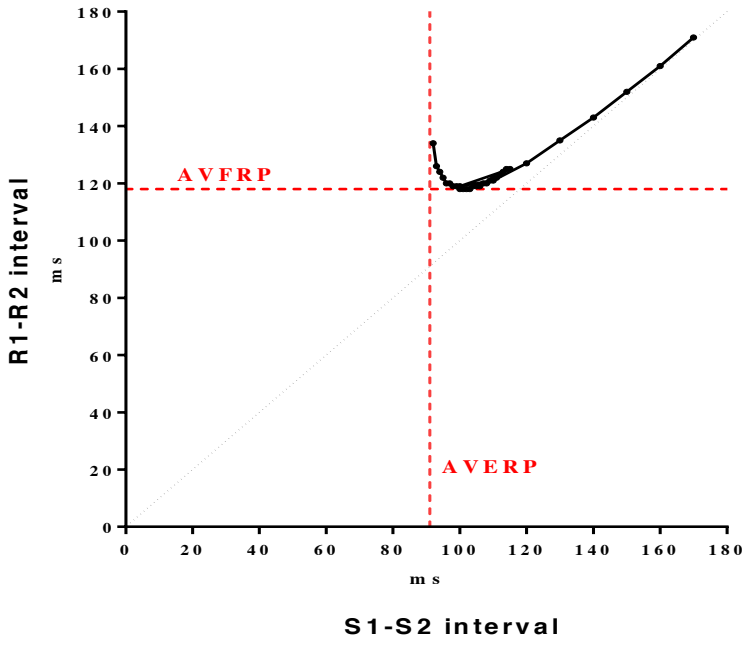

Figure 2.2: AV nodal conduction curve. The R1 and R2 interval i.e output of the AV node is plotted against the S1-S2 interval (the interval between two paced atrial beats) i.e the AV nodal input. The dotted line showed the projected path the output takes if AV nodal conduction doesnot cause delay with shorter coupling intervals. The AVERP is defined as the highest S1-S2 interval at which AV conduction fails and is read from the X-axis. The AVFRP is defined as the shortest R1-R1 interval that the AV node conducts and is read from the y-axis. Adapted from Temple.[103]

2.2.7 Drugs

CsCl (Sigma Aldrich, Poole, UK) was used at a 2 mM concentration to block I_f. Ryanodine (Sigma Aldrich, Poole, UK) was used at a 2 μM concentration was used to block RyR channels (block Ca^{2+} release from the sarcoplasmic reticulum).

2.2.8 Perfusion system

The perfusion system incorporated a reservoir chamber, heat exchangers and a perfusion bath which were 'jacketed' in order to allow warmed water to be pumped through them via a waterbath. The temperature of the waterbath was adjusted to ensure a temperature of 36.5 ± 0.5°C of the Tyrode's solution within the perfusion system. Fluid was recirculated in the system using a Gilson Minipuls 3 pump (Gilson, USA) with a four way adaptor to control both inflow and outflow. The final design of the perfusion system incorporated two parallel inflow circuits with equal flow rates each supplying 25 ml/min giving a total perfusion flow of 50 ml/min. One inflow was directed at the AV node and the other supplied the whole chamber. Two outflow circuits were also used to match the inflow circuits. They were arranged so that one outflow circuit was positioned at the bottom of the chamber and the other was elevated to the desired perfusion fluid level. The efficiency of the pump was altered by adjusting the pressure applied to the perfusion tubing so that the return circuits were able to pump greater volumes than the perfusion circuits. In this way a 'feedback' loop was created so that the chamber was filled to a desired level but would not exceed the desired level. With the final perfusion system AV node conduction parameters were stable over several hours (Figure 2.3).

2.2.9 Mapping of earliest activation

Mapping of earliest activation was performed using two bipolar electrodes, which were positioned using micromanipulators. The first bipolar electrode was positioned on the septal aspect of the RA. Once a good atrial signal was obtained this electrode was no longer moved and was used as a 'fiduciary point' for subsequent mapping.

The second electrode was moved across the surface of the RA. At each point the timing of atrial activation relative to the fiduciary point was recorded until the roving electrode recorded the earliest activity compared with that of the fiduciary point. A photograph was taken and the position of the roving electrode was used to mark the position of the SN (Figure 2.4).

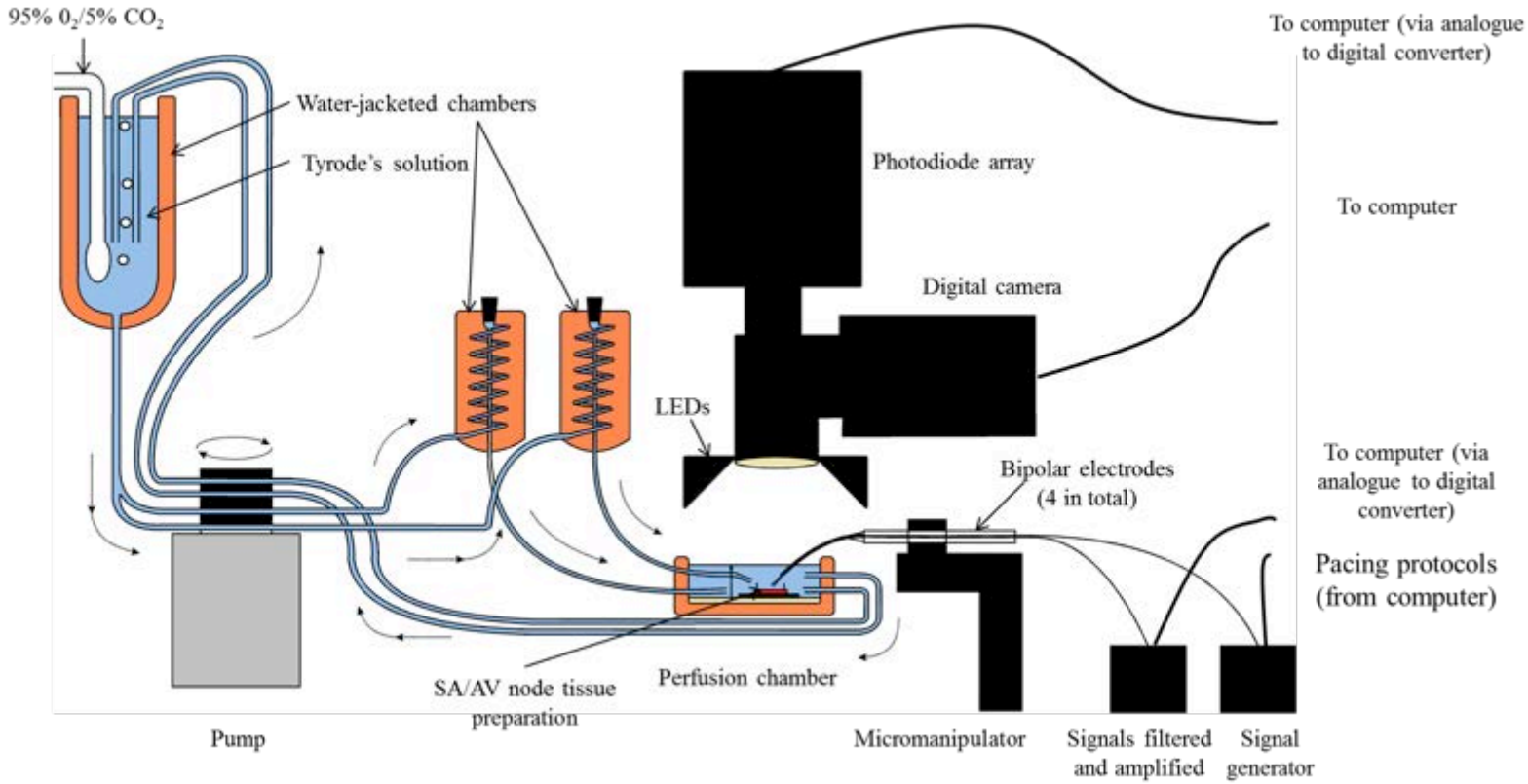

Figure 2.3: Diagram of the experimental setup for the isolated SA/AV node preparation. The perfusion circuit used two parallel inflows into the perfusion chamber to achieve a high flow rate and to direct the perfusion directly at the AVN as well as into the chamber. The outflow used two parallel tubes with the upper of the two tubes used to control the depth of fluid in the perfusion chamber. Experiments were performed using bipolar electrodes for pacing and recording signals. Adapted from Temple.[103]

2.2.10 Mapping of the His bundle

A bipolar electrode was positioned along the tricuspid valve annulus and moved using the micromanipulator until both an atrial and a second discrete sharp signal was recorded, i.e. an atrial and a His signal. Another electrode was positioned at the point of the earliest activation determined as described above. A third electrode was positioned on the septal aspect of the atrium between the fossa ovalis and the tricuspid valve annulus in a position near the 'fast pathway'. A fourth electrode was positioned between the coronary sinus and the tricuspid valve annulus in a location near the 'slow pathway' (Figure 2.4).

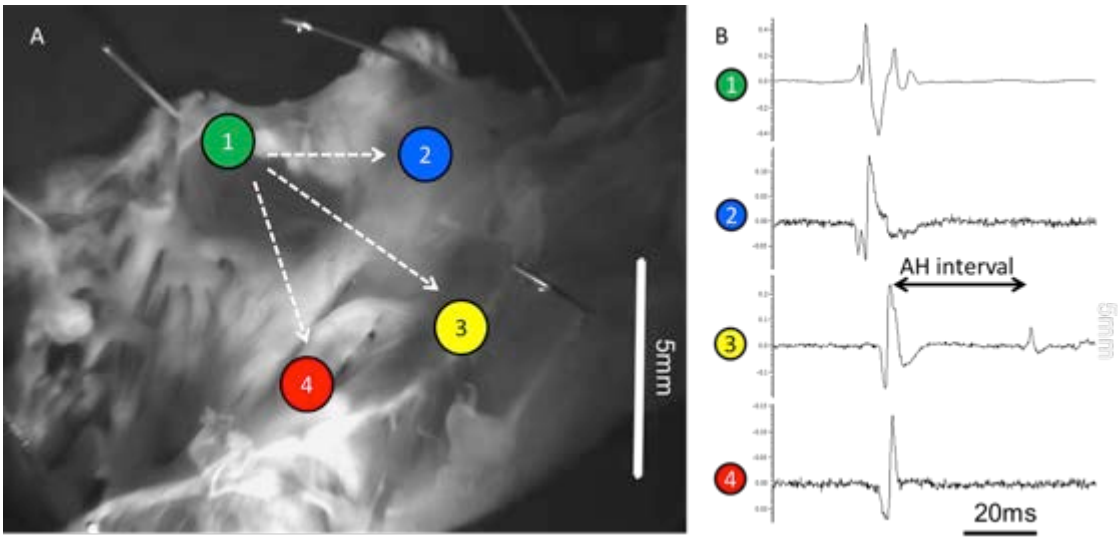

Figure 2.4: Bipolar recording from the AV node preparation. A) Photograph of preparation. Once the His bundle had been identified the other three electrodes were positioned. Electrode 1 was positioned at the site of earliest activation (the SN). Electrode 2 was positioned at the atrial septum, electrode 3 was at the His electrode and electrode 4 was positioned between the coronary sinus and the tricuspid valve annulus. B) Bipolar recordings from the 4 electrodes marked in A. Earliest activation was at electrode 1 and latest at electrode 4. This represents rapid atrial activation spreading from the SA node (marked with white dashed arrows). At the His signal (electrode 3) there was a discrete pause which was followed by a second smaller sharp deflection. This second deflection is the His signal. The time between the atrial and His signal is the AH interval. Adapted from Temple.[103]

2.3 Results

2.3.1 Electrophysiological measurements: comparison of young and old hearts

The comparison between young and old hearts showed that sinus node cycle length, AH interval, Wenkebach cycle length, AVNERP and AVFRP prolong with ageing. Table 2.1 and Figures 2.5-2.8 show the electrophysiological changes seen with ageing. Figure 2.9 shows the AV conduction curves of all young and old hearts under baseline conditions.

Table 2.1: Changes in the electrophysiological measurements with ageing

AVNERP, Atrioventricular nodal effective refractory period; AVFRP, Atrioventricular functional refractory period.

	Sinus node cycle length (ms)	AH interval (ms)	Wenkebach cycle length (ms)	AVNERP (ms)	AVFRP (ms)
Young Heart	259.10± 12.33	41.33 ± 3.60	148.70 ± 6.32	103.20 ± 7.16	141.10±8.87
Old Heart	370.50 ± 23.10	63.60 ± 5.144	216.80 ± 31.44	168.30 ± 6.811	184.80±8.2
p value	**0.0002**	**0.0049**	**0.0038**	**0.0002**	**0.01**
95% CI	58.19-164.7	7.65 – 36.88	25.72-110.4	39.03 - 91.03	10.7 -75.01

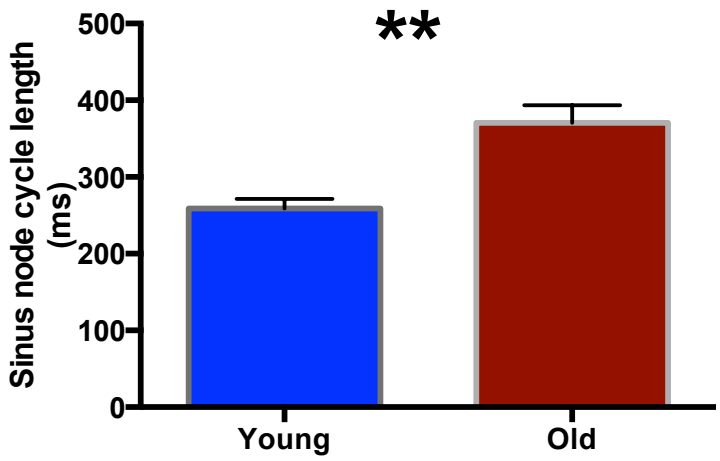

Figure 2.5: Sinus node cycle length prolongation with ageing. Mean±SEM shown. ** p < 0.0005

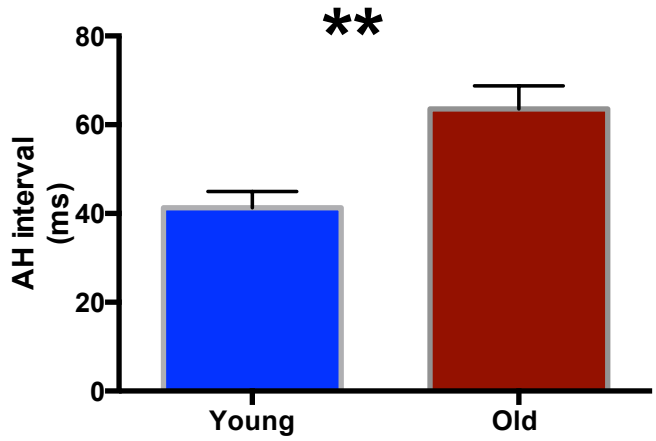

Figure 2.6: AH interval prolongation with ageing. Mean±SEM shown. ** p < 0.005

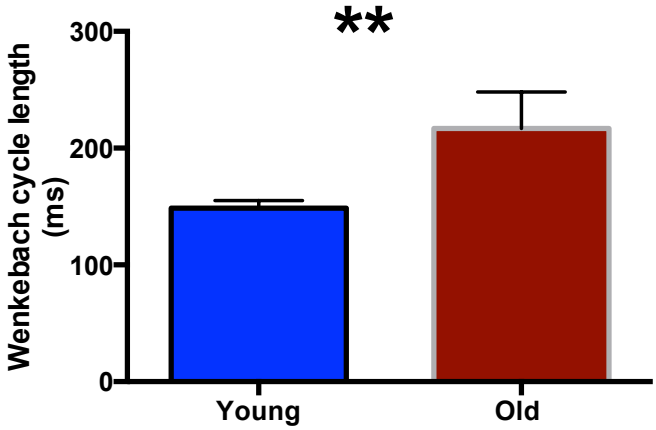

Figure 2.7: Wenckebach cycle length prolongation with ageing. Mean±SEM shown. ** p < 0.005

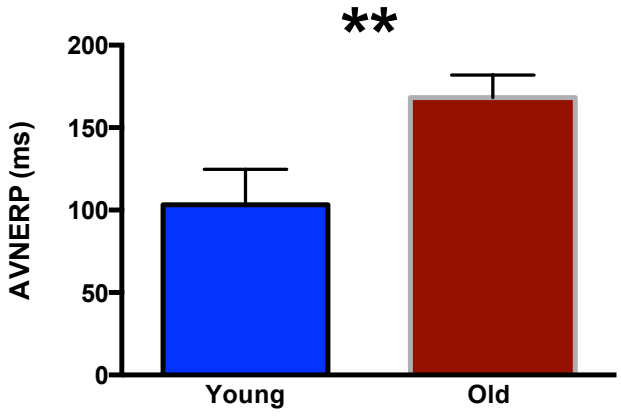

Figure 2.8: AV nodal effective refractory period prolongation with ageing. Mean±SEM shown. ** p < 0.0005

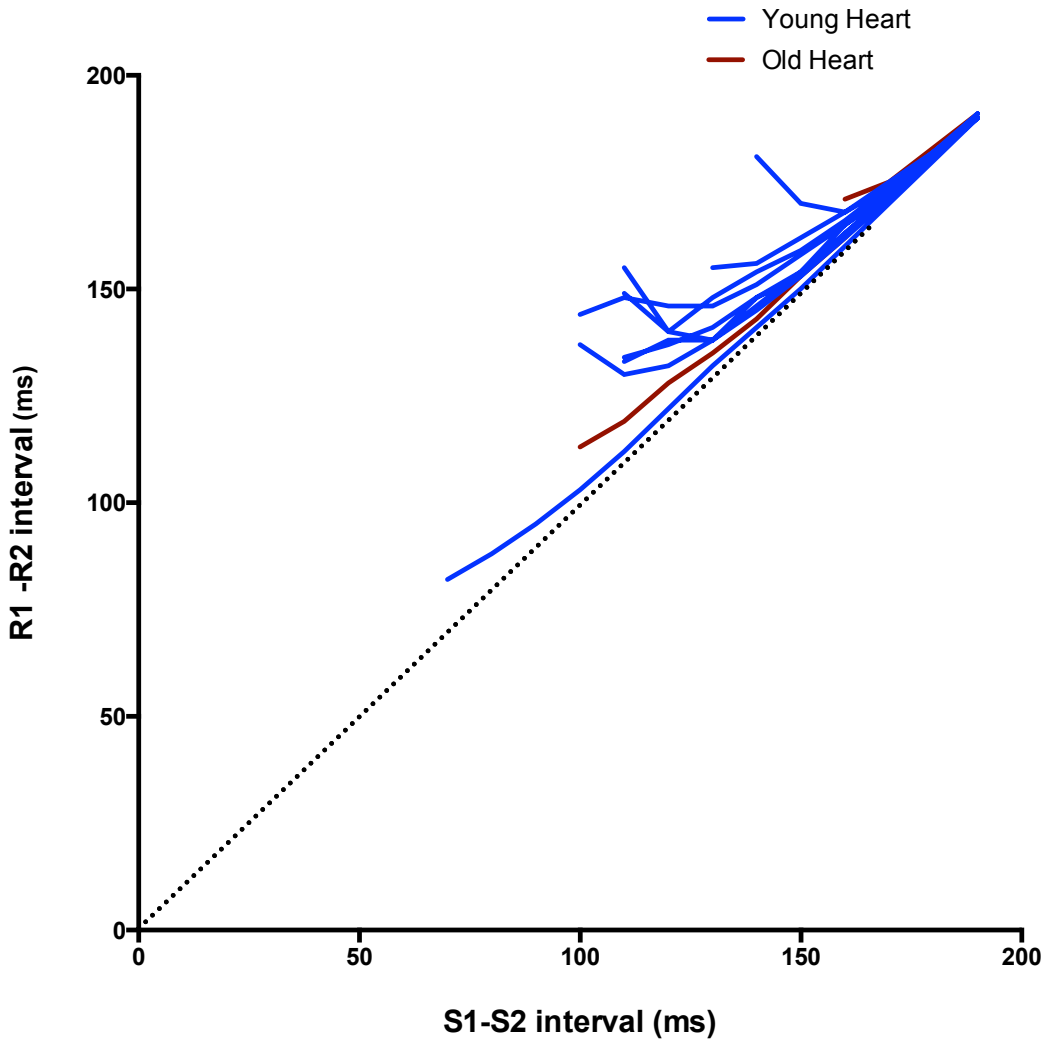

Figure 2.9: Comparison of AV conduction curves in young and old hearts. On X-axis the R1-R2 interval (AV nodal output in response to S1-S2) is plotted against S1-S2 interval (the interval between two paced atrial beats. The dotted line showed the projected AV nodal output (R1-R2 interval) if there was no decremental conduction through the AVN i.e. R1-R2 interval = S1-S2 interval. The AV conduction curves show the classical hockey stick appearance and no discontinuity suggesting dual AV nodal physiology is not evident.

2.3.2 Electrophysiological measurements in young hearts: application of Cs^+ and ryanodine

The application of Cs^+ and ryanodine in young hearts has yielded interesting results. I have shown that blocking I_f with Cs^+ and blocking RyR2 with Ryanodine results in a prolongation of the sinus node cycle length, AH interval and Wenkebach cycle length. AVNERP significantly prolonged with Cs^+, but the prolongation with Ryanodine didnot reach statistical significance. The measurement of AVNERP was only possible in three young hearts as Ryanodine prolonged the Wenckebach cycle length quite substantially. Tables 2.2-2.5 and Figures 2.10-2.13 shows electrophysiological changes in young hearts after application of Cs^+ and ryanodine. In addition, Figure 2.14

shows the AV conduction curves after application of Cs^+ with changes in the AVFRP in young hearts.

Table 2.2: Changes in sinus node cycle length after application of Cs^+ and Ryanodine in young hearts

Young hearts	Baseline	Cs^+ (2 mM)	Ryanodine (2 µM)	p value (95% Confidence interval, CI)
Sinus node cycle length (ms)	259.1± 12.33	342.8±21.96		0.0001 (61.116-135.0)
Sinus node cycle length (ms)	241.1± 9.63		369.8±25.4	0.0002 (65.38-141.1)

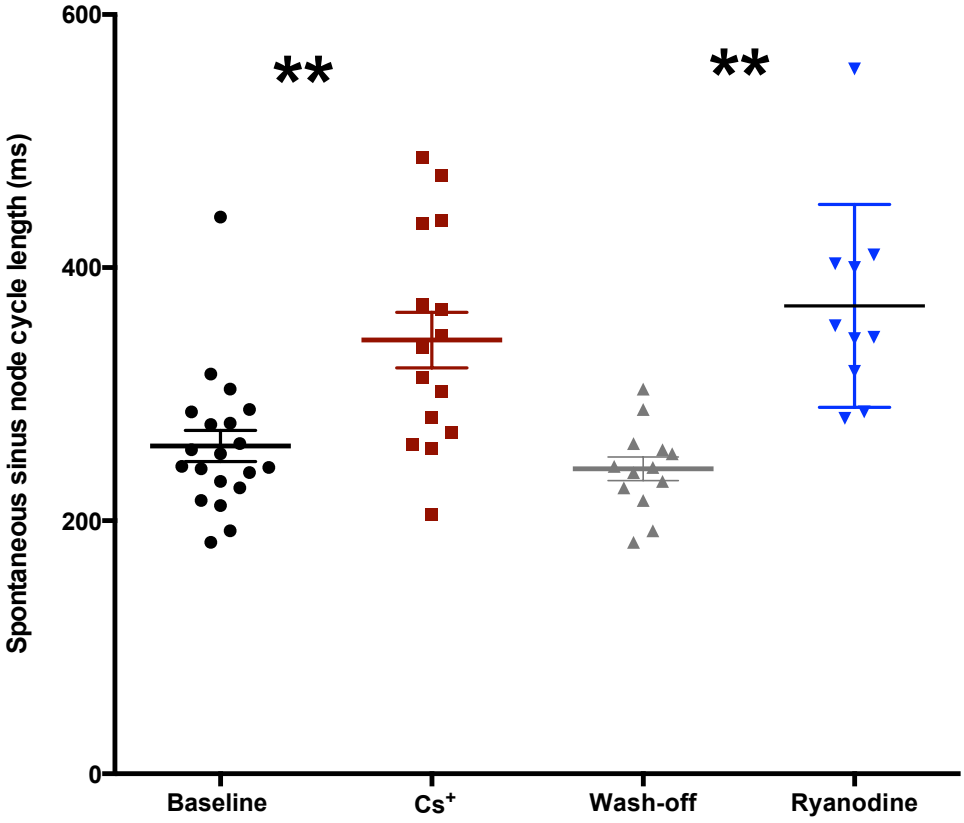

Figure 2.10: Changes in the sinus node cycle length in young hearts after application of Cs^+ and Ryanodine. Mean±SEM shown. The figure shows results at baseline, after Cs^+ application, after Cs^+ wash-off and after ryanodine application. ** $p < 0.0005$

Table 2.3: Changes in AH interval after application of Cs^+ and Ryanodine in young hearts.

Young hearts	Baseline	Cesium (2 mM)	Ryanodine (2 µM)	ρ value (95% Confidence interval, CI)
AH interval (ms)	43.1± 3.62	51.67±5.144		0.0076 (2.38-12.28)
AH interval (ms)	47.00± 6.08		59.00±7.72	0.01 (5.35-28.93)

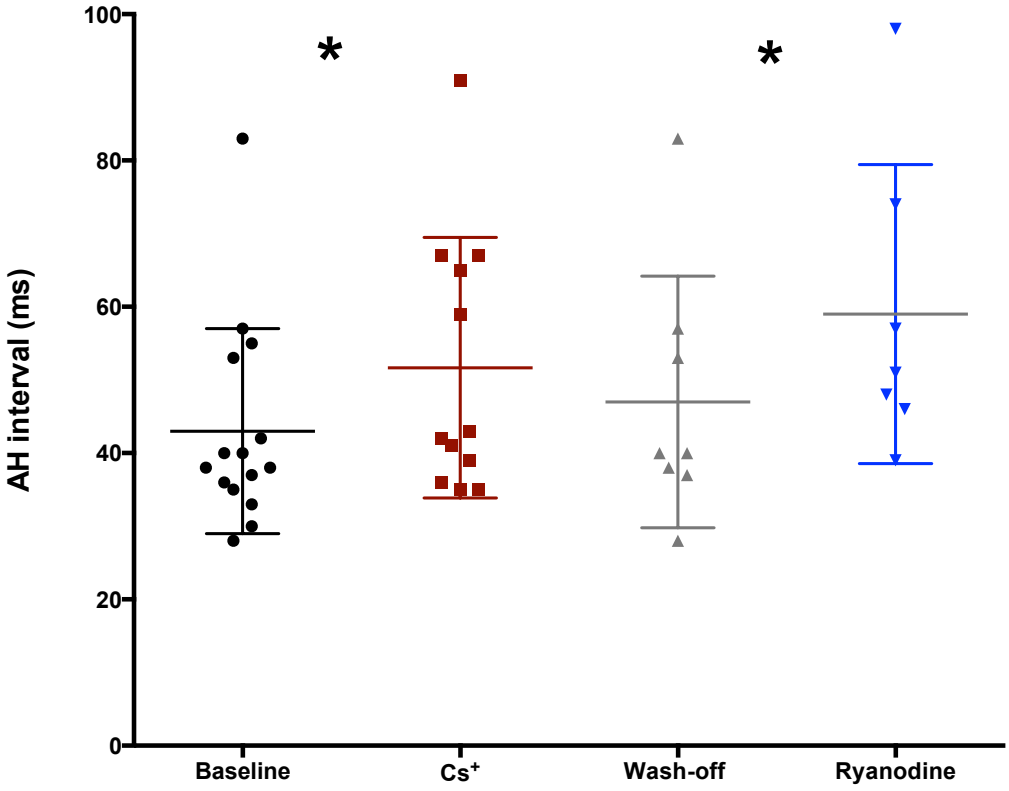

Figure 2.11: Changes in atrio-Hisian (AH) interval in young hearts after application of Cs^+ and ryanodine. Mean±SEM shown. The figure shows results at baseline, after Cs^+ application, after Cs^+ wash-off and after ryanodine application. * $\rho < 0.05$

Table 2.4: Changes in Wenkebach cycle length after application of Cs^+ and Ryanodine in young hearts.

Young hearts	Baseline	Cesium (2 mM)	Ryanodine (2 µM)	p value (95% Confidence interval, CI)
Wenkebach cycle length (ms)	165.9±10.58	179.3±16.03		0.0254 (3.22-40.93)
Wenkebach cycle length (ms)	161.5±11.69		205.1±22.71	0.017 (13.86-105.4)

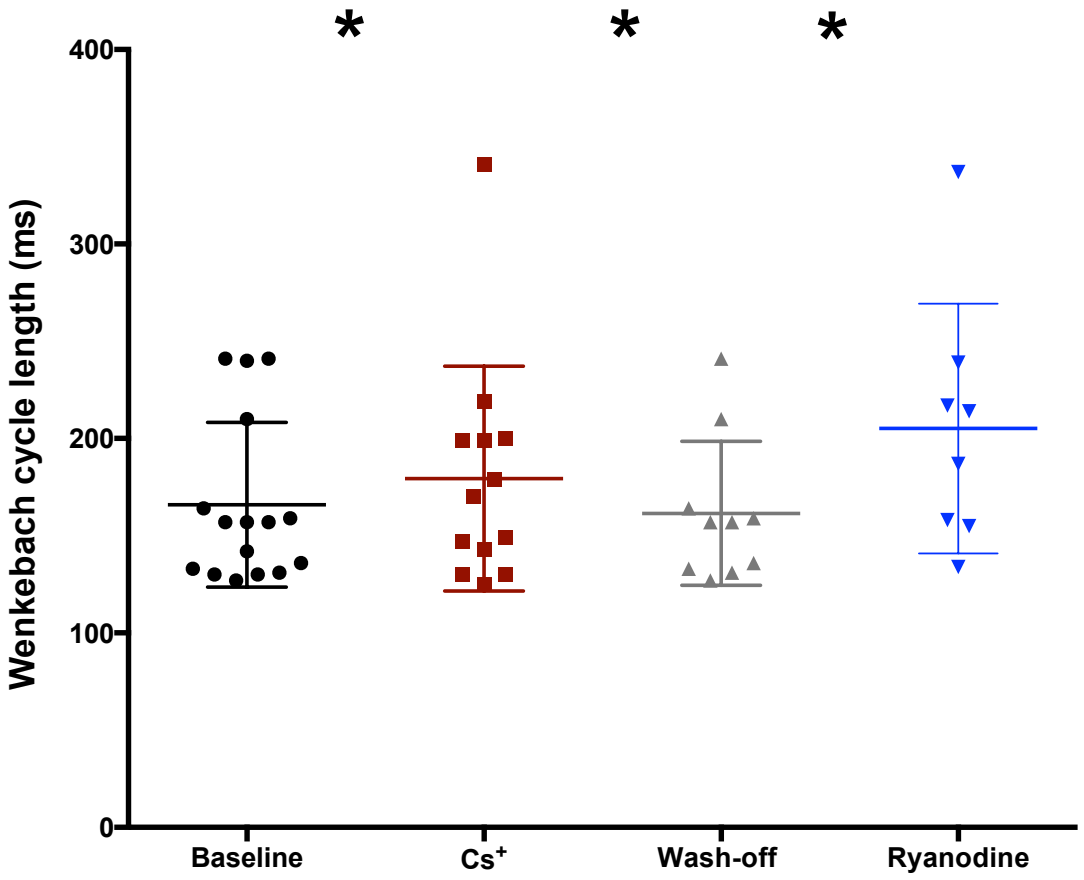

Figure 2.12: Changes in the Wenkebach cycle length in young hearts after application of Cs^+ and ryanodine. Mean±SEM shown. The figure shows results at baseline, after Cs^+ application, after Cs^+ wash-off and after Ryanodine application. * $p < 0.05$

Table 2.5: Changes in AVNERP after application of ion channel blockers Cs^+ and Ryanodine in young hearts.

Young hearts	Baseline	Cesium (2 mM)	Ryanodine (2 µM)	p value (95% Confidence interval, CI)
AVNERP (ms)	103.3 ± 6.40	124.9 ± 10.68		0.0214 (4.018 – 39.18)
AVNERP (ms)	95.33 ± 5.925		127.3 ± 15.07	0.07 (-7.76 to 71.45)

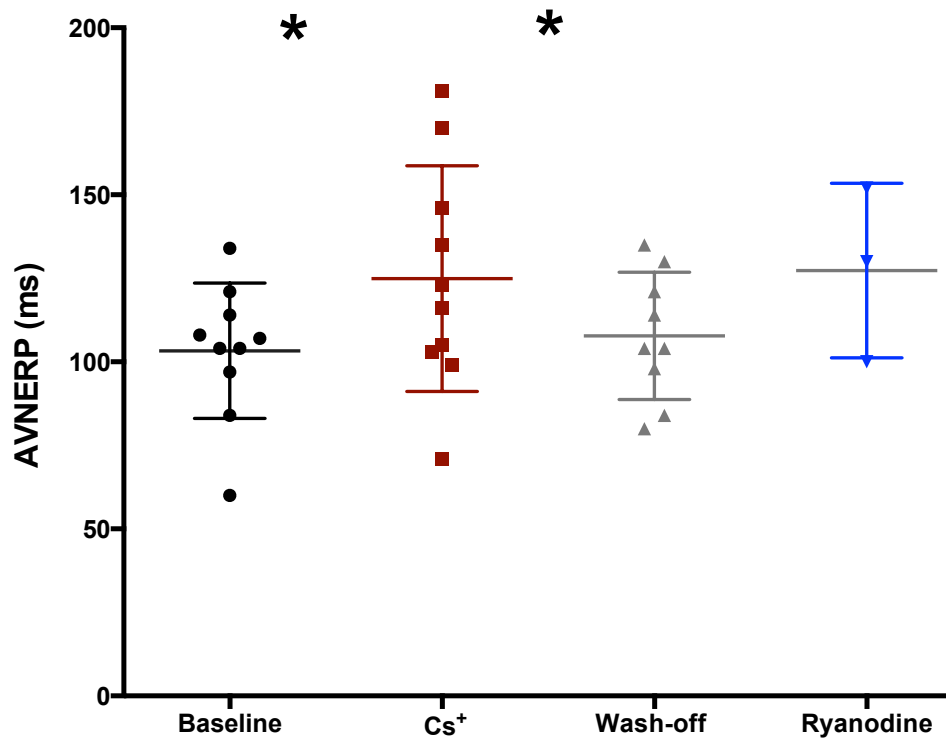

Figure 2.13: Changes in the AVNERP in young hearts after application of Cs^+ and Ryanodine. Mean±SEM shown. The figure shows results at baseline, after Cs^+ application, after Cs^+ wash-off and after ryanodine application. * $p < 0.05$

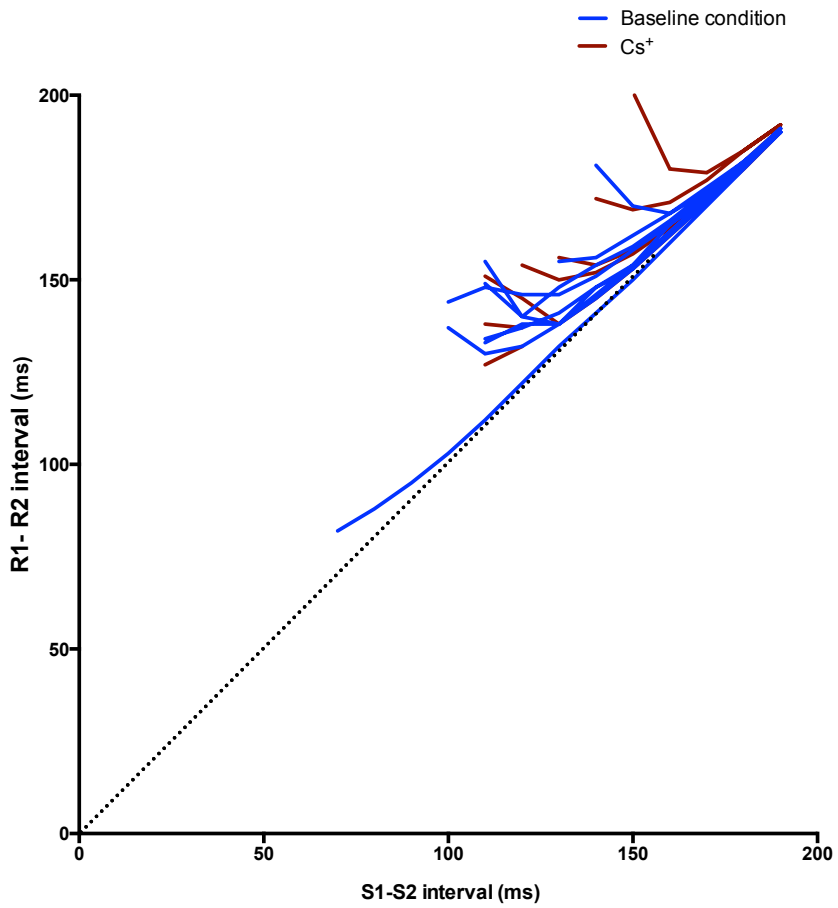

Figure 2.14: AV conduction curves in all young hearts after application of Cs^+. On X-axis the R1-R2 interval (AV nodal output in response to S1-S2) is plotted against S1-S2 interval (the interval between two paced atrial beats. The dotted line showed the projected AV nodal output (R1-R2 interval) if there was no decremental conduction through the AVN i.e. R1-R2 interval = S1-S2 interval. The AV conduction curves show the classical hockey stick appearance and no discontinuity suggesting dual AV nodal physiology is not evident.

2.3.3 Electrophysiological measurements in old hearts: Application of cesium and ryanodine.

The application of Cs^+ and Ryanodine in old hearts has provided interesting results. The application of Cs^+ and Ryanodine did prolong the sinus node cycle length. However, Cs^+ effects on the AH interval, Wenkebach cycle length and AVNERP was minimal in old hearts. Ryanodine though did prolong the AH interval and Wenkebach cycle length. The AVNERP measurement was not possible with ryanodine as the S1 drive train of 200 ms resulted in the Wenkebach phenomenon in all old hearts after application of Ryanodine. Tables 2.6-2.9 and Figures 2.15-2.19 show the electrophysiological changes in the old hearts. Figure 2.20 and 2.25 showed the Mean and SEM of young and old hearts electrophsyiolgoical measurements with and without drugs. Figures 2.20 to 2.25 show the electrophsysiological measuresments in young and old hearts with and without drugs.

Table 2.6: Changes in sinus node cycle length after application of Cs^+ and ryanodine in old hearts.

Old Heart	Baseline	Cesium (2 mM)	Ryanodine (2 µM)	p value (95% Confidence interval, CI)
Sinus node cycle length (ms)	374.0 ± 27.96	522.0 ± 70.17		0.038 (61.11-135.0)
Sinus node cycle length (ms)	368.4 ± 25.81		507.8 ± 75.52	0.048 (1.31- 275.9)

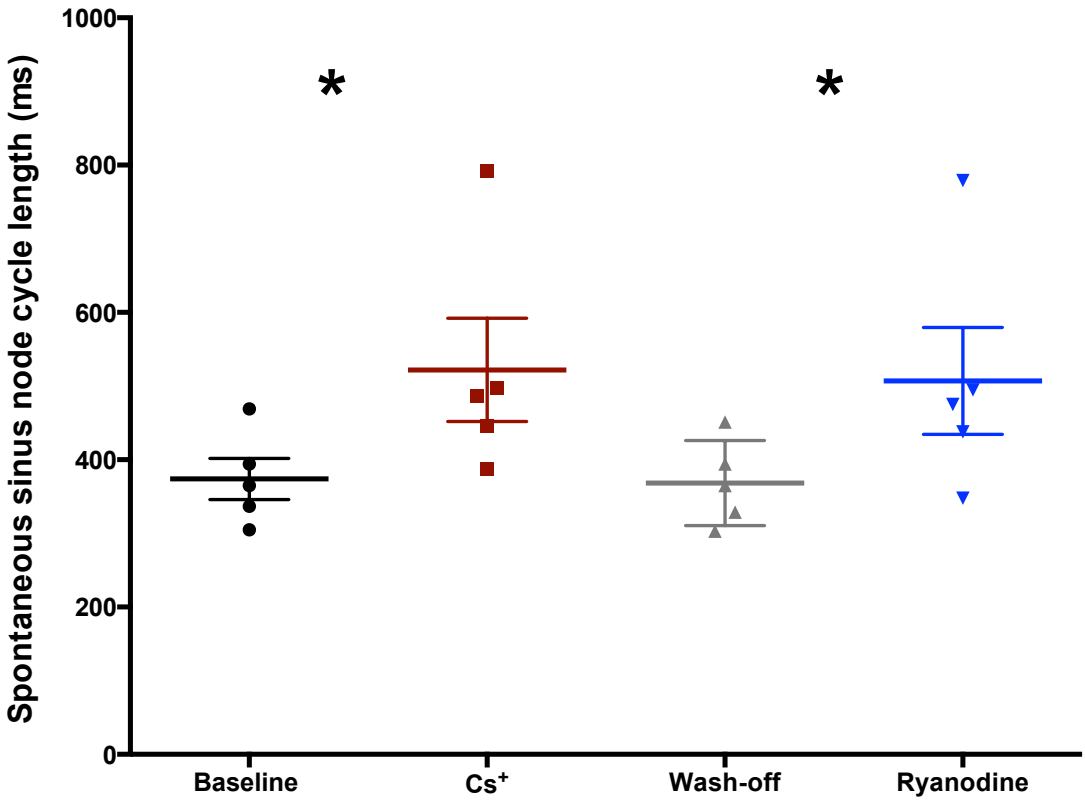

Figure 2.15: Changes in the sinus node cycle length in old hearts after application of Cs^+ and ryanodine. Mean±SEM shown. The figure shows results at baseline, after Cs^+ application, after Cs^+ wash-off and after ryanodine application. * $p < 0.05$

Table 2.7: Changes in AH interval after application of Cs^+ and ryanodine in old hearts.

Old hearts	Baseline	Cesium (2 mM)	Ryanodine (2 µM)	p value (95% Confidence interval , CI)
AH interval (ms)	63.60 ± 5.14	61.40 ± 4.844		0.48 (-10.77 – 5.77)
AH interval (ms)	58.20 ± 3.30		81.00 ± 6.61	0.01 (8.87-36.72)

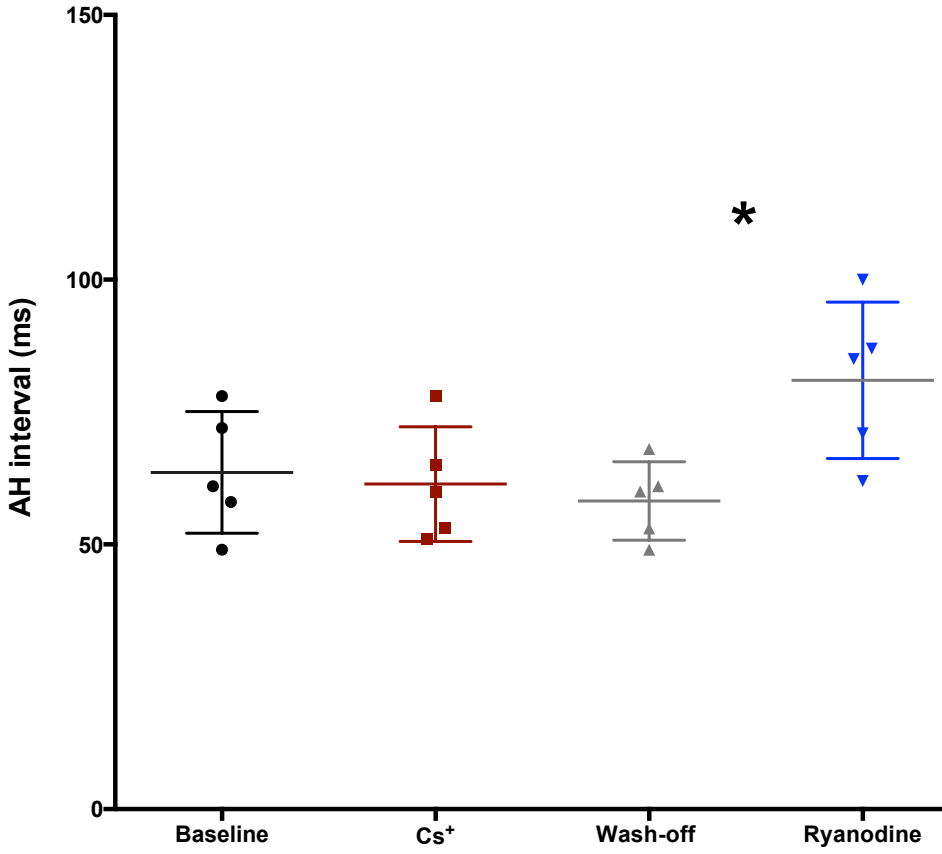

Figure 2.16: Changes in the AH interval in old hearts after application of Cs^+ and ryanodine. Mean±SEM shown. The figure shows results at baseline, after Cs^+ application, after Cs^+ wash-off and after ryanodine application. * $\rho < 0.05$

Table 2.8: Changes in Wenkebach cycle length after application of Cs^+ and ryanodine in old hearts.

Old Heart	Baseline	Cesium (2 mM)	Ryanodine (2 µM)	p value (95% Confidence interval, CI)
Wenkebach cycle length (ms)	216.8 ± 31.44	220.0 ± 30.28		0.63 (16.21 -22.71)
Wenkebach cycle length (ms)	220.08 ± 32.24		276.8 ± 38.72	< 0.02 (11.77-100.2)

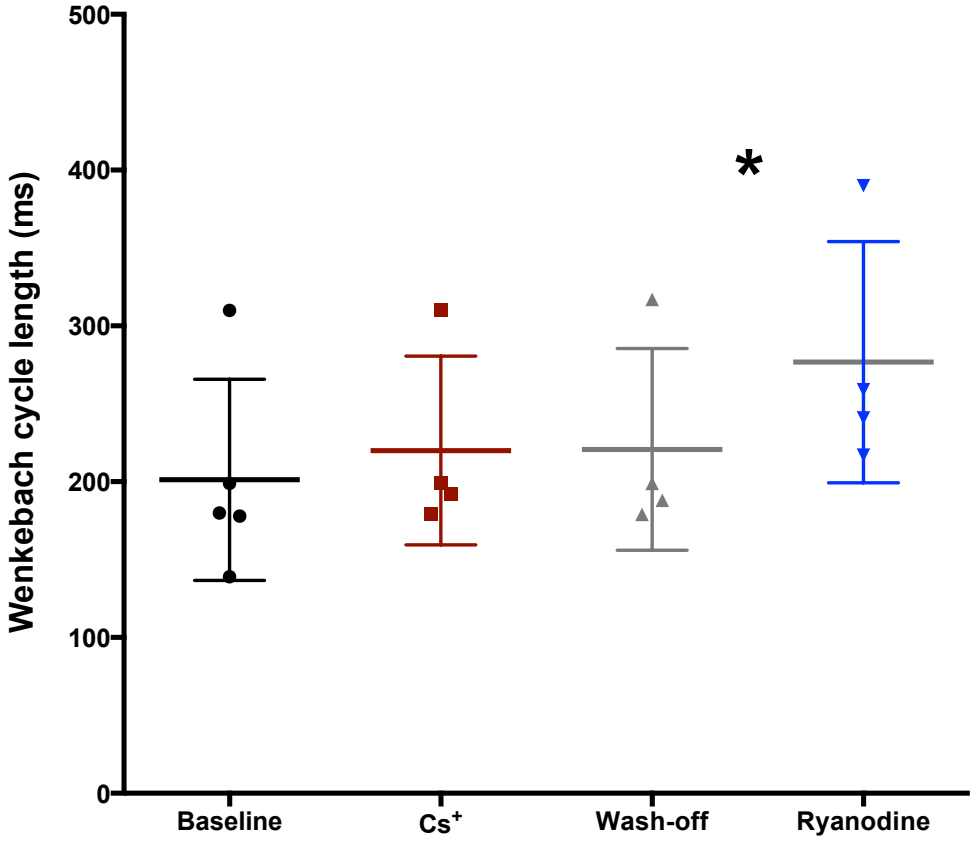

Figure 2.17: Changes in the Wenkebach cycle length in old hearts after application of Cs^+ and ryanodine. Mean±SEM shown. The Figure shows results at baseline, after Cs^+ application, after Cs^+ wash-off and after ryanodine application. * $p < 0.05$

Table 2.9: Changes in AVNERP after application of Cs^+ in old hearts.

Old hearts	Baseline	Cesium (2 mM)	ρ value (95% Confidence interval, CI)
AVNERP (ms)	168.3 ± 6.811	159.8 ± 6.35	0.16 (-23.05 – 6.005)

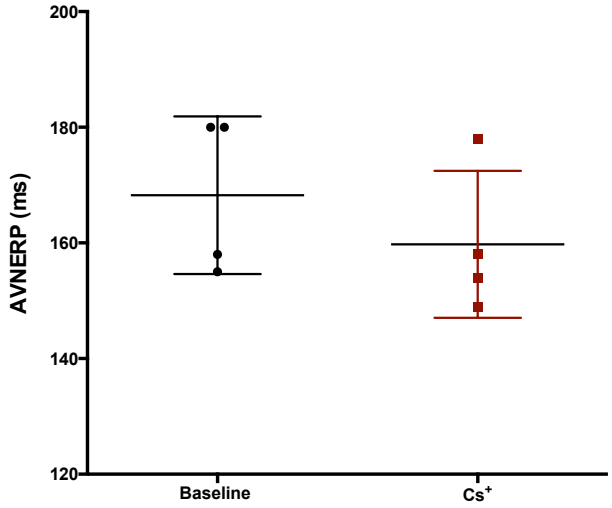

Figure 2.18: Changes in the AVNERP in old hearts after application of Cs^+. The Figure showed results at baseline and after Cs^+ application.

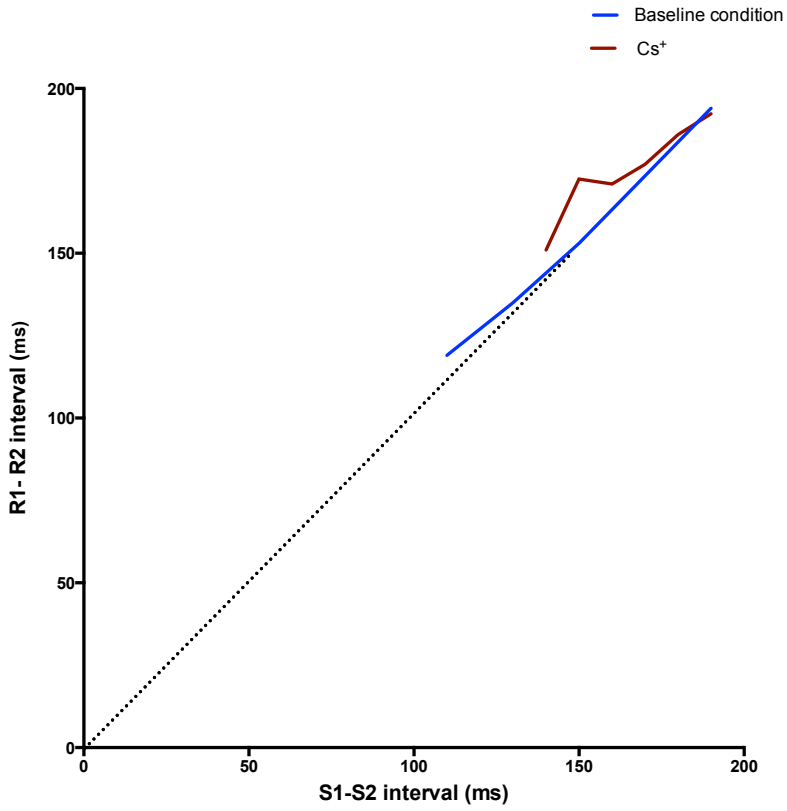

Figure 2.19: AV conduction curves in old hearts after application of cesium. On X-axis the R1-R2 interval (AV nodal output in response to S1-S2) is plotted against S1-S2 interval (the interval between two paced atrial beats. The dotted line showed the projected AV nodal output (R1-R2 interval) if there was no decremental conduction through the AVN i.e. R1-R2 interval = S1-S2 interval. The AV conduction curves show the classical hockey stick appearance and no discontinuity suggesting dual AV nodal physiology is not evident.

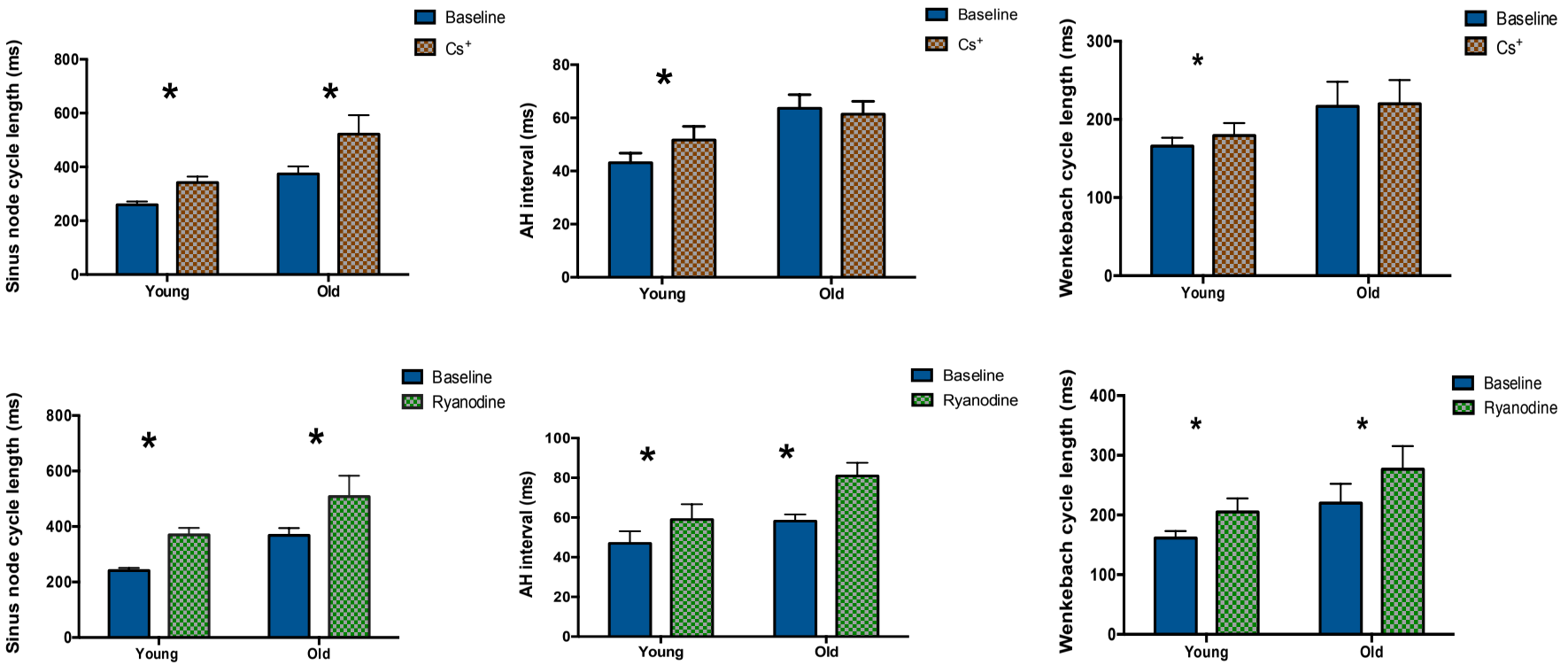

Figure 2.20: Electrophysiological measurement in young and old hearts with and without drugs. Mean±SEM are shown. * $p < 0.05$

2.4 Discussion

Ageing has been associated with impaired AV nodal function. Multiple studies have described these changes with ageing including prolonged PR, AH, HV interval, increased Wenkebach cycle length and AVNERP. My study demonstrated prolonged sinus node cycle length with ageing. I have also shown that in aged rats AH interval, Wenkebach cycle length, AVNERP and AVNFRP prolonged. My study findings are in agreement with previous studies performed on rats.[86,90,96] The changes in the functional experiment correlates with my immunohistochemistry experiments, which have shown changes in the ion channel expression, calcium handling proteins and gap junction protein with ageing. These results have been discussed in detail in chapter 4.

My study has yielded important results concerning the cellular mechanisms of AV nodal conduction and its remodelling with ageing. I have been able to demonstrate the effect of I_f i.e. membrane clock and calcium clock (Ca^{2+} release from the SR) on AV nodal conduction. I have also shown changes in the effect of these "clocks" with ageing.

It is important here that I describe the calcium clock and membrane clock mechanisms responsible for the phase 4 of action potential in nodal cells (both sinus node and AVN cells) in greater detail because that will help the reader understand the phase 4 deplorization in pacemaker cells. The effects of I_f blockage and the ryanodine effects on RyR2 will then be easier to understand.

The calcium clock mechanism underline the RyR2 mediated spontaneous Ca^{2+} release or Ca^{2+} sparks from SR. These local oscillatory Ca^{2+} releases in phase 4 activates the forward mode of Na^{+}-Ca^{2+} exchanger generating inward membrane current $I_{Na\text{-}Ca}$. This causes the late deplorization driving the resting membrane potential towards -40mV, which results in activation of L-type calcium channels thus generating the action potential. The L-type calcium channel mediates further calcium induced calcium release from SR depleting SR Ca^{2+} content which then synchronizes SR to reuptake Ca^{2+} via SERCA. This timely refilling ensures that the RyR2 channels are ready for the next cycle of oscillatory calcium release. On the other hand, the theory behind I_f current or membrane clock is the activation of HCN4 channels during the late phase of the action potential. They are fully activated at a membrane potential close of -100mV resulting in the inward current (primarily Na^{+}) that changes the membrane potential to -40mV that results in activation of L-type calcium channels, which in turn generate the action potential. Of note, that in both these mechanism the final pathway is the activation of L-type calcium channels ($Ca_v1.3$).[104]

The role of the membrane clock and Ca^{2+} clock in determining the automaticity of the SN is well established.[104] However, the evidence for a role in AV nodal conduction is lacking and whether these are involved in the changes seen in the AV nodal conduction with ageing is also not known. Previous studies have analysed the automaticity of the AV node. A study by our group in 2008 by Liu et al., measured the effect of I_f block in the mouse SN and AVN by using Cs^+ (I_f blocker) and ZD7288 (I_f blocker).[100] They have shown that both of these reduce the automaticity of the SN and AVN by increasing cycle length. The effect of these agents was more pronounced in the SN as compared to the AVN. The study by Kim et al., in 2010 also showed that ZD7288 slows the AVJ rate by 35%.[101] A recent study by Verrier et al., on anesthetised pig model of atrial fibrillation has shown the ventricular rate during atrial fibrillation can be reduced by combined administration of Ivabradine (I_f blocking agent) and Ranolazine (membrane stabilizer, reduce peak and late I_{Na} and delayed rectifier K^+ current). The combination of these agents results in increased PR and AH intervals during pacing to a greater degree than the additive effects of single agents. It also reduced ventricular rate during AF by 23%.[102] More recently, a study has shown that blocking I_f with Ivabradine can reduce ventricular rate during atrial fibrillation in anesthesised pigs, and increase AH interval in sinus rhythm in rate dependent manner.[105] The study by Mesrica et al., showed that suppressing I_f conductance by expressing non functional HCN4 subunit results in AV block.[106] These experiments suggest the role of I_f on AV nodal conduction. My study have confirmed that blocking the I_f results in prolongation of AH interval, WB cycle length, AVNERP and AVFRP in young rats.

The effect of ryanodine on RyR2 channels is complex. It has been shown that ryanodine act as a functional blocker of RyR2 channels. Essentially it means that ryanodine suppresses the oscillatory calcium release from the sarcoplasmic reticulum. It has been described that ryanodine effects on cardiac SR reduces the Ca^{2+} handling ability of SR by forming a long lasting subconductance state of the Ca^{2+} release channel. This results in depletion of the SR calcium content whereby it is possible that this subconductance state increase cytosolic basal calcium concentration. On the other hand cardiac myocyte can maintain the intracellular Ca^{2+} content by Na^+-Ca^{2+} exchanger. So the increase cytosolic Ca^{2+} can be effectively extruded from the cell by the Na^+-Ca^{2+} exchanger.[107]

Calcium handling proteins especially RyR2 affecting AV nodal conduction has not been described before. The studies have analysed the automaticity of the AVN with

Ryanodine use. A study by our group in 2008 by Nikmaram et al., showed that inhibition of RyR2 in mice results in decreased automaticity of the AVN by increasing AV nodal cycle length.[99] Another study by Kim et al., in dogs, showed that Ryanodine reduced the AVJ automaticity by 83%.[101] My study confirms that blocking Ca^{2+} release from RyR receptors using Ryanodine results in impaired AV nodal conduction, prolonging the AH interval and WB cycle length.

The RyR block in old rats also results in prolongation of AH interval and WB cycle length. The AH interval is prolonged by 39% in the old as compared with 25% in young hearts, which suggest increased sensitivity to Ryanodine with ageing. The effect of I_f and Ryanodine with ageing is interesting as we have shown that with ageing the effect of the membrane clock on AV nodal conduction decreases and the sensitivity to Ryanodine increases. This could explain the dysfunction or prolongation in AV nodal conduction seen with ageing.

I propose that these cellular mechanisms i.e. membrane clock (I_f) and calcium clock, act in conjunction with each other to maintain the background excitability or depolarization reserve in the young AVN allowing it to conduct efficiently. I_f blockage or blocking oscillatory release of Ca^{2+} from the SR by Ryanodine could result in impairment of conduction by increasing the slope of phase 4 depolarization. This increasing slope results in decreased activity of forward mode of Na^{+}-Ca^{2+} exchanger. This in turn results reduce $I_{Na\text{-}Ca}$ thus taking longer for the cells to reach the membrane potential necessary to activate the L-type calcium channel. This effect on the action potential affects the action potential propagation as well, as the successive cells need more time to reach the excitation threshold to generate the action potential, which ultimately increases the conduction time across the AVN. These can further deteriorate in disease states resulting in increased incidence of AV block (2^{nd} and 3^{rd} degree AV block) seen with ageing.[108]

A word of caution is necessary here because of the complexity of ryanodine action on the RyR2 channels and the basal cytosolic calcium concentration. The ryanodine blockage can increase basal cytosolic calcium levels although its effect is to inhibit oscillatory Ca^{2+} release. However another mechanism that can affect AV nodal conduction if the basal cytosolic calcium concentration is higher, is the gap junction conductance. It has been described that intracellular calcium concentration can decrease the gap junctional conductance which can ultimately results in impairement in AV nodal conduction.[130]

Chapter 3

3. Histology

3.1 Introduction

Structural changes in ageing AVN has been previously described in the studies.[80-85] I have explained in section 1.11.1 that the location and morphology of the AVN changes with ageing. The AVN in adult heart is located more on the slope of the intraventricular septum. The length of the INE increase and becomes equal to CN length in adolescent heart.[80] The ageing has also been associated with fibrofatty infiltration of the AVN with an increase in the collagen content.[83-85]

3.2 Methodology

3.2.1 Species used and sample size

Male Wistar-Hanover rats were used in this study. Young rats (aged 3 months, n=8) and old rats (aged 24 months, n=9) were commercially purchased and humanely killed in accordance with United Kingdom Animals Scientific Procedures Act 1986. Schedule 1 killing was performed on these animals via carbondioxide inhalation followed by swift dislocation of neck. The chest was opened, and heart removed and placed in ice cold Tyrode's solution.

3.2.2 Dissection and freezing of whole heart

The dissection of heart was performed while bathing the heart in Tyrode's solution. The excess connective tissue, parts of the trachea and lungs were removed from the heart. Tyrode's solution was then infused through the aorta and pulmonary artery to remove excess blood from the heart. The heart was then submerged in isopentane cooled to -50^0C, with the help of liquid nitrogen, which immediately froze the tissue. Hearts were then stored at -80^0C until further use.

3.2.3 Cryosection

The frozen whole heart was mounted on a metal plate (cryostat chuck) with the help of OCT (the embedding medium) and warmed until -17^0C. The heart was oriented to take sections from the posterior to anterior direction. The 20-µm sections were cut and placed in pairs on superfrost plus slide (positively charged surface for better tissue adhesion). Approximately 24 sections were taken every 700 µm. The slides were then stored at -80^0C until further use.

Appendix 1 showed the detailed summary of the cryosection performed on each heart. It also showed selection of slides after Masson's trichome stain for detailed light microscopy, picrosirius red stain, and immunohistochemistry.

3.2.4 Histological stains

Histological stains include Masson's Trichome stain (MT) and picrosirius red (PR) stain. These two staining protocols have been performed on sections from each level to identify the different regions of the AV junctional area. Only after MT staining of serial sections, the different regions of the AVJ can be recognised histologically. The staining protocols were not only helpful for identifying appropriate slides for immunohistochemical analysis but they were also used to study the morphology of different regions of the AVJ. Picrosirius red stain was used for collagen signal estimation for the assessment of fibrosis.

3.2.4.1 Solutions

1. 0.01M Phosphate Buffer saline (PBS); containing in mM: Na_2HPO_4, 77; $Na_2H_2PO_4$, 23; pH 7.4 (Sigma, UK).

2. Putchler's Picrosirus red soloution; 0.5gm of Sirius red F3B (Sigma, UK) dissolved in 500mls of saturated aqueous picric acid (Sigma, UK).

3. Acetic acid water: 5 milliters (mls) of glacial acetic acid (Fischer Scientific, UK) was dissolved in 1 liter of distilled water.

3.2.4.2 Fixative's

1. Bouin's Fluid; 75 ml of saturated (1.2 % W/V) aqueous picric acid, 25ml of formalin (40% W/V) formaldehyde, and 5 ml of glacial acetic acid (Sigma).
2. 10% neutral buffered Formalin (Sigma).

3.2.4.3 Solvents

Ethanol, Histoclear and xylene (BDH).

3.2.4.4 Mounting medium

DPX (BDH).

3.2.4.5 Masson's trichome (MT) staining protocol

The MT stain was performed on serial sections to identify different structures of the AVJ. Figure 3.1 summarizes the MT staining protocol. With this technique under the light microscope the nuclei are stained dark blue to black, the connective tissue is royal blue and cardiac myocytes are pink. I have been able to differentiate various regions of the AVJ with this technique when examined with light microscopy. Three different magnification protocols (8X, 10X, 63X) were used to correctly identify these regions. The regions include inferior nodal extension (INE), compact node (CN), proximal penetrating bundle (PPB), and distal penetrating bundle (DPB). With the use of immunohistochemistry and confocal microscopy these regions have been further investigated. Appendix 1 lists the slides of the regions investigated.

3.2.4.6 Picrosirius red (PR) staining protocol

The PR stain was performed on adjacent MT sections. The detail of the selected slides on which the PR stains was performed has been listed in Appendix 1. Figure 3.2 showed the PR staining protocol. With this technique, under the bright field microscope, the muscle and cytoplasm are expected to be yellow and the collagen red. Under the polarised microscope the large collagen fibers are red, whereas the thin collagen fibers are green.

3.2.4.7 Principles of Picrosirius red staining and polarized light

Collagen staining with PR stain and the use of polarized microscopy has been first described by Puchtler et al.,[109] in 1973 and then further improved by Junqueira et al., [108] in 1979. PR staining is based on the principle that Sirius red (being an acid dye) stains collagen by interacting with its basic groups. The dye molecule via its sulphonic acid groups attaches to collagen fibres in a parallel fashion (long axis). This theory forms the basis of bisference seen and is used with the polarised microcscopy. Polarised microscopy involved use of a "polariser" which blocks the transmitted light when

oriented at 90^0 angle to the tissues. This effect then illuminates the bisference (green and red) against a dark background.

The combination of picrosirius red and polarised light microscopy also uses the molecular organisation of collagen. The collagen molecule is birefringent because of its anisotropic molecular organisation and it appears brighter with birefringence enhanced when viewed with polarized light, which is also anisotropic. Anisotropy essentially means directionally dependent and the polariser allows the light to be transmitted in only one direction blocking all other thus allowing the collagen molecule which is also anisotropic to be illuminated. [111]

3.2.4.8 Statistical analysis

SPSS version 19.0 and Prism 6 for Mac has been used for data entry and statistical analysis. Independent t-test and one-way ANOVA was used to compare means and compute p value, p value of 0.05 or less is considered as statistically significant.

3.2.4.9 Collagen signal estimation

Volocity software was used to measure collagen signal intensity in arbitrary units on images (20 X magnification) across different components of the AVJ.

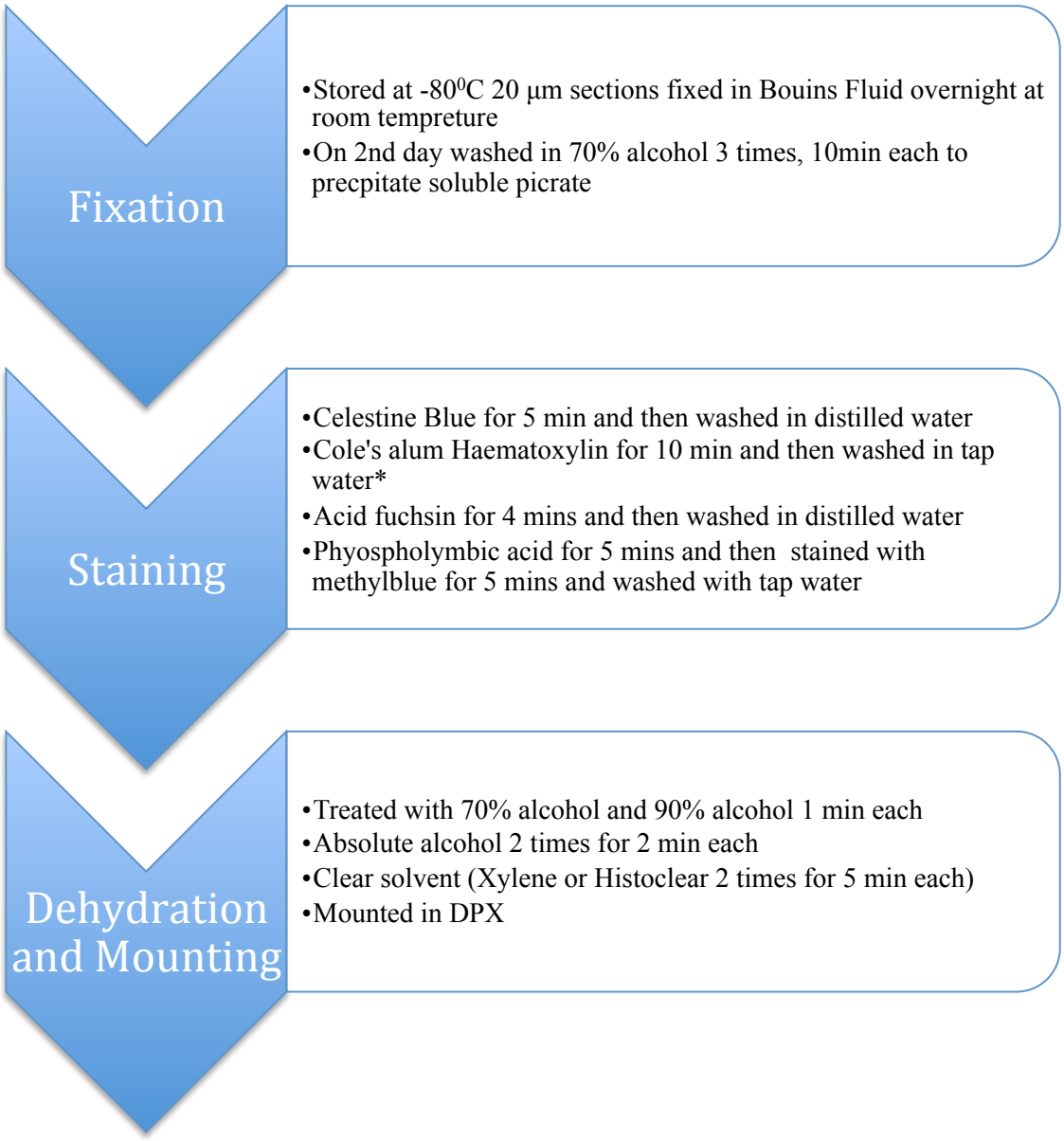

Figure 3.1: Masson Trichome staining protocol.[112]

*After staining with Celestine blue and Cole's alum haematoxylin the nuclei were checked with light microscope if they were too lightly stained then the Celestine blue step was repeated but if they were too dark they were placed in a differentiator for 5 seconds and rewashed in tap water and rechecked again.

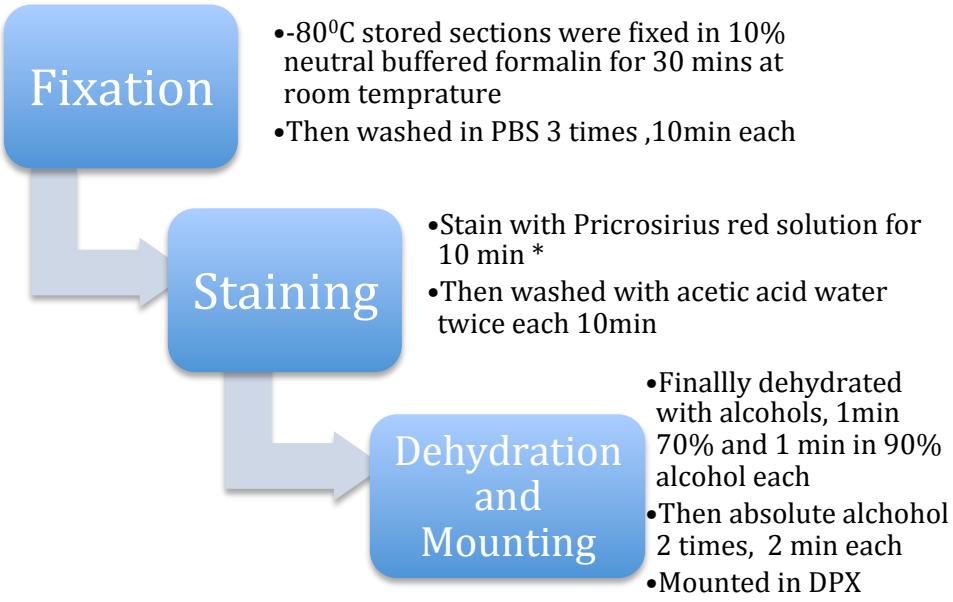

Figure 3.2: Picrosirius red protocol
*10 minutes staining with PR solution is only suitable for brightfield microscopy. If polarized microscope is used then the 1 hour staining with PR solution in necessary.

3.3. Results

3.3.1 Identification of the AVN

The AVN has been differentiated from the atrial (AM) and ventricular muscle (VM) by its characteristic position in the triangle of Koch. With MT stain, the staining pattern of the AVN is also different from atrial and ventricular muscle. The AVN stained lighter and separated from VM (interventricular septum) by a layer of connective tissue (Figure 3.8). The AVN showed high density of nuclei. The cells were arranged in an interweaving and irregular manner, whereas cells of atrial and ventricular muscle contained lower density of nuclei, cells were larger and regularly arranged (Figure 3.9). The differentiation between the CN (compact node) and the INE (inferior nodal extension) is more difficult just on the basis of MT stain, however it was primarily performed based on the location of these components and cellular orientation. The INE is located posteriorly whereas the CN is located closer to the penetrating bundle. The CN is the nodal tissue to be seen just before the central fibrous body if the approach is from posterior to anterior, which is the approach I used in cryosectionning. Cellular orientation is also different in the INE as compared to the CN. Cells are more parallel to each other

in the INE as compared to the CN, where no regular structural pattern is seen. Figure 3.6 and Figure 3.7 illustrates the cellular orientation in the young INE and CN respectively.

3.3.2 Identification of the penetrating bundle

The penetrating bundle is clearly seen when nodal tissue penetrates the central fibrous body. It is characteristically engulfed by the central fibrous body and surrounded by the connective tissue. The penetrating bundle can be divided into two distinct zones, the proximal penetrating bundle when it penetrates the central fibrous body and the distal penetrating bundle or His bundle when the penetrating bundle is located inferior to the central fibrous body with connective tissue layer only seen at the superior side of the bundle. The cells of the penetrating bundle appears to be arranged more regularly than the AVN cells but in comparison with the AM and VM still contain high density of nuclei. The AM and VM has lower density of nuclei and cells are more regular in appearance than the cells of PB. These structures are shown in Figure 3.8-3.9.

3.3.3 Comparison of the three-dimensions of AVN in young and old rats heart

The young rats are smaller in size and of lower weight as compared to older animals and the heart size are also smaller and have lower weight in young 3 month old rats as compared to old 24 month rats as shown in Figure 3.3. I have measured the three dimensions of the AVJ structures in both young and old rat heart. Appendix 2 showed all the measurements performed, Table 3.1 showed the statistical analysis and Figure 3.4 showed the graphical representation of the statistical analysis. I have performed these analysis on eight hearts (four from young and four from old rats) in which the boundaries of the components of the AVJ are clearly defined.

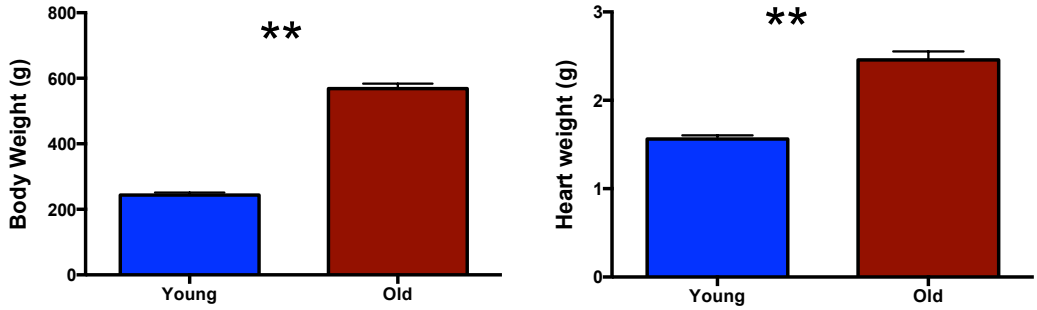

Figure 3.3: Body and Heart weight of young and old rat. Mean±SEM are shown. ** ρ <0.001

Not all components of the AVJ can be accurately measured, as the boundaries of the INE were less clearly defined in MT stained sections especially in the older animals, thus not included in the analysis. However, the boundaries of the CN and the PB can be

easily traced in the MT stain. I have found that the anterior-posterior length of the CN, the PPB and the DPB/His bundle are approximately of equal size in young and old rat's heart. This finding is quite unexpected as the younger animals have lower weight and heart size. I expected the antero-posterior length to be increased in the old rats. The diameter across horizontal axis was increased with ageing in the CN, however the comparison between the old and the young CN didn't reach statistical significance. Similarly, the height of the CN across the vertical axis is higher in the CN then the young CN but again didn't reach statistical significance (Table 3.1, Figure 3.4). The difference was observed in the height of the PPB and the DPB/His bundle across vertical axis, higher in old rat hearts that reaches statistical significance on comparison. On the other hand, the width of the PPB and DPB across horizontal axis in the old rats heart is slightly increased but did not reach statistical significance (Table 3.1, Figure 3.4).

I can conclude from the above data that with ageing the anteroposterior length of the CN, PPB and DPB/His bundle does not change. On the other hand, the height of the PPB and DPB increased with age. Although differences were observed across horizontal axis of the CN, PPB and DPB, statistical significance is not reached. Figures 3.7, 3.8 and 3.9 show the images taken at low magnification to illustrate the height and width of the CN, PPB and DPB/His bundle respectively.

Table 3.1: Comparison between young and old rat hearts. Difference in compact node (CN), proximal penetrating bundle (PPB), distal penetrating bundle or His (DPB/His) three-dimensional size (at low, 10X magnification), number of nuclei (at high, 63X magnification) (Statistically significant results are shown in red with p value <0.05 or <0.01).

	Length (antero-posterior axis) µm	Width (horizontal axis) µm	Height (Vertical axis) µm	Number of nuclei seen per high power field
Young CN (Mean± SEM)	555±62	558±56	198±42 ρ <0.05	182±14 ρ <0.01
OldCN (Mean± SEM)	545 ± 59	599±48	456 ±131 ρ <0.05	110.25±16 ρ <0.01
Young PPB (Mean±SEM)	320 ± 16	443±37	338±49 ρ <0.05	209±10 ρ <0.01
Old PPB (Mean ±SEM)	340±25	451± 28	663±116 ρ <0.05	141±6 ρ <0.01
Young His (Mean±SEM)	890±19	453±68	304±13 ρ <0.05	191±12 ρ <0.01
Old His (Mean±SEM)	870±58	403±18	600±66 ρ <0.05	129±3 ρ <0.01

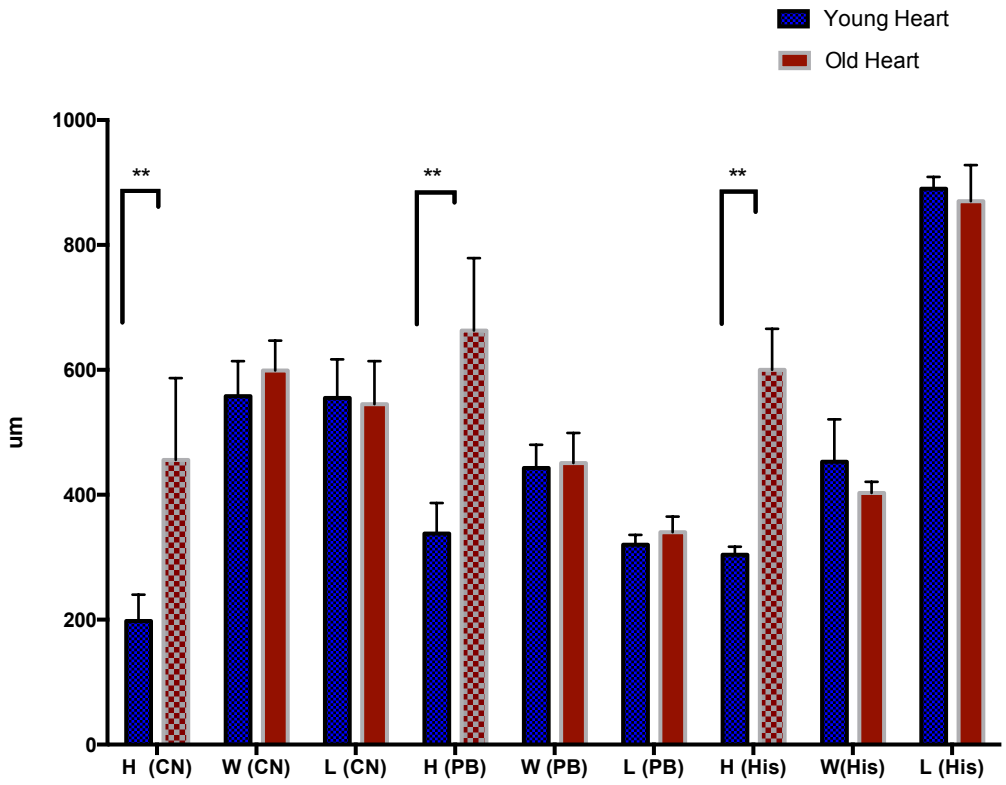

Figure 3.4: Comparison of three-dimensional structure of the AVJ showing significant difference in height in each component (measured in µm). CN, compact Node, PB, proximal penetrating bundle, His, His bundle or distal penetrating bundle, Height (H), Width (W), Length (L). **ρ <0.05.

3.3.4 Comparison of cellular architecture of the AVN in young and old rat hearts

The cellular orientation and architecture of the INE cannot be clearly seen in the old rat hearts. The images taken suggest that the cells of the INE in the young rat's heart are more regularly arranged than in old rats (Figure 3.6). The CN cells with ageing becomes loosely packed and showed no regular pattern of arrangement (Figure 3.7). The nuclei are counted for each rat heart from the high magnification (63X) image. The number of nuclei in the young CN is higher than the old CN (Table 1, Figure 3.4). The mean difference between the numbers of nuclei is 65% higher in young CN, it has been compared with independent t-test and results are statistically significant with a p value of <0.01. This could suggest increased cell size and hypertrophy of the cells of the old CN. The comparison between the cell sizes cannot be made, as the cell boundaries are less well defined in the old CN. However, the cell size estimation has been achieved by immunolabelling for membrane marker (caveolin3) and described in the section 4.6.

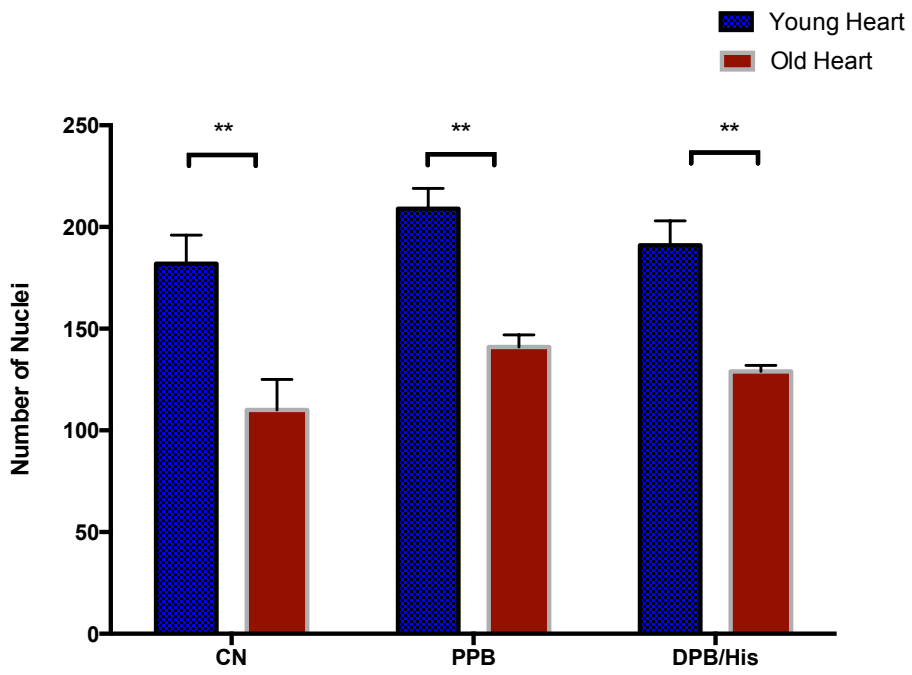

Figure 3.5: Comparison of number of nuclei seen per high power field (63X) in CN (compact node), PPB (proximal penetrating bundle), DPB/His (distal Penetrating Bundle /His bundle). Mean±SEM are shown. ** p <0.01**.**

3.3.5 Comparison of cellular architecture of the PPB and the DPB in young and old rat's heart

The PPB and DPB of the young rat hearts show increase number of nuclei in comparison with the old rat hearts; PPB (48%) and DPB/His (48%) (Table 3.1 and Figure 3.5). The p value computed is <0.01 via independent t-test. The nuclei are counted for each rat heart from the high magnification (63X) image. The cells are more loosely packed in the old PPB and DPB, less regularly arranged and cell boundaries are less regularly defined in comparison with the young PPB and DPB cells (Figure 3.8 and 3.9).

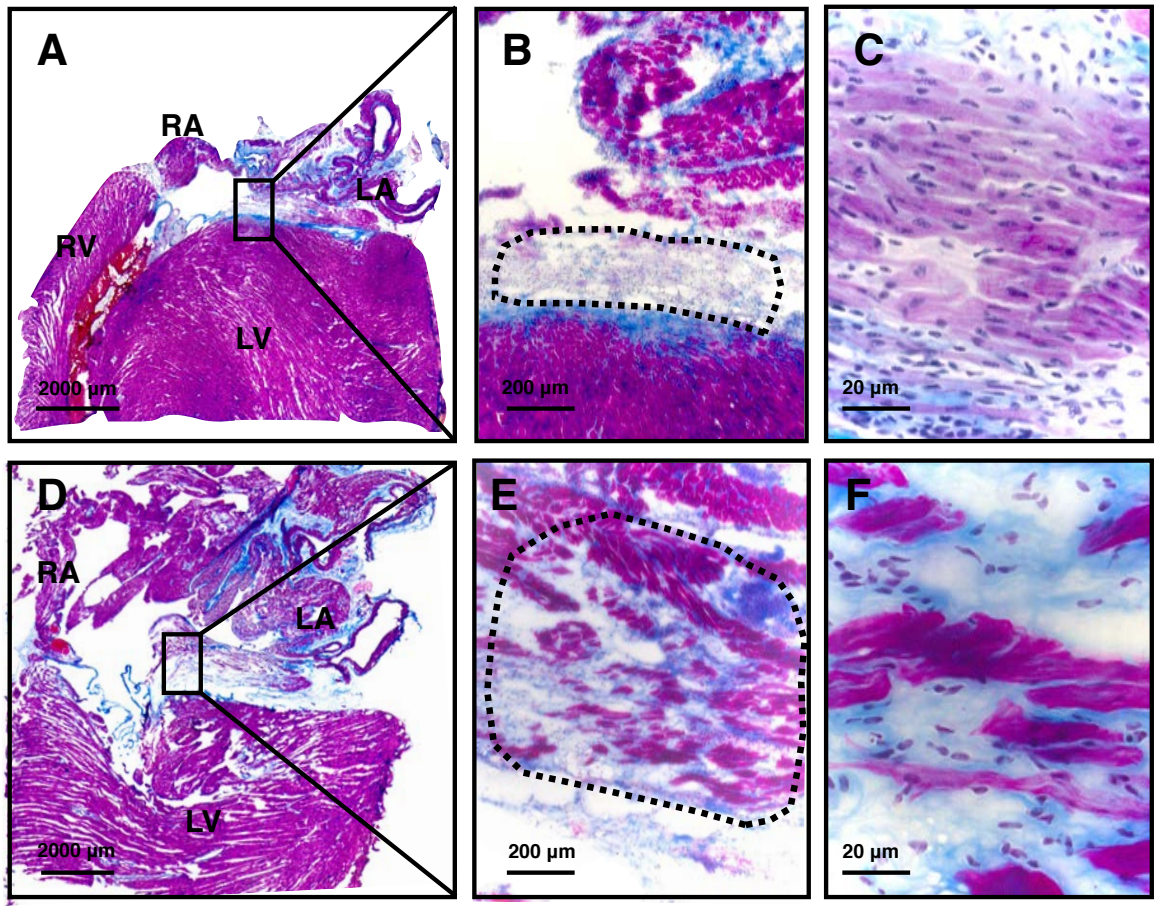

Figure 3.6: Masson's trichome. Young and old inferior nodal extension (INE). Top panel (A,B,C) show sections at INE level at different magnification in young heart and bottom panel (D,E,F) shows the comparable images in old heart at INE level. INE is marked with black dotted line. Myocytes are pink/ purple and nuclei are black blue in high magnification images (C, F). Left atrium (LA), right atrium (RA), left ventricle (LV), right ventricle (RV). Bar is shown in each image. Red colour seen in A and D is clotted blood.

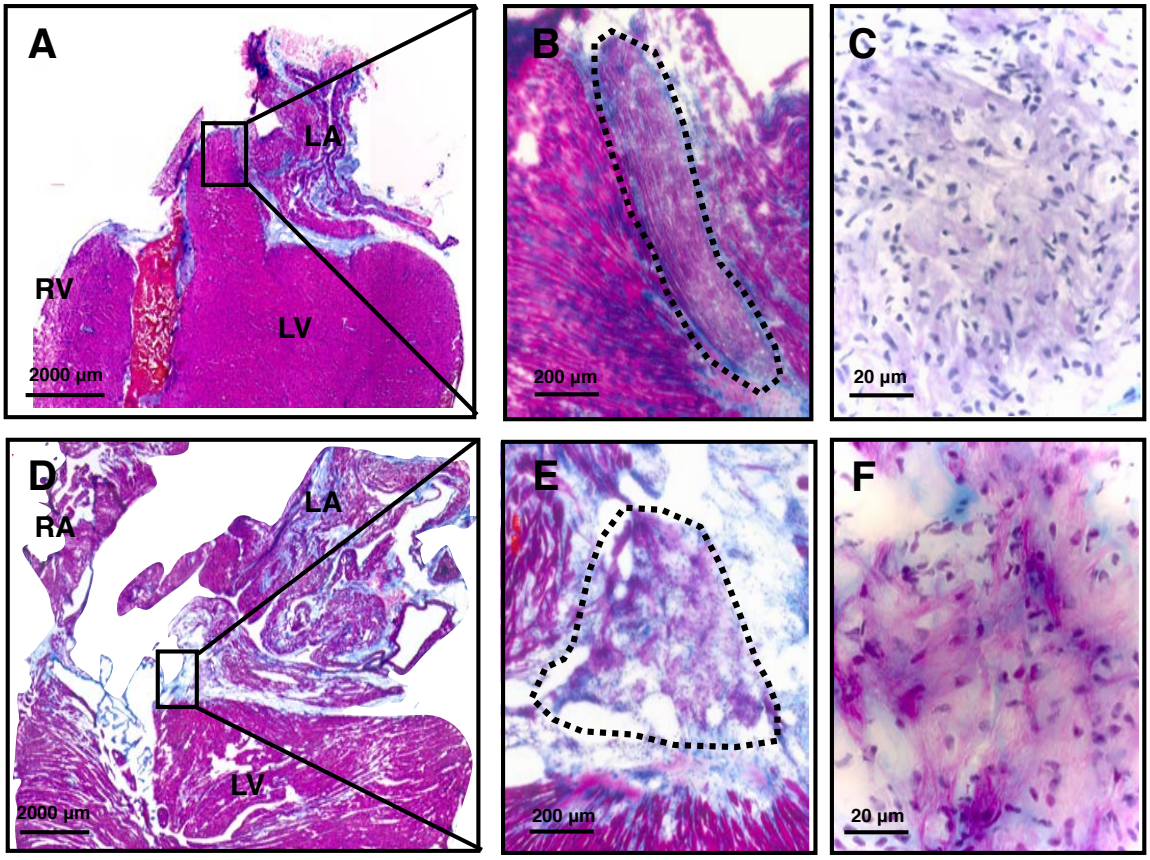

Figure 3.7: Masson's trichome. Young and old compact node (CN). Top panel (A,B,C) show sections at CN level at different magnification in young heart and bottom panel (D,E,F) shows the comparable images in old heart at CN level. CN is marked with black dotted line. Myocytes are pink/purple and nuclei are black blue in high magnification images (C, F). Left atrium (LA), right atrium (RA), left ventricle (LV), right ventricle (RV). Bar is shown in each image. Red colour seen in A is clotted blood.

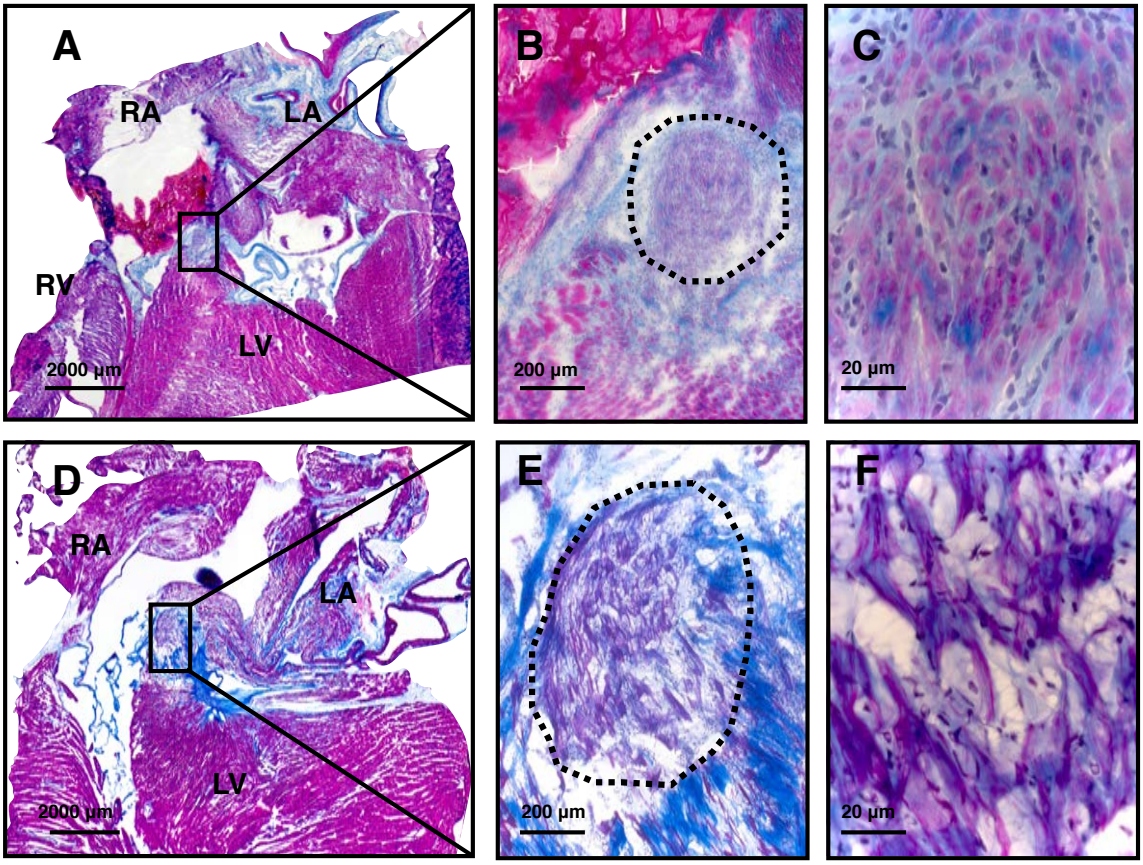

Figure 3.8: Masson's trichome. Young and old proximal penetrating bundle (PPB). Top panel (A,B,C) show sections at PPB level at different magnification in young heart and bottom panel (D,E,F) shows the comparable images in old heart at PPB level. PPB is marked with black dotted line. Myocytes are pink/purple and nuclei are black blue in high magnification images (C, F). Left atrium (LA), right atrium (RA), left ventricle (LV), right ventricle (RV). Bar is shown in each image. Red colour seen in A is clotted blood.

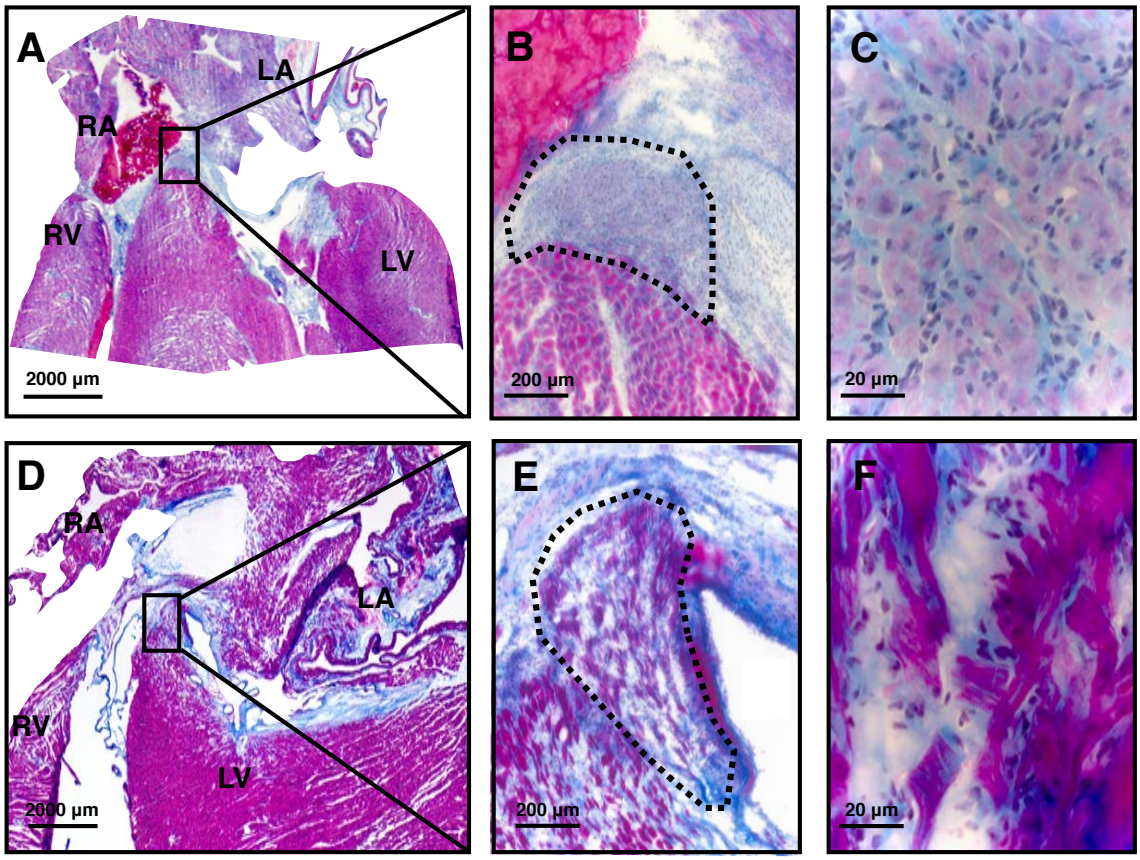

Figure 3.9: Masson's trichome. Young and old distal penetrating bundle (DPB/His). Top panel (A,B,C) show sections at DPB level at different magnification in young heart and bottom panel (D,E,F) shows the comparable images in old heart at DPB level. His is marked with black dotted line. Myocytes are pink/purple and nuclei are black blue in high magnification images (C, F). Left atrium (LA), right atrium (RA), left ventricle (LV), right ventricle (RV). Bar is shown in each image. Red colour seen in A is clotted blood.

3.3.7 Comparison of collagen signal intensity of young and old rat's heart

Tissue sections from the INE, CN, PPB and His bundle were stained with PR. The collagen fibres appear red and cytoplasm yellow when analysed with light microscopy. However, the picrosirius red images when analysed with polarised microscopy showed thick red collagen fibers and thin green collagen fibers. I have performed two protocol of staining. I have used light microscopy and polarized microscopy to confirm our findings. Volocity software was used to measure signal intensity on images taken with polarised microscope. Table 3.2 showed collagen signal estimation via polarised microscope. All polarised microscope slides are listed in Appendix 1. There is no significant age dependent change noticed in the total collagen protein content in the CN and PPB. However, the total protein collagen content increased with ageing in the His bundle (Table 3.2). Polarised microscopy analysis showed increase in signal intensity of thin green fibers in the CN, PPB and DPB or His bundle. Figures 3.10 - 3.12 show the graphs of collagen signal estimation. Figures 3.13-3.17 show the picrosirius red images with light microscope and polarised microscope.

Table 3.2: Statistical analysis: collagen signal estimation via polarised microscope in young and old rat heart's compact node (CN), proximal penetrating bundle (PPB), distal penetrating bundle or His (DPB/His). Red (thick fibers), green (thin fibers), combine (sum of both red and green fiber signal estimation (statistically significant results are shown in red).

	Collagen signal red	Collagen signal green	Collagen signal combine
Young hearts CN (Mean and SEM)	10.22±0.41	10.37±0.48 p<0.005	20.60±0.78
Old hearts CN (Mean and SEM)	11.91±2.12	12.66±0.48 p<0.005	24.58±2.48
Young hearts PPB (Mean and SEM)	11.17 ±0.79	9.73±0.58 p<0.05	21.41±1.51
Old hearts PPB (Mean and SEM)	12.84±0.90	10.97±0.54 p<0.05	22.88±1.52
Young hearts DPB/ His (Mean and SEM)	9.52±0.53	8.18±0.43 p<0.05	17.70±1.51 p<0.05
Old hearts DPB/His (Mean and SEM)	11.66±1.37	10.37±0.25 p<0.05	22.03±1.52 p<0.05

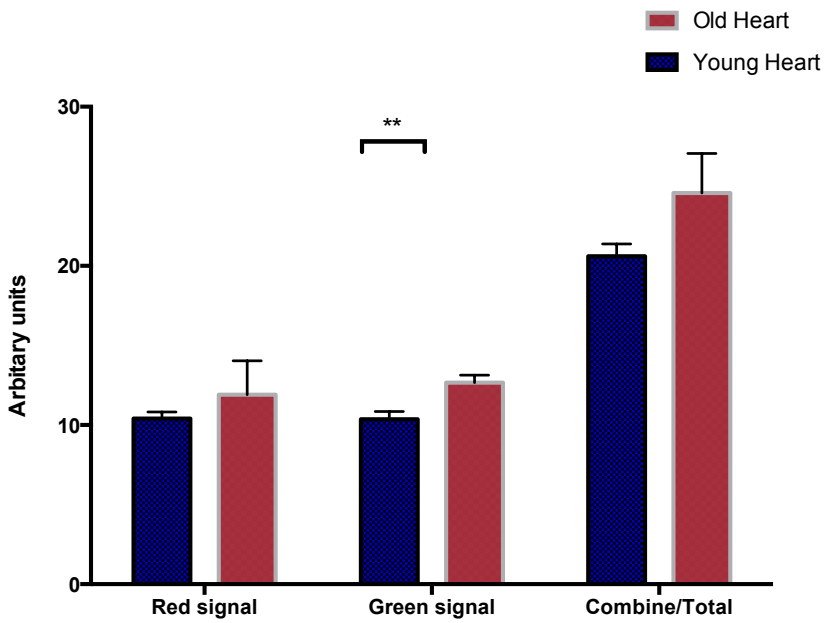

Figure 3.10: Comparison of collagen signal estimation of compact node (CN) via polarised microscope. Red (thick fibers), green (thin fibers), combine (sum of both red and green). Mean±SEM are shown. ** p <0.005.

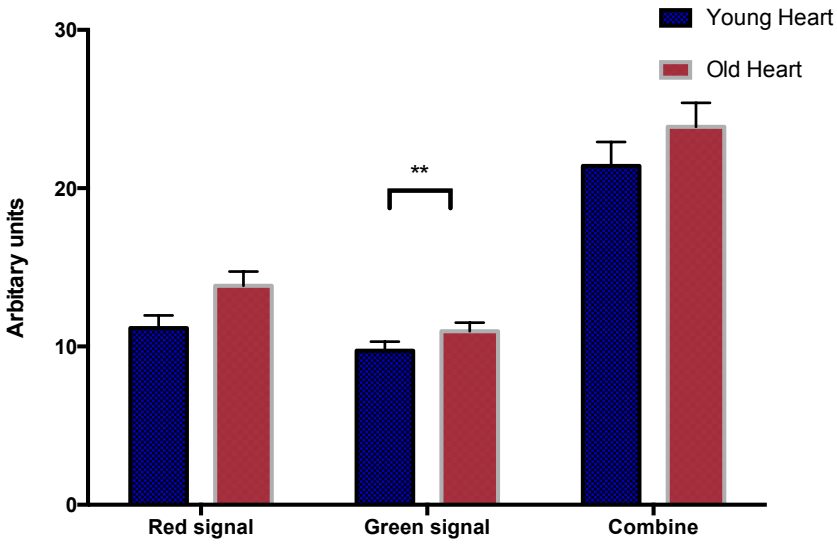

Figure 3.11: Comparison of collagen signal estimation of proximal penetrating bundle (PPB) via polarized microscope. Red (thick fibers), green (thin fibers), combine (sum of both red and green). Mean±SEM are shown. * p <0.05.

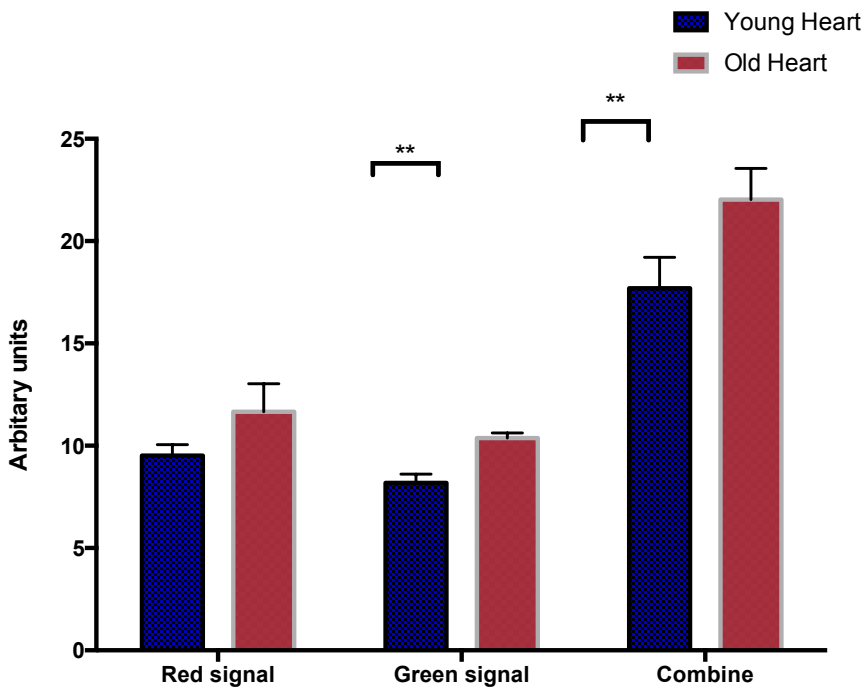

Figure 3.12: Comparison of collagen signal estimation of distal penetrating bundle (DPB or His) via polarized microscope. Red (thick fibers), green (thin fibers), combine (Sum of both red and green). Mean±SEM are shown. * p <0.05.

3.3.8 Summary of Results

In summary, the cells of the CN and PB showed an age-dependent decrease in the number of nuclei. The cells are loosely packed with no regular pattern of arrangement seen in the old CN and PB. In comparison the cells of the young CN and PB are more regularly arranged, and have a higher number of nuclei. This indicates apoptosis or hypertrophy of cells in the old rats.

There is an age dependent increase in the thin green fibre collagen content as measured by collagen signal intensity in the CN, PPB and the DPB/His via polarised microscope, whereas no difference is observed in thick collagen fibres content. Total collagen content increase with ageing in the His bundle but not in other regions of the AVJ.

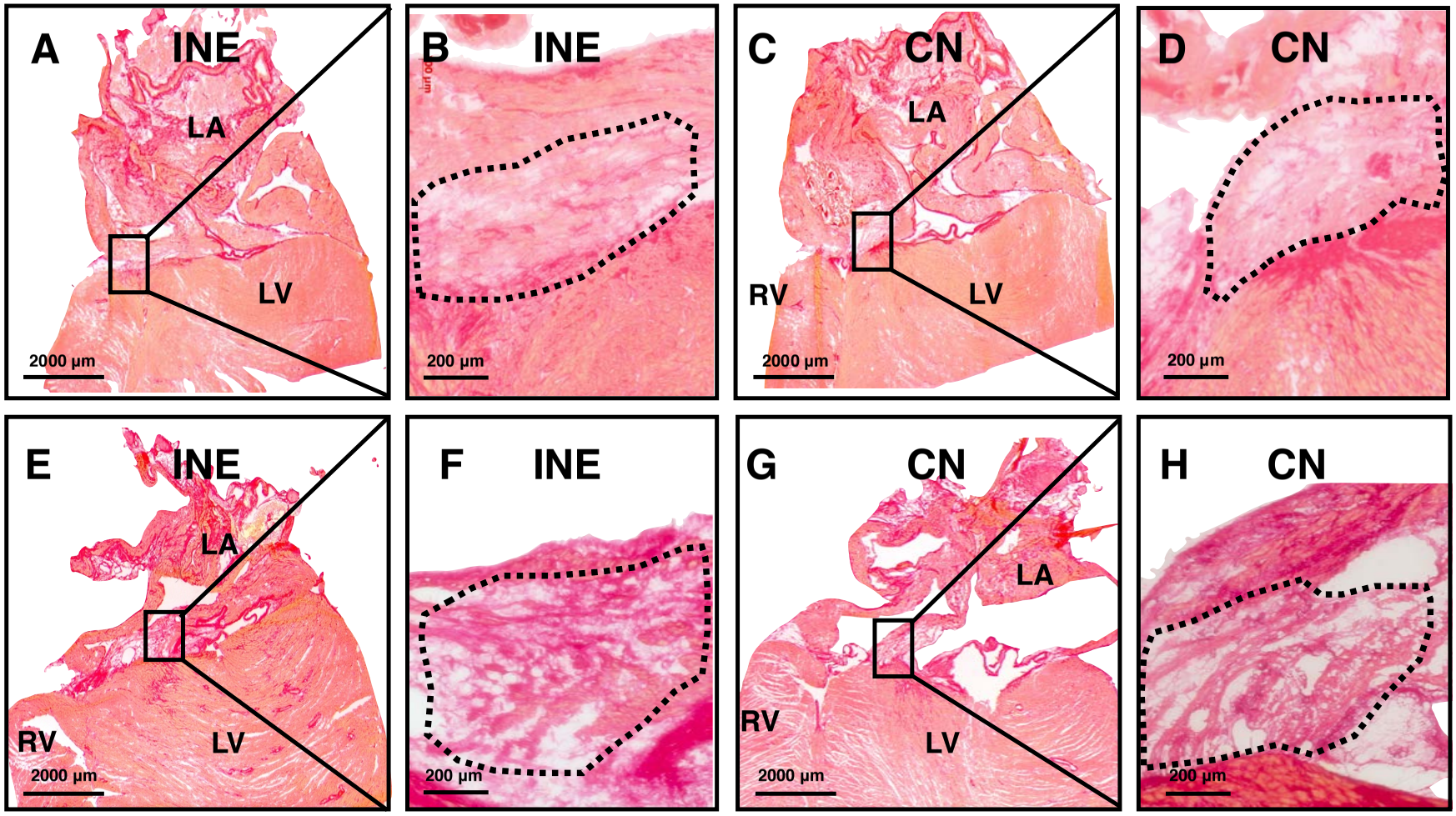

Figure 3.13: Picrosirius red stain (light microscopy) Young and old inferior nodal extension (INE) and compact node (CN). Top panel shows the sections in young heart and bottom panel shows the comparable images in old heart. The INE and CN are marked with black dotted line. Bar is shown in each image.

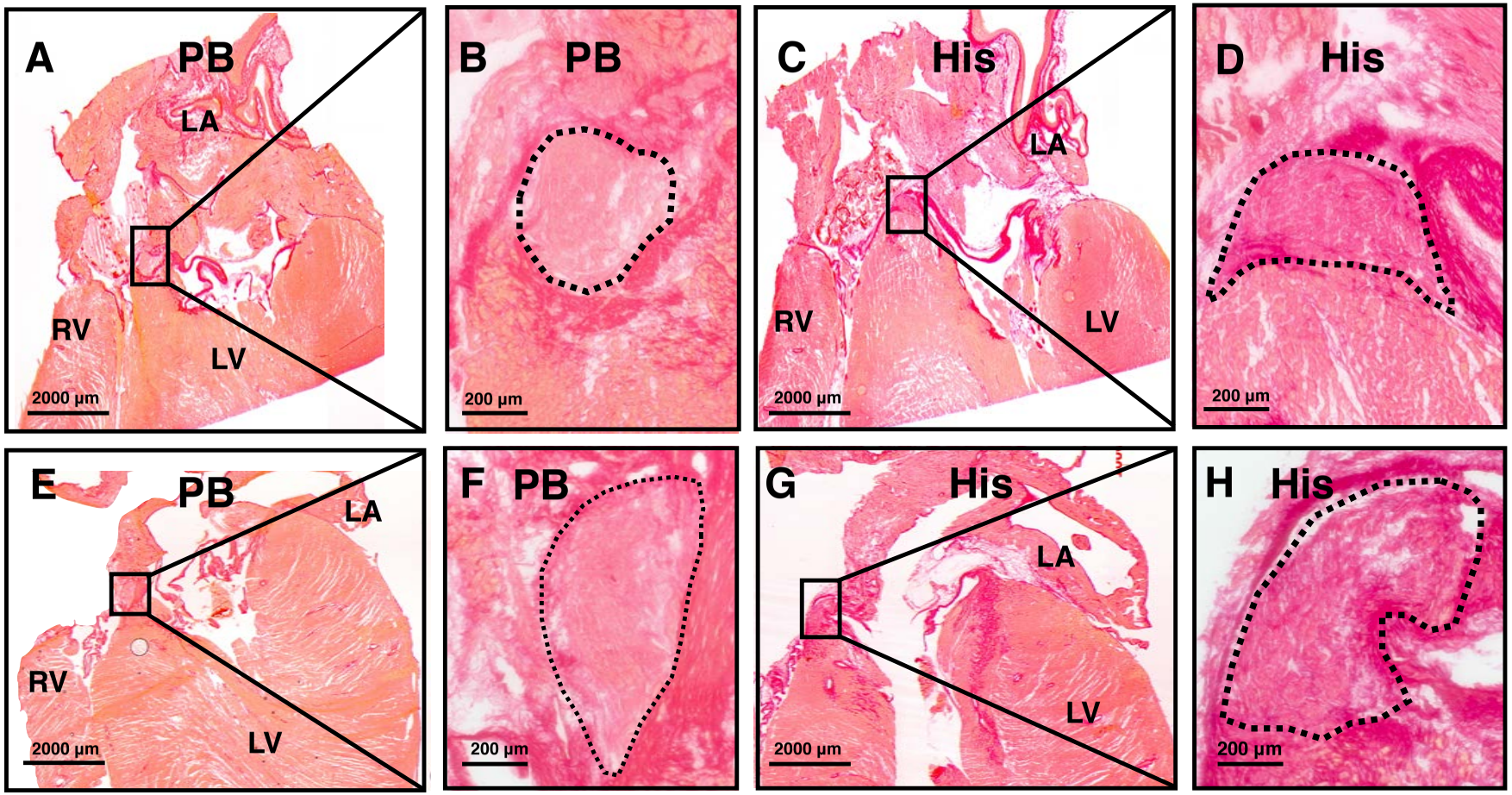

Figure 3.14: Picrosirius red stain (light microscopy) Young and old proximal penetrating bundle (PPB) and distal penetrating bundle (DPB/His). Top panel shows the sections in young heart and bottom panel shows the comparable images in old heart. The PPB and His are marked with black dotted line. Bar is shown in each image.

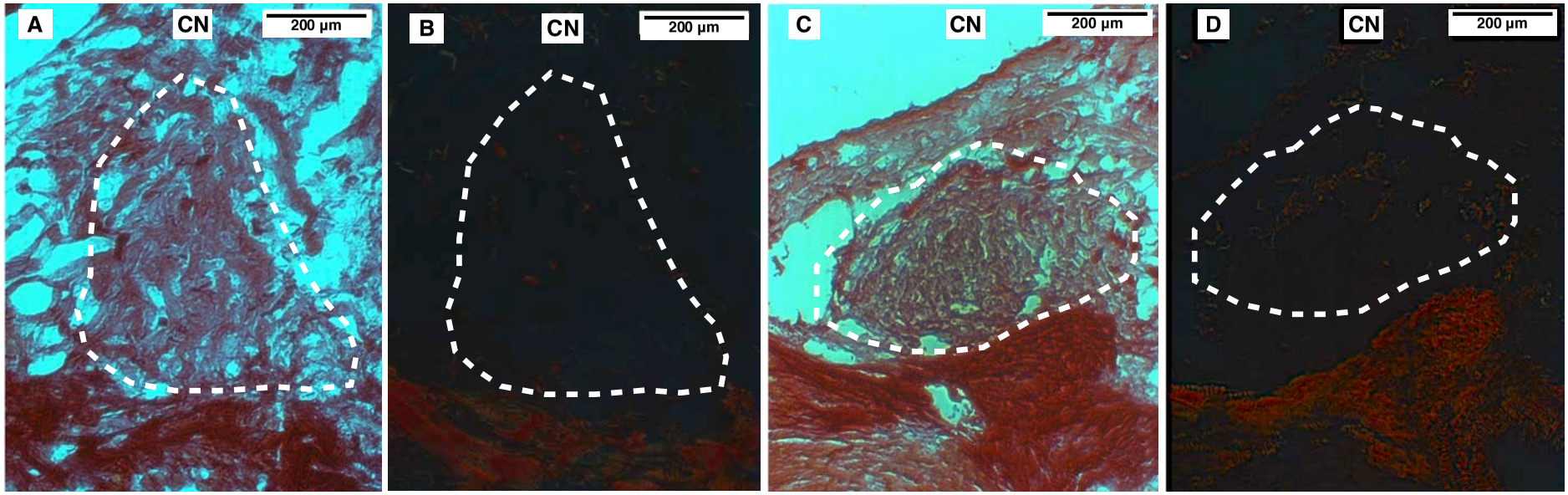

Figure 3.15: Picrosirius red stain. Images of the young and old compact node (CN) with light and polarized microscope. (A) young heart bright field image, (B) same image taken with polarized microscope. (C) The old CN bright field microscope image, (D) same image taken with polarized microscope. Red and green bisference can be easily seen with dark background; red bisference represent thick collagen fibers, green bisference represent thin collagen fibers. The CN is marked with white dotted line. Bar is shown in each image.

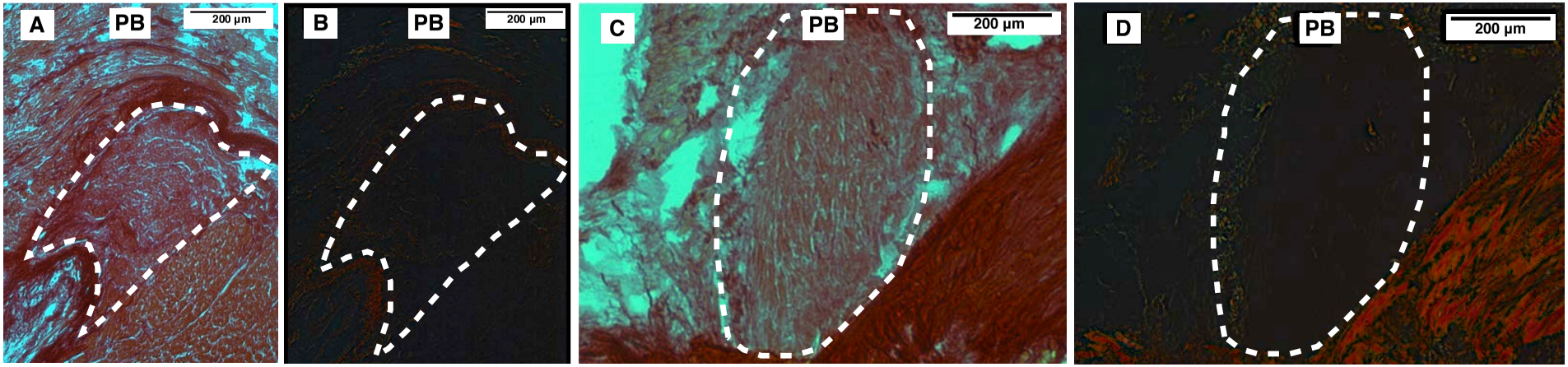

Figure 3.16: Picrosirius red stain: Images of the young and old proximal penetrating Bundle (PPB). (A) young PPB bright field image, (B) same image taken with polarized microscope. (C) old PB bright field image, (D) same image taken with polarized microscope. Red and green bisference represent thick and thin collagen fibers respectively. The PPB is marked with white dotted line. Old PPB shows high green bisference.

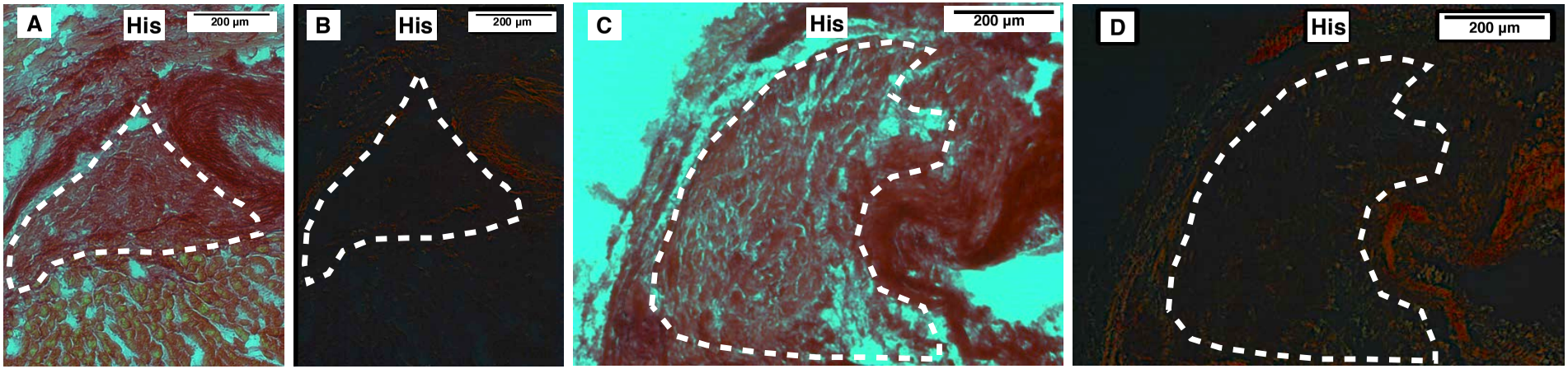

Figure 3.17: Picrosirius red stain: Images of young and old DPB or His Bundle (His). (A) Young His bright field image, (B) same image taken with polarized microscope. (C) old His bright field image, (D) same image taken in polarized microscope. Red and green bisference represent thick and thin collagen fibers respectively. The His is marked with a white dotted line.

3.4 Discussion and Conclusion

In terms of cellular architecture our findings correlate well with the previous studies performed on ageing animals and humans. I have noticed decrease in number of nuclei with ageing, which is also reported by Fujino et al.,[82] they demonstrated decreased number of cells in the AVN with ageing. Buruljanowa reported increased cellular hypertrophy with ageing.[83] Both these findings correlate with my finding of decrease in number of nuclei with ageing. This finding could suggest apoptosis and/or cellular hypertrophy with ageing. Furthermore, they have reported that the cells of the AVN and PB are more loosely arranged with ageing, which supports my findings.

I have not been able to locate any study that demonstrates comparison of the CN and PB between young and old hearts in three dimensions, which can correlate with my findings. However, these findings merit further discussion. First, the dimensions of the INE especially in the old rat heart could not be accurately measured. It is possible that the limitations of the techniques used to demonstrate INE architecture could be one of the reasons. The other important aspect is the antero-posterior length of the CN, PPB and DPB/His. Approximately similar length is quite unexpected as with ageing the cell size clearly increase which is demonstrated in this study. The horizontal and vertical axis measurements increase with ageing. This elucidates an important concept that with ageing the distance that the action potential needs to travel across AVJ remains constant however the PR interval and AH interval prolong as shown in section 2.3.1, which suggests that it is likely related with cellular changes.

The issue of fibrosis in the conducting tissues of the heart with ageing needs careful analysis. I have shown in the literature review (section 1.11.1) that across different studies fibrosis has been uniformly linked with ageing. The study by Sandusky[113] in large breed dogs also suggest increased fibrosis in the AVN with ageing. However, a recent study on SN by Yanni et al.,[87] has demonstrated decreased mRNA expression of type I and III collagen in ageing rats. In the SN the total collagen content decreases which has been measured by collagen signal estimation. My findings in terms of fibrosis are quite interesting. I have shown that with ageing there is no significant difference in total collagen content and thick red collagen fibres but in terms of thin green collagen fibres there seems to be age dependent increase. My findings correlate with the studies described earlier however I have described the issue of fibrosis in more detail in terms of thick and thin collagen fibres which could be the reason behind different findings by Yanni et al.[87]

In summary, the structural histological findings seen correlate with previous studies performed on the AVN with ageing. The changes with ageing observed in this study may well explain slowing of conduction across the AVJ with ageing that were described in functional studies in section 2.3.1. DiFrancesco group has demonstrated that the destruction of the HCN4 positive cells in the SN and AVN can results in deep bradycardia and AV block[51] that correlates with our findings of reduction in the number of nuclei. Reduced number of nuclei indicates decrease in number of cells with ageing, could be responsible for impaired AV nodal conduction i.e prolonged AH interval. Furthermore, the cellular architecture disruption or myocardial disarray and apoptotsis can result in decreased expression of proteins/ion channels important in cell-to-cell communication and action potential propagation. These results are explained in greater detail in chapter 4.

Chapter 4

4. Immunofluorescence

4.1 Introduction

The changes in the ion channel expression, calcium handling protein and gap junction proteins with ageing in the atrioventricular junction has not been described in the literature. I have described in this chapter the immunohistochemcial experiments performed to identify the changes in the expression of proteins important in the AVN conduction.

4.2 Methodology

The species used and sample size have been described in the histology section. The methods of dissection, freezing of the whole heart and cryosection have been described in the histology section.

4.2.2 Solutions and chemicals used

4.2.2.1 Solutions

1. 0.01M Phosphate Buffer saline (PBS); containing in mM: Na_2HPO_4, 77; $Na_2H_2PO_4$, 23; pH 7.4 (Sigma).

2. 0.1% Triton-X100 (Sigma) was used to penetrate the tissue.

3. 1% Bovine serum albumin (BSA) (Sigma).

4.2.2.2 Fixative

1. 10% neutral buffered Formalin (Sigma).

2. Methanol (Sigma)

4.2.2.3 Primary and secondary antibodies

All primary and secondary antibodies used are summarized in table 4.1 and 4.2 respectively.

4.2.2.4 Mounting medium

Vectshield (H-1000), Vector laboratories, Peterborough, UK.

4.2.2.5 Statistical analysis

SPSS version 19.0 for Mac and Prism 6 have been used for data entry and statistical analysis. Independent t-test and one-way ANOVA was used to compare means and compute p value and 95% confidence intervals. p value = < 0.05 is considered as statistically significant.

4.2.2.6 Signal estimation

Volocity software was used to measure signal intensity in arbitrary units of high magnification images (63X magnification) across different components of the AVJ. Signals are measured in at least four high magnification images taken from four different hearts for each region of the AVJ. The process of signal estimation is explained in Figure 4.1. The mean of the arbitrary units from all these images are taken and plotted on the graph with standard error of mean.

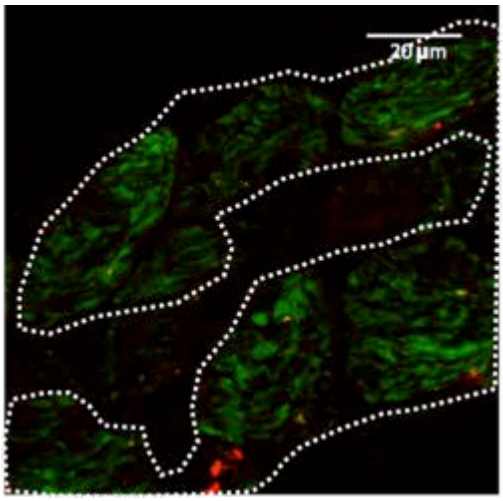

Figure 4.1: Signal estimation using Volocity software. The high magnification image of His bundle (63X) is shown with a white dotted line encircling the areas of signal estimation. The dark areas (no tissues) are not included in the signal estimation. Signals are estimated in arbitrary units.

4.2.3 Principle of immunofluorescence and immunofluorescence protocol

Immunofluorescence is the detection of a specific protein of interest (antigen) in tissue section using primary antibodies. The immunohistochemical technique with fluorescent secondary antibody i.e., immunofluorescence has been well defined. Smith and Barton [114,115] technique has been used extensively in our group with excellent results.[86,87,116] The primary antibodies bind specifically to the protein of interest (antigen) in tissue sections. These primary antibodies are then in turn detected by specific fluorescent secondary antibody (conjugated with fluorochromes) raised against them. The fluorescent secondary antibody can be visualised using a confocal microscope. The principle of confocal laser scanning microscopy is described in a separate section below. Figure 4.2 explains the principle of immunofluorescence.

The primary antibodies are of two types, either monoclonal or polyclonal. Both have different advantages. The hybridoma cells produce monoclonal antibodies, which are immortal cells of B-cell lineage. (i.e a hybrid cell line that is created by fusing a mortal antibody-producing B-lymphocyte with an immortalised myeloma line; the hybridoma line is immortal and produces a continuous supply of a particular monoclonal antibody). Monoclonal antibodies are active against only one region of the antigen, therefore they are more specific. On the other hand, polyclonal antibodies are active against many regions of the antigen. Polyclonal antibodies are produced by injecting host laboratory animals with the specific antigen. The serum of these animals is then collected and purified as it contains other antibodies directed against different parts of antigen. Polyclonal antibodies have the advantages of producing stronger labelling as compared to monoclonal antibody however they are less specific. [117] The tissue sections can be single or double-labelled with primary antibodies raised in different animals (as shown in Figure 4.2).

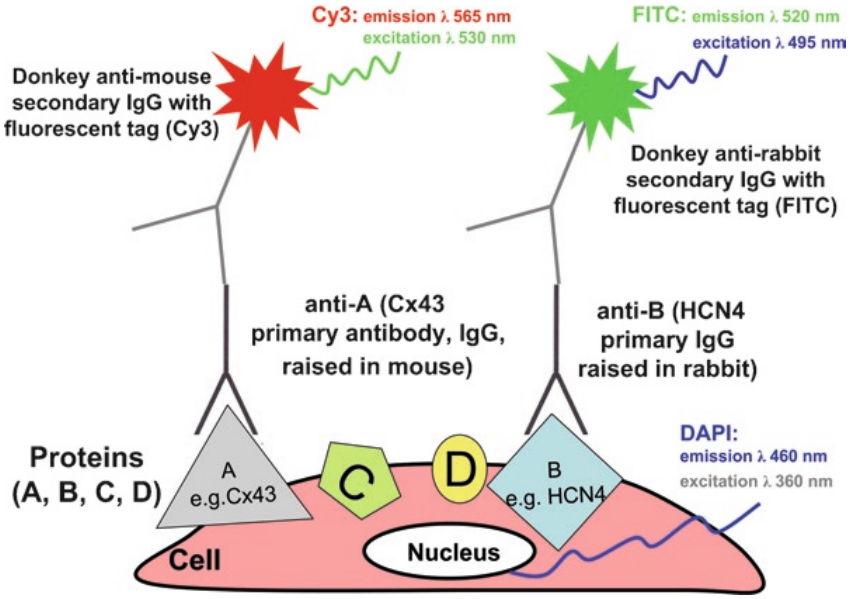

Figure 4.2: Principle of immunofluorescence (Adapted from Morris et al [117] Detection and measurement of cardiac ion channels, cardiac electrophysiology: Methods and Models: Springer US 2010). Two primary antibodies are shown bound to their respective antigens on the surface of a cell. The anti-A primary antibody (raised in mouse) binds to antigen A (Cx43), whereas the anti-B primary antibody (raised in rabbit) binds to antigen B (HCN4). The primary antibody binds to the antigen with its Fab fragment. The secondary antibody normally binds to the Fc portion of the primary antibody molecule in a species-specific manner. The secondary antibody, therefore, binds to antibodies raised in a particular species (e.g., anti-mouse and anti-rabbit). The secondary antibodies contain fluorescent tags such as Cy3 (indocarbocyaninne) and FITC (fluorescein isothiocyanate), which can be visualized using an epifluorescence or confocal laser scanning microscope.

Table 4.1: Details of primary antibodies used in immunohistochemistry experiments on AVJ and their respective western blot experiments on left ventricular tissue. The antibodies that produced specific signals are shown in red. The dilution shown gives best results in the test experiments. The test experiments are repeated with different concentration to select the best dilution for the final experiments.

Protein	Catalogue ♯	Molecular weight	Company	Species	Dilution
HCN4	APC-052	158 kda	Almone	Rabbit	1:50
HCN1	APC-056	50-100 (two bands)	Almone	Rabbit	1:100
RyR2	MA1-83782	565kda	Thermo	Mouse	1:50
SERCA2a	A010-20	100 kda	Badrilla	Rabbit	
Cx43	ACC-201	43-47kda	Chemicon Almone	Mouse Rabbit	1:100
Cx40	SC-20466	40 kda (43-55kda)	Santa cruz Chemicon	Goat Rabbit	1:50
Cx45	SC-25716	±45	Santa cruz	Rabbit	1:100
$Ca_V1.3$	ACC-005	>250	Almone	Rabbit	1:50
Ca_v 3.1	ACC-021	121-250 (two bands)	Almone	Rabbit	1:50/1:100/1:400
$Ca_v1.2$	ACC-022	200-250	Almone	Rabbit	1:50/1:100/1:400
$Na_v1.5$	ASC-013	250	Almone	Rabbit	1:50
$K_v1.4$	APC-007	96	Almone	Rabbit	1:50/1:100/1:400
$K_v7.1$ (LQT1)	APC-022	75	Almone	Rabbit	1:50/1:100/1:400
$K_v11.1$ (ERG)	APC-016	117-205	Almone	Rabbit	1:50/1:100/1:400
$K_{ir}2.1$	APC-026	±70	Almone	Rabbit	1:50/1:100/1:400
$K_{ir}3.4$	APC-027	50-75 (two bands)	Almone	Rabbit	1:50/1:100/1:400
Cav3	610421	18 kda	BD transduction	Mouse	1:50
Alpha Actinin	A-7811	100kd	Sigma	Mouse	1:50

Table 4.2: Summary of secondary antibodies used.

Secondary Antibody	Catalogue ♯	Dilution	Company
Donkey anti-rabbit FITC	AP182F	1:100	Millipore lab
Donkey anti-mouse Cy3	AP192F	1:400	Millipore lab
Donkey anti-goat Alexa Flur 488	A11055	1:100	Life technologies

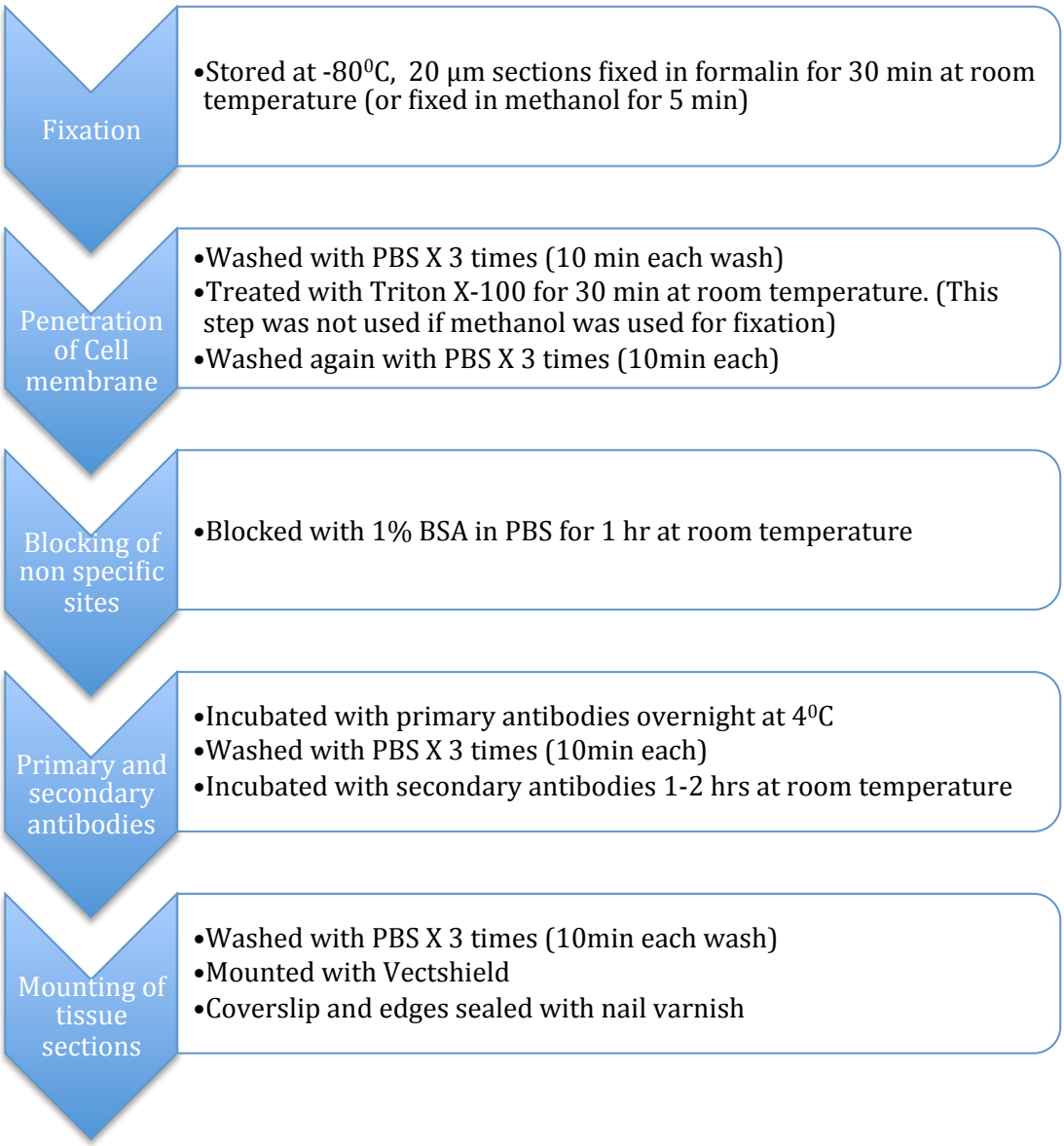

Figure 4.3: Immunofluorescence protocol

Fixation: The formalin has good penetration of tissue section and fixes tissue by primarily reacting with amino acids to form cross-linking methyl bridges. This results in low permeability to macromolecules and the structure of cytoplasmic protein is preserved. Tissues can also be fixed by using methanol.

Penetration of cell membrane: Triton-X 100 penetrate the cell membrane thus allows the antibody to reach antigens located on the cytoplasmic site of the cell membrane.

Blocking of non-specific sites: 1% BSA blocks binding of the primary antibody to nonspecific sites and thus reduces background labelling.

Labelling with primary and secondary antibody: Different concentrations of primary and secondary antibody is used. Antibodies were diluted with 1% BSA in PBS. The details of the antibodies used in the experiments are given in Table 4.1 and 4.2.

Mounting: Vectshield prevent fading of the fluorescent signal and sealing with nail varnish prevent drying of tissues.

4.2.4 Confocal laser scanning microscopy

Single or double-labelled sections were scanned using confocal microscopy. A Zeiss confocal microscope was used in this study and PASCAL LSM software was used. The confocal microscope differs from a conventional microscope because it employs laser and has two confocal pinholes (Figure 4.4). These pinholes allow only light from the plane of focus to reach the detector. Out of focus light is removed from the image by the use of a suitably positioned pinhole. This produces an image of high resolution. The confocal principle is combined with a scanning system utilizing laser light source. This builds up an image by scanning the sample point by point in X and Y direction. The detector of reflected light from the sample comes from a photomultiplier tube. The signal from the photomultiplier tube is converted to a digital form that contains information on the position of laser in the image and the amount of light coming from the sample. A computer is used to store the intensity value of each point (called pixels) from the detector, and presents these in the correct order on a high-resolution video monitor to display the image.

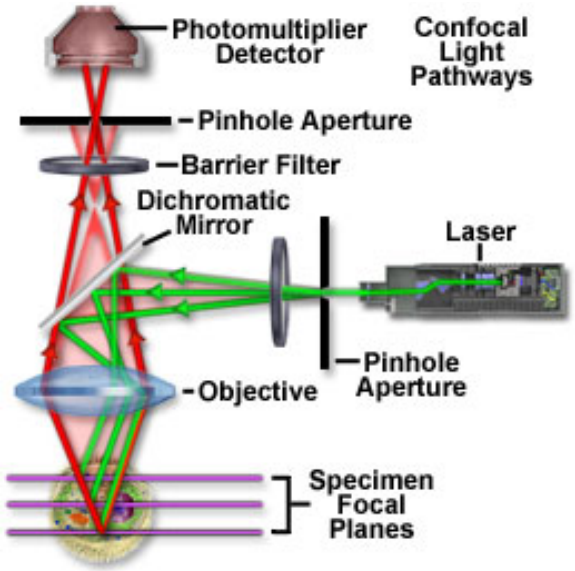

Figure 4.4: **Prinicples of confocal microscopy**

Table 4.3: Summary of excitation and emission wavelengths used for detection of secondary antibody conjugated with fluorochromes

Flourochromes	Excitation wave length (nm)	Emission wave length (nm)	Laser
FITC	496 (blue light)	518 (green light)	Argon
Cy3	556 (green light)	574 (red light)	Krypton

4.3 Western blot experiments

4.3.1 Species used and sample size

Western blot experiments to confirm antibody specificity were performed on the left ventricular tissue of four young hearts (3 months old). Male Wistar-Hanover rats were used in this study. The dissection and freezing protocol has been described earlier in the histology.

4.3.2 Solutions and Chemicals

1. TBS (Tris-buffered saline) (20 mM Tris and 150 mM NaCl)
2. TBST (TBS with 1 ml of Tween 20)
3. NuPage LDS buffer (4X)
4. 3% Bovine serum albumin (BSA, Sigma).
5. NuPage MOPS LDS running buffer (Life technologies, UK)
6. Ponceau S (Sigma)
7. Transfer buffer (Transfer buffer 800ml 1x tris-glycine running buffer 200 ml methanol)
8. Sodium hydroxide (NaOH 0.1M, Sigma)
9. Methanol (Sigma)
10. Chemiluminescene solution (ECL, mixing H_20_2 2 ul with provided solution 1 and 2 each 1.5ml, Biorad, UK)

4.3.3. Primary and secondary antibodies

1. All primary antibodies used for western blot experiments are summarized in Table 4.1.
2. 1% HRP Conjugated antibody (anti-rabbit, anti-goat, anti-mouse, Bio rad, UK)

4.3.4. Western Blot Protocol

The western blot protocol is described in Figure 4.5.

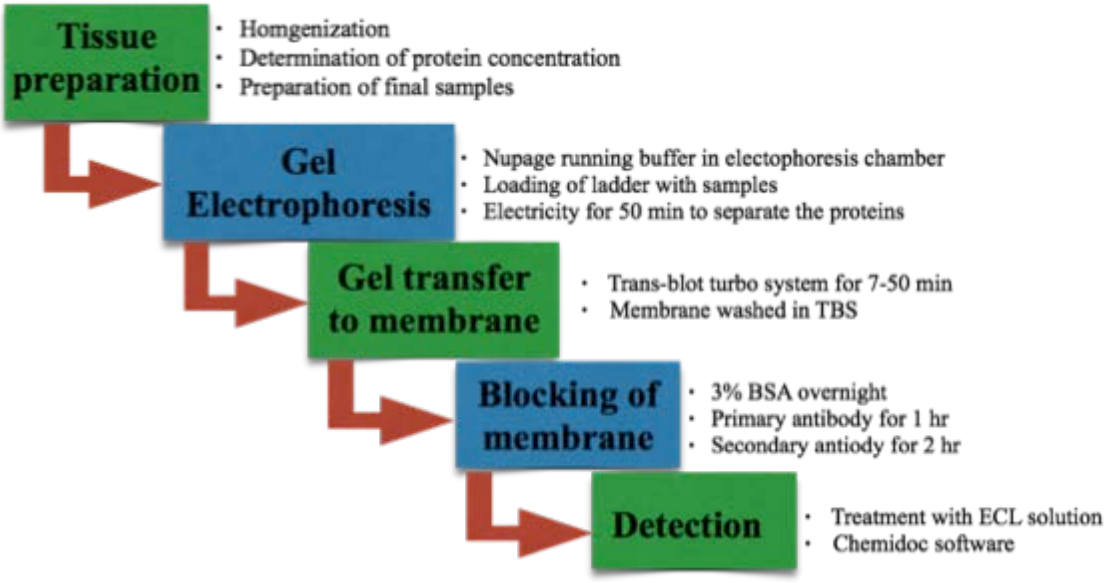

Figure 4.5: Western Blot protocol.

Tissue preparation: The collected tissue sample was homogenised. Quant-iT assay (Invitrogen, Life technologies, UK) was then used to determine protein concentration. In the Quant-iT assay, buffer 199 µL, and reagent 1µL was used to make working solution 200uL. Working solution (190 µL) is then mixed with standard solution (10 µL) from the kit to make 200 µL standard solution. Protein samples (1-20 µL) are also mixed with 190 µL of working solution. The tubes of protein samples and standards are read in the Qubit flourometer (Life technologies, UK) to determine the protein concentration. The protein samples (7.5 µL) were then mixed with NuPage LDS sample buffer-4X (2.5 µL) to make 10 µL final solution.

Gel electrophoresis: The Novex (life technologies, UK) system was used for gel electrophoresis. The NuPage MOPS-LDS running buffer was used to fill the electrophoresis chambers. The NuPage Tris-Glycine precast gel cassette was used. The samples and ladder were loaded with gel loading tips. Electricity was run for 50 min to separate the proteins. The gel maintains the polypeptide in a denatured state thus allowing separation of the protein by their molecular state. Smaller proteins migrate faster and proteins are thus separated according to their size (kDa).

Tranfer: The Trans-blot turbo transfer system was used to transfer gel on the membrane. The transblot mini or midi transfer pack was used. The gel and the transfer pack were then placed in the transblot turbo transfer system for 7-50 min to complete transfer. The membrane was then rinsed in TBS and then stained in Ponceau S for 5 min. The membrane was rinsed in millipore water to see bands and then 0.1M NaOH was used to clear gel.

Blocking with antibodies: The membrane was then blocked in 3% BSA in TBS overnight. The membrane was then incubated in primary antibody in 1% BSA for 2 hours. After washing with TBST the membrane was incubated in appropriate secondary antibody for 2 hours.

Detection/Visualization: Bio rad Chemidoc-XRS imaging system was used to image membranes. Chemiluminescene solution (ECL) was then prepared and placed on to membrane. The image was then taken and visualised on the chemi-doc software.

4.3.5. Results

Analysis of western blot experiments was performed on left ventricular tissue to assess the specificity of the primary antibodies. The experiments were successful for the variety of the protein expected to be present in the left ventricular tissue. The successful western blot experiment results are shown with the respective immunofluorescence image. Table 4.1 lists antibodies that were successful (i.e., specific) for either or both immunohistochemical and western blot experiment. The microdissection of each component of the AVJ for western blot experiments was not attempted, as it would result in contamination of the AVJ samples from surrounding atrial and ventricular muscle.

Immunohistochemical images and western blot data shown in the subsections of this chapter are only for the antibodies that produced required/specific signals.

4.4 Changes in the expression of HCN4 in the AVJ with ageing

4.4.1 Introduction

HCN channels or hyperpolarisation activated cyclic nucleotide gated channel are responsible for I_f current. The I_f current was first described in the SN almost 40 years ago.[118] The special characteristics of the I_f current includes: activation on hyperpolarisation from a threshold of about -45 mV and maximam activation at about -100mV, a mixed Na^+ and K^+ current with a reversal potential of about -10/-20mV (inward current in the diastolic range) and finally modulation by internal cAMP (cyclic adenosine monophosphate).

HCN channels are voltage gated as well as cycle nucleotide gated channels. They are formed of six transmembrane domains S1 to S6 and a C terminus with cyclic nucleotide binding domain. Figure 4.6 shows the structure of HCN channels.

Four isoforms of HCN channels have been identified and they differ in properties including tissue distribution, channel kinetics and cAMP activity. HCN3 channel is expressed only in the neuron and will not be discussed further. On the other hand, HCN1, 2 and 4 channels are expressed both in the heart and brain. HCN4 is the most highly expressed channel in the cardiac conduction system and thus is commonly used as a marker of the cardiac conduction system.[51,119,120] HCN2 channel has a slower kinetics than HCN1 but faster than HCN4. HCN2 is activated at more negative potentials than HCN1 and HCN4. HCN2 is also more sensitive to cAMP as compared to HCN2 and HCN4.[118-121]

Multiple studies documented HCN channels abundance in the AVJ. In the human atrioventricular node HCN4 mRNA was more abundant than HCN1 and HCN2 mRNA in the CN. HCN4 mRNA and protein is also abundantly expressed in the INE, CN and PB compared to atrial and ventricular myocardium.[24] HCN1 is expressed more in the CN than the PB and ventricular muscle in human. Greener et al., showed similar results in the rabbit AVJ. HCN4 mRNA is abundantly expressed in the INE. HCN1 mRNA is significantly more abundant in all areas of the AVJ as compared to the atrial and ventricular myocardium.[24] Dobrzynski et al., also showed that the site of origin of junctional pacemaker is in the INE with high expression of HCN4 in the rabbit heart.[22]

HCN4 gene knockout studies on mice showed conflicting results in terms of AV nodal conduction. HCN4 knockout mice die in utero at day 10-11,[122] thus analysis of PR or PQ interval is impossible. Studies have been conducted using Cre/loxP-system that involves selective deletion of HCN4 ion channels. The study by Herrman et al.,[123]

showed no effect on PR interval. However Baruscotti and colleagues[54] showed severe bradycardia associated with higher degrees of AV block (2:1 and 4:1 2nd degree AV block) with HCN4 deletion. Thus the role of HCN4 in the AV conduction remains elusive.

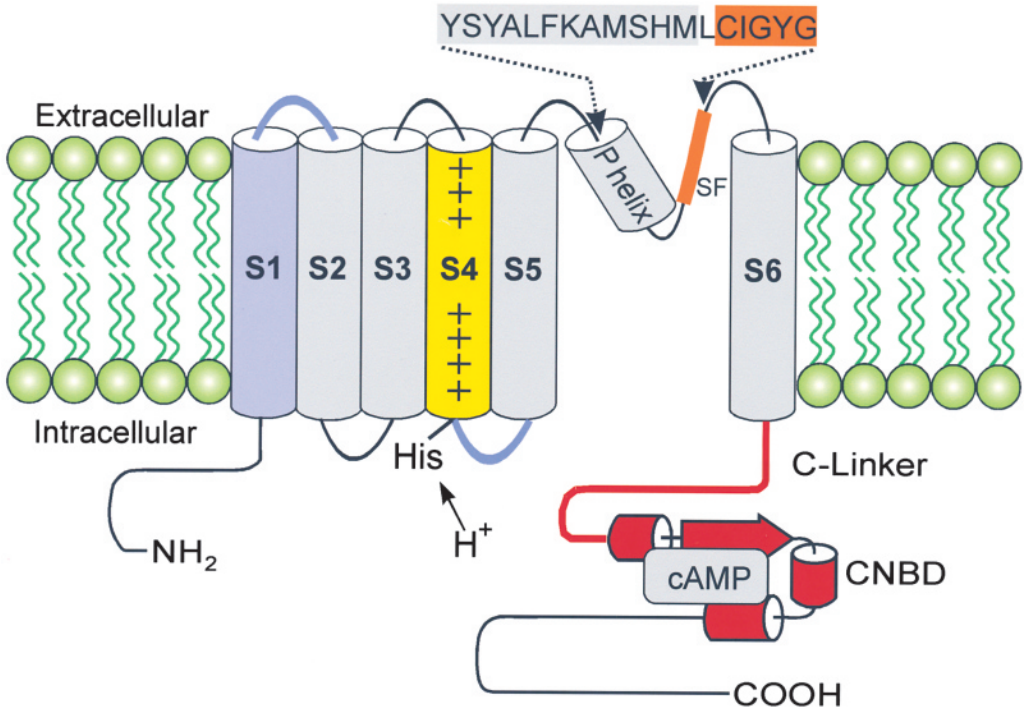

Figure 4.6: Structural model of hyperpolarisation-activated cyclic nucleotide-gated (HCN) channel. The channel displays two functional parts: (a) the transmembrane core region consisting of the six transmembrane segments (S1–S6) and the ion-conducting pore loop between S5 and S6, and (b) the modulatory C terminus containing the C linker and the cyclic nucleotide-binding domain (CNBD). The function of the cytosolic N terminus is not yet known. The voltage sensor of the channel is formed by the positively charged S4 helix that contains nine regularly spaced Arg or Lys residues at every third position. The S1 helix, the extracellular S1–S2 linker, and the intracellular S4–S5 linker, which are involved in activation gating are highlighted. Adapted from Biel et al.[120]

4.4.2 Methods

Methodology has been explained in detail in section 4.1.

4.4.3 Results

4.4.3.1 Age related changes in the expression of HCN4

Table 4.4 and Figure 4.7 showed changes in HCN4 expression with ageing in each component of the AVJ conduction axis. No significant difference in the INE, CN and PPB bundle in HCN4 expression with ageing was found. There is a decrease in HCN4 expression in the His bundle with p-value=0.05.

Figure 4.8 shows low magnification images, double labelled with HCN4 and Cx43. HCN4 is used as a marker of the CCS. HCN4 is highly expressed in the

CCS and poorly expressed in atrial and ventricular tissues. On the other hand expression of Cx43 is poor in the CCS and high in the atrial and ventricular tissues. The reason of double labelling was to identify the conduction system separate from the surrounding atrial, ventricular tissues and in the case of penetrating bundle from the central fibrous body. The primary antibody against HCN4 was raised in rabbit and secondary fluorescent antibody used was FITC, which emits green fluorescence. The primary antibody against Cx43 was raised in mouse and the secondary fluorescent antibody used was anti-mouse Cy3, which emits red fluorescence.

Figure 4.9 shows high magnification images of HCN4 double labelled with Cx43 corresponding with each component of the AVJ conduction axis. Cx43 expression will be discussed in more detail in the next section. HCN4 green signal is stronger in the His bundle of young hearts as compared to the His bundle of old hearts. No expression of HCN4 was seen in the working myocardium of atria and ventricle thus was not analyzed.

4.4.4 Discussion

HCN4 expression in the INE, CN and PPB with ageing was consistent with the study by Tellez et al., on ageing SN. In the SN no significant change in the immunofluorescence signal intensity or mRNA was detected. However, downregulation of HCN4 in ageing DPB/His bundle has not been previously documented.

The role of HCN4 is not firmly established in the AV nodal conduction. Although HCN4 is responsible for I_f current, studies have conflicting results in terms of decreased conduction across the AVJ following deletion of HCN4 as already mentioned. Functional studies that involve use of ion channel blocker Cs^+ to block HCN4 and then measuring AV nodal conduction have not been reported before our study. My finding of decrease in HCN4 expression in the His bundle correlate with our functional results, which showed that there is no changes seen in the AV nodal conduction in the ageing rats after application of Cs^+. It is possible that HCN4 has a very limited role in the AV conduction in ageing and thus may not be a major player in the AV conduction in ageing.

Table 4.4: Statistical analysis of HCN4 expression in young and old heart's AVJ. Statistically significant results are shown in red.

HCN4 expression	Inferior nodal extension (INE)	Compact node (CN)	Proximal penetrating bundle (PB)	Distal penetrating bundle (His)
Young hearts (Mean and SEM)	29.91±2.04	32.77±2.09	27.48±1.71	33.23±1.21
Old hearts (Mean and SEM)	32.09±1.60	33.36±2.61	30.68±0.75	27.66±2.83
p-value and 95% confidence interval	0.55 (-5.20 to 9.57)	0.8 (-6.18 to 7.35)	0.17 (-1.50 to 7.91)	0.05 (-11.16 to 0.03)

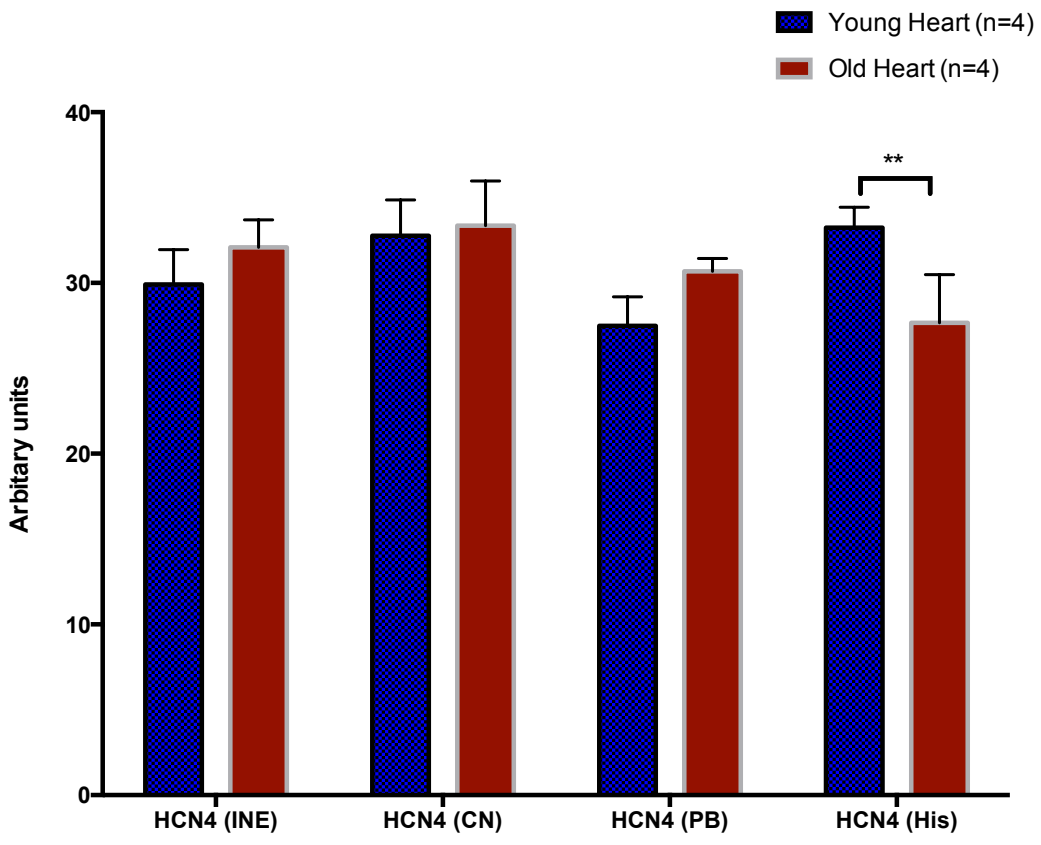

Figure 4.7: Changes in HCN4 expresson in AVJ with ageing
Inferior nodal extension (INE), compact Node (CN), proximal penetrating bundle (PB), distal penetrating bundle or His bundle. Signal intensity measured with Volocity software. Mean±SEM shown. ** p=0.05

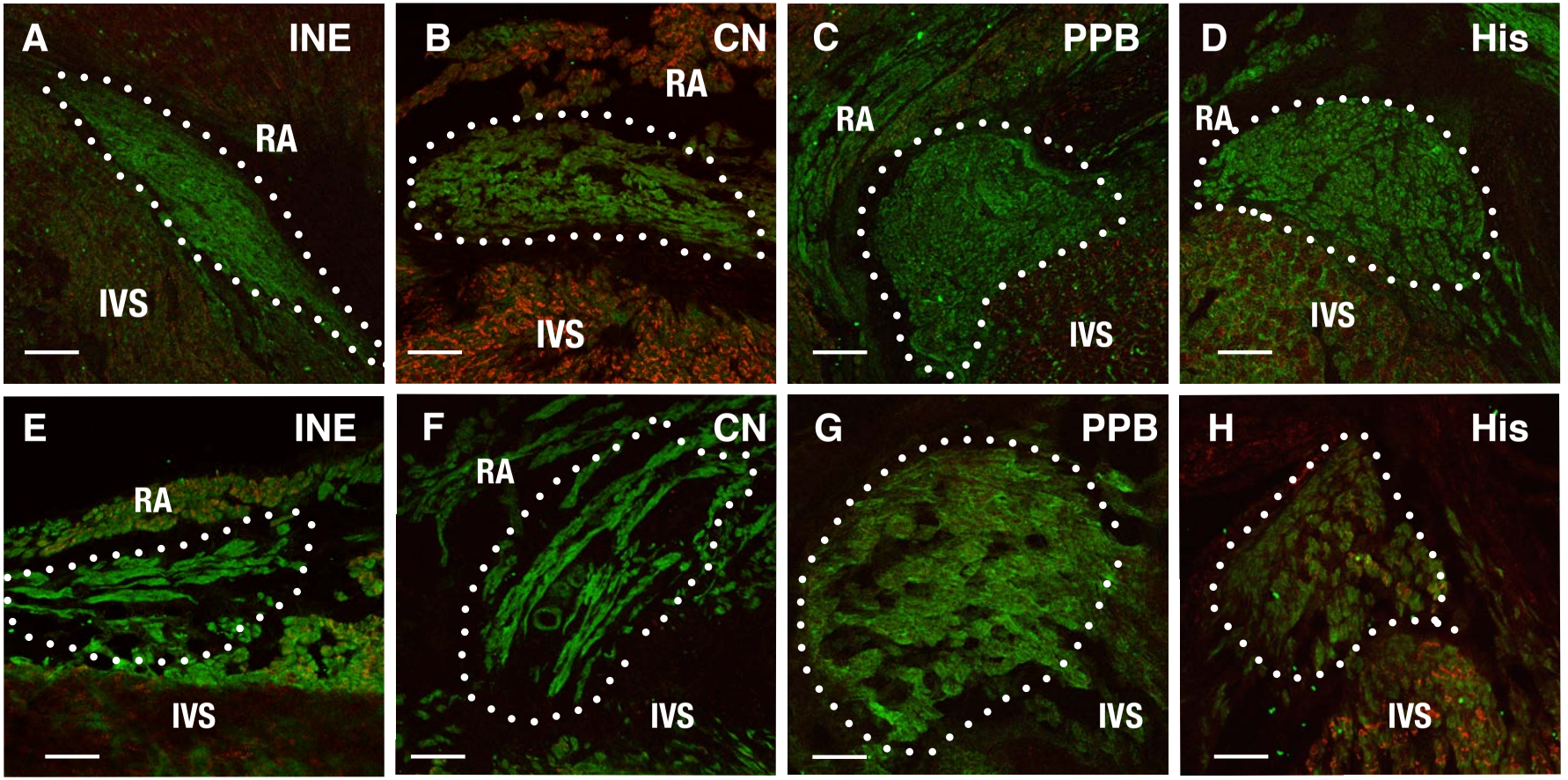

Figure 4.8: Confocal microscope low magnification images of the AVJ with HCN4 (green) and Cx43 (red) immunolabelling. Inferior nodal extension (INE), compact node (CN), proximal penetrating bundle (PPB), distal penetrating bundle/His bundle (His). Top panel shows the AVJ components in young hearts and bottom panel shows the AVJ components in old heart. Poor Cx43 expression is shown in the INE and CN. Bar=200μm

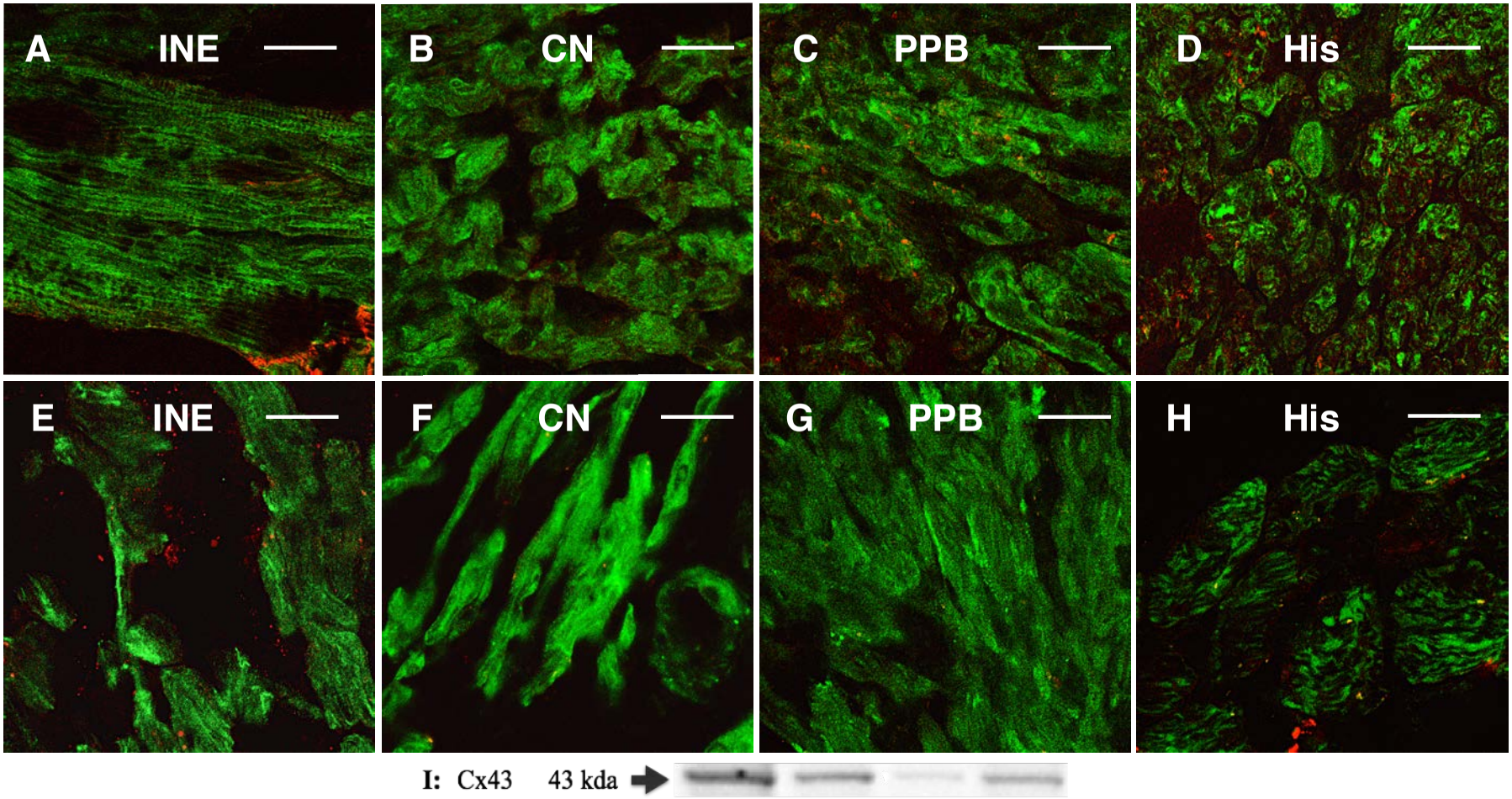

Figure 4.9: Confocal microscope high magnification images of the AVJ with HCN4 (green) and Cx43 (red) immunolabelling. Inferior nodal extension (INE), compact node (CN), proximal penetrating bundle (PPB), distal penetrating bundle/His bundle (His). Top panel shows the AVJ components in young hearts and bottom panel shows the AVJ components in old heart. Poor Cx43 expression is shown in the INE and CN. Lower right hand corner of image A show the right atrial tissue with Cx43 expression. Western blot of Cx43 on left ventricular tissue along with molecular weight is shown in image **I**. Bar=20μm

4.5 Changes in the expression of Connexins in the AVJ with ageing

4.5.1 Introduction

Gap junctions are unique structures that allow intercellular communication. They are low resistance non-selective ion channels, thus important in electrical and chemical coupling between myocardial cells, which are imperative for the transmission and propagation of the action potential. Connexins are the proteins that form the gap junctions. To date 20 members of connexins family have been identified in humans and 21 members in mice.[124]

The structure of the gap junction channel is described in Figure 4.10. Six connexins proteins combines to form connexon, which when attached or docked to the connexon of the other neighbouring cell, form a gap junction channel.[125] The connexon can be homomeric (all six connexins belongs to the same type) or heteromeric (different connexins forming connexons). Single connexins consists of four highly conserved α-helical transmembrane segments separated by two extracellular and one intracellular loop. The amino and carboxy terminals are located intracellularly. The connexins differ mainly in the sequence of their intracellular loops and carboxy terminal.[126]

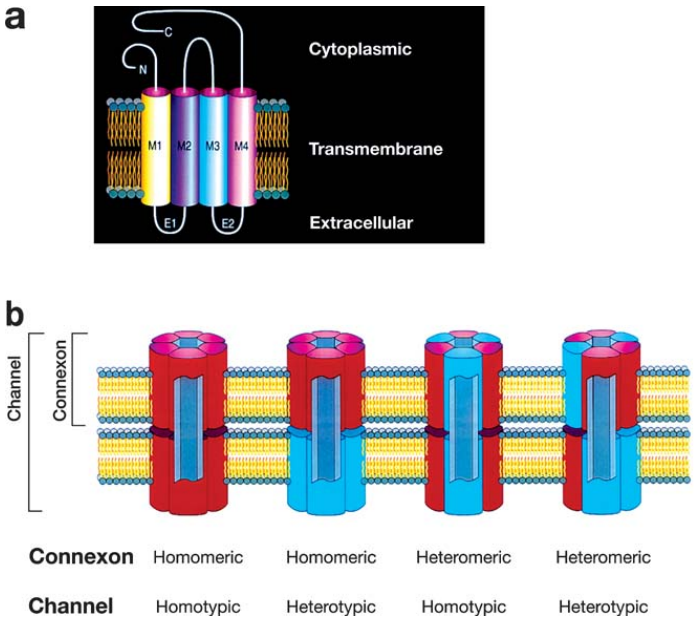

Figure 4.10: Gap junction structure illustration. (A). Structure of a single connexin protein. M1–M4 represent the four transmembrane domains, E1 and E2 the two intracellular loops; the amino (N) and carboxy (C) termini are intracellular. (B). Part of a gap junction plaque showing several channels interconnecting two cells and the composition of an individual channel from two half-channels (connexons) which are composed of connexin proteins and the scheme explain the composition of homotypic and heterotypic channels from homomeric and heteromeric connexons. Adapted from Kumar et al., 1996.[127]

The major isoforms of the connexins family that are expressed in the heart include Cx30.2/31.9, Cx40, Cx43, and Cx45. The connexins family allows conductance of structure with molecular weight of less than 1 kda. Cx40 form large conductance gap junction channel (~200 ps), Cx43 medium conductance (~75ps), Cx45 small conductance (~20ps) and Cx30.2/31.9 smallest conductance (~9ps) channels.[128,129] The Cx30.2/31.9 is unique as it forms heterotypic gap junction channels with other connexins and heterotypic channels have small conductance (15-18 ps).[129] The conductance of the gap junctions is affected by transjunctional voltage, intracellular pH, Ca^{2+} concentrations, phosphorylation state of connexins and extracellular fatty acid composition.[130,131]

The compact node (CN) has been shown to have low level of expression of the major cardiac isoform, Cx43, which is responsible for cell-to-cell communication throughout most of the myocardium, specifically in the atrial and ventricular myocardium.[24,58,59] Hucker et al., reported high level of Cx43 expression in the human INE compared to leftward extension and the upper part of the compact node.[41] However, majority of other studies showed Cx43 to be largely absent from INE.[24,36,132] Cx43 expression in the AV junction appears to be higher in the penetrating or His bundle and the lower part of the CN or lower nodal bundle (LNB).[24,36,132]

The high-conductance Cx40 expression is expressed in the working atrial myocardial tissue (with the exception of rat and rabbit heart).[133,134] Cx40 tends to express higher in the cardiac conduction system in areas where high conductance is required. Thus low level of Cx40 mRNA is seen in the INE.[135] The CN, PB or His bundle and both bundle branches showed high expression of Cx40 mRNA.[135] The pattern of expression of the Cx40 and Cx43 is fitting with fast conduction of action potential in the atrial muscle (~80 cm/s), slower conduction in the INE (~10 cm/s), and very fast conduction in the PB, His bundle, and Purkinje fibers (~150 cm/s).[136] The only exception is the finding of higher expression of Cx40 in the CN, which is known to have slow conduction velocity.

There is evidence that Cx45 is the main connexins responsible for the cell-to-cell conductance in the AVN.[58,124,137] It has been shown that the ultra small conductance Cx30.2 is expressed in the AVN of mice.[138] However, its human counterpart Cx31.9 mRNA and protein is poorly expressed in all tissues of AVJ in humans. It is unlikely, therefore, to be functionally important in humans.[61]

The gene knockout studies in mice shed some more light into connexins function in the AVN. Homozygous knockout of Cx43 and Cx45 is incompatible with survival[139,140], however the heterozygous knockout of Cx43 and Cx45 separately does not show alteration in any electrocardiographic parameters, including the PR interval.[141] The

homozygous loss of Cx40 results in slowing of conduction across the AVN and His purkinje system and/or AV conduction block.[142,143] In addition to this, the homozygous loss of Cx30.2 results in acceleration of conduction across the AVN and His bundle that become normalized if both Cx40 and Cx30.2 is knocked out.[142] A possible explanation for this could be the different location of Cx40 and Cx30.2 in the AVN conduction axis. Another explanation is the heterotypic and/or heteromeric gap junction channels with a combination of both Cx30.2 and Cx40. It has been shown that Cx30.2 can influence voltage-dependent gating in the gap junction channels if co-expressed with other connexins. Cells expressing Cx30.2 with Cx43 or Cx45 exhibited voltage dependent gating intermediate between either connexins alone whereas Cx30.2 dominate the voltage dependence gating if co-expressed with Cx40.[144]

The expression of connexin is also altered if the intercalated discs are affected. Knockout of N-cadherin (the cellular structural protein) has been shown to disrupt the intercalated disc with loss of adherens junctions and desmosomes.[124] Cx43 and Cx40 were rapidly down regulated in the myocardium after the loss of N-cadherin, which was associated with reduction in ventricular conduction velocity. These observations can be important with disease state and ageing as the disruption of the cellular architecture may also contribute towards altered connexins expression.

4.5.2 Methods

4.5.2.1 Immunofluorescence for Cx43 and Cx40

Methodology has been explained in detail in section 4.1. Appendix 1 shows details of the slides selected for immunohistochemistry.

Tissue sections used to measure changes in expression of Cx43 and Cx40 were double labelled. Tissue sections used for Cx43 were also labelled with HCN4. Tissue sections used for Cx40 were also labelled with caveolin3. Caveolin3 is a structural protein that delineates the cell boundary, thus enabled me to identify myocardial cells. The primary antibody against Cx40 was raised in goat and the secondary fluorescent antibody used was anti-goat FITC, which emits green fluorescence. The primary antibody against caveolin3 was raised in mouse and the secondary fluorescent antibody used was anti-mouse Cy3, which emits red fluorescence.

4.5.3 Results

4.5.3.1 Age dependent change in the expression of Cx43

Table 4.5 and Figure 4.11 show the age-related change in the expression of Cx43. The INE and CN have poor expression of Cx43, therefore their signal intensity measurements are not included in the final analysis. The proximal penetrating bundle (PPB) and distal penetrating bundle (DPB)/His bundle showed significant age dependent decrease in Cx43 expression. The comparable high magnification images of both young and old hearts showing Cx43 expression in the AVJ are shown in Figure 4.9.

Table 4.6 and Figure 4.12 show no change with ageing in the expression of Cx43 in different chambers of heart: left atrium, left ventricle, right atrium and right ventricle. The high magnification images of left, right atria and ventricles can be seen in Figure 4.13.

4.5.3.2 Age dependent change in the expression of Cx40

Table 4.7 and Figure 4.14 show change in Cx40 expression with ageing. Cx40 expression tends to increase with age reaching statistical significance in the INE and CN. The low expression of Cx40 is seen in INE as compared to the CN, PPB and His bundle. The Cx40 expression tends to increase with age in the PB and His bundle.

Figure 4.15 shows images of the components of the AVJ. The images of the PPB showed distinct Cx40 negative region in the upper part of PPB and Cx40 positive region in the lower part of PPB. In the distal penetrating bundle i.e., His bundle, this distinction is lost and Cx40 expression becomes homogenous. This pattern of expression remains preserved with ageing. Figure 4.15 also shows caveolin3, which is discussed in section 4.5.

4.5.4 Discussion

The age related changes in the expression of Cx43 and Cx40 across the AVJ showed interesting results. Cx43 expression in the PPB and His bundle decreases with ageing, which correlate with the functional experiments that have been performed in multiple studies.[86,94,96] The functional experiments showed increased AH and HV intervals, increased AV Wenkebach cycle length. These studies were described in section 1.11.3. What is the reason for this reduced Cx43 expression? It could be the results of disruption of cellular architecture that has been seen with ageing in our histology experiments. The loss of intercalated discs as we have described earlier can results in down regulation of Cx43. Our findings of decreased Cx43 expression in the penetrating bundle are similar to the findings of other studies performed on SN node with ageing.

Jones et al.,[145] demonstrate an increase in the Cx43 negative area in the guinea pig SN. Similar findings has been seen in the rats by Yanni et al.,[87] which showed an increase in the volume of the SN lacking Cx43.

The interesting observation in this study is increase in the expression of Cx40 in the INE and CN. In the PPB and His bundle no significant change in the signal intensity as well as in the pattern of expression was observed. Cx40 being the largest conductance channel is expected to decrease with age as the conduction velocity across the AVJ is slower. This increase in Cx40 expression is surprising and may well be the result of heterotypic association with other connexins like Cx30.2 and/or Cx45. As we have described earlier that if Cx40 co-expressed with Cx30.2, the Cx30.2 dominates the voltage dependent gating resulting in decreased conduction across the gap junction channel. The effect of co-expression of Cx40 with Cx45 is not known. I have tried experiments with a Cx45 antibody but signal seen was non-specific.

There was no significant change in Cx43 expression in different heart chambers with ageing although there is a tendency of down regulation of Cx43 with ageing (including both atria and ventricles). Tellez et al.,[86] showed no significant difference in Cx43 mRNA and protein expression with ageing in the right atrium. This is consistent with our findings. The study by Boengler et al.,[146] showed reduction in Cx43 expression with ageing in left ventricular myocardium. However the comparable data in this study is from 4 week old rats to 9 month old rats, which is different to our study groups. (Our study has young rats 3 months old and old rats 24 months old).

Table 4.5: Statistical analysis of Cx43 expression in young and old heart's AVJ. Statistically significant results are shown in red.

Cx43 expression	Proximal penetrating bundle (PB)	Distal penetrating bundle (His)
Young hearts (Mean and SEM)	19.65±0.82	22.01±2.80
Old hearts (Mean and SEM)	15.55±1.09	17.97±0.50
p-value and 95% confidence interval	0.005 (-6.87 to -1.31)	0.027 (-7.57 to -0.49)

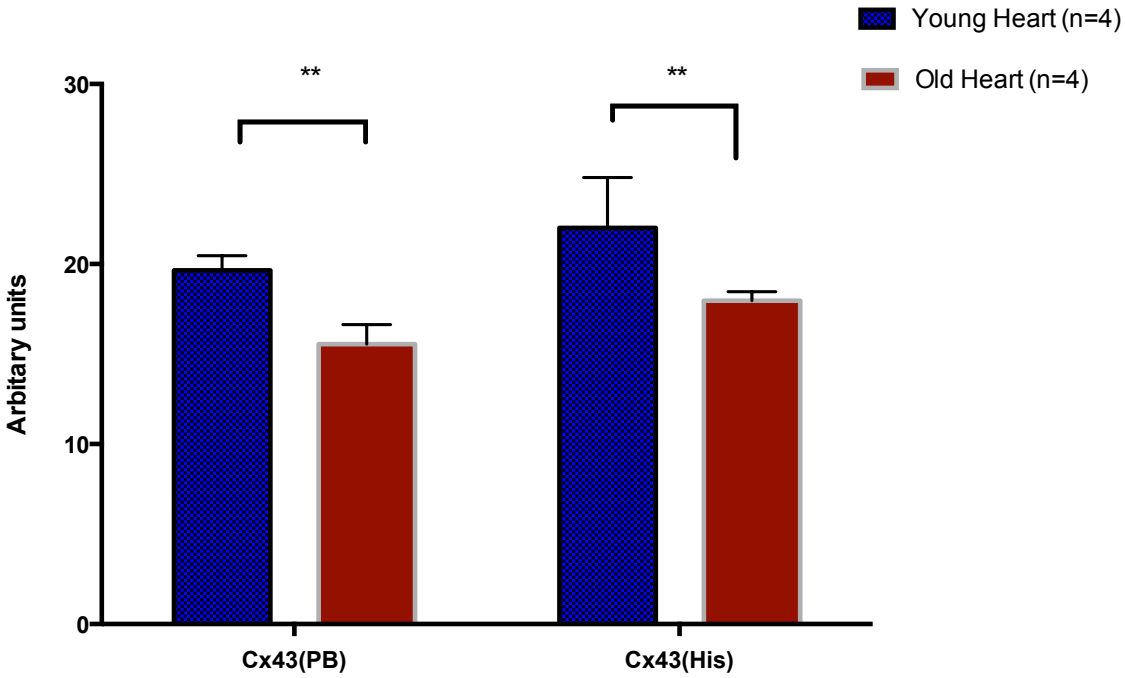

Figure 4.11: Changes in Cx43 expresson in AVJ with ageing. Proximal penetrating bundle (PB), distal penetrating bundle or His bundle. Signal intensity measured with Volocity software. Mean±SEM are shown, ** $p < 0.05$.

Table 4.6: Statistical analysis of Cx43 expression in young and old heart's working myocardium

Cx43 expression	Left Ventricle	Left atrium	Right Ventricle	Right atrium
Young hearts (Mean and SEM)	41.22±2.83	36.27±1.52	44.18±2.12	40.05±1.89
Old hearts (Mean and SEM)	38.76±2.25	33.33±1.75	43.31±4.43	34.44±3.43
p-value and 95% confidence interval	0.52 (-10.33 to 5.41)	0.42 (-6.83 to 2.96)	0.85 (-10.8 to 8.81)	0.16 (-13.75 to 2.52)

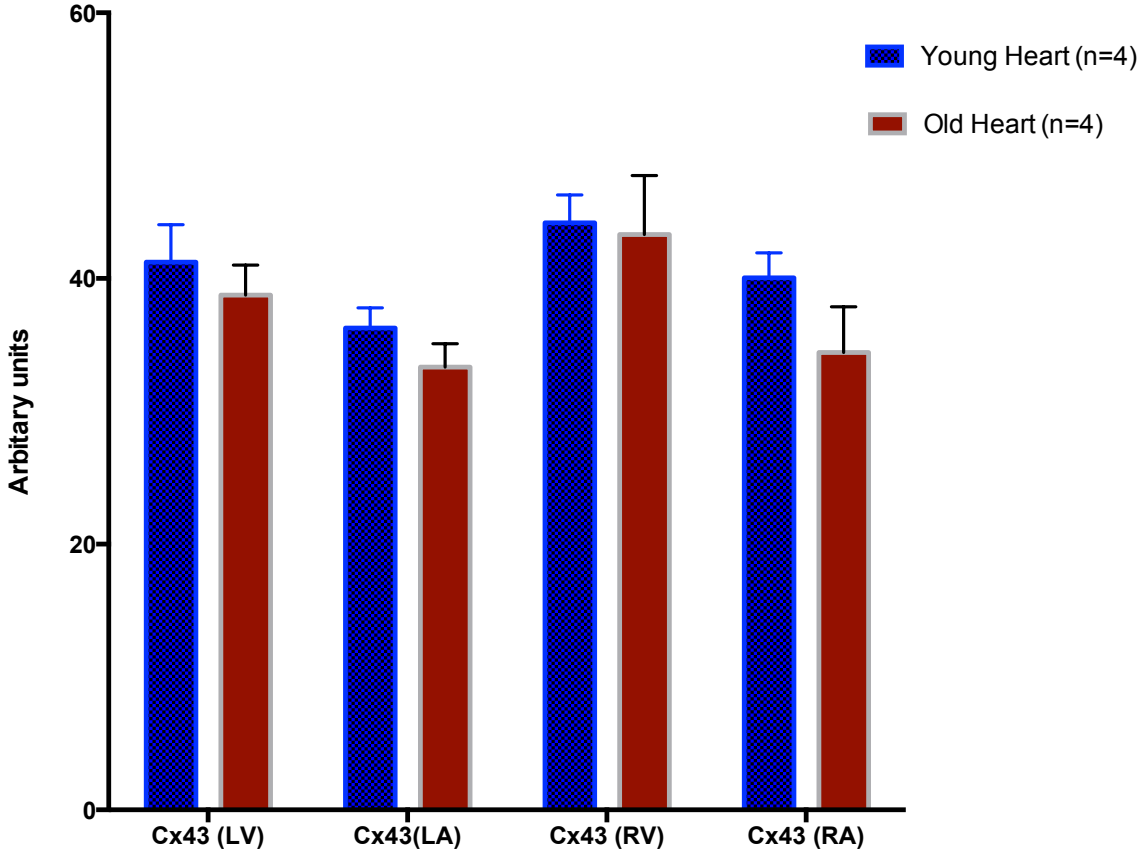

Figure 4.12: Changes in Cx43 expresson in different heart chambers with ageing
Left ventricle (LV), left atrium (LA), right ventricle (RV), right atrium (RA). Signal intensity measured with Volocity software. Mean ±SEM are shown, ** $p < 0.05$.

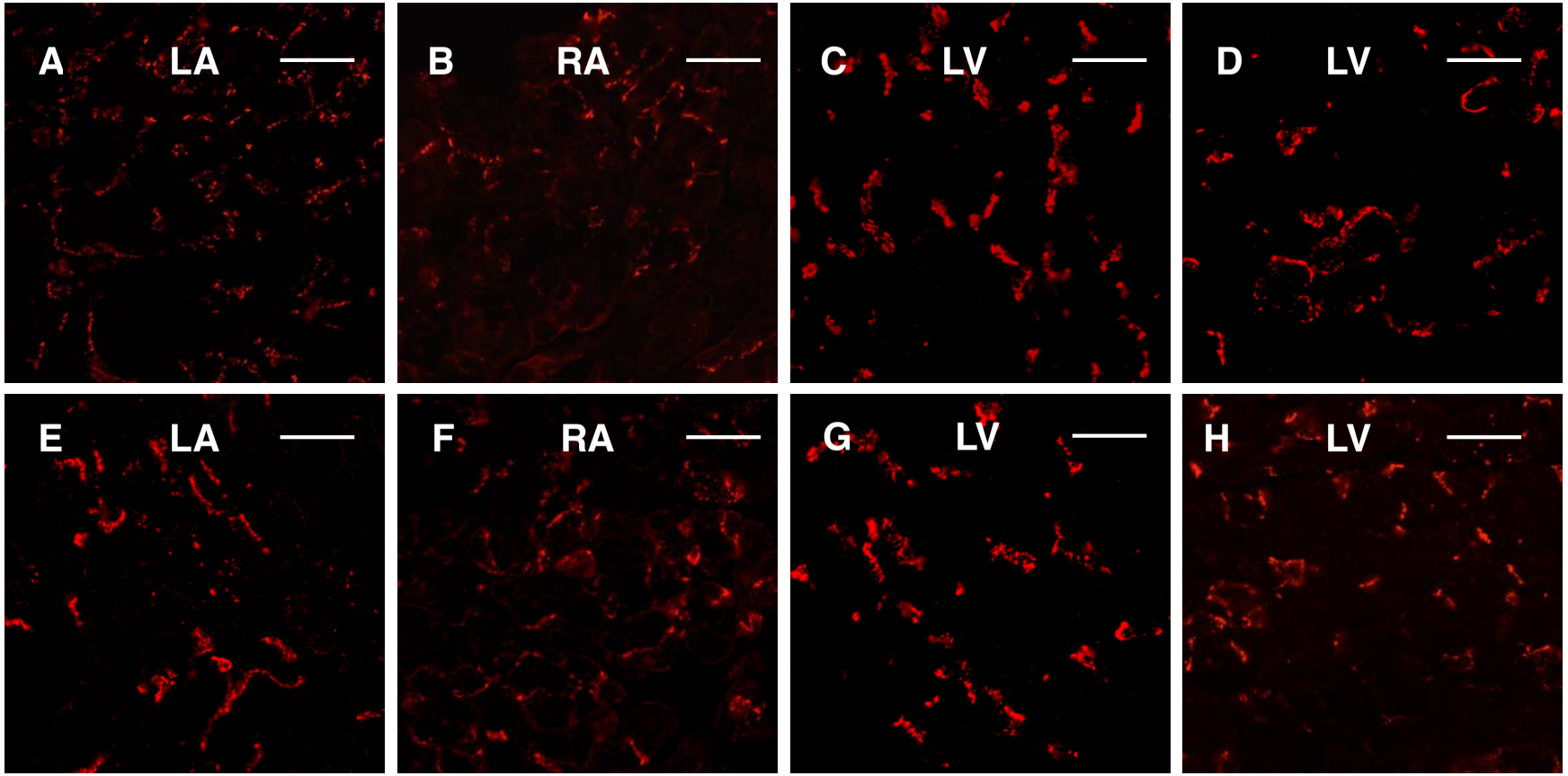

Figure 4.13: Confocal microscope high magnification images of the AVJ with Cx43 (red) immunolabelling. Left atrium (LA), right atrium (RA), left ventricle (LV), right ventricle (RV). Top panel shows the working myocardium in young hearts and bottom panel shows the working myocardium in old heart. Bar =20 μm

Table 4.7: Statistical analysis of Cx40 expression in young and old hearts AVJ. Statistically significant results are shown in red.

Cx40 expression	Inferior nodal extension (INE)	Compact node (CN)	Proximal penetrating bundle (PB)	Distal penetrating bundle (His)
Young hearts (Mean and SEM)	3.08±0.67	2.21±1.34	6.99±3.01	6.93±3.16
Old hearts (Mean and SEM)	5.62±0.53	8.61±0.97	8.38±1.61	10.01±1.25
ρ-value and 95% confidence interval	0.01 (0.67 to 4.39)	0.005 (2.42 to 10.45)	0.13 (-9.6 to 61.56)	0.28 (-2.82 to 8.97)

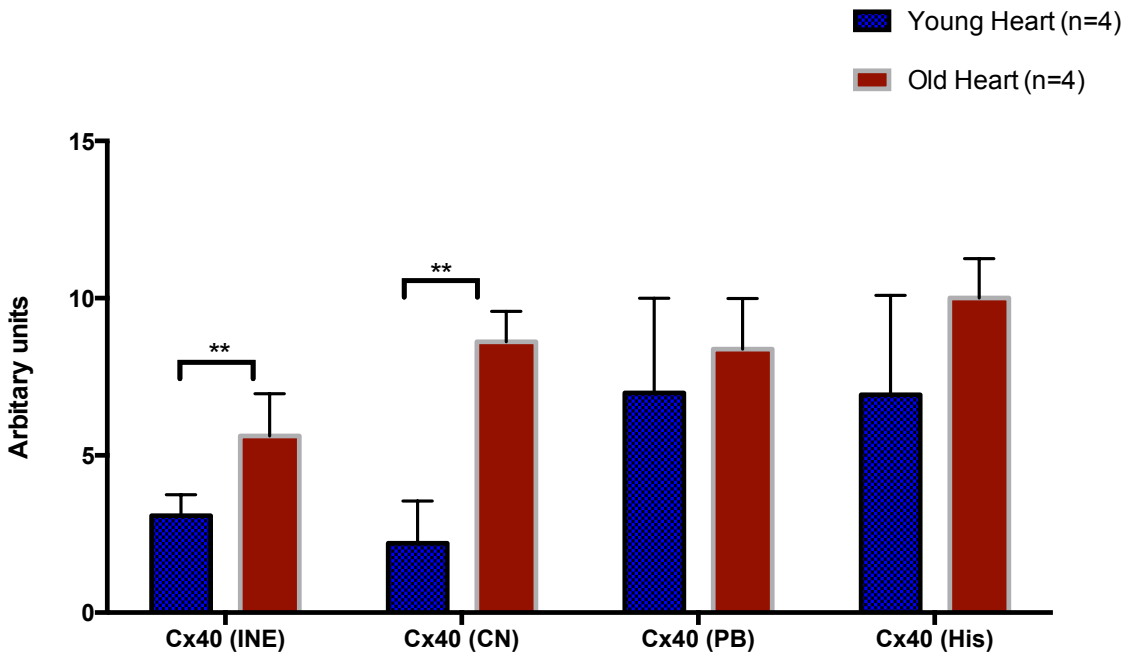

Figure 4.14: Changes in Cx40 expresson in AVJ with ageing
Inferior nodal extension (INE), compact Node (CN), proximal penetrating bundle (PB), distal penetrating bundle or His bundle. Signal intensity measured with Volocity software. Mean±SEM are shown, ** $p < 0.05$.

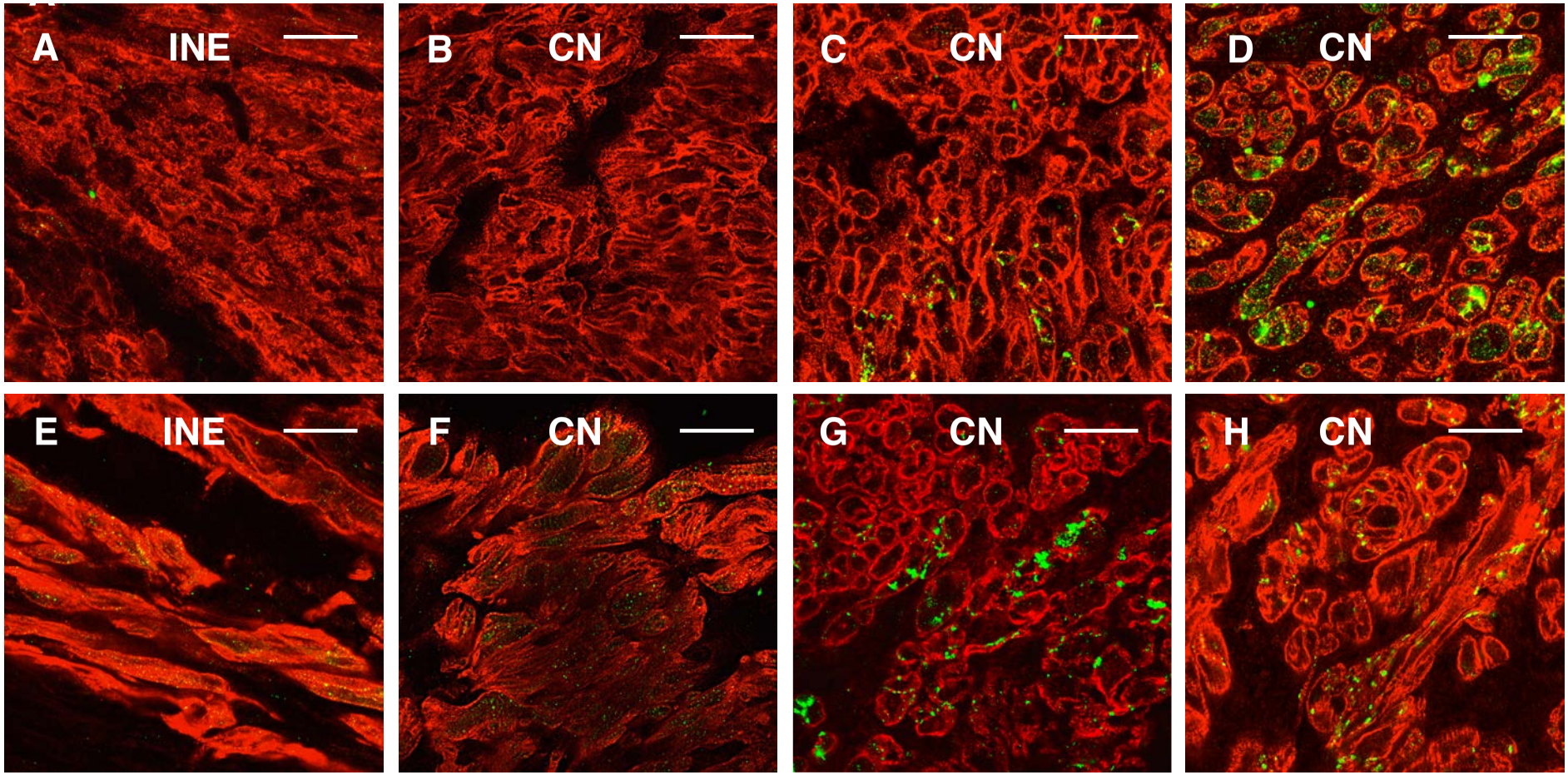

Figure 4.15: Confocal microscope high magnification images of the AVJ with Cx40 (green) and Cav3 (red) immunolabelling. Inferior nodal extension (INE), compact node (CN), proximal penetrating bundle (PPB), distal penetrating bundle/His bundle (His). Top panel shows the AVJ components in young hearts and bottom panel shows the AVJ components in old heart. Cx40 expression increase with ageing as shown in the INE and CN. Lower right hand corner of image A show the right atrial tissue with Cx43 expression. Bar=20μm

4.6 Changes in the expression of structural proteins and cellular diameter in the AVJ with ageing

4.6.1 Introduction

Structural proteins including caveolin3 and alpha actinin were used to identify the age-associated structural changes in the AVJ. The measurement of the signal intensity was performed to assess up or down regulation of these proteins with ageing. These proteins were also used to confirm the changes in the cellular architecture and cell diameter noticed in histology experiments described in chapter 3.

The plasma membrane or cell surface membrane is a mixture of proteins, cholesterol and lipids including glycolipids and sphingolipids. The cholesterol and sphingolipids combine with each other to form *lipid rafts or liquid ordered microdomains*. Caveolae are a subset of these lipid rafts and caveolins are major proteins that interact with cholesterols to form caveolae. Caveolae are 50-100 nm in size, shaped as invaginated flask shaped structures of plasma membrane and are present in most cell types including muscle cells.[147,148] The structure of caveolae is further explained in Figure 4.16. Several ion channels including HCN channels, L-type Ca^{2+} channels, Na^{+} channels and others are localised in caveolae. This subcellular localization to caveolae may allow the regulation of these channels.

Six different subtypes of caveolin have been identified that are encoded by three separate genes (Cav1, Cav2, Cav3). Caveolin3 is a major protein (encoded by Cav3) expressed specifically in myocytes and is critical to the formation of caveolae in these cells. Cav3 is present in cardiomyocytes as well as skeletal muscle and smooth muscle cells.[149] Mutation in Cav3 results in autosomal limb girdle muscular dystrophy.[148] Caveolae are abundantly present in ventricular, atrial and nodal cells. Cav3 has been identified as essential for the formation of caveolae in cardiomyocytes based on knockout mice studies.[148]

Alpha actinin is a universally expressed protein that is a primitive molecule within a family of actin cross-linking proteins.[151] The muscle and non-muscle isoforms of alpha actinin has been characterised. The non-muscle form binds to actin in a calcium sensitive manner, whereas the actin biniding of the muscle isoform is not calcium dependent. The alpha actinin is found at Z disk in the sarcomere where it cross-links the actin filaments to adjacent sarcomere. Figure 4.17 shows the structure and location of alpha actinin.[151,152]

Alpha actinin has also been closely associated with integrins and thus forms an important part of the cellular cytoskeleton. The deficiency of alpha actinin isoforms has been described in the literature resulting in skeleletal myopathy and also right ventricular and dilated cardiomyopathy.[153,154]

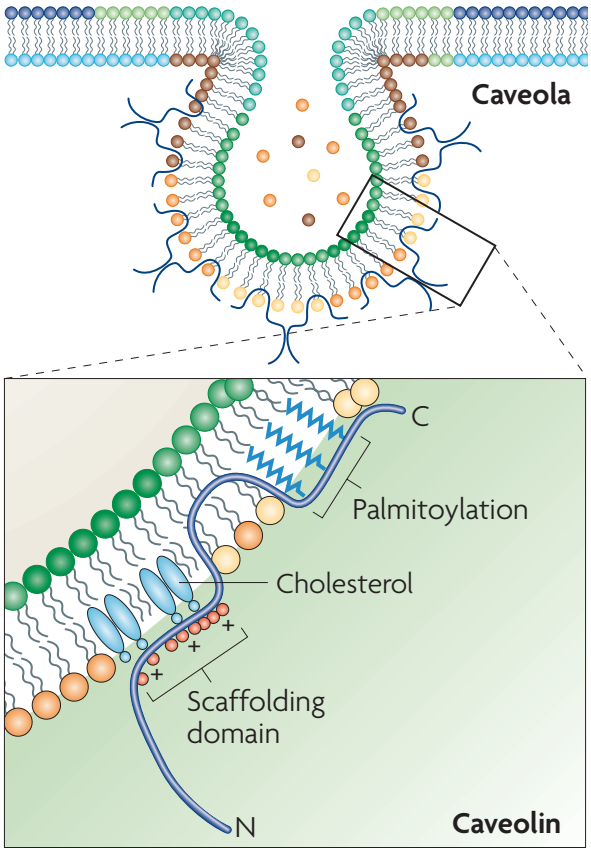

Figure 4.16: The structure of caveola and caveolin. This indicates how caveolin is inserted into the caveolar membrane, with the N and C termini facing the cytoplasm and a putative 'hairpin' intramembrane domain embedded within the membrane bilayer. The scaffolding domain, a highly conserved region of caveolin, might have a role in cholesterol interactions through conserved basic (+) and bulky hydrophobic residues (red circles). The C-terminal domain, which is close to the intramembrane domain, is modified by palmitoyl groups that insert into the lipid bilayer. The complex structures that are formed by interconnected caveolae can occupy a large area of the plasma membrane.[147]

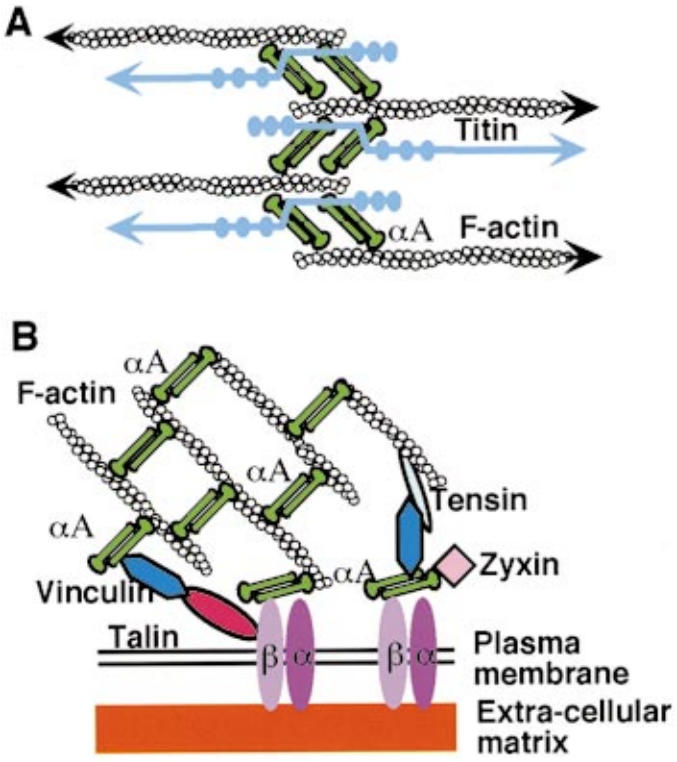

Figure 4.17: Domain structure of α-actinin and its function in the sarcomeric Z Disk and its focal contacts. (A) In the muscle Z disk, α-actinin cross-links antiparallel actin filaments from adjacent sarcomeres. Titin acts as a molecular ruler for the sarcomere and interacts with two different parts of α-actinin, at the center of the α-actinin rod and with the calmodulin-like domain. (B) A simplified representation of a focal contact showing α-actinin linking the actin cytoskeleton to membrane-associated structures. Focal contacts are points where cultured cells are attached tightly to the extracellular matrix via transmembrane receptors such as integrins (α and β in figure). α-Actinin has been shown to interact with β integrins as well as with the focal contact components such as vinculin and zyxin. Thus, it may connect integrins to actin filaments either directly or indirectly, involving proteins such as talin.[155]

4.6.2 Methods

Methodology has been explained in detail in section 4.1.

4.6.3 Results

4.6.3.1 Age related changes in the expression of Caveolin3 and alpha actinin.

Table 4.8 and Figure 4.18 shows changes in expression of alpha actinin with ageing in the AVJ. The alpha actinin expression is down regulated with ageing in the INE, whereas in the CN it is upregulated. These results are statistically significant. There is also a modest increase in the expression of alpha actinin with ageing in the PPB and DPB. No significant difference has been observed in the alpha actinin expression with ageing in the working myocardium (Table 4.9 and Figure 4.20). Figure 4.19 shows high magnification images of alpha actinin corresponding with each component of the AVJ. The striated pattern of labelling appears to be disrupted with ageing.

Table 4.10 and Figure 4.21 shows changes in Cav3 in the AVJ with ageing. There is significant down regulation of the channel expression with ageing in the His bundle. In the working myocardium down regulation is only seen in the right atrium. The results are summarised for working myocardium in Table 4.11 and Figure 4.22.

Figure 4.25 show the labelling of Cav3 within cell membrane in all regions of the heart. The cellular diameter was measured from 20 cells in transverse orientation in the high magnification images (63X) for the components of AVJ (Table 4.12 and Figure 4.23) and from 50 cells in the heart chambers (Table 4.13 and Figure 4.24). Hypertrophy is observed across all regions of the AVJ and atrioventricular conduction axis and also in all chambers of the heart with ageing.

4.6.4 Discussion

The pattern of expression of alpha actinin and caveolin3 confirmed the disorganised cellular architecture with ageing that has been observed with Masson's trichome stain described in chapter 3. The cellular architecture in the young INE, CN, PB and His bundle are much regular as compared with ageing hearts. The cell size is also increase with ageing confirming cellular hypertrophy. The disruption of cellular architecture in the AVJ may well be associated with the prolongation of the AV conduction (discussed in chapter 2) and the changes in the connexins discussed early in this chapter. It has been noted that when the cytoskeletal proteins such as integrins are disturbed decrease in the expression of Cx43 and Cx40 has been observed.[156]

Table 4.8: Statistical analysis of Alpha actinin expression in young and old hearts AVJ. Statistically significant results are shown in red.

Alpha actinin expression	Inferior nodal extension (INE)	Compact node (CN)	Proximal penetrating bundle (PB)	Distal penetrating bundle (DPB or His)
Young hearts (Mean and SEM)	66.50±7.71	60.71±1.40	57.86±7.87	37.93±6.27
Old hearts (Mean and SEM)	41.97±4.90	72.12±2.34	65.90±10.00	55.86±11.43
p-value and 95% confidence interval	0.04 (-48.80 to -0.24)	0.007 (4.19 to 18.63)	0.56 (-22.41 to 38.49)	0.18 (-10.90 to 46.84)

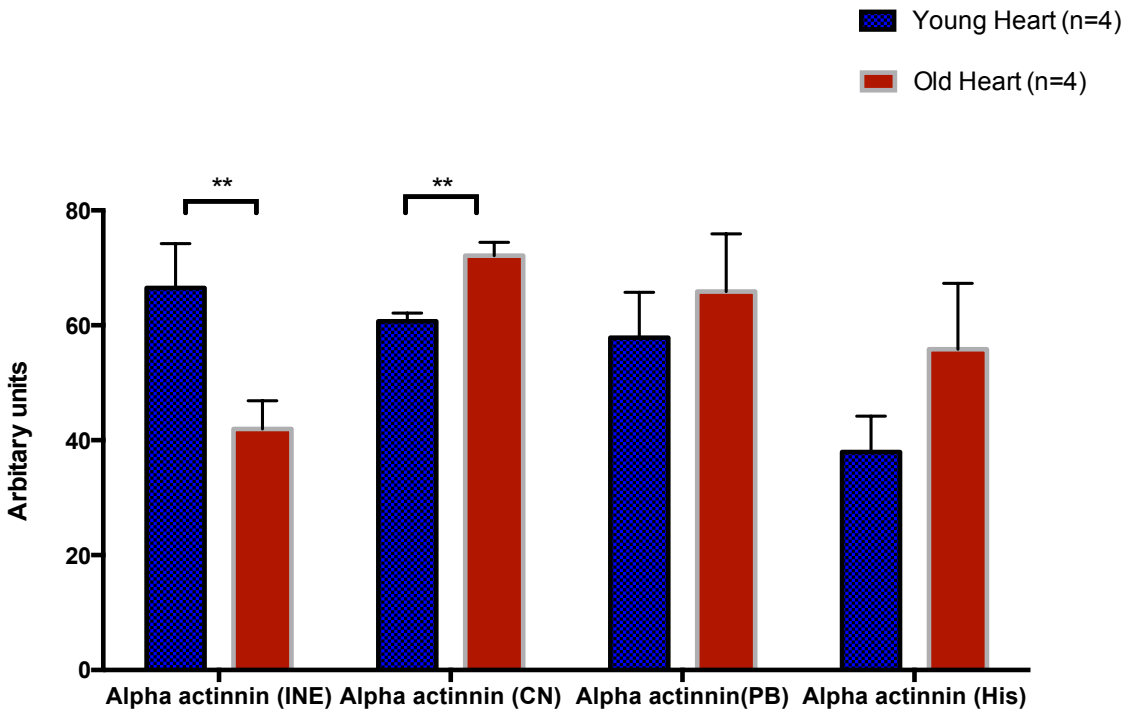

Figure 4.18: Changes in Alpha actinin expression in the AVJ with ageing
Inferior nodal extension (INE), compact Node (CN), proximal penetrating bundle (PB), distal penetrating bundle or His bundle. Signal intensity measured with Volocity software. Mean±SEM are shown ** $p < 0.05$.

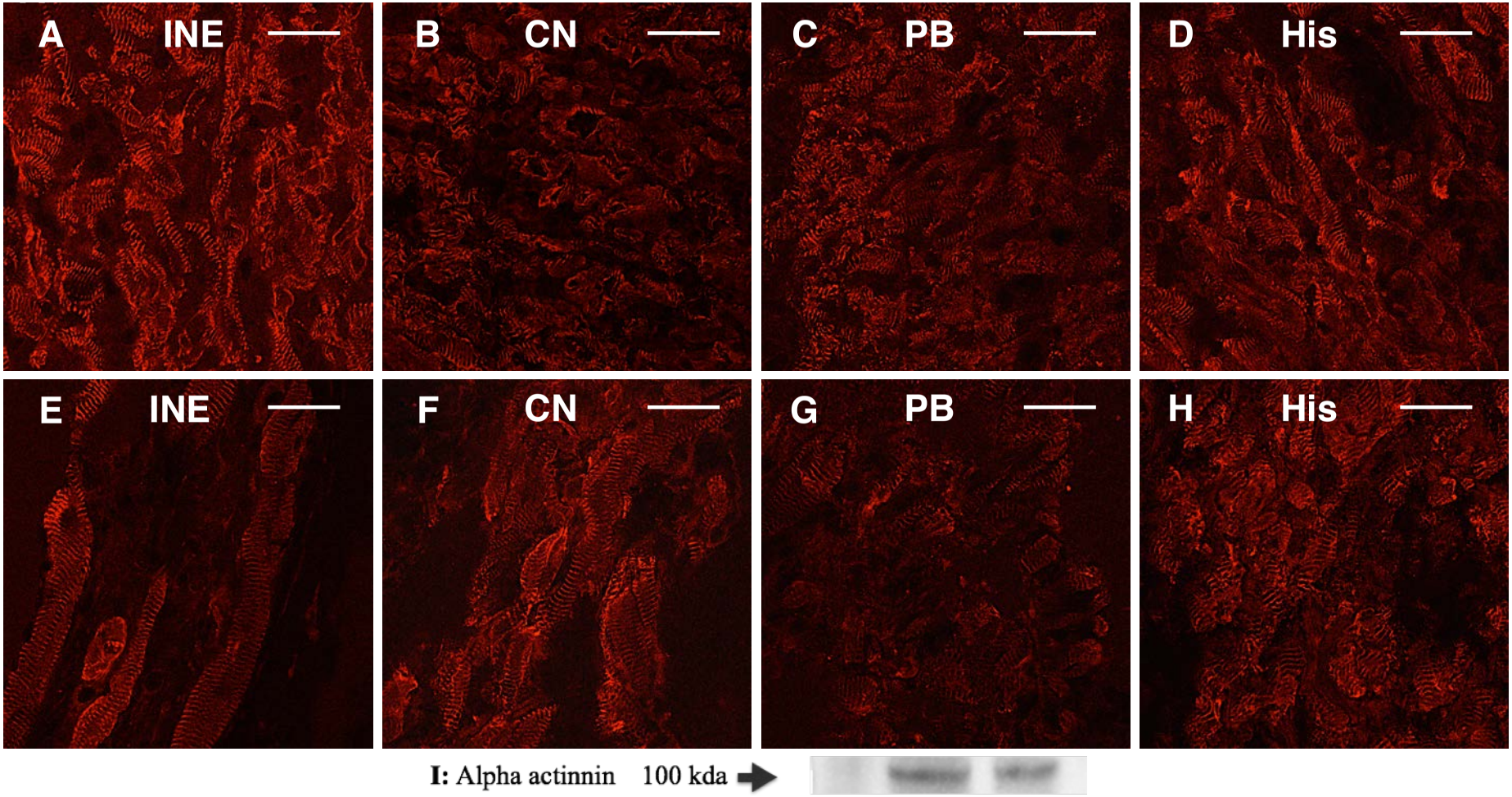

Figure 4.19: Confocal microscope high magnification images of the AVJ with alpha actinin (red) immunolabelling. Inferior nodal extension (INE), compact node (CN), proximal penetrating bundle (PPB), distal penetrating bundle/His bundle (His). Top panel shows the AVJ components in young hearts and bottom panel shows the AVJ components in old heart. Bar=20 μm. Western blot result is shown in Image I.

Table 4.9: Statistical analysis of Alpha actinin expression in young and old hearts working myocardium.

Alpha-actinin expression	Left Ventricle	Left atrium	Right Ventricle	Right atrium
Young hearts (Mean and SEM)	63.61±6.73	75.78±6.86	84.58±11.47	83.02±4.39
Old hearts (Mean and SEM)	55.05±6.73	62.26±6.80	78.88±4.48	95.34±10.14
p-value and 95% confidence interval	0.366 (-28.29 to 11.16)	0.196 (-35.02 to 7.97)	0.59 (-28.17 to 16.76)	0.26 (-11.13 to 35.77)

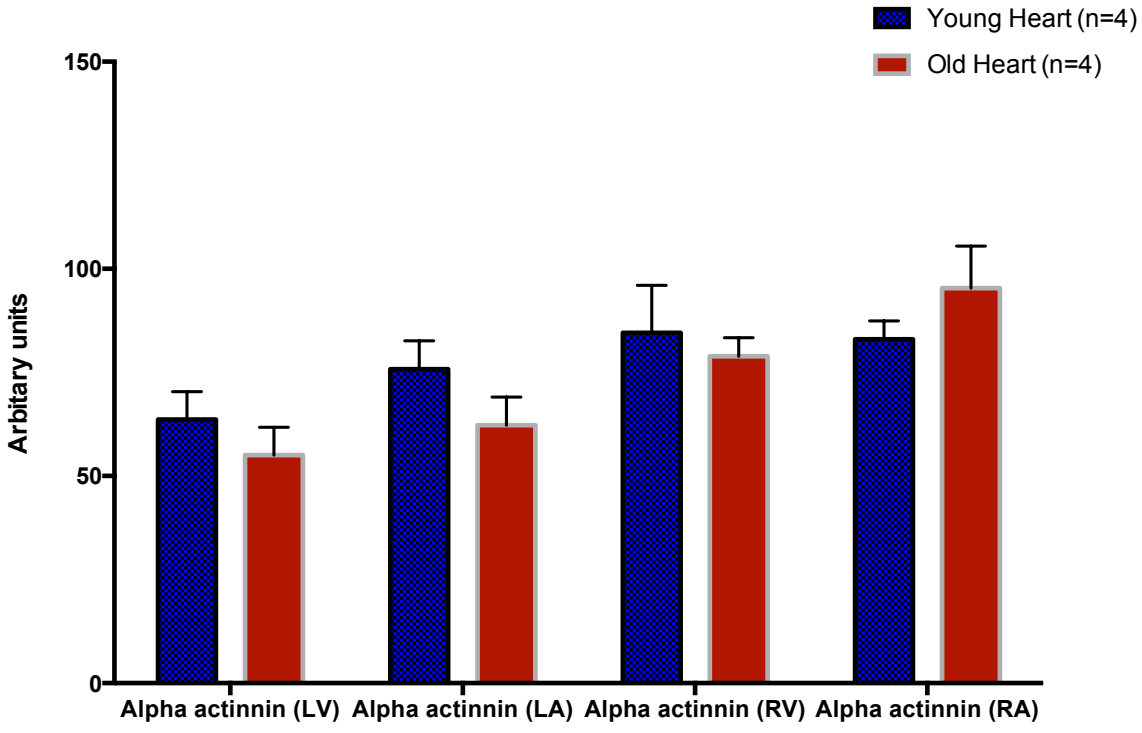

Figure 4.20: Changes in Alpha actinin expression in different heart chambers with ageing.
Left ventricle (LV), left atrium (LA), right ventricle (RV), right atrium (RA). Signal intensity measured with Volocity software. Mean ±SEM are shown.

Table 4.10: Statistical analysis of Cav3 expression in young and old hearts AVJ. Statistically significant results are shown in red.

Caveolin 3 expression	Inferior nodal extension (INE)	Compact node (CN)	Proximal penetrating bundle (PB)	Distal penetrating bundle (His)
Young hearts (Mean and SEM)	96.62±7.13	94.90±10.41	77.11±7.34	84.88±8.04
Old hearts (Mean and SEM)	94.38±3.98	75.10±5.59	103.09±17.74	53.95±8.71
ρ-value and 95% confidence interval	0.774 (-18.93 to 14.43)	0.16 (-49.48 to 9.9)	0.135 (-9.6 to 61.26)	0.035 (-59.52 to -2.33)

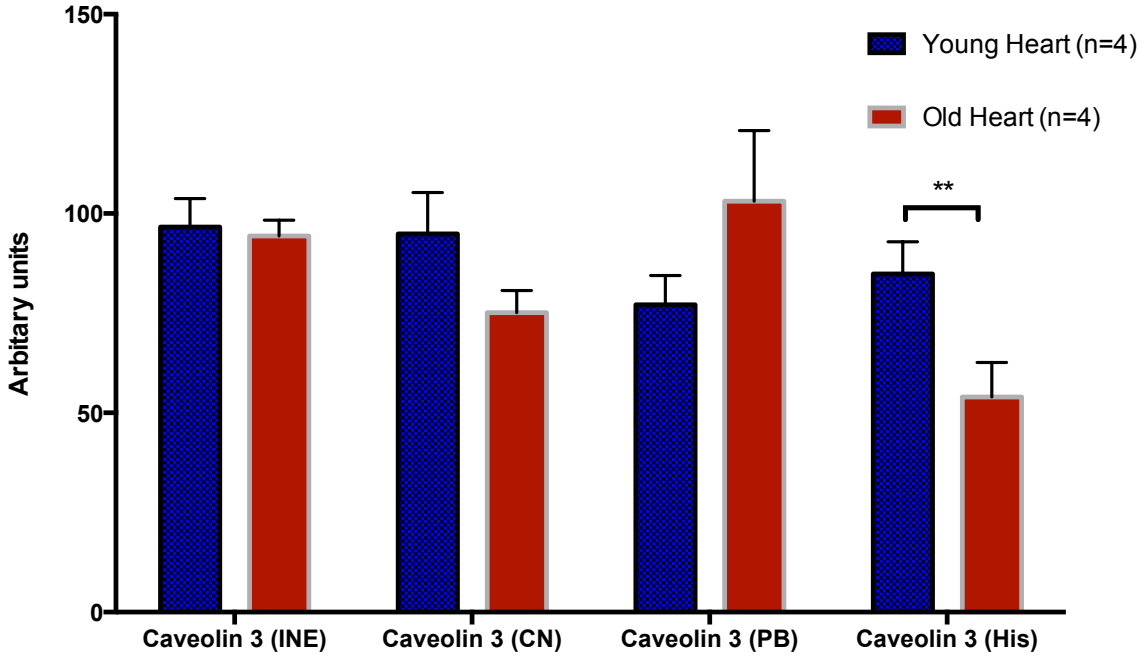

Figure 4.21: Changes in Caveolin 3 expresson in AVJ with ageing. Inferior nodal extension (INE), compact Node (CN), proximal penetrating bundle (PB), distal penetrating bundle or His bundle. Signal intensity measured with Volocity software. Mean ±SEM are shown, ** p <0.05.

Table 4.11: Statistical analysis of Caveolin3 expression in young and old hearts working myocardium. Statistically significant results are shown in red.

Caveolin3 expression	Left Ventricle	Left atrium	Right Ventricle	Right atrium
Young hearts (Mean and SEM)	81.83±7.11	94.78±7.40	87.46±7.90	98.96±7.38
Old hearts (Mean and SEM)	70.26±5.40	73.33±6.97	71.80±5.29	63.10±8.72
p-value and 95% confidence interval	0.21 (-30.39 to 7.25)	0.068 (-44.57 to 1.67)	0.11 (-35.39 to 4.08)	0.005 (-59.53 to -12.17)

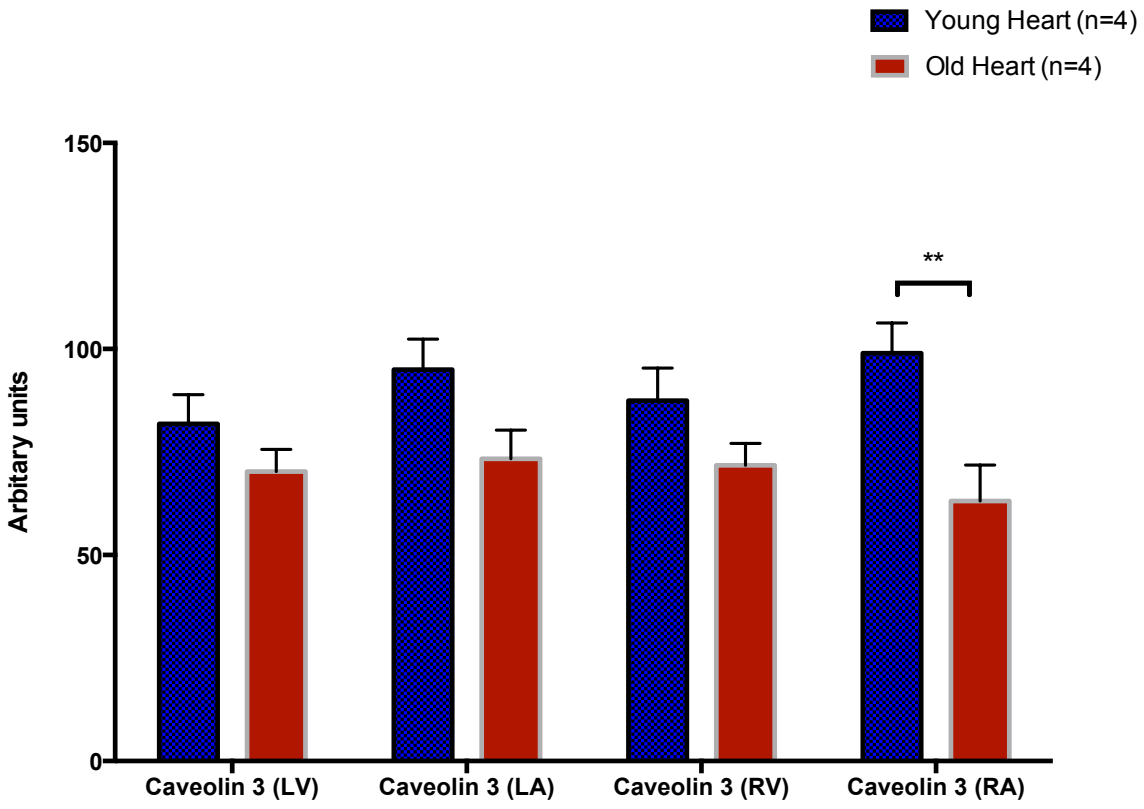

Figure 4.22: Changes in Caveolin 3 expresson in different heart chambers with ageing. Left ventricle (LV), left atrium (LA), right ventricle (RV), right atrium (RA). Signal intensity measured with Volocity software. Mean ±SEM are shown, ** p <0.05.

Table 4.12: Statistical analysis of cellular diameter (µm) in young and old hearts AVJ. 20 cells were measured from each region of the AVJ in four hearts. Statistically significant results are shown in red.

Cellular diameter (µm)	Inferior nodal extension (INE)	Compact node (CN)	Proximal penetrating bundle (PB)	Distal penetrating bundle (DPB or His)
Young hearts (Mean and SEM)	8.29±0.42	7.31±0.25	7.10±0.19	6.99±0.26
Old hearts (Mean and SEM)	13.19±0.82	8.83±2.69	9.25±0.25	7.97±0.16
p-value and 95% confidence interval	0.0001 (3.2 to 6.8)	0.005 (0.48 to 2.56)	0.0001 (1.49 to 2.80)	0.002 (0.38 to 1.58)

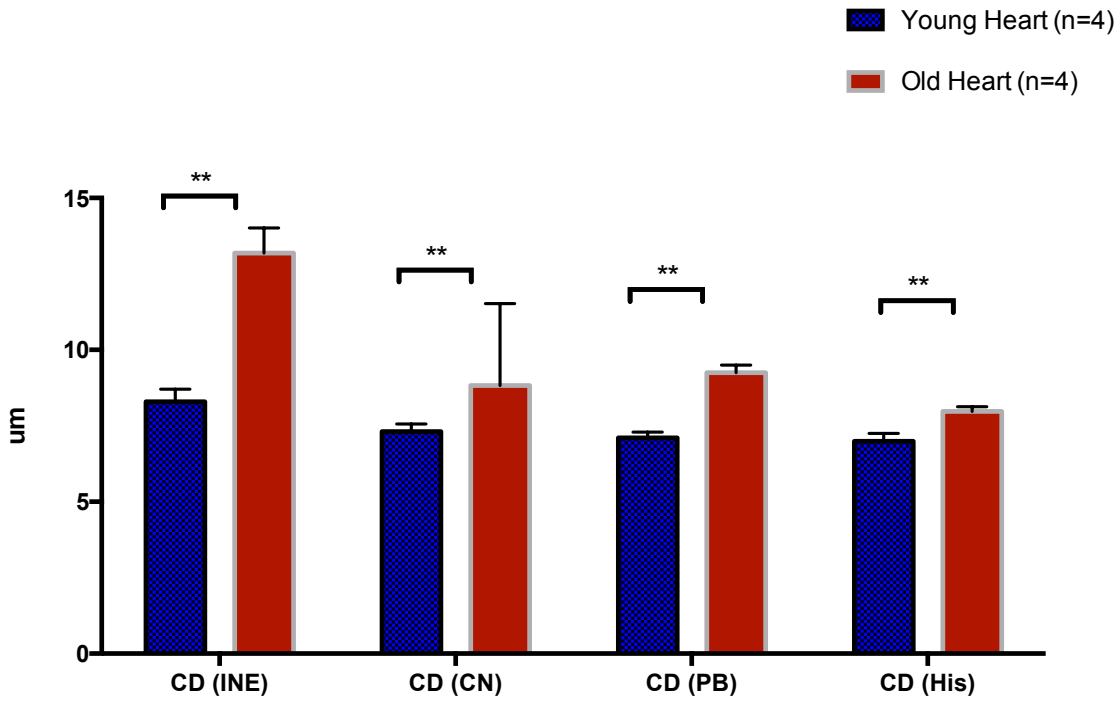

Figure 4.23: Changes in cellular diameter (µm) in AVJ with ageing.
Inferior nodal extension (INE), compact node (CN), proximal penetrating bundle (PB), distal penetrating bundle or His bundle (His), cellular diameter (CD). Mean ±SEM are shown. ** $p < 0.05$

Table 4.13: Statistical analysis of cellular diameter (µm) in young and old hearts working myocardium. 50 cells were measured from each heart. Statistically significant results are shown in red.

Cellular diameter(µm)	Left Ventricle	Left atrium	Right Ventricle	Right atrium
Young hearts (Mean and SEM)	16.25±0.30	10.13±0.19	15.21±0.31	10.31±1.71
Old hearts (Mean and SEM)	19.04±0.34	15.17±0.34	19.38±0.30	14.23±3.38
p-value and 95% confidence interval	0.0001 (1.87 to 3.71)	0.0001 (4.28 to 5.78)	0.0001 (3.29 to 5.03)	0.0001 (2.81 to 5.02)

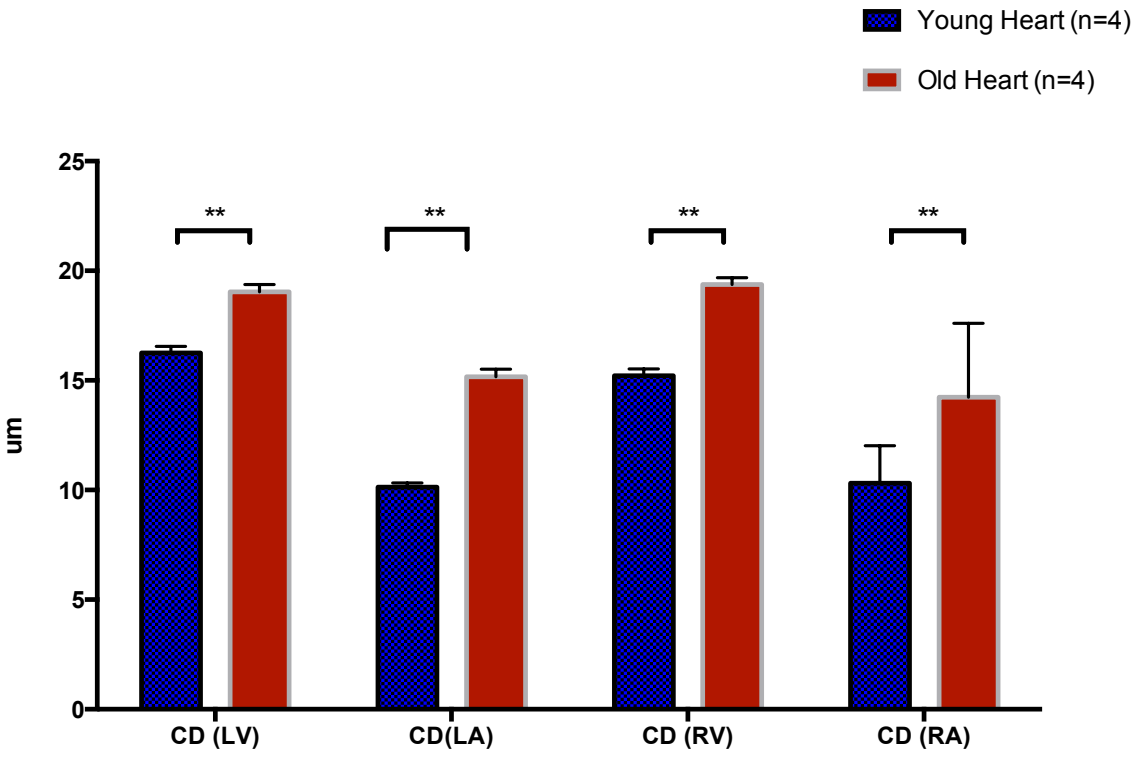

Figure 4.24: Changes in celluar diameter (µm) in different heart chambers with ageing. Left ventricle (LV), left atrium (LA), right Ventricle (RV), right atrium (RA), cellular diameter (CD). Signal intensity measured with Volocity software. Mean ±SEM are shown. ** p <0.05.

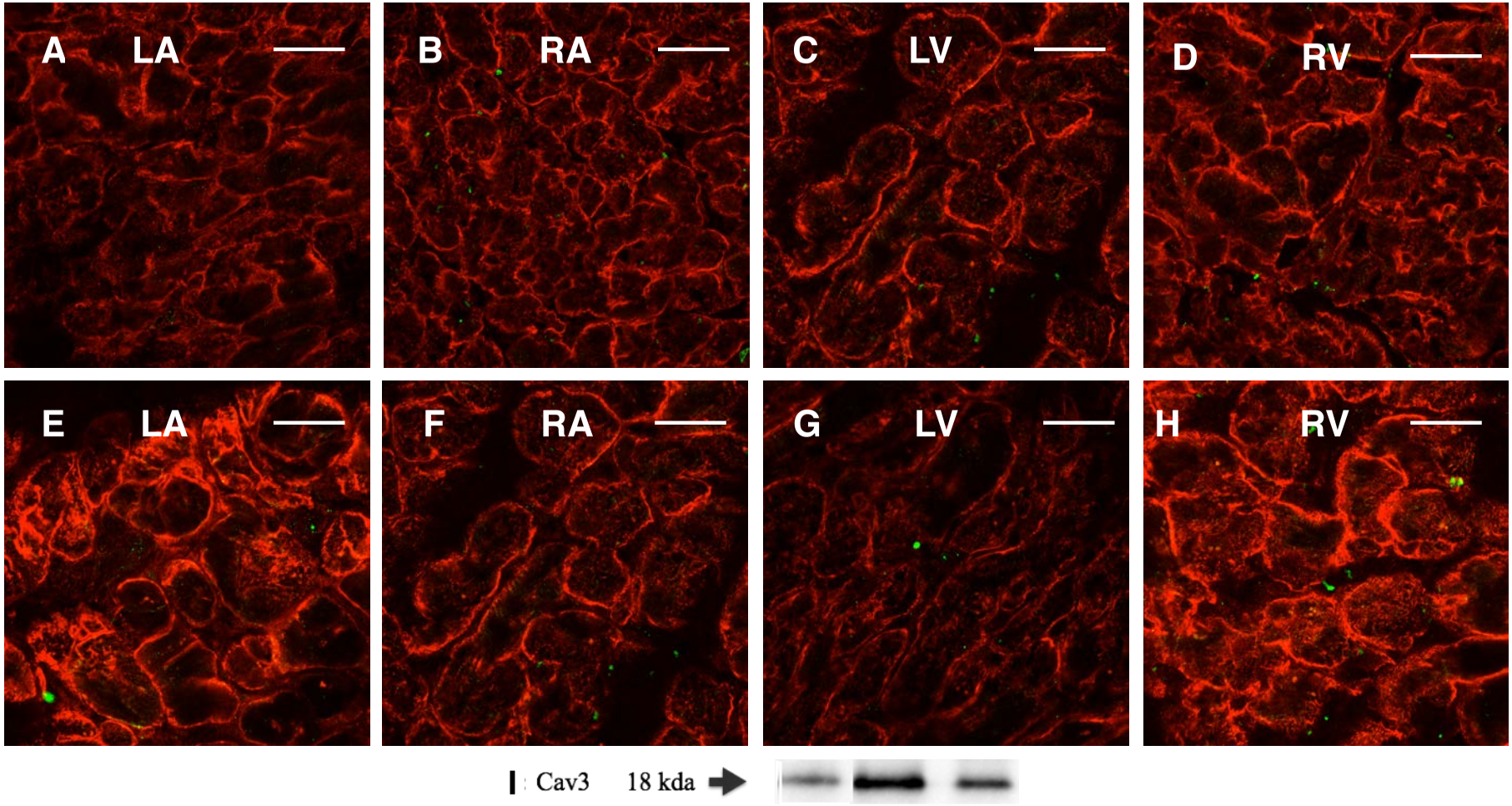

Figure 4.25: Confocal microscope high magnification images of different chamber of the heart with Cav1.3 (red) immunolabelling. Left atrium (LA), right atrium (RA), left ventricle (LV), right ventricle (RV). Top panel shows the working myocardium in young hearts and bottom panel shows the working myocardium in old heart. Bar=20 µm. Western blot experiment on left ventricle tissue with molecular weight is shown in Image I.

4.7 Changes in the expression of $Na_v1.5$ in the AVJ with ageing

4.7.1 Introduction

Cardiac sodium channels are essential for action potential propagation from SN to the ventricular muscle. Cardiac Na^+ channels are transmembrane proteins consisting of α and β subunits. There are four β subunits and they are all expressed in the heart. The β subunits modulate channel gating, interact with the extracellular matrix and function as cell adhesion molecules.[157] The α-subunit is the principal component and is responsible for channel gating and has essential elements to control the channel function.

$Na_v1.5$ is the principal α subunit in the heart that is encoded by SCN-5a gene. It is responsible for inward sodium current (I_{Na}) causing first phase of action potential, resulting in rapid depolarisation of the myocardium. $Na_v1.5$ like the other voltage gated sodium channel is formed of four homologous domains. Each domain is made up of six transmembrane domains (S1-S6) and region (S5-S6 pore loop) that control ion selectivity and permeation. Figure 4.26 describe the $Na_v1.5$ ion channel in further detail.

Yoo et al., performed a comprehensive study of the localization of Na^+ channels isoforms in the AVJ in rats. The study showed protein expression via immunohistochemistry and concluded that $Na_v1.5$ was abundant in the atrial and ventricular myocardium and left bundle branch, it was present at a reduced level in the INE and transitional layer but absent in the CN and penetrating bundle.[45] However, Greener et al., on the rabbit AVN showed that $Na_v1.5$ mRNA is less abundant in the INE as compared to atrial muscle but it tends to be abundant in the penetrating bundle.[24] In a human study, there was lower expression of $Na_v1.5$ in the INE and CN as compared to the penetrating bundle.[135] In essence, the findings of all three studies showed lower expression of $Na_v1.5$ in the INE and CN in the AVJ as compared to atrial and ventricular muscle. However, $Na_v1.5$ was not completely absent in these tissues.

The homozygous gene knockout study of SCN5a is not possible as it is essential for survival, however the heterozygous knockout of SCN5a has been performed in mice.[114] The studies on heterozygous SCN5a deficient mice showed normal survival and functional studies showed PR interval prolongation together with increased in AVNERP. The study by Van Veen et al., showed general slowing of conduction across all four chambers of the heart especially in aged mice heterozygously deficient in SCN5a,

unfortunately the conduction velocity across the AVN was not performed in this study.[156] In addition, the SCN5a mutation is known to be associated with AV conduction block.[70,72]

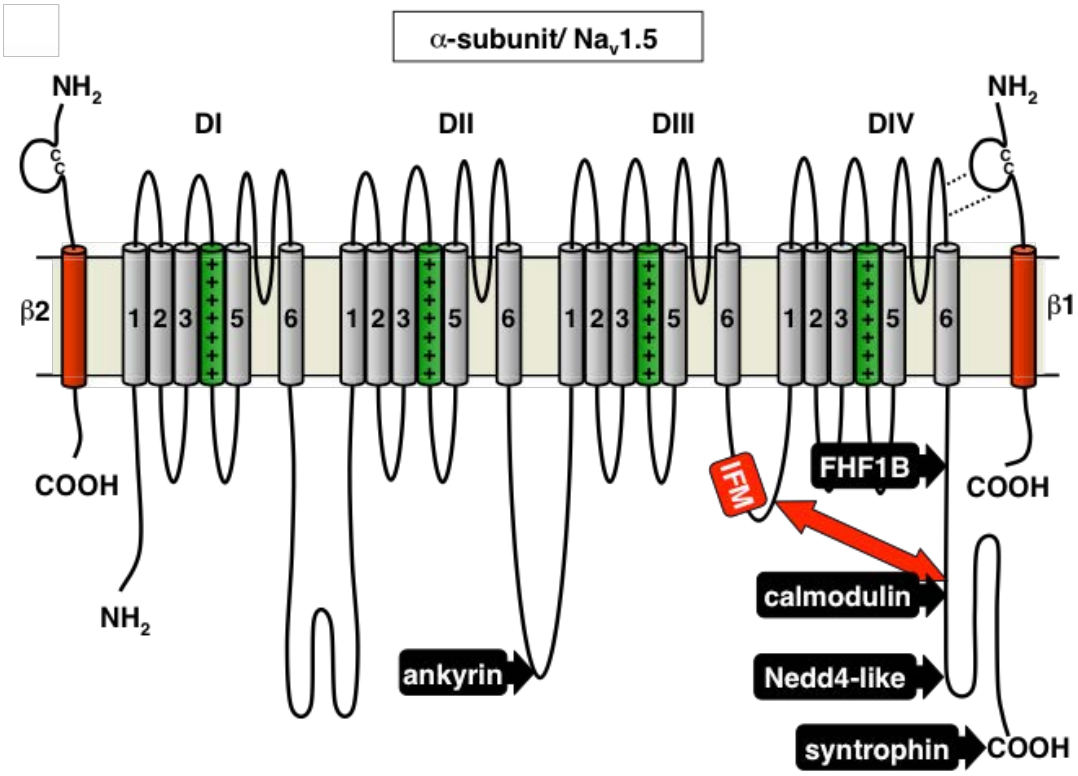

Figure 4.26: Schematic representation of the α subunit of $Na_v1.5$, the two associated β subunits, and interacting proteins. The predicted membrane topology of the β subunit of Nav1.5 is illustrated together with the 1 and 2 subunits (in red). DI–DIV indicate the four homologous domains of the α subunit; segments 5 and 6 are the pore-lining segments and the S4 helices (green) serve as voltage sensors. The extracellular domain of the β1 subunit, comprising an immunoglobulin-like fold, interacts with the α-subunit loop as shown (dotted lines); the β2 subunit binds covalently to the α-subunit via a disulfide bound. The isoleucine- phenylalanine-methionine (IFM) residues are key amino acids for fast inactivation gating. Five proteins that have been reported to interact with Nav1.5 are represented schematically with their approximate binding sites. The red arrow indicates the intramolecular interaction between the III–IV linker and the C terminus (C-T) domain. Adapted from Abriel and Kraus et al.[159]

4.7.2 Methods

Methodology has been explained in detail in section 4.1.

4.7.3 Results

4.7.3.1 Age related changes in the expression of $Na_v1.5$

Table 4.14 and Figure 4.27 showed changes in $Na_v1.5$ expression with ageing in the AVJ. The Figure shows that $Na_v1.5$ is expressed in all components of the AVJ with less expression in the INE. In ageing significant age related downregulation

was observed in the CN and PPB. The changes in the INE and His bundle are not significant. However, $Na_v1.5$ had a tendency of upregulation in the His bundle with ageing. Figure 4.28 shows high magnification images of $Na_v1.5$ expression in CN, PPB and His bundle. The higher intensity of $Na_v1.5$ signals was seen in the CN as compared to His bundle. It could be possible that the signal intensity was measured in the Lower nodal bundle (LNB) in some of the section and that may have affected the results.

Table 4.15 and Figure 4.29 show changes in $Na_v1.5$ in the working myocardium with ageing. There is significant downregulation of $Na_v1.5$ expression with ageing in left ventricle, left atrium and right atrium. The downregulation in the right ventricle did not reach statistical significance. Figure 4.30 showed corresponding images from each of the four chambers of the young and old heart.

4.7.4 Discussion

Age related downregulation of $Na_v1.5$ in the CN and PPB correlates with the functional ageing studies that show an increased in the AV nodal conduction time in heterozygous deficient SCN5a mice and an increased in AVNERP as mentioned earlier.[112]

The study by Veen et al.,[156] in heterozygous SCN5a deficient mice have compared the conduction velocity, Cx43 expression and cellular architecture in the young and old mice. They have shown that in older heterozygous mice reduced SCN5a is associated with fibrosis and disarrangement of Cx43, which results in profound conduction impairment in working myocardium particularly in the left ventricle. This effect is not as pronounced in young mice. Unfortunately, the AVN conduction properties in this study were not published thus it is difficult to say whether the result could be applied to our findings. Similar results have been shown in another study.[158]

In conclusion, reduced $Na_v1.5$ expression with ageing in the AVJ suggests that the AVN conduction velocity could be affected with age related changes noticed.

Table 4.14: Statistical analysis of $Na_v1.5$ expression in young and old hearts AVJ. Statistically significant results are shown in red.

$Na_v1.5$ expression	Inferior nodal extension (INE)	Compact node (CN)	Proximal penetrating bundle (PB)	Distal penetrating bundle (His
Young hearts (Mean and SEM)	55.10±1.49	92.17±3.59	87.40±4.98	70.24±5.71
Old hearts (Mean and SEM)	46.53±4.61	66.45±8.22	66.28±5.12	93.49±4.34
p-value and 95% confidence interval	0.28 (-27.96 to10.84)	0.029 (-47.79 to -3.74)	0.023 (-38.46 to-3.76)	0.06 (-1.26 to 48.17)

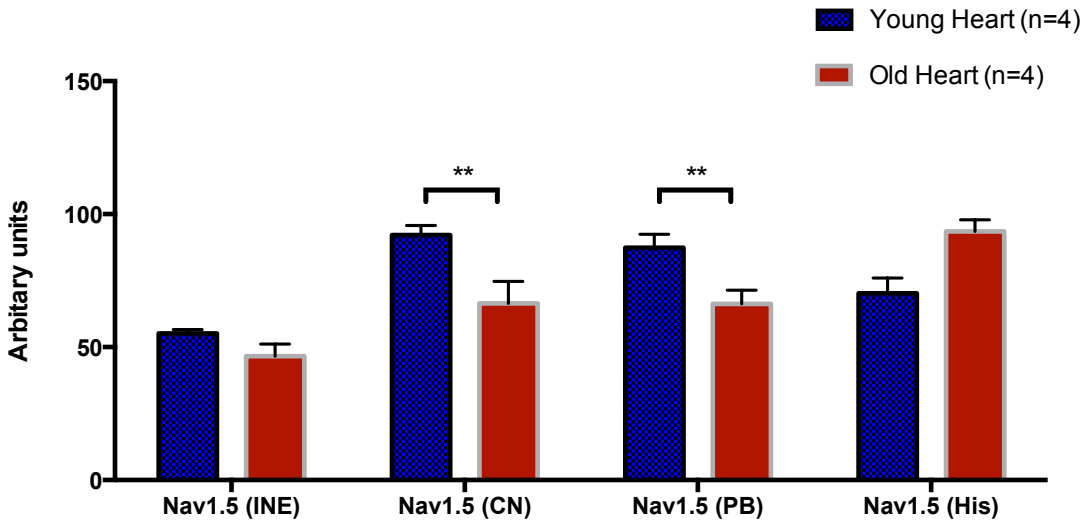

Figure 4.27: Changes in $Na_v1.5$ expresson in AVJ with ageing. Inferior nodal extension (INE), compact node (CN), proximal penetrating bundle (PB), distal penetrating bundle or His bundle (His). Signal intensity measured with Volocity software. Mean±SEM are shown, ** p <0.05.

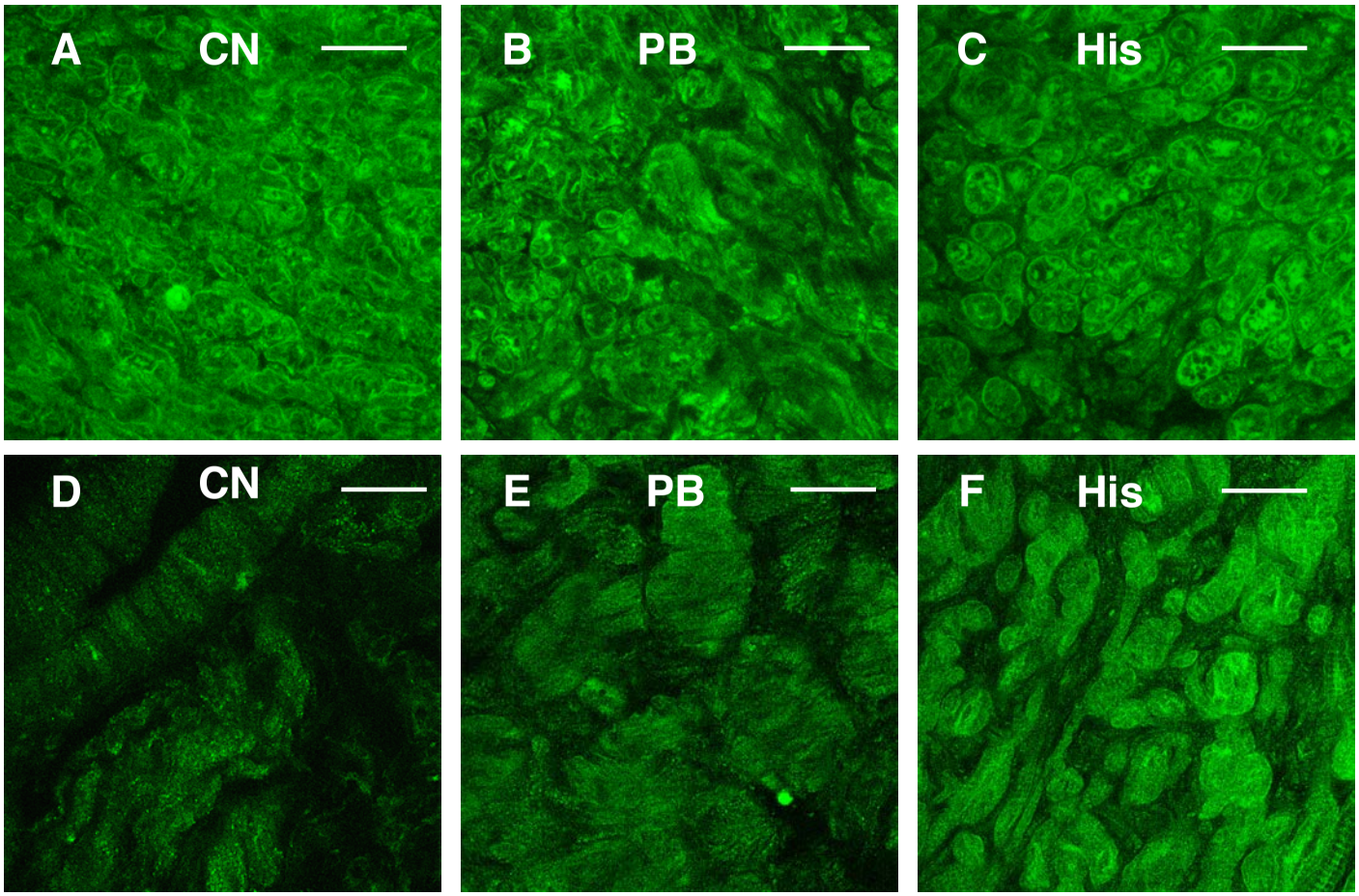

Figure 4.28: Confocal microscope high magnification images of the AVJ with Nav1.5 (green) immunolabelling. Compact node (CN), proximal penetrating bundle (PPB), distal penetrating bundle/His bundle (His). Top panel shows the AVJ components in young hearts and bottom panel shows the AVJ components in old heart. Bar=20 μm

Table 4.15: Statistical analysis of $Na_v1.5$ expression in young and old hearts working myocardium. Statistically significant results are shown in red.

$Na_v1.5$ expression	Left Ventricle	Left atrium	Right Ventricle	Right atrium
Young hearts (Mean and SEM)	106.58±6.75	116.10±5.62	94.29±5.78	122.41±4.12
Old hearts (Mean and SEM)	76.90±7.55	87.71±3.97	83.77±6.24	75.98±6.85
p-value and 95% confidence interval	0.016 (-52.46 to -6.89)	0.004 (-45.67 to -11.11)	0.25 (-30.74 to 9.71)	0.0001 (-64.45 to -28.40)

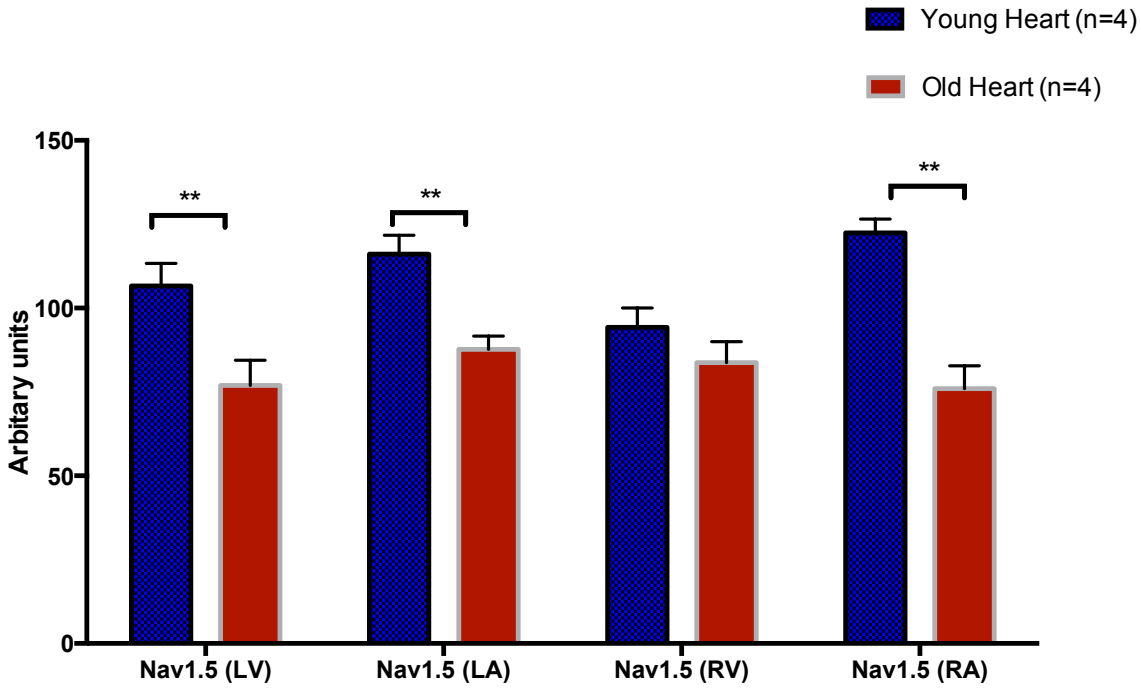

Figure 4.29: Changes in Nav1.5 expresson in different heart chambers with ageing. Left ventricle (LV), left atrium (LA), right Ventricle (RV), right atrium (RA). Signal intensity measured with Volocity software. Mean ±SEM are shown. ** $p < 0.05$.

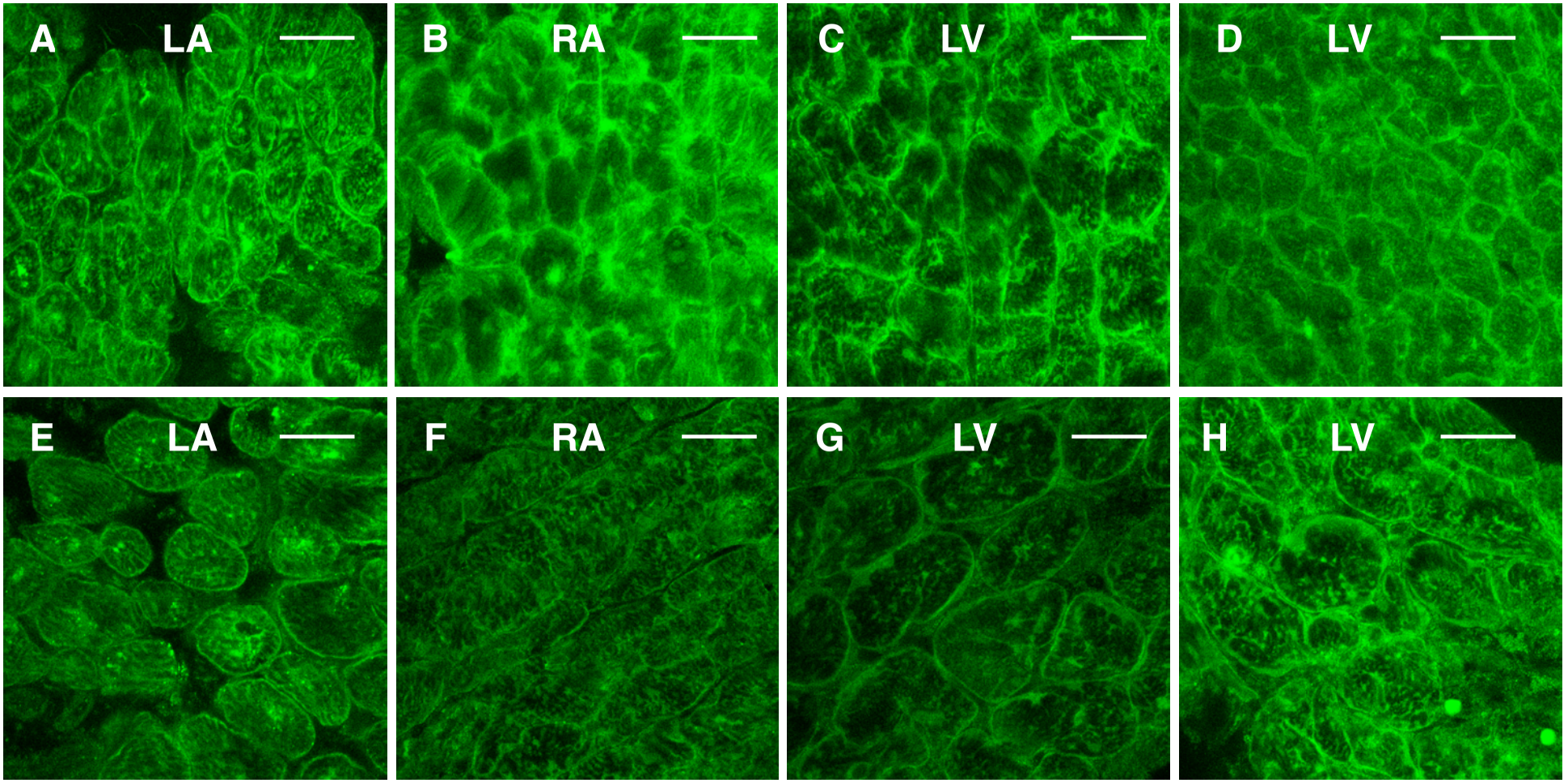

Figure 4.30: Confocal microscope high magnification images of the AVJ with Nav1.5 (green) immunolabelling. Left atrium (LA), right atrium (RA), left ventricle (LV), right ventricle (RV). Top panel shows the working myocardium in young hearts and bottom panel shows the working myocardium in old heart. Bar=20 μm

4.8 Changes in the expression of calcium handling proteins and L-Type calcium channel, $Ca_v1.3$ in the AVJ with ageing

4.8.1 Introduction

The calcium clock mechanism underlies the novel concept of oscillatory Ca^{2+} release (Ca^{2+} clock) from the sarcoplasmic reticulum in the sino-atrial nodal cells. This mechanism being responsible for automaticity has been subject of much debate in the recent past. Few argue that the calcium handling proteins play an important role in the regulation of heart rhythm. The calcium handling proteins include Ryanodine sensitive calcium release channel (RyR) located in the junctional portion of the sarcoplasmic reticulum (SR). The rapid release of calcium from SR mediated by RyR is fundamental not only in impulse generation and regulation in the pacemaker cells but also in the excitation-contraction coupling in the skeletal and cardiac muscle cells.[161]

Ryanodine receptors are the largest ion channel known to exist. Three different isoforms have been characterised. RyR1 in the skeletal muscle, RyR3 only in the brain and RyR2 principally in the myocardium but can also be found in the brain and gestational tissue.[162] RyR2 forms homotetrameric transmembrane calcium channel on the SR. RyR2 channel is composed of carboxy and amino terminals on the cytosolic side of the SR. The carboxy terminus is anchored to the SR by 4 to 10 membrane spanning hydrophobic motifs and a very large cytoplasmic domain that is in close connection with outer cell membrane L-type calcium channel ($Ca_v1.2$ and $Ca_v1.3$).[162] Figure 4.31 showed the schematic representation of the ryanodine channel.

The study by Greener et al.,[135] on the human AVN confirms the presence of RyR2 mRNA in the INE and CN but much less as compared to atrial and ventricular muscle. The penetrating bundle and His bundle also have high concentration of RyR2 mRNA as compared to INE and CN. Similar findings have also been seen in the rabbit AVJ.[24]

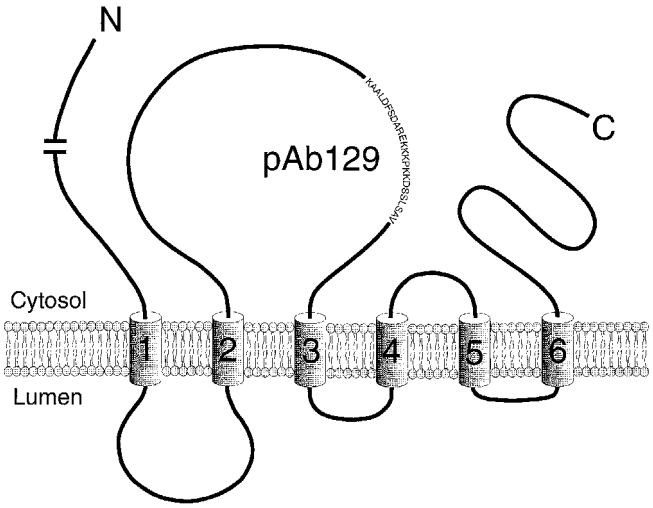

Figure 4.31: A working model of the transmembrane topology of the RyRs with six putative transmembrane segments. The epitope for the RyR2-specific antibody pAb129 is shown in the cytoplasmic loop present between transmembrane segments 2 and 3. The relative lengths of regions between putative transmembrane segments are shown by solid lines.[160]

The sarcoplasmic reticulum calcium pump (SERCA2a) is another important calcium handling protein that involves active reuptake of calcium into the SR. SERCA is an ATPase that's has more than 10 different isoforms encoded by three different genes. SERCA2 gene encoded two different isoforms SERCA2a and 2b. SERCA-2a is specifically seen in the cardiac and skeletal muscle. SERCA2a has higher rate of Ca^{2+} uptake than SERCA2b. The homozygous loss of SERCA2a results in switch in the cardiac isoform to SERCA2b, which results in higher mortality and cardiac malformation.[161]

The structure of voltage gated calcium channels has been described in detail in Figure 4.31. Ca^{2+} channels play an important role in the AVN conduction and have been described in chapter 1. Both L-type and T-type calcium channels responsible for I_{CaL} and I_{CaT} respectively, have been found in the AVN.[45,46] Greener et al., study on ion channel transcripts measured via qPCR technique in rabbits and the study in humans showed that expression of $Ca_v1.3$ is more abundant in the nodal tissues including the CN, INE and distal penetrating bundle as compared to atrial and ventricular muscle in which $Ca_v1.2$ is more abundant.[24,135]

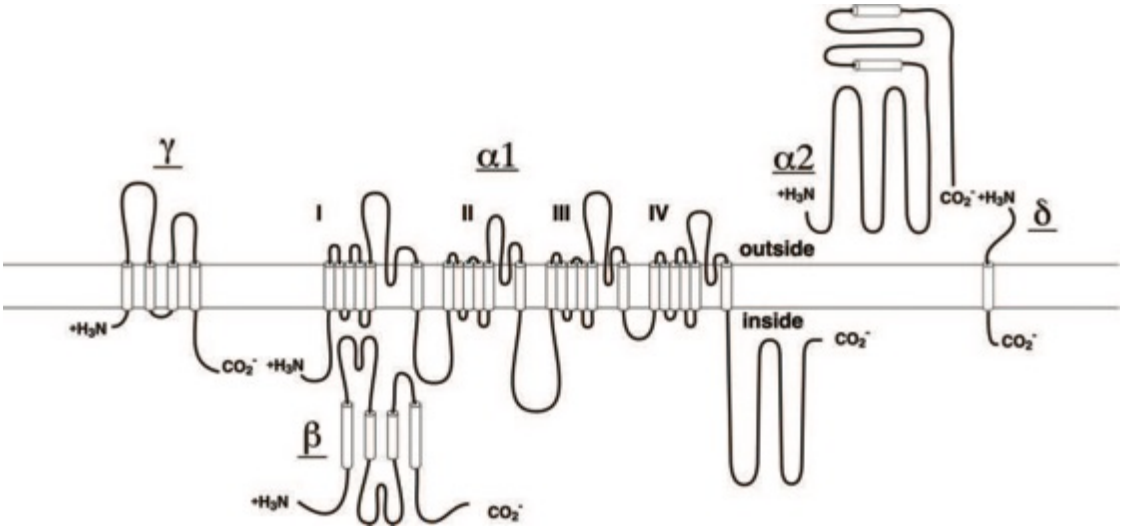

Figure 4.32: The structure of voltage gated calcium channel adapted from Catterall et al.[164] The calcium channels are composed of four or five subunits that are shown. The multiple alpha subunits determine the different subtypes of the voltage gated calcium channels. The α1 subunit is the largest subunit and includes the conduction pore, voltage sensor and gating apparatus. The α1 subunit is organized into four homologus domain (I to IV) with six transmembrane segments (S1 to S6) in each domain.

4.8.2 Methods

Methodology has been explained in detail in section 4.1.

4.8.3 Results

4.8.3.1 Age related changes in the expression of Calcium handling proteins and $Ca_v1.3$.

Table 4.16 and Figure 4.33 show changes in expression of RyR2 with ageing in the AVJ. Significant downregulation was observed in the RyR2 expression in the CN and PPB with ageing. No significant changes were observed in the INE and His bundle with ageing. The corresponding high magnification images can be seen in Figure 4.34, which show a striated pattern of labelling.

In the working myocardium, RyR2 expression decreases with ageing in the left ventricle. Modest decrease is also seen in other parts of working myocardium, however it didnot reach statistical significance. Table 4.17 and Figure 4.35 show changes in the expression of RyR2 in the working myocardium. Figure 4.36 show corresponding high magnification images, which show a striated pattern of labelling. The expression of RyR2 is much higher in the working myocardium in comparison with the components of the AVJ

SERCA2a showed significantly increased expression in the PPB with ageing. However, no significant changes have been seen in other components of the AVJ. There is a trend of up regulation in the His bundle but it is not significant. Table 4.18 and Figure

4.37 show changes in the expression of SERCA2a in the AVJ. Table 4.19 and Figure 4.38 show changes in the expression of SERCA2a in the working myocardium. No significant changes were observed in the working myocardium although there was a trend of decreased expression with ageing in all parts of working myocardium. Figure 4.39 shows corresponding images in the AVJ. This figure shows striated pattern of labelling.

The changes in $Ca_v1.3$ expression with ageing include increased expression in the PPB. No significant change has been observed in other components of AVJ. Table 4.20 and Figure 4.41 show these changes. Figure 4.41 shows corresponding high magnification images. $Ca_v1.3$ expression is poor in the working myocardium thus was not analysed.

4.8.4 Discussion

The substantial age dependent decrease in RyR2 expression with ageing in the CN and PPB correlate with the ageing study on the SN by Tellez et al.[86] Tellez et al., showed significant decrease in RyR2 mRNA and protein expression in the SN. It is possible that reduced RyR2 expression results in decreased conduction across the AVN by reducing cytosolic calcium concentration.

On the other hand the reduced RyR2 in the PPB (decreased calcium release from SR) and increased expression of SERCA2a (increased re uptake of calcium in the SR) in the PPB may also contribute to decreased intracellular Ca^{2+} transient, thus decreasing conduction across the AVJ. Increased SERCA2a may results in decreasing cytosolic Ca^{2+} concentration with active reuptake or cause increase SR calcium concentration, which may allow more calcium release from the SR. Increased $Ca_v1.3$ in the PPB however will increase the calcium concentration promoting increased conduction across the AVJ. Increased SERCA2a and $Ca_v1.3$ has been observed with ageing in the SN.[86] The changes that are seen in $Ca_v1.3$ levels could be as a consequence of RyR2 downregulation. I have also not measured phospholamban during this study. It is likely that changes phospholamban levels modulate activity of the SERCA-2a, which in turn effect cystosolic calcium concentration. Phospholamban is a protein that in unphosphorylated state inhibits SERCA but this inhibition is lost once it is phosphorylated by protein kinase A.

Whether these results in the PPB are actually offset each other's effect is difficult to predict. However the reduced RyR2 in the CN is likely to cause delay in the impulse propagation across the AVN.

Table 4.16: Statistical analysis of RyR2 expression in young and old hearts AVJ. Statistically significant results are shown in red.

RyR2 expression	Inferior nodal extension (INE)	Compact node (CN)	Proximal penetrating bundle (PB)	Distal penetrating bundle (DPB or His)
Young hearts (Mean and SEM)	38.67±4.19	59.83±4.67	36.36±1.92	29.58±1.72
Old hearts (Mean and SEM)	38.90±5.98	36.42±0.56	29.44±2.39	28.43±1.18
ρ-value and 95% confidence interval	0.846 (-23.17 to 19.63)	0.031 (-42.67 to -4.13)	0.042 (-13.53 to -0.29)	0.68 (-7.2 to 4.90)

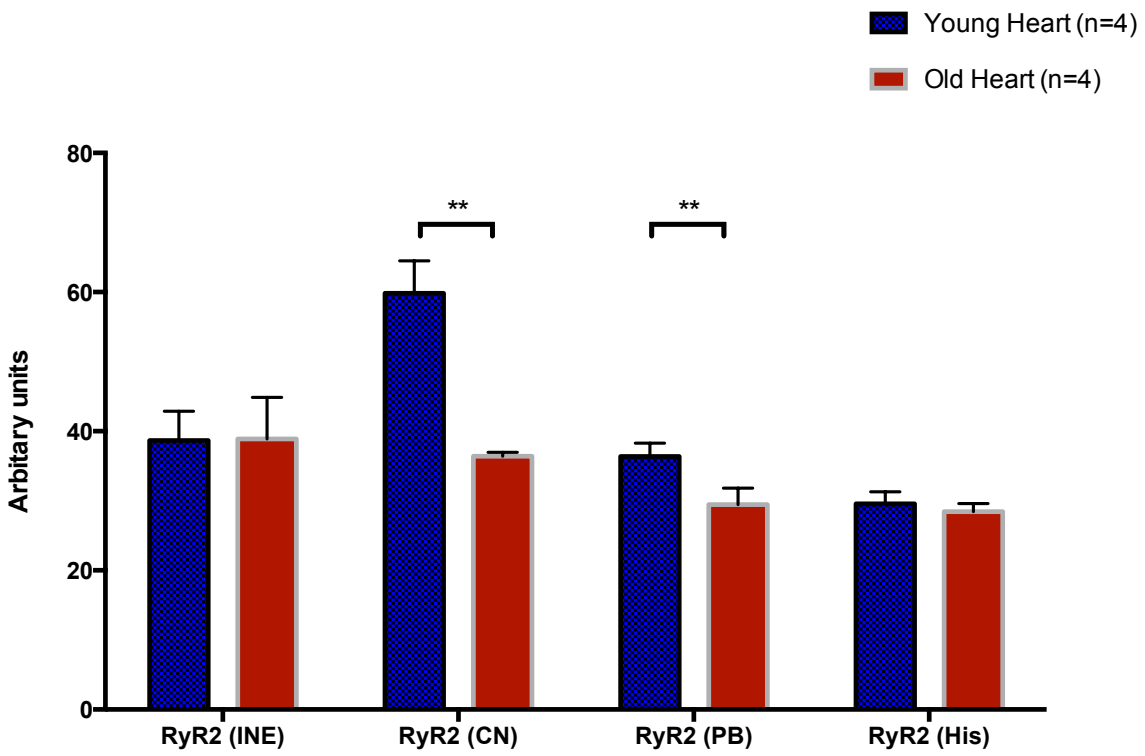

Figure 4.33: Changes in RyR2 expresson in AVJ with ageing. Inferior nodal extension (INE), compact node (CN), proximal penetrating bundle (PB), distal penetrating bundle or His bundle (His). Signal intensity measured with Volocity software. Mean±SEM are shown, ** p <0.05.

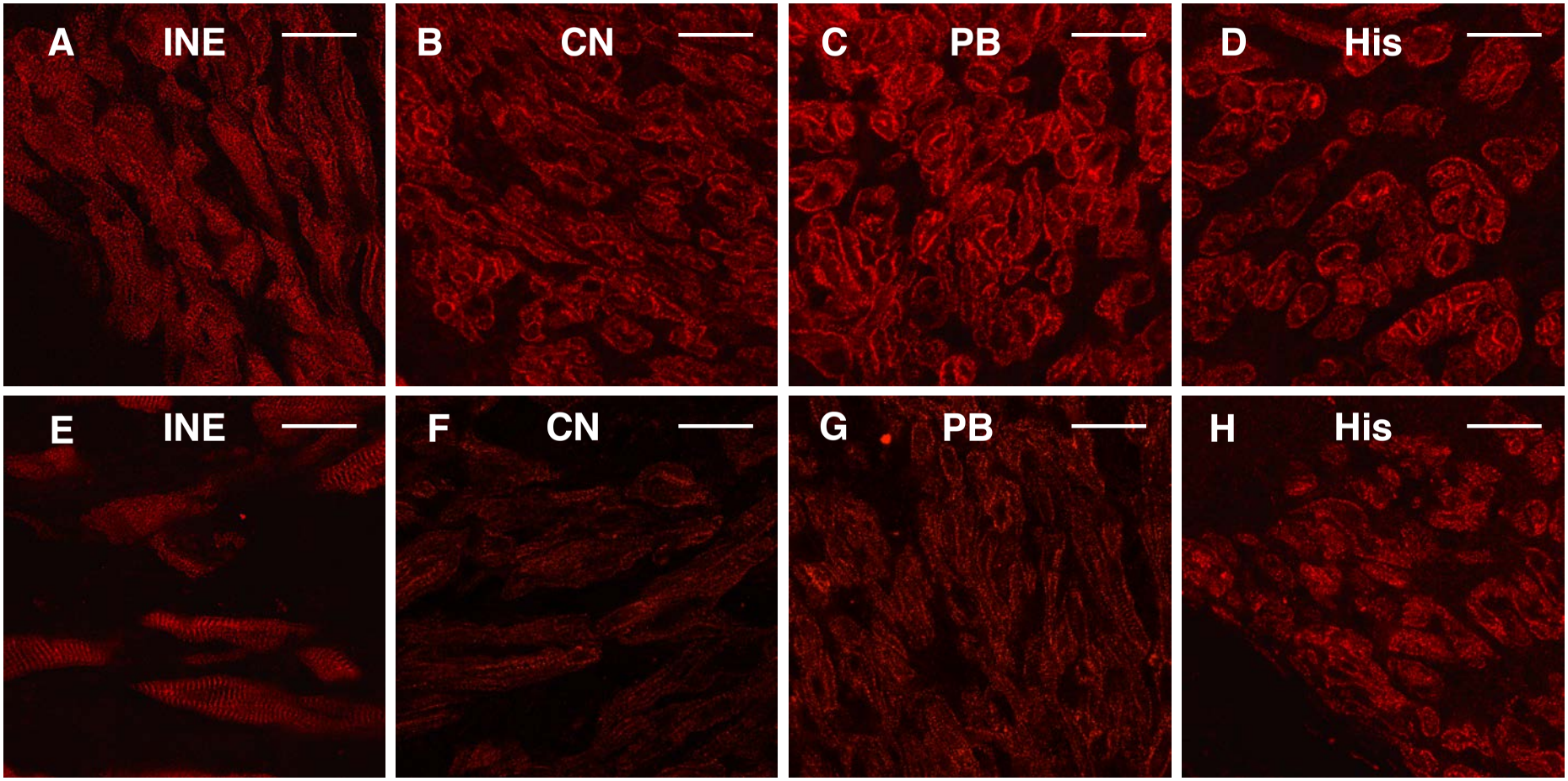

Figure 4.34: Confocal microscope high magnification images of the AVJ with RyR2 (red) immunolabelling. Inferior nodal extension (INE), compact node (CN), proximal penetrating bundle (PPB), distal penetrating bundle/His bundle (His). Top panel shows the AVJ components in young hearts and bottom panel shows the AVJ components in old heart. Bar=20 μm

Table 4.17: Statistical analysis of RyR2 expression in young and old hearts working myocardium. Statistically significant results are shown in red.

RyR2 expression	Left Ventricle	Left atrium	Right Ventricle	Right atrium
Young hearts (Mean and SEM)	69.56±3.34	70.92±4.73	64.39±6.70	61.43±5.47
Old hearts (Mean and SEM)	60.16±2.62	65.14±3.68	53.86±4.01	61.83±4.67
ρ-value and 95% confidence interval	0.034 (-18.02 to -0.78)	0.342 (-18.00 to 6.43)	0.166 (-25.78 to 4.73)	0.956 (-14.85 to 15.66)

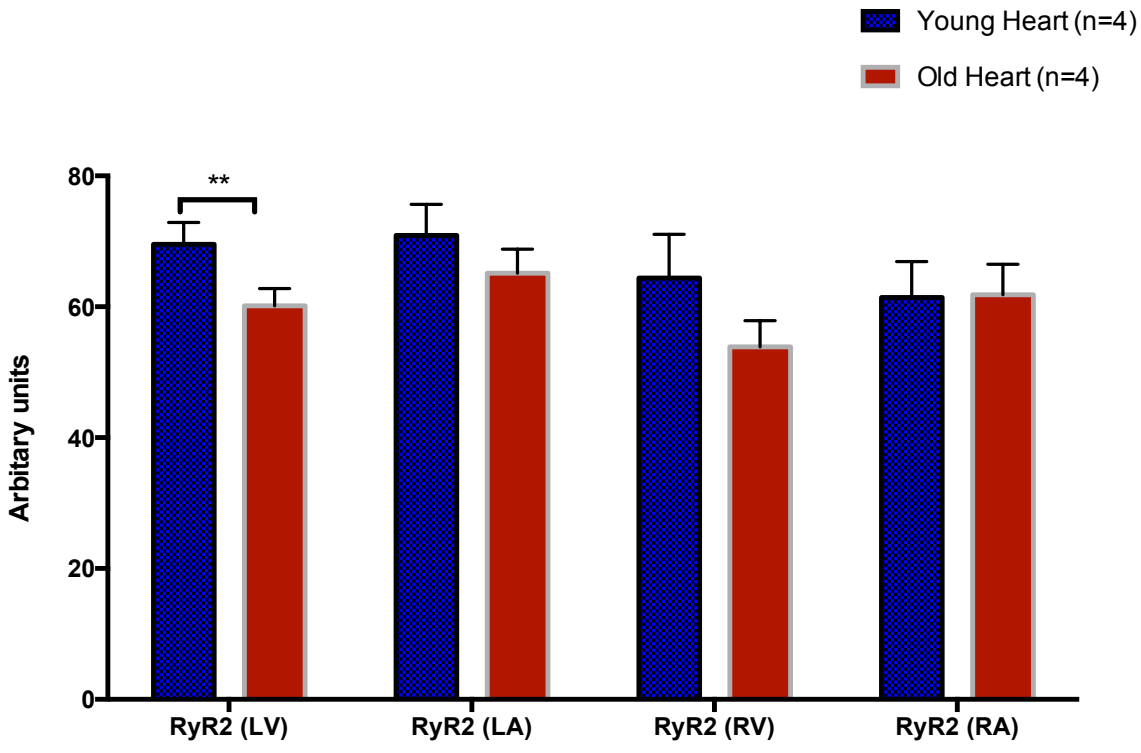

Figure 4.35: Changes in RyR2 expresson in different heart chambers with ageing. Left ventricle (LV), left atrium (LA), right Ventricle (RV), right atrium (RA). Signal intensity measured with Volocity software. Mean ±SEM are shown. ** $p < 0.05$.

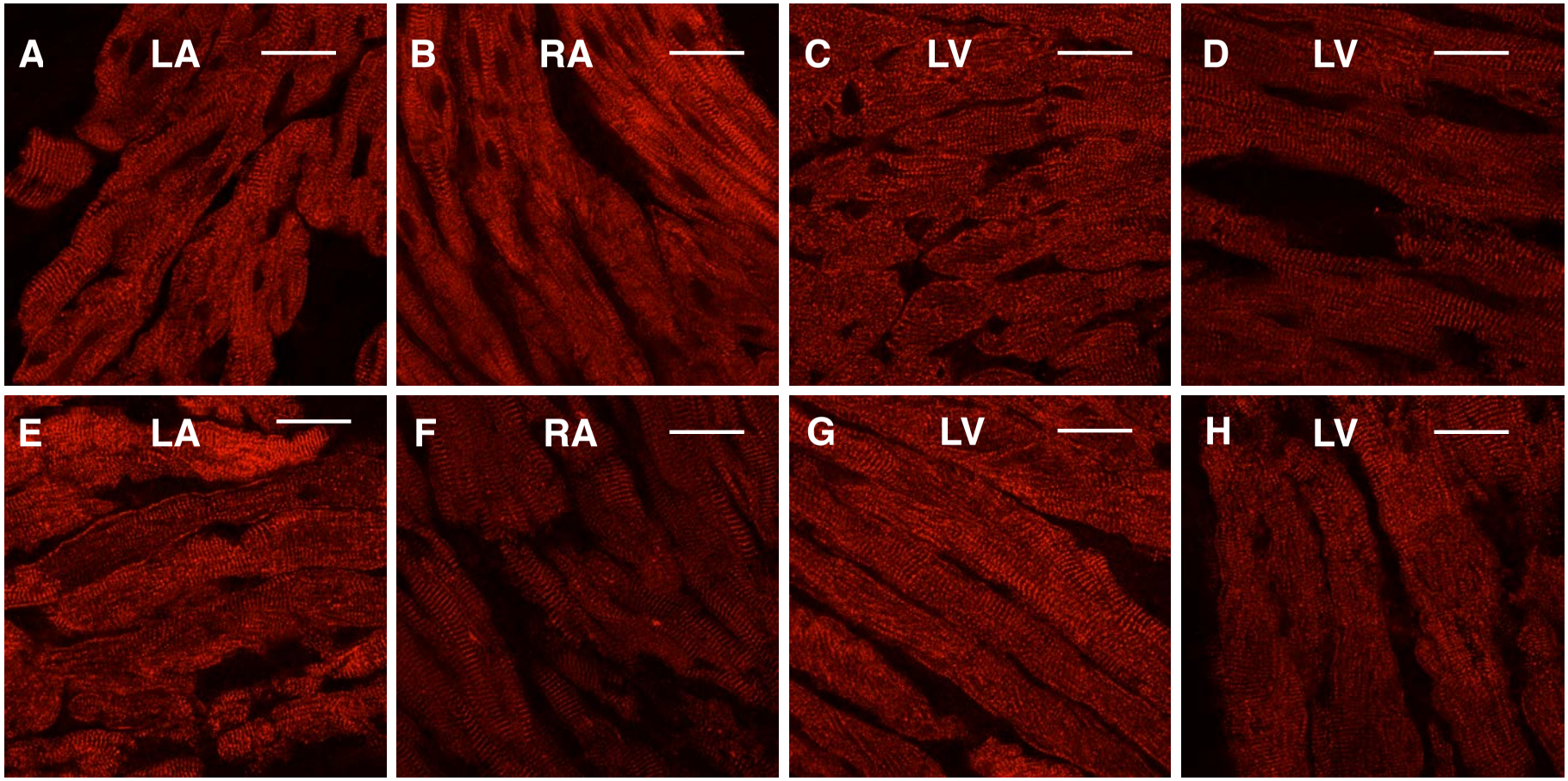

Figure 4.36: Confocal microscope high magnification images of the AVJ with RyR2 (red) immunolabelling. Left atrium (LA), right atrium (RA), left ventricle (LV), right ventricle (RV). Top panel shows the working myocardium in young hearts and bottom panel shows the working myocardium in old heart. Bar=20 μm

Table 4.18: Statistical analysis of SERCA2a expression in young and old hearts AVJ. Statistically significant results are shown in red.

SERCA2a expression	Inferior nodal extension (INE)	Compact node (CN)	Proximal penetrating bundle (PB)	Distal penetrating bundle (DPB or His)
Young hearts (Mean and SEM)	98.64+_4.81	46.29+_7.82	32.80+_0.93	72.24+_2.20
Old hearts (Mean and SEM)	102.58+_6.85	34.65+_5.36	44.80+_1.51	102.24+_24.18
ρ-value and 95% confidence interval	0.73 (-25.74 to 33.62)	0.123 (-27.23 to 3.95)	0.0001 (7.32 to 16.67)	0.106 (-8.20 to 68.21)

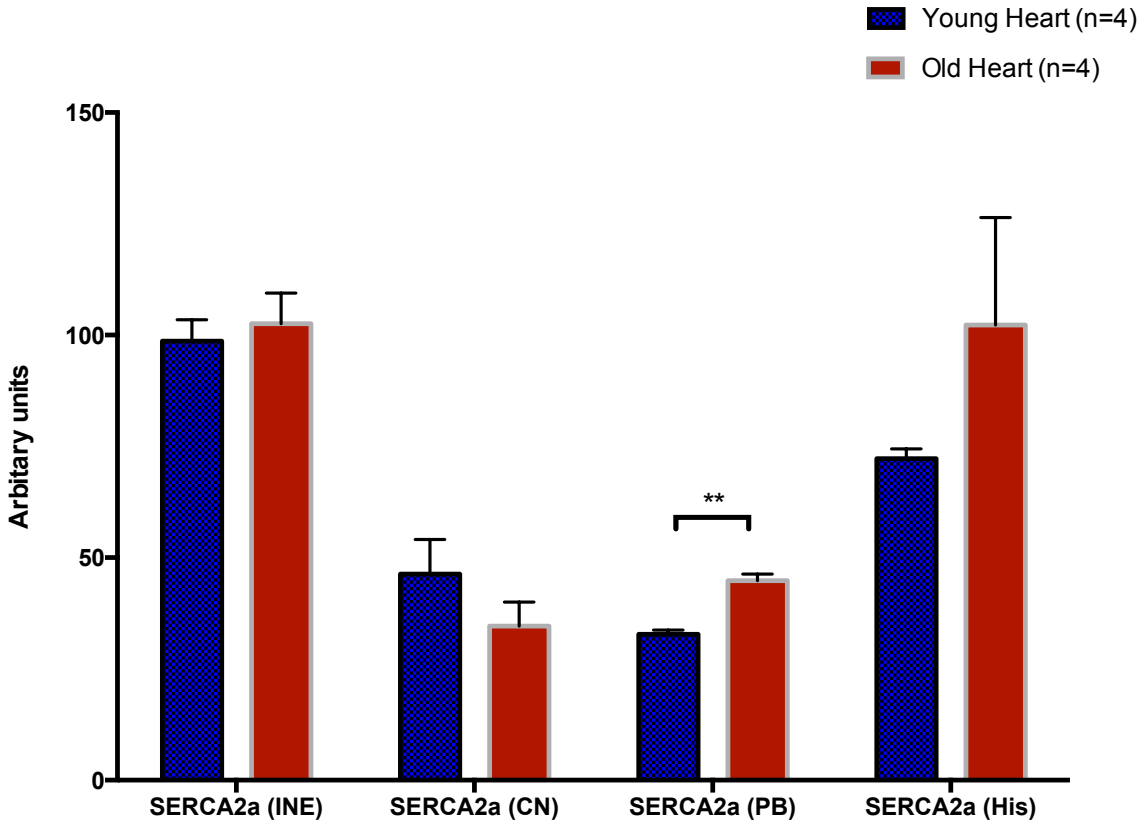

Figure 4.37: Changes in SERCA2a expresson in AVJ with ageing. Inferior nodal extension (INE), compact node (CN), proximal penetrating bundle (PB), distal penetrating bundle or His bundle (His). Signal intensity measured with Volocity software. Mean±SEM are shown, ** p <0.05.

Table 4.19: Statistical analysis of SERCA2a expression in young and old hearts

SERCA2a expression	Left Ventricle	Left atrium	Right Ventricle	Right atrium
Young hearts (Mean and SEM)	80.74±3.30	72.37±5.05	74.88±4.48	82.13±3.26
Old hearts (Mean and SEM)	69.09±6.25	55.50±6.74	70.95±8.51	64.46±10.51
p-value and 95% confidence interval	0.131 (-27.40 to 4.11)	0.09 (-37.78 to 4.02)	0.75 (-31.23 to 23.52)	0.224 (-50.40 to 15.05)

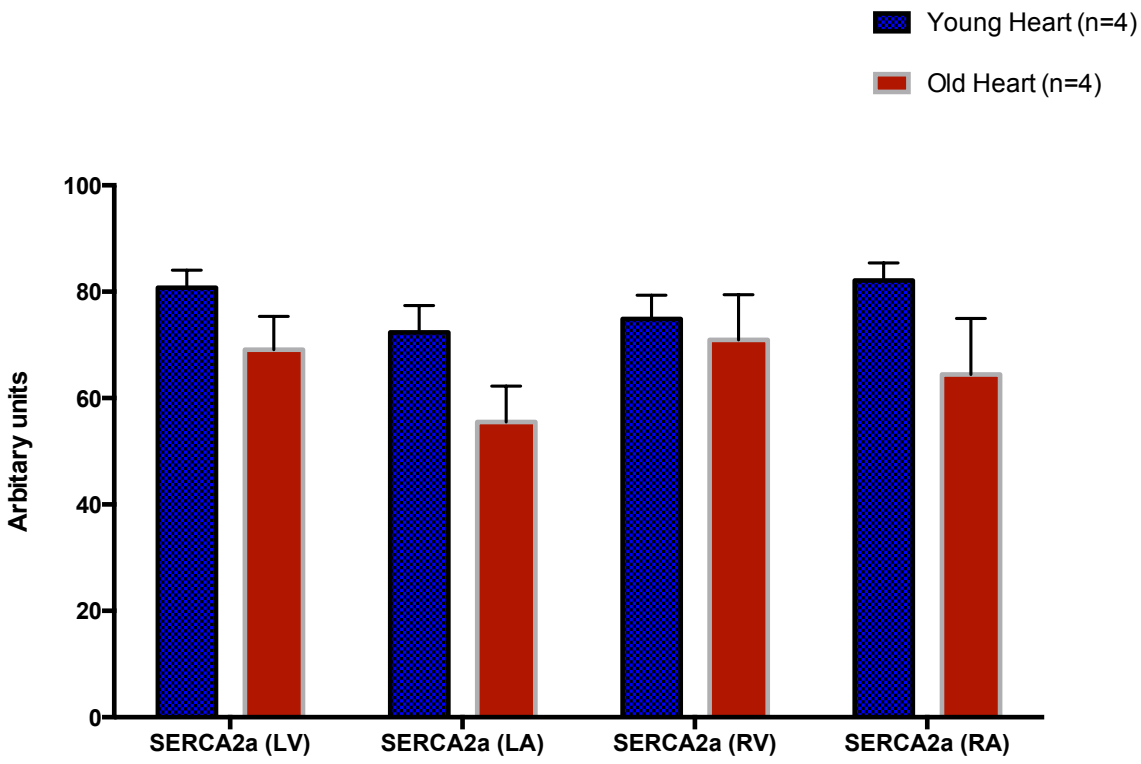

Figure 4.38: Changes in SERCA 2a expresson in different heart chambers with ageing. Left ventricle (LV), left atrium (LA), right Ventricle (RV), right atrium (RA). Signal intensity measured with Volocity software. Mean ±SEM are shown. ** p <0.05.

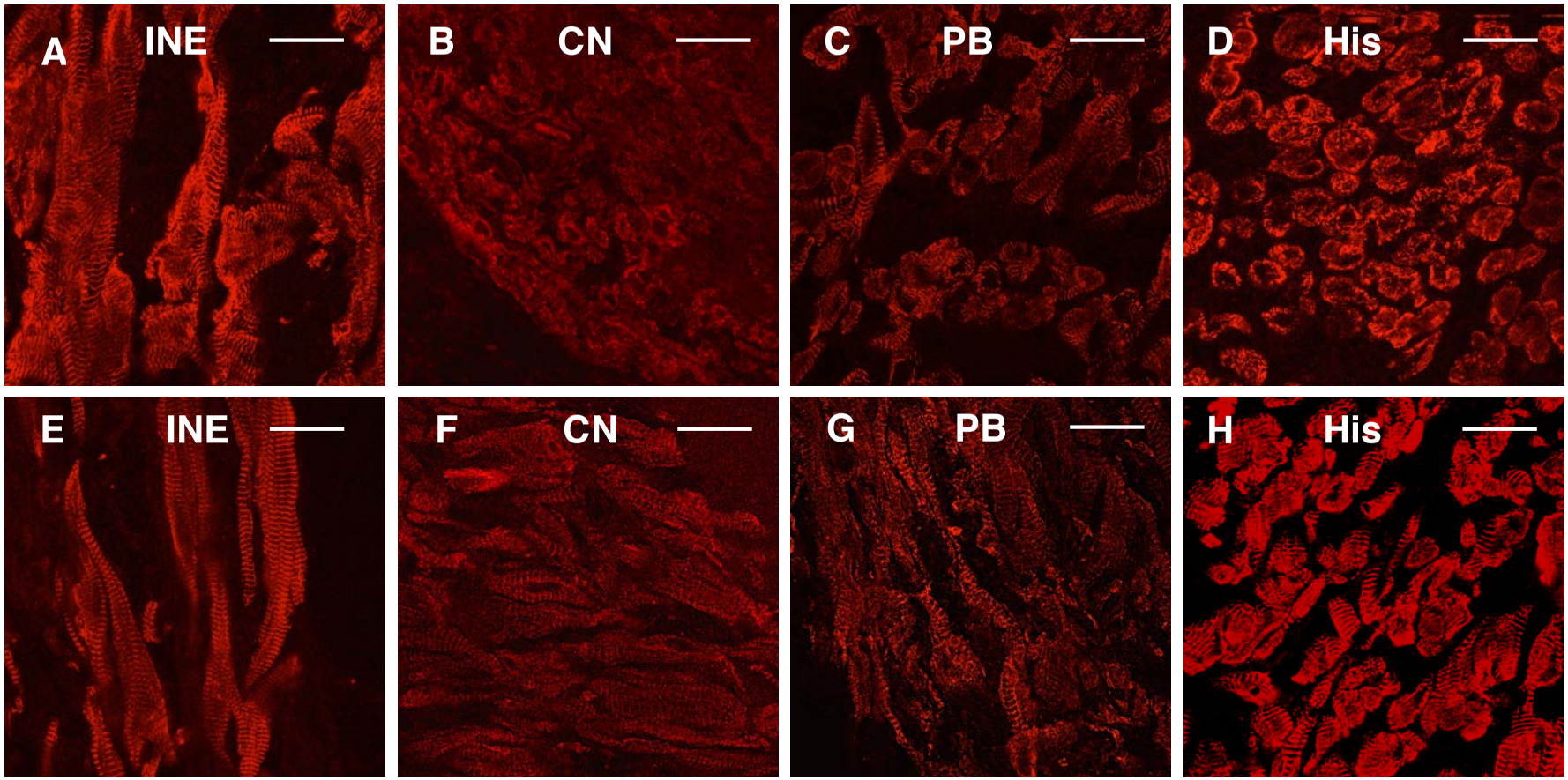

Figure 4.39: Confocal microscope high magnification images of the AVJ with SERCA2a (red) immunolabelling. Inferior nodal extension (INE), compact node (CN), proximal penetrating bundle (PPB), distal penetrating bundle/His bundle (His). Top panel shows the AVJ components in young hearts and bottom panel shows the AVJ components in old heart. Bar=20 μm

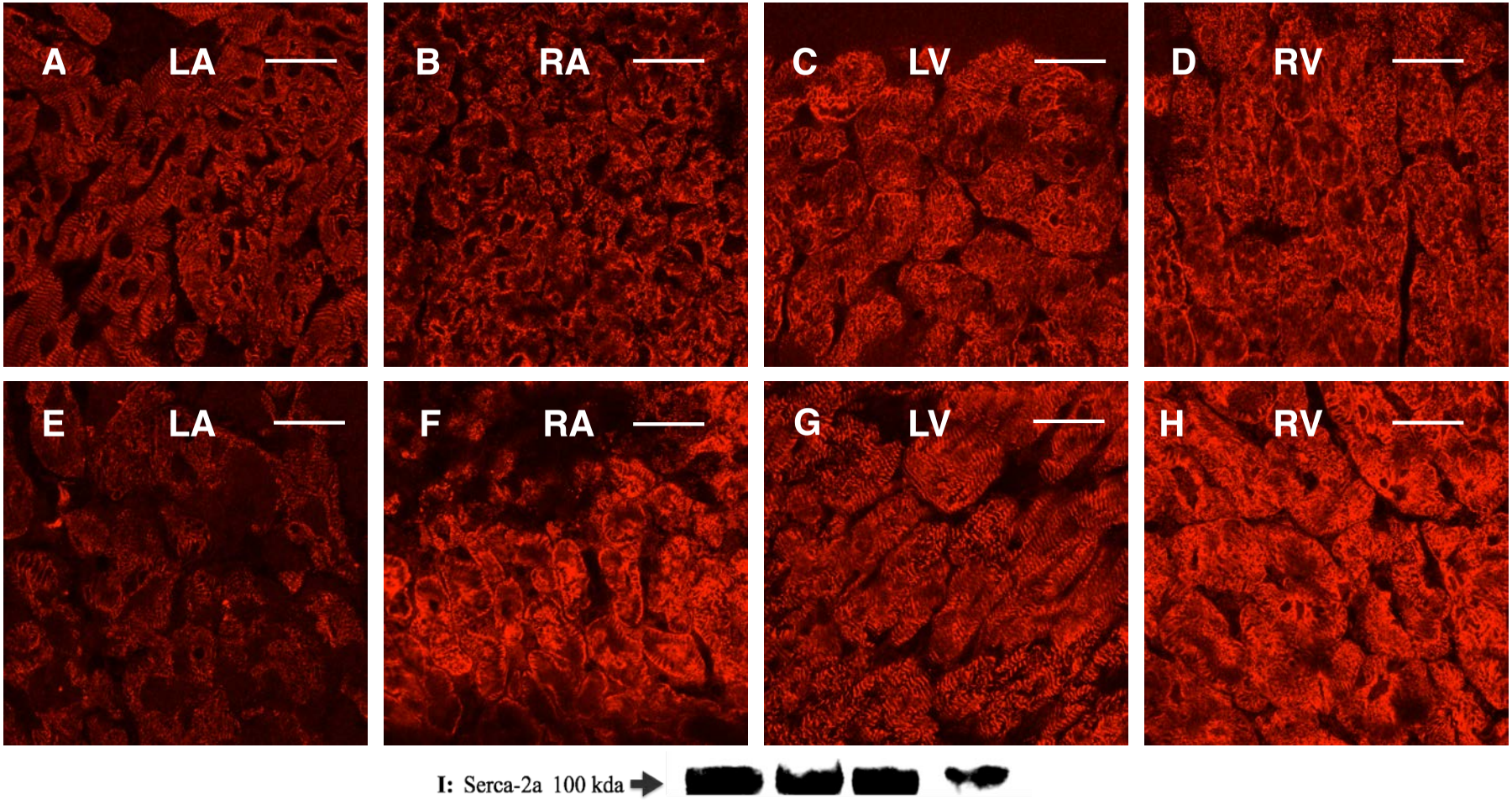

Figure 4.40: Confocal microscope high magnification images of the differentt heart chambers with SERCA2a (red) immunolabelling. Left atrium (LA), right atrium (RA), left ventricle (LV), right ventricle (RV). Top panel shows the working myocardium in young hearts and bottom panel shows the working myocardium in old heart. Bar=20 μm

Table 4.20: Statistical analysis of $Ca_v1.3$ expression in young and old hearts AV junction.

$Ca_v1.3$ expression	Inferior nodal extension (INE)	Compact node (CN)	Proximal penetrating bundle (PB)	Distal penetrating bundle (His
Young hearts (Mean and SEM)	16.91±8.45	21.46±2.49	7.53±0.42	23.36±2.70
Old hearts (Mean and SEM)	6.57±4.64	21.07±2.45	17.99±2.68	20.08±2.19
ρ-value and 95% confidence interval	0.24 (-23.17 to 19.63)	0.91 (-8.46 to 7.69)	0.004 (3.99 to 16.96)	0.4 (-13.25 to 6.68)

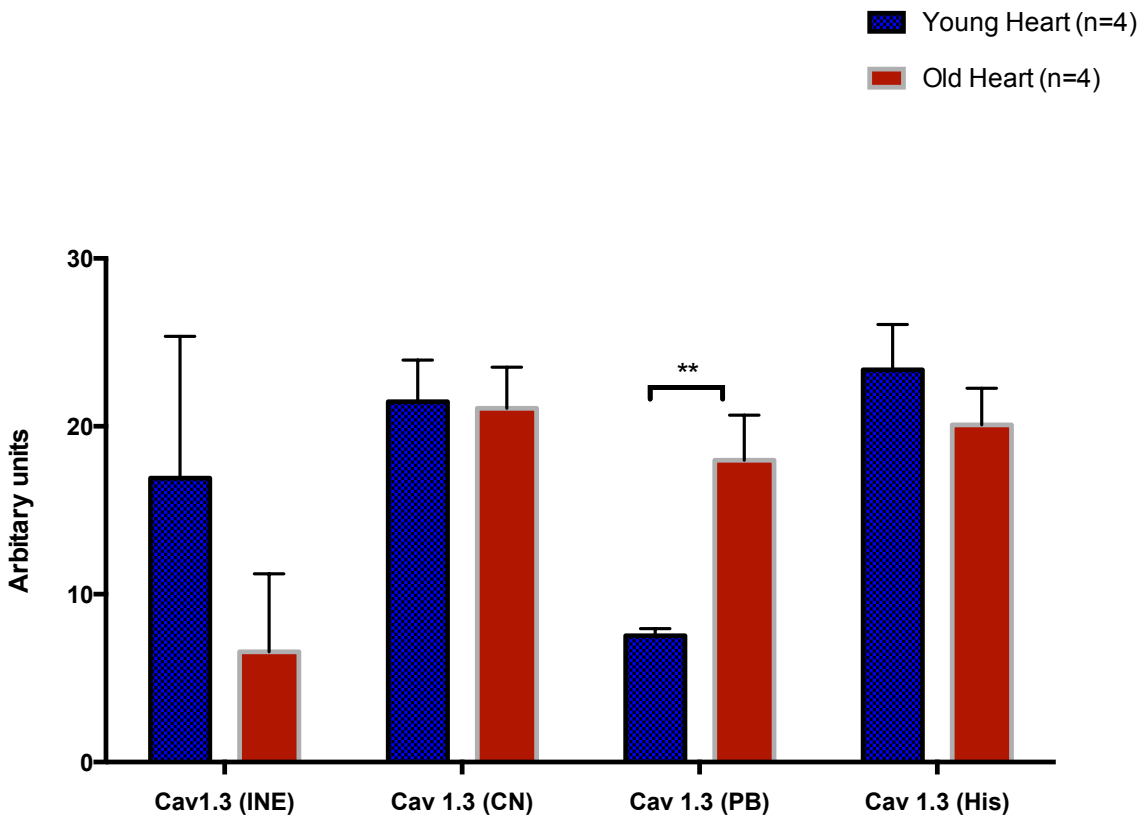

Figure 4.41: Changes in Cav1.3 expresson in AVJ with ageing. Inferior nodal extension (INE), compact node (CN), proximal penetrating bundle (PB), distal penetrating bundle or His bundle (His). Signal intensity measured with Volocity software. Mean±SEM are shown, ** p <0.05.

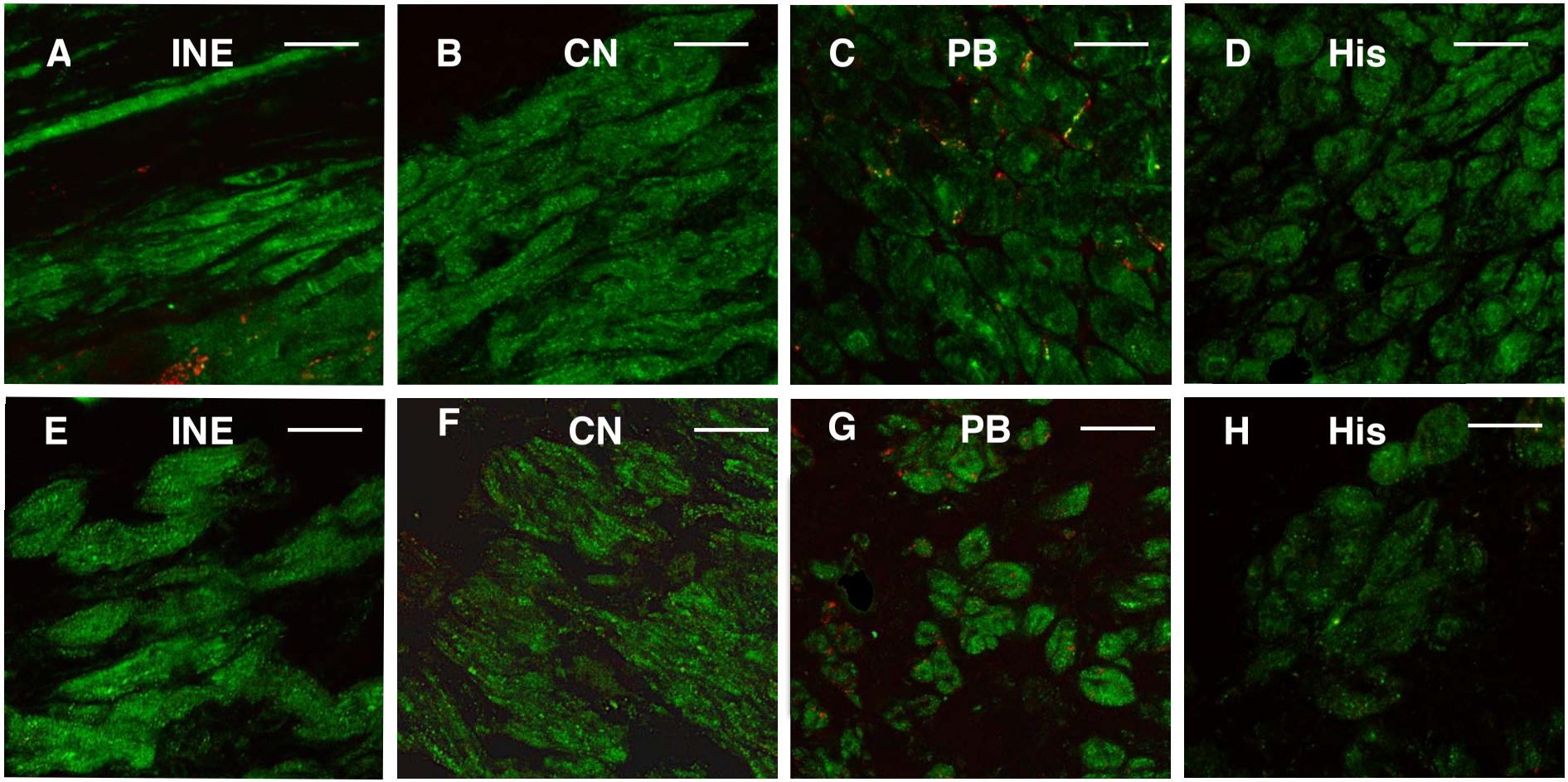

Figure 4.41: Confocal microscope high magnification images of the AVJ with Cav1.3 (green) immunolabelling. Inferior nodal extension (INE), compact node (CN), proximal penetrating bundle (PPB), distal penetrating bundle/His bundle (His). Top panel shows the AVJ components in young hearts and bottom panel shows the AVJ components in old heart. Bar=20 μm

4.9 Summary of immunofluorescence experiments

Ageing related expression changes in the ion channels, connexins, Ca^{2+} handling proteins and structural proteins across the AVJ is complex. Table 4.21 summarises changes in the proteins investigated with ageing across the AVJ and their possible effect on the AVN conduction.

The only significant change in the INE with ageing is increase expression of Cx40. The other ion channels including $Ca_v1.3$ and calcium handling proteins did not show any significant difference in the INE with ageing.

In CN, decrease expression of $Na_v1.5$ and RyR2 with ageing was oberved. Cx40 expression increase with ageing in the CN. The probable net effect of these changes is prolongation of the AV conduction, if we assume that the Cx40 expression is either heterotypic or heteromeric channels with Cx30.2 or Cx45. Unfortunately immunofluorescence for Cx45 could not be performed as the primary antibodies (commercially available) showed non-specific signal.

The ion channel expression changes in the PPB are more interesting. The changes across both DPB and PPB are different with ageing. The PPB being closer to the CN is likely to have more N cells as compared to the DPB or His bundle. Cx43, $Na_v1.5$ and RyR2 decrease significantly with ageing in the PPB. $Ca_v1.3$ and SERCA2a increase with ageing. No significant changes are seen in HCN4 and Cx40 in the PPB. Decrease in Cx43 and $Na_v1.5$ expression with ageing can lead to prolongation of AV conduction. The changes in the His bundle with ageing is only decrease expression of Cx43 and HCN4, which may prolong AV conduction. The findings of only few changes in the expression of ion channels in the His bundle correlate with the electrophysiological changes, which showed the prolongation of AH interval is much more than HV interval with ageing, as shown in the section 1.11.3. The HV interval contribution to PR prolongation with ageing is modest and AH interval prolongation is the primary reason of PR interval prolongation with ageing.

Changes in the expression pattern of structural proteins including alpha actinin and caveolin3 were also observed with ageing. The alpha actinin confirmed irregular cellular architecture with ageing. The changes in caveolin3 expression with ageing in the His bundle may prolong AV conduction by indirectly effecting ion channel expression in the caveolae. The irregular cellular architecture as I have discussed earlier can downregulate ion channel expression.

There are few limitations in the immunofluorescence experiments. K^+ channels, Cx45, HCN1 and $Ca_v3.1$ were not investigated as a lot of commercially available primary antibodies that have been tested against these proteins produced nonspecific staining. This is the potentially confounding, as these channels are important in determining the AV conduction properties.

In conclusion, protein expression in the AVJ showed important changes with ageing. These results may explain the functional changes that have been seen with ageing in chapter 2. It will be interesting to find out if similar changes are seen in humans with ageing. These changes can likely make the ageing AVN vulnerable to disease/insult resulting in increased incidence of AV block.

Table 4.21: Summary of the changes seen with ageing in the ion channels and structural protein. Inferior nodal extension (INE), Compact node (CN), Proximal penetrating bundle (PPB), Distal penetrating bundle or His bundle (His) (↑ upregulation) (↓ downregulation) (= no significant change)

Ion Channel/Structrual protein	INE	CN	PPB	His bundle	Possible Effect on AV conduction
Cx43	=	=	↓	↓	Prolong
Cx40	↑	↑	=	=	Accelerates
HCN4	=	=	=	↓	Prolong
$Na_v1.5$	=	↓	↓	=	Prolong
RyR2	=	↓	↓	=	Prolong
SERCA2a	=	=	↑	=	Unknown
Ca_v 1.3	=	=	↑	=	Accelerates
Alpha actinin	↓	↓	=	=	No effect
Caveolin3	=	=	=	↓	Unknown

Chapter 5

Clinical effects of AV nodal and cardiac conduction system disease in elderly patients with syncope

5.1 Introduction

AVN disease is the most common reason for pacemaker implantation in elderly individuals.[165] AVN disease is commonly manifested on the routine electrocardiogram (ECG) as heart block. The heart block varies from prolonged PR interval or 1st degree heart block to complete heart block with complete AV dissociation. While the finding of complete heart block on the routine ECG results in pacemaker implantation, the prolonged PR interval is commonly perceived as benign finding especially in middle aged population.[166] This prolonged PR interval usually coexists with the other CCS abnormalities manifested on routine ECG as left axis deviation (LAD), right bundle branch block (RBBB) or left bundle branch block (LBBB). With the exception of LBBB, these CCS abnormalities are also considered as benign findings. However, recently a study has shown that prolonged PR interval is associated with increased incidence of atrial fibrillation, pacemaker implantation and increased mortality in general population.[167] The significance of a prolonged PR interval and CCS abnormalities are not known in elderly individuals with syncope.

Syncope (or transient loss of consciousness, T-LOC, with loss of postural tone) is a common occurrence. The incidence and prevalence of syncope in the adult population is variably reported in studies. In the Framingham study, it has been shown that at least 3% of adults have experienced a single episode of syncope in their life time.[168] However a relatively recent study noted the cumulative life time incidence to be as high as 35% in adult population.[167] Syncope has been widely reported as the reason for 1-6% of emergency room or accident and emergency department visits. About one third of these patients required hospital admission.[170,171,172,173] Increasing incidence of syncope has been reported in the elderly population.[170] Recurrent syncope especially in the ever increasing elderly population may result in increased mortality and morbidity including frequent hospital admissions, physical injury and loss of independence. In the elderly population it is difficult to establish the exact cause of syncope, even with extensive investigation. The studies have shown that history, examination and the ECG are key determinant to establish the cause and further management.[174,175] Causes of syncope are varied but common causes include cardiac syncope (arrhythmias and cardiac ischemia), orthostatic hypotension, neurologic causes and neurally mediated hypotension. Studies have shown that cardiac syncope has the worst prognosis.[170] In the evaluation of syncope, the ECG has been recommended by both the European and American guidelines.[174,175] The 12-lead ECG in elderly patients often shows conduction tissue abnormalities (ECG-CTA) including first degree AV block (PR interval > 200ms, LAD, RBBB (QRS >120msec), LBBB (QRS duration >120msec). I have compared outcomes in elderly patients (>65 years) presenting with ECG-CTA with elderly patients (>65 years) presenting with a normal ECG.

5.2 Methodology

Patients attended a Rapid Access Blackout Triage Clinic (RABTC). RABTC received referrals from both primary and secondary care. The twice weekly, RABTC is staffed by specialist nurses and a cardiologist. Specialist nurses in arrhythmia, falls and epilepsy assess patients using a web-based blackouts assessment Tool, which included a risk assessment for “Red Flag” features. The red flags include an abnormal ECG. A cardiologist provided a medical overview of the patients.

2586 patients were assessed in the RABTC during the study period (1st January 2007 till 1st January 2013). Of the initial patients assessed only patients with syncope (T-LOC) and > 65 years of age were included in the final analysis. Patients were divided in two groups. Group A included the patients with normal baseline ECG (84 patients). Group B

included patients with conduction tissue abnormalities (65 patients) with ECG-CTA. In Group B patients 38 patients had first degree AV block, 15 had left axis deviation, 8 had right bundle branch block and had left bundle branch block). Group B is further subdivided in to two groups depending on pacemaker implantation. Outcome data was then calculated and compared amongst patients with and without permanent pacing.

The data were collected retrospectively from hospital electronic records. Microsoft Excel for Mac 2011 and Prism version 6 was used for data analysis. Chi square test was used to calculate p-values, odds ratio and 95% confidence interval in mortality analysis. Kaplan-Meir curve was also performed for survival comparison between the two groups. Paired t-test was used to calculate p value and 95% confidence intervals in continuous variables.

5.3 Results

Baseline characteristics of all patients included in the final analysis are mentioned in table 5.1. Baseline characteristics showed a slight difference including a higher proportion of females (62%) in Group B. In terms of comorbidities, Group B patients had a lower percentage of ischemic heart disease and chronic obstructive pulmonary disease however the comorbidities were largely similar between the two groups. Group B patients were diagnosed with cardiac syncope more commonly as compared to patients in Group A. On the other hand reflex or vasovagal syncope was commonly observed in Group A patients. High proportions of atrio-ventricular (AV) nodal disease are seen in Group B patients as almost 58% of patients had a prolonged PR interval. The AV nodal disease frequently coexisted with LAD, RBBB and LBBB.

The outcome analysis is shown in Tables 5.2 and 5.3. Patient with conduction tissue abnormalities (Group B) showed worse prognosis with higher mortality during the mean follow up of 3.6 years (SD 2.0). Recurrent syncope was more common and they also had higher number of hospital admissions. The Kaplan-Meir curves in Figure 5.1 showed that the survival curves separates early but with long follow up, less differentiation was observed between the two group.

The decision of permanent pacing was the clinical decision that was taken by the individual cardiologist who assessed the patient. Permanent pacing didn't seem to alter the mortality risk amongst Group B patients, however the symptomatic improvement and reduced hospital admission were seen in patients after permanent pacemaker implantation. The Kaplan-Meir curve is quite interesting among Group B patients (Figure

5.2). It shows that with long term follow up, the curves start to separate suggesting a possible favourable prognosis amongst ECG-CTA patients with permanent pacing.

Table 5.1: Baseline characteristics of study population.

Variable	**Group A (Normal ECG) n (%)**	**Group B (Conduction tissue abnormalities)**	**ρ Value (NS=non significant)**
Patients	84	65	
Men	32 (38%)	Male 32 (49%)	NS
Women	52 (62%)	Female 33 (51%)	NS
Age	75±7 sd	77±8 sd	NS
First degree AV block	None	38 (58%)	< 0.0001
Left axis deviation	None	15 (23%)	<0.0001
Right bundle branch block	None	8 (12%)	<0.0001
Left bundle branch block	None	14 (21%)	<0.0001
Cardiac syncope	11 (13%)	32 (49%)	<0.0001
Reflex or vasovagal syncope	44(54%)	21(32%)	<0.05
Orthostatic hypotension	11 (13%)	7 (10%)	NS
Epilepsy	7 (9%)	1 (1.5%)	<0.05
Undiagnosed	6 (8%)	4 (6%)	NS
Vestibular syncope	1 (1%)	0	NS
Transient ischaemic attacks	1 (1%)	0	NS
Ejection fraction (<30%)	0	1 (1.5%)	NS
Ejection fraction (30-50%)	0	4 (6%)	NS
Mitral regurgitation	1 (1%)	1 (1.5%)	NS
Aortic Stenosis	0	1 (1.5%)	NS
Prosthetic Heart valve	1 (1%)	2 (3%)	NS
Comorbidities (1 or more)	43 (51%)	31 (48%)	NS
Comorbidities (2 or more)	28 (33%)	20 (31%)	NS
Hypertension	18 (21%)	17 (26%)	NS
Ischemic heart disease	10 (11%)	6 (9%)	NS
Chronic obstructive pulmonary disease	7 (8%)	1 (1.5%)	<0.05
Diabetes Mellitus	1 (1%)	3 (4.5%)	NS
Congenstive heart failure	0	1 (1%)	NS
Smoker/Exsmoker	7 (8%)	4 (6%)	NS
Chronic kidney disease (CKD 3 or above)	3 (4%)	1 (1.5%)	NS
Cerebrovascular disease	2 (3%)	0	NS
Medication (2 or more)	24 (28%)	18 (27%)	NS
Follow up (years)	3.6 (SD 2.0)	3.1 (SD 1.6)	NS

Table 5.2: Mortality and Morbidity

Variables	Group A (Normal ECG)	Group B (Conductions system abnormalities	P Value NS (Not significant)	95% confidence interval
Number of patients.	84	65		
All cause mortality	5 (6%)	11 (15%)	**< 0.05** Chi square test	0.10 to 0.94 (OR 0.31)
Recurrent syncope	61 (73%)	53 (81%)	**< 0.05** Paired t-test	**-0.20 to -0.04**
Implantation of Permanent Pacemaker	12 (14%)	31 (47%)	**<0.0001** Paired t-test	0.13 to 0.45
Implantable loop recorder implantation	22 (26%)	16 (24%)	NS	
Hospital admissions (Patients)	44 (52%)	44 (67%)	NS	
Number of Hospital admissions /patients/year	1.77	2.25	NS	
Injury/Fracture	38 (45%)	33 (51%)	NS	

Table 5.3: Outcome data after permanent pacemaker implantation in Group B patients

Variables	Group B1 (Post PPM)	Group B2 (No PPM)	P Value NS (Not significant)	95% confidence interval
Number of patients.	31 (47%)	34 (53%)	NS	
All cause mortality	5 (16%)	6 (17%)	**NS**	
Recurrent syncope reduction/Symptomatic improvement after PPM and/or medical management	23 (74%)	14 (41%)	**<0.001**	-0.56 to -0.09
No Hospital admissions after PPM and/ or medical management.	20 (64%)	12 (35%)	**<0.001**	-0.45 to -0.12

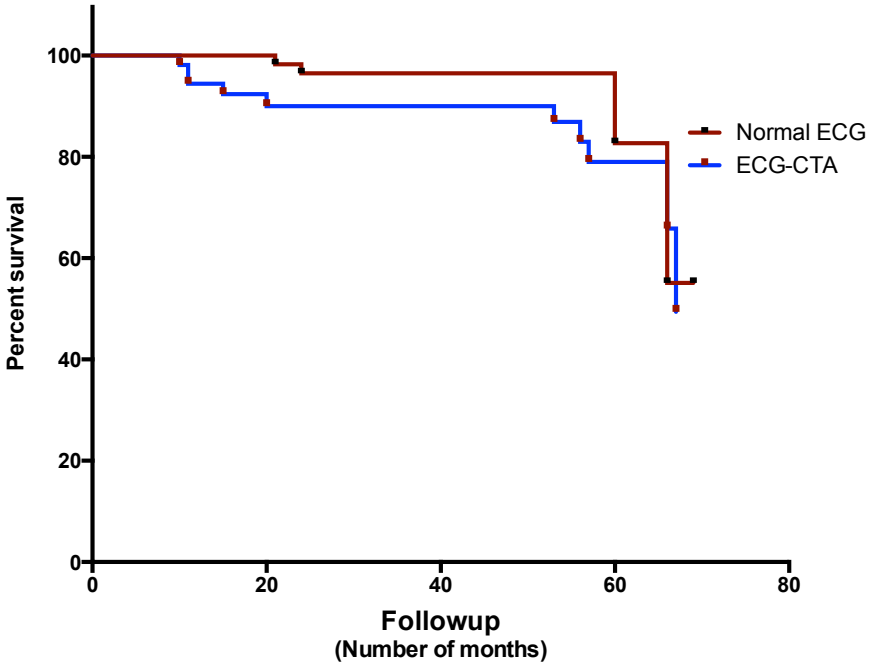

Figure 5.1: Kaplan-Meir curve to show survival analysis between Group A and Group B patients. The curves separate quite early indication worse prognosis in patients with conduction tissue abnormalities. With longer followup this difference becomes negligible. The curves are significantly different as calculated by Gehan-Breslo-Wilcoxon test (ρ-value <0.05, 95% confidence interval 0.15 to 1.36).

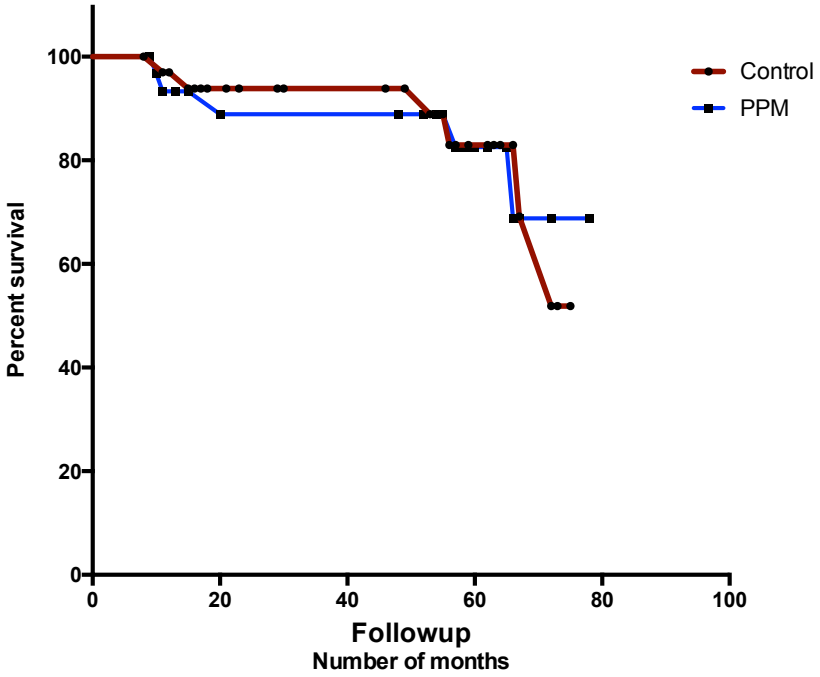

Figure 5.2: Kaplan-Meir curve to show survival analysis in Group B patients. No significant difference is seen however the curves starts to separate with longer followup data which may suggest improve prognosis in later years after pacemaker implanataion. The curves are not significantly different as calculated by Gehan-Breslo-Wilcoxon test.

5.3 Discussion

In our study we have compared outcomes in patients with TLOC with a normal ECG with those who presented with conduction tissue abnormalities (prolonged PR interval, LAD, RBBB, and LBBB). These conduction tissue abnormalities are often termed 'soft' and especially in elderly individuals they usually have been attributed to conduction system fibrosis with a possible exception of left bundle branch block. These findings especially in patients with syncope, should merit further investigation.

Recent studies evaluating the prognosis of these findings especially with AV nodal disease or prolonged PR interval in middle aged population showed conflicting results. A study based on the Framingham heart study population showed that prolonged PR interval is associated with atrial fibrillation, increased incidence of pacemaker implantation, and increased risk of mortality in general population.[165] Another study in patients with stable coronary artery disease showed that a prolonged PR interval is associated with increased heart failure related hospitalisation and mortality.[175] However, the Aro et al., study showed that PR interval prolongation in the middle aged population is partially transient and doesnot result in increased mortality. This obviously cannot be extended to the elderly population who are likely to have fixed and permanent conduction tissue abnormalities. Further to this, the recent finding of prolonged PR interval in those over 75 years is an important clinical predictor of pacemaker implantation in patients with syncope.[176]

It is already known that cardiac syncope confers poor prognosis especially in elderly patients.[168] However, my study identifies for the first time that findings of ECG-CTA confers poor prognosis in elderly patients (>65 years) with T-LOC or syncope. I have not shown that treating those with permanent pacemaker implantation results in improved mortality. However my study does demonstrate decreased hospital admission rate and symptomatic improvement with permanent pacing.

My findings of mortality benefit with permenant pacing could be limited because of the number of follow up years. It is possible that these ECG-CTA are early signs of structural heart disease although the moderate to severe left ventricular systolic dysfunction was found in only 7.5% of patients. Our study also identified important baseline characteristics in elderly patients with syncope. Epilepsy is an infrequent diagnosis in elderly patient with TLOC or syncope found in only 9% of Group A patients

and only 1% of Group B patients. This is also an uncommon finding in the young to middle aged population.[179]

This study was based on electronic records entered by a variety of individuals, which include specialist nurses, junior doctors and cardiologists. Although care has been taken to make sure the data is robust it is possible that the follow up data may not be complete for every individual. The outcome data, including mortality data has been verified again to maintain the authenticity. The other limiting factor of the study is the groups are not sex matched which could have an effect on the outcome data.

5.4 Conclusion

The findings of conduction tissue abnormalities especially in elderly patients with syncope should be carefully evaluated and investigated. These abnormalities are associated with increased morbidity and mortality. Permanent pacing in these individuals shows favorable results and should be considered.

Chapter 7

7.1 Summary and future directions

Ageing is associated with decline in the function of the AVN. This study confirms that the conduction time (AH interval) prolongs and the recovery properties of AV node (AVNERP and AVFRP) decline with ageing. The AV nodal disease (prolonged PR interval) as shown in Framingham heart study is associated with atrial fibrillation, permanent pacemaker implantation and increased mortality.[167] The Atherosclerosis risk in the communities (ARIC) study in patients with stable coronary artery disease also showed that prolonged PR interval is associated with increased risk of atrial fibrillation.[177] I have also demonstrated in my clinical study that in elderly patients with syncope or transient loss of consciousness, the cardiac conduction system disease including AV nodal disease is associated with increased mortality and morbidity.

This study demonstrates the effect of I_f current and the role of intracellular calcium release from the SR via RyR2 channel as an important mechanisms in AV nodal conduction. The changes observed by blocking these currents with ageing shed more light towards ion channel remodelling. My immunohistochemistry experiments showed that ion channels, calcium handling proteins and connexins were remodelled with ageing. Single cell studies with patch clamp technique to elucidate the changes in the ionic current with ageing would be helpful in establishing the effect of these ionic currents in greater detail.

My study has yielded important results concerning the cellular mechanisms of AV nodal conduction and its remodelling with ageing. For the very first time, we have been able to demonstrate the effect of I_f current i.e. membrane clock and calcium clock (calcium release from the SR) on the AV nodal conduction. We have also shown the changes in these "clocks" with ageing. The role of membrane clock and calcium clock in determining the automaticity of the SN is well established.[106] However, the evidence for their role in AV nodal conduction is lacking and whether these are involved in changes of AV nodal conduction with ageing was also not known. Previous studies have analyzed the automaticity of the AV node and not the AV nodal conduction. The studies by Liu et al.,[100] and Marger et al., in mice showed that blocking I_f current reduces the automaticity of the AVN.[49] Kim et al., also shown similar results.[101] The recent study in pig shown that blocking I_f with modulating I_{Na} can reduce AV conduction to a greater degree than blocking these current individually.[102] Another evidence come more recently by the same group, they have shown that blocking I_f with Ivabradine can prolong AH conduction in sinus rhythm and also reduce ventricular rate during atrial fibrillation in anesthetized pigs.[105] Mesirca et al., has also shown that affecting I_f results in AV block.[106] These experiments suggest the role of I_f on AV nodal conduction. My study has confirmed that blocking I_f result in prolongation of AH interval, WB cycle length, AVNERP and AVFRP in young rats.

Similar findings have been observed in the studies affecting calcium dynamics with Ryanodine. The block of RyR2 can decrease the automaticity of the AVN.[99,101] Our study confirms the role of blocking oscillatory calcium release from RyR receptors using Ryanodine results in impaired AV nodal conduction prolonging AH interval and WB cycle length. Another study has also demonstrated that blocking L-type calcium channels with Isardipine results in decreased automaticity of the AVN.[49] It is possible that the release of calcium from the SR depends on influx of calcium via these voltage sensitive calcium channels and both mechanisms are also important in AV nodal conduction.

The role of RyR blockage with ageing is associated with prolonging AH interval and WB cycle length. The increased sensitivity to ryanodine with ageing together with almost no effect of blocking I_f suggest that the ageing AVN is more dependent on calcium dynamics for AV nodal conduction. This suggests the role of background excitability of the AVN cells in the AV nodal conduction. Does less background excitability in cardiac conduction system tissues result in decreased conduction? The AVN is unique in that aspect. It is more excitable (increase automaticity) than the bundle branches, purkinje cells and also delays conduction. If we decrease the automaticity we

can certainly delay conduction as shown in my functional experiments. The probable explanation is the decreased automaticity due to the increased slope of phase 4 depolarisation (via hyperpolarising membrane current). This may effect the action potential propagation as the successive cells need more time to reach the excitation threshold to generate the action potential, which ultimately increases the conduction time across the AVN.

For the first time, this study has reported down regulation of HCN4 (His), RyR2 (CN, PB) and Cx43 (PB, His) with ageing, whereas the up regulation of SERCA2a (CN, PPB), $Ca_v1.3$ (His) and Cx40 (INE, CN) is seen. These findings in my study demonstrate that changes in protein expression can explain the functional changes seen with ageing. Increased fibrosis, decreased Cx43, decreased HCN4, decreased RyR2, increased SERCA2a expression and decrease $Na_v1.5$ are likely to increase conduction time. The finding of changes in caveolin3 and alpha actinin is likely to have no effect on the conduction time seen with ageing. Perhaps the increased expression of Cx40 and $Ca_v1.3$ is a compensatory mechanism. Cx40 co-expression with other connexins can explain increased expression with ageing. Future work should include mRNA expression to further further improve understanding of ion channel remodelling seen with ageing. The computer modelling of these changes in the ion channels, calcium handling proteins and gap junctions will be needed to integrate the results.

Gene knockout studies have shown multiple ion channels including HCN4[54], $Ca_v3.1$[48] and Cx40[143] associated with AV nodal conduction disease. The slowing of AV conduction has also been reported in genetic diseases caused by SCN5a mutation,[74] CACNA1d ($Ca_v1.3$) and CACNA1c ($Ca_v1.2$) mutation. Recently, a genome wide association study has shown that there are several ion channel loci associated with prolonged PR interval.[180] These ion channel loci include genes coding for $Na_v1.5$ (SCN5a), caveolin and Tbx3-Tbx5 (transcription factors important in the development of the CCS).

There are few limitations in my study. Because of the time constraints in getting the old rats (24 months) I have not been able to perform electrophysiological experiments with other ion channel blocker specifically calcium channel blockers. That would further increase our understanding the role of calcium channels in the AVN conduction with ageing. Secondly, I have not been able to perform the immunohistochemistry experiment on the K^+ channels, HCN2 and Cx45. I have tried multiple commercially available antibodies but didn't get the specific signals required for the correct interpretation of the data. Thirdly, another quantitative method like western blot or qPCR to confirm our

immunohistochemistry results would increase the authenticity of the results further however again because of time constraints this was not possible.

From the data shown in this thesis, I conclude that the decline in the function of AVN with ageing is likely the result of ion channel, connexins and calcium handling proteins remodelling together with fibrosis. This remodelling with ageing may be associated with further worsening of the AV nodal function seen in high degrees of AV block (2^{nd} and 3^{rd} degree AV block) requiring permanent pacemaker implantation.

Ageing has already become the cornerstone of most disease patterns that we see today. The AV nodal disease and cardiac conduction system abnormalities with ageing are already well known. AV nodal disease is the most common indication for permanent pacemaker implantation and pacemaker implantation is highest in elderly individuals.[165] The permanent pacemaker implantation is associated with multiple complications and efforts to develop a biological pacemaker have been actively pursed. The genetic therapy for various diseases with the discovery of whole human genome looks promising now and for that we need more information about the basic concepts that underly the AV nodal dysfunction with ageing.

References

1. Akiyama, T. Sunao Tawara: Discoverer of the atrioventricular conduction system of the heart. *Cardiology Journal* 17, 428–433 (2010).
2. Suma, K. Sunao Tawara: a father of modern cardiology. *Pacing and Clinical Electrophysiology*, 24, 88-96 (2001).
3. Silverman, M. and Grove, D. Why Does the Heart Beat? *Circulation*, 113 (23), 2775-2781 (2006).
4. Tawara, S., Suma, K. and Shimada, M. *The conduction system of the mammalian heart: an anatomico-histological study of the atrioventricular bundle and the Purkinje fibers*. Imperial college press (2000).
5. Anderson, R. H., Yanni, J., Boyett, M., Chandler, N. and Dobrzynski, H. The anatomy of the cardiac conduction system. *Clinical Anatomy*. 99–113 (2009).
6. Boyett, M R. 'And the beat goes on' The cardiac conduction system: the wiring system of the heart. *Experimental Physiology,* 94 (10) 1035-1049 (2009).
7. Keith, A. and Flack, M. The form and nature of the muscular connections between the primary divisions of the vertebrate Heart. *Journal of Anatomy and Physiology,* **41,** 172–189 (1907).
8. Hering, H E. Evidence that the delay of the excitation transfer between atrium and ventricle of Säugethierherzens is in Tawara's node. *European Journal of Physiology,* 131 (10-12) 572-580 (1910*)*.
9. Davies, M. and Anderson, R. *The conduction system of the heart*. (Butterworth-Heinemann, 1983).
10. Lewis, T. *The mechanism and graphic registration of the heart beat*. Shaw and sons, London (1925).
11. Christoffels, V., Smits, G., Kispert, A., and Moorman A F M. Development of the Pacemaker Tissues of the Heart. *Circulation Research,* 106, 240-254 (2010).
12. Moorman, A. F. M. and Christoffels, V. M. *Novartis Foundation Symposia*. 250**,** 25–43 (John Wiley & Sons, 2003).
13. Lieberman, M. The spread of excitation in the embryonic Chick Heart. *The Journal of General Physiology,* 49**,** 365–379 (1965).
14. Moorman, A. and Christoffels, V. Cardiac chamber formation: development, genes, and evolution. *Physiology Reviews,* 83 (4) 1223-1267 (2003).
15. Hoogaars, W. M. H., Barnett, P., Moorman, A. F. M. and Christoffels, V. M. T-box factors determine cardiac design. *Cellular and Molecular Life Sciences,* 64, 646–660 (2007).
16. Hoogaars, W. M. H., Engel A, Brons, J. F., Verkerk, A. O., de Lange, F. J., Wong, L. Y. E., Bakker, M. L., Clout, D. E., Wakker, V., Barnett, P., Ravesloot, H. J., Moorman, A. F. M., Verheijck, E., and Christoffels, V. M. Tbx3 controls the sinoatrial node gene program and imposes pacemaker function on the atria. *Genes and Development,* 21, 1098–1112 (2007).
17. Moorman, A., Anderson, R. and Lamers, W. Development of the myocardium of the atrioventricular canal and the vestibular spine in the human heart. *Circulation Research,* 88 (4) 395-402 (2001).
18. Anderson, R. H. and Yen Ho, S. The morphology of the specialized atrioventricular junctional area: The evolution of understanding. *Pacing and Clinical Electrophysiology*, 25, 957–966 (2002).
19. Meijler, F. and Janse, M J. Morphology and electrophysiology of the mammalian atrioventricular node. *Physiology Reviews*, 68 (2) 608-647 (1988).
20. Inoue, S., and Becker, A. Posterior extensions of the human compact atrioventricular node: a neglected anatomic feature of potential clinical significance. *Circulation*, 97 (2) 188-193 (1998).
21. Kurian, T., Ambrosi, C., Hucker, W., Fedorov, V. V. and Efimov, I. R. Anatomy and electrophysiology of the human AV node. *Pacing and Clinical Electrophysiology* 33, 754–762 (2010).
22. Dobrzynski, H. Nikolski, V. P., Sambelashvili, A. T., Greener, I. D., Yamamoto, M.,

Boyett, M. R., and Efimov, I. R. Site of origin and molecular substrate of atrioventricular junctional rhythm in the rabbit heart. *Circulation Research,* 93, 1102-1110 (2003).
23. Hucker, W. and Nikolski, V. Optical mapping of the atrioventricular junction. *Journal of Electrocardiology,* 38, 121-125 (2005).
24. Greener, I., Tellez, J., Dobrzynski, H., Yamamoto, M., Graham, G. M., Billeter, R., & Boyett, M. R. (2009). Ion channel transcript expression at the rabbit atrioventricular conduction axis. *Circulation: Arrhythmia and Electrophysiology*, *2*, 305–315 (2009).
25. Mazgalev, T. and Tchou, P. J. *Atrial-AV nodal electrophysiology: A View from the millennium*. (Wiley-Blackwell 2000).
26. Moe, G., Preston, J., and Burlington, H. Physiologic evidence for a dual A-V transmission system. *Circulation Research*, *4*, 357–375, (1956).
27. Denes, P., Wu, D., Dhingra, R., Amat-y-Leon, F., Wyndham, C., & Rosen, K. M. Dual atrioventricular nodal pathways. A common electrophysiological response. *Heart*, *37* (10), 1069–1076 (1975).
28. Casta, A., Wolff, G., Mehta, A., & Tamer, D. Dual atrioventricular nodal pathways: A benign finding in arrhythmia-free children with heart disease. *The American Journal of Cardiology*, *48*, 1013–1018 (1980).
29. Carvalho, A. D. Spread of activity through the atrioventricular node. *Circulation Research*, *8*, 801–809 (1960).
30. Billette, J. Atrioventricular nodal activation during periodic premature stimulation of the atrium. *The American Journal of Physiology*, *252* (1 Pt 2), H163–77 (1987).
31. Efimov, I. R., Nikolski, V. P., Rothenberg, F., Greener, I. D., Li, J., Dobrzynski, H., & Boyett, M. Structure-function relationship in the AV junction. *The Anatomical Record*, *280A*(2), 952–965 (2004).
32. Munk, A. A., Adjemian, R. A., Zhao, J., Ogbaghebriel, A. and Shrier, A. Electrophysiological properties of morphologically distinct cells isolated from the rabbit atrioventricular node. *Journal of Physiology (London)* **493 (3),** 801–818 (1996).
33. Ren, F., Niu, X., Ou, Y., Han, Z., Ling, F., & Zhou, S. Morphological and electrophysiological properties of single myocardial cells from Koch triangle of rabbit heart. *Chinese Medical Journal*, *119*, 2075–2084 (2006).
34. Efimov, I. and Mazgalev T. N. High-resolution, three-dimensional fluorescent imaging reveals multilayer conduction pattern in the atrioventricular node. *Circulation*, *98*, 54–57 (1998).
35. Bharati, S.. Anatomic-morphologic relations between AV nodal structure and function in the normal and diseased heart. In T. N. Mazgalev and P. J. Tchou, *Atrial-AV nodal electrophysiology: A view from the millenium*. Wiley-Blackwell (2000).
36. Li, J., Greener, I. D., Inada, S., Nikolski, V. P., Yamamoto, M., Hancox, J. C., Zhang, H., Billeter, R., Efimov, I. R., Dobrzynski, H., and Boyett, M. R. Computer Three-Dimensional Reconstruction of the Atrioventricular Node. *Circulation Research*, *102*(8), 975–985 (2008).
37. Rosen, K., Mehta, A., & Miller, R. A. Demonstration of dual atrioventricular nodal pathways in man. *The American Journal of Cardiology*, *33*, 291–294 (1974).
38. Mazgalev, T., Yen Ho, S., & Anderson, R. H. Anatomic-Electrophysiological Correlations Concerning the Pathways for Atrioventricular Conduction. *Circulation*, *103*, 2660–2667 (2001).
39. Issa, Z., Miller, J., and Zipes, D. *Clinical arrhythmology and electrophysiology: a companion to Braunwald's heart disease* (1st ed.). Saunders, Elsevier. (2009).
40. Murgatroyd, F., Krahn, A. D., Klein, G. J., Skanes, A. C., & Yee, R. *Handbook of cardiac electrophysiology: A practical guide to invasive EP studies and catheter Ablation* (1st ed.). Remediaca publishing limited (2002).
41. Hucker, W. J., Mccain, M. L., Laughner, J. I., Iaizzo, P. A. and Efimov, I. R. Connexin 43 expression delineates two discrete pathways in the human atrioventricular junction. *The Anatomical Record* **291,** 204–215 (2008).
42. Petrecca, K., Amellal, F., Laird, D. W., Cohen, S. A. and Shrier, A. Sodium channel distribution within the rabbit atrioventricular node as analysed by confocal microscopy. *Journal of Physiology (Lond.)* **501,** 263–274 (1997).

43. Carvalho, A. D. *The specialized tissues of the heart*, Elsevier (1961).
44. Marger, L., Mesirca, P., Alig, J., Torrente, A., Dübel, S., Engeland, B., Kanani, S., Fontanaud, Pierre., Striessnig. J., Shin, H. S., Isbrandt, D., Ehmke, H., Nargeot, J., and Mangoni, M. E. Pacemaker activity and ionic currents in mouse atrioventricular node cells. *Channels*, *5*(3), 241–250 (2014).
45. Yoo, S., Dobrzynski, H., Fedorov, V. V., Xu, S., Yamanushi, T. T., Jones, S. A., Yamamoto, M., Nikolski, V. P., Efimov, I. R., and Boyett, M. R. Localization of Na+ Channel Isoforms at the Atrioventricular Junction and Atrioventricular Node in the Rat. *Circulation*, *114*(13), 1360–1371 (2006).
46. Liu, Y., Zeng, W., Delmar, M. and Jalife, J. Ionic mechanisms of electronic inhibition and concealed conduction in rabbit atrioventricular nodal myocytes. *Circulation* **88,** 1634–1646 (1993).
47. Zipes, D. P. and Mendex, C. Action of manganese Ions and tetrodotoxin on atrioventricular nodal transmembrane potentials in isolated rabbit hearts. *Circulation Research* **32,** 447–454 (1973).
48. Mangoni, M. E., Traboulsie, A., Leoni, A.-L., Couette, B., Marger, L., Khai Le, Q., Kupfer, E., Cohen-Solal, A., Vilar, J., Shin, H. S., Escande, D., Charpentier, F., Nargeot, J., and Lory, P., (2006). Bradycardia and slowing of the atrioventricular conduction in mice lacking CaV3. 1/α1G T-type calcium channels. *Circulation Research*, *98*, 1422–1430 (2006).
49. Marger, L., Mesirca, P., Alig, J., Torrente, A., Dübel, S., Engeland, B., Kanani, S., Fontanaud, Pierre., Striessnig. J., Shin, H. S., Isbrandt, D., Ehmke, H., Nargeot, J., and Mangoni, M. E.Functional roles of Ca v1.3, Ca v3.1 and HCN channels in automaticity of mouse atrioventricular cells. *Channels*, *5*(3), 251–261 (2014).
50. Baig, S. M., Koschak, A., Lieb, A., Gebhart, M., Dafinger, C., Nürnberg, G., Ali, A., Ahmad, I., Sinnegger-Brauns, M. J., Brandt, N., Engel, J., Mangoni, M. E., Farooq, M., Khan, H. U., Nürnberg, P., Striessnig, J., and Bolz, H. J. Loss of $Ca_v1.3$ (CACNA1D) function in a human channelopathy with bradycardia and congenital deafness. *Nature Neuroscience*, *14*(1), 77–84 (2011).
51. Ludwig, A., Zong, X., Jeglitsch, M., Hofmann, F. and Biel, M. A family of hyperpolarization-activated mammalian cation channels. *Nature* **393,** 587–591 (1998).
52. DiFrancesco, D. The role of the funny current in pacemaker activity. *Circulation Research* **106,** 434–446 (2010).
53. Bucchi, A., Barbuti, A., Baruscotti, M. and DiFrancesco, D. Heart rate reduction via selective 'funny' channel blockers. *Current Opinion in Pharmacology,* **7,** 208–213 (2007).
54. Baruscotti, M., Bucchi, A., Viscomi, C., Mandelli, G., Consalez, G., Gnecchi-Rusconi, T., Montano, N., Casali, K. R., Micheloni, S., Barbuti, A., and DiFrancesco, D. Deep bradycardia and heart block caused by inducible cardiac-specific knockout of the pacemaker channel gene Hcn4. *Proceedings of the National Academy of Sciences of the United States of America*, *108*(4), 1705–1710. **108,** 1705–1710 (2011).
55. Mazgalev, T., Dreifus, L. S., Michelson, E. L. and Pelleg, A. Vagally induced hyperpolarization in atrioventricular node. *American Journal of Physiology,* **251,** H631–43 (1986).
56. Clemo, H. F. and Belardinelli, L. Effect of adenosine on atrioventricular conduction. I: Site and characterization of adenosine action in the guinea pig atrioventricular node. *Circulation Research* **59,** 427–436 (1986).
57. Shibasaki, T. Conductance and kinetics of delayed rectifier potassium channels in nodal cells of the rabbit heart. *Journal of Physiology (Lond.)* **387,** 227–250 (1987).
58. Coppen, S. R. and Severs, N. J. Diversity of Connexin expression patterns in the atrioventricular node: Vestigial consequence or functional Specialization? *Journal of Cardiovascular Electrophysiolgy* **13,** 625–626 (2002).
59. Gourdie, R., Severs, N., Green, C., Rothery, S., Germroth, P., & Thompson, R. P. The spatial distribution and relative abundance of gap-junctional connexin40 and connexin43 correlate to functional properties of components of the cardiac atrioventricular conduction system. *Journal of Cell Science*, *105*, 985–991. (1993).
60. Boyett, M., Inada, S., Yoo, S., Li, J., Liu, J., Tellez, J., Greener, I., Honjo, H., Billeter,

R., Lei, M., Zhang, H., Efimov, I., and Dobrzynski, H. Connexins in the sinoatrial and atrioventricular nodes. In S. Dhein, *Cardiovascular gap junctions* (Vol. 42, pp. 175–197). Karger Publishers (2006).

61. Kreuzberg, M. M., Liebermann, M., Segschneider, S., Dobrowolski, R., Dobrzynski, H., Kaba, R., Rowlinson, G., Dupont, E., Severs, N. J., and Willecke, K. Human connexin31.9, unlike its orthologous protein connexin30.2 in the mouse, is not detectable in the human cardiac conduction system. *Journal of Molecular and Cellular Cardiology*, *46*(4), 553–559 (2009).
62. Kreuzberg, M. M., Sohl, G., Kim, J.-S., Verselis, V. K., Willecke, K., and Bukauskas, F. F. Functional Properties of Mouse Connexin30.2 Expressed in the Conduction System of the Heart. *Circulation Research*, *96*(11), 1169–1177 (2005).
63. Petrecca, K. and Shrier, A. Spatial distribution of nerve processes and beta-adrenoreceptors in the rat atrioventricular node. *Journal of Anatomy* **192,** 517–528 (1998).
64. Prystowsky, E., Jackman, W., Rinkenberger, R. L., Heger, J. J., & Zipes, D. P. Effect of autonomic blockade on ventricular refractoriness and atrioventricular nodal conduction in humans. Evidence supporting a direct cholinergic action on Ventricular muscle refractoriness. *Circulation Research*, *49*, 511–518 (1981).
65. Akhtar, M., Damato, A. N., Caracta, A. R., Batsford, W. P., Josephson, M. E., and Lau, S. H. Electrophysiologic effects of atropine on atrioventricular conduction studied by His bundle electrogram. *The American Journal of Cardiology*, *33*(3), 333–343 (1974).
66. Berkowitz, W., Wit, A., & Lau, S. The effects of propranolol on cardiac conduction. *Circulation*, *40 (6)*, 855–862 (1969).
67. Taggart, P., Boyett, M. R., Logantha, S., and Lambiase, P. D. Anger, Emotion, and Arrhythmias: From Brain to Heart. *Frontiers in Physiology*, *2*, 1–11 (2011).
68. Brugada, P. and Brugada, J. Right bundle branch block, persistent ST segment elevation and sudden cardiac death: a distinct clinical and electrocardiographic syndrome. A multicenter report. *Journal of American College of Cardiology.* **20,** 1391–1396 (1992).
69. Tan, H., Bezzina, C. R., Smits, J. P., Verkerk, A. O., and Wilde A. A. M. Genetic control of sodium channel function. *Cardiovascular Research* **57,** 961–973 (2003).
70. Schott, J. J., Alshinawi, C., Kyndt, F., Probst, V., Hoorntje, T. M., Hulsbeek, M., Wilde, A. A., Escande, D., Mannens, M. M., and Marec, H. Le. Cardiac conduction defects associate with mutations in SCN5A. *Nature Genetics*, *23*(1), 20–21. Schott, J. J. *et al.* Cardiac conduction defects associate with mutations in SCN5A. *Nature Genetics.* **23,** 20–21 (1999).
71. Tan, H. L., Bink-Boelkens, M. T., Bezzina, C. R., Viswanathan, P. C., Beaufort-Krol, G. C., van Tintelen, P. J., Van den Berg, M. P., Wilde, A. A., and Balser, J. R. A sodium-channel mutation causes isolated cardiac conduction disease. *Nature*, *409*(6823), 1043–1047 (2001).
72. Kyndt, F., Probst, V., Potet, F., Demolombe, S., Chevallier, J. C., Baro, I., (2001). Novel SCN5A mutation leading either to isolated cardiac conduction defect or Brugada syndrome in a large French family. *Circulation*, *104*(25), 3081–3086 (2001).
73. Wang, D., Viswanathan, P., Balser, J., George, A. L., & Benson, D. W. Clinical, genetic, and biophysical characterization of SCN5A mutations associated With atrioventricular conduction block. *Circulation*, *105*, 341–346 (2002).
74. McNair, W., Ku, L., Taylor, M., Fain, P., Dao, D., Wolfel, E., & Mestroni, L. SCN5A Mutation Associated With Dilated Cardiomyopathy, Conduction Disorder, and Arrhythmia. *Circulation*, *110*, 2163–2167 (2004).
75. Viswanathan, P. and Balser, J. R. Inherited Sodium Channelopathies A Continuum of Channel Dysfunction. *Trends in Cardiovascular Medicine, 14, 28-35* (2004).
76. Boutjdir, M., Chen, L., Zhang, Z., Tseng, C. E., El-Sherif, N., & Buyon, J. P. Serum and immunoglobulin G from the mother of a child with congenital heart block induce conduction abnormalities and inhibit L-type calcium channels in a rat heart model. *Pediatric Research*, *44*, 11–19 (1998).
77. Qu, Y., Xiao, G.-Q., Chen, L. and Boutjdir, M. Autoantibodies from mothers of children with congenital heart Block downregulate cardiac L-type Ca^{2+} channel. *Journal of Molecular and Cellular Cardiology* **33,** 1153–1163 (2001).

78. Hu, D., Barajas-Martinez, H., Nesterenko, V. V., Pfeiffer, R., Guerchicoff, A., Cordeiro, J. M., Curtis, A. B., Pollevick, G. D., Wu, Yu., Burashnikov, E., and Antzelevitch, C. (2010). Dual variation in SCN5A and CACNB2b underlies the development of cardiac conduction disease without Brugada syndrome. *Pacing and Clinical Electrophysiology*, *33* (3), 274–285. (2010).
79. Oka, Y., Itoh, H., Ding, W.-G., Shimizu, W., Makiyama, T., Ohno, S., Nishio, Y., Sakaguchi, T., Miyamoto, A., Kawamura, M., Matsuura, H., and Horie., M. Atrioventricular block-induced Torsades de Pointes with clinical and molecular backgrounds similar to congenital long QT syndrome. *Circulation Journal : Official Journal of the Japanese Circulation Society*, *74*(12), 2562–2571 (2010).
80. Waki, K., Kim, J. S. and Becker, A. E. Morphology of the human atrioventricular node is age dependent: a feature of potential clinical significance. *Journal of Cardiovasc Electrophysiolgy,* **11,** 1144–1151 (2000).
81. Blaufox, A., Rhodes, J., and Fishberger, S. Age related changes in dual AV nodal physiology. *Pace-Pacing and Clinical Electrophysiology*, *23*, 477–480 (2000).
82. Fujino, M., Okada, R. and Arakawa, K. The relationship of aging to histological changes in the conduction system of the normal human heart. *Japan Heart Journal,* **24,** 13–20 (1983).
83. Buruljanowa, I., Wassilew, G., and Radanov, S. Age-related structural changes in the stimuli-conducting system of the human heart. *Zentralbl Allg Pathology*, *133*, 433–438 (1987).
84. Gottwald, M., Gottwald, E., and Dhein, S. Age-related electrophysiological and histological changes in rabbit hearts Age-related changes in electrophysiology. *International Journal of Cardiology,* **62,** 97–106 (1997).
85. Song, Y., Laaksonen, H., Saukko, P., Toivonen, S. and Zhu, J. Histopathological findings of cardiac conduction system of 150 Finns. *Forensic Science International,* **119,** 310–317 (2001).
86. Tellez, J. O., Mączewski, M., Yanni, J., Sutyagin, P., Mackiewicz, U., Atkinson, A., Inada, S., Beresewicz, A., Billeter, R., Dobrzynski, H., and Boyett, M. R. Ageing-dependent remodelling of ion channel and Ca2+ clock genes underlying sinoatrial node pacemaking. *Experimental Physiology*, (96), 1163–1178 (2011).
87. Yanni, J., Tellez, J., Sutyagin, P., Boyett, M. R., and Dobrzynski, H. Structural remodelling of the sinoatrial node in obese old rats. *Journal of Molecular and Cellular Cardiology*, 48, 653-662 (2010).
88. Lim, S. H., Anantharaman, V., Teo, W. S., Goh, P. P. Tan, A. T. Comparison of treatment of supraventricular tachycardia by Valsalva maneuver and carotid sinus massage. *Annals of Emergency Medicine,* **31,** 30–35 (1998).
89. Chow, L. T., Chow, S. S., Anderson, R. H. and Gosling, J. A. Autonomic innervation of the human cardiac conduction system: changes from infancy to senility--an immunohistochemical and histochemical analysis. *The Anatomical Record* **264,** 169–182 (2001).
90. Kusumoto, F., Lurie, K., Dutton, J., Capili, H., and Schwartz, J. B. Effects of aging on AV nodal and ventricular beta-adrenergic receptors in the Fischer 344 rat. *American Journal of Physiology,* 1408–1415 (1994).
91. Kavanagh, K. M., Wyse, D. G., Mitchell, L. B. and Duff, H. J. Cardiac refractorines: Age-dependence in normal subjects. *Journal of Electrocardiology,* **22,** 221–225 (1989).
92. Kuo, C. T., Wu, J. M., Lin, K. H. and Young, M. L. The effects of aging on AV nodal recovery properties. *Pacing and Clinical Electrophysiology,* **24,** 194–198 (2001).
93. Lin, M.-H., Young, M. L., Wu, J. M., and Wolff, G. (1997). Developmental changes of atrioventricular nodal recovery properties. *The American Journal of Cardiology*, *80*, 1178–1182 (1997).
94. Taneja, T., Windhagen, M., Passman, R., Goldberger, J., and Kadish, A. Effects of sex and age on electrocardiographic and cardiac electrophysiological properties in adults. *Pacing and Clinical Electrophysiology*, *24*, 16–21 (2001).
95. Schwartz, J., & Craft, N. (1995). Effects of age on intrinsic heart rate, heart rate variability, and AV conduction in healthy humans. *American Journal of Physiology,*1441–1452 (1995).

96. Schmidlin, O., Bharati, S., Lev, M. and Schwartz, J. B. Effects of physiological aging on cardiac electrophysiology in perfused Fischer 344 rat hearts. *American Journal of Physiology,* **262,** H97–105 (1992).
97. Schwartz, J., and Gibb, W. (1991). Aging effects on heart rate variation. *Journal of Gerontology*, *46*, 99–106 (1991).
98. D'Este, D., Bertaglia, E., Zanocco, A., Reimers, B. & Pascotto, P. Electrophysiological properties of the atrioventricular node and ageing: evidence of a lower incidence of dual nodal pathways in the elderly. *Europace* **3,** 216–220 (2001).
99. Nikmaram, M. R., Liu, J., Abdelrahman, M., Dobrzynski, H., Boyett, M. R., and Lei, M. Characterization of the effects of Ryanodine, TTX, E-4031 and 4-AP on the sinoatrial and atrioventricular nodes. *Progress in Biophysics and Molecular Biology*, *96*(1-3), 452–464 (2008).
100. Liu, J., Noble, P. J., Xiao, G., Abdelrahman, M., Dobrzynski, H., Boyett, M. R., Lei, M., and Noble, D. Role of pacemaking current in cardiac nodes: Insights from a comparative study of sinoatrial node and atrioventricular node. *Progress in Biophysics and Molecular Biology*, *96*(1-3), 294–304 (2008).
101. Kim, D., Shinohara, T., Joung, B., Maruyama, M., Choi, E. K., On, Y. K., Han, S., Fishbein, M. C., Lin, S. F., and Chen, P. S. Calcium Dynamics and theMechanisms of Atrioventricular Junctional Rhythm. *Journal of American college of cardiology*, *56*(10), 805–812 (2010).
102. Verrier, R. L., Silva, A. F. G., Bonatti, R., Batatinha, J. A. P., Nearing, B. D., Liu, G. X., et al. (2014). Combined Actions of Ivabradine and Ranolazine reduce ventricular rate during atrial fibrillation. *Journal of Cardiovascular Electrophysiology*, 1–7 (2014).
103. Temple, I. P. Arrhythmogenesis in Pulmonary Hypertension. *PhD Thesis, University of Manchester* 1–240 (2014).
104. Lakatta, E. G. and DiFrancesco, D. What keeps us ticking: a funny current, a calcium clock, or both? *Journal of Molecular and Cellular Cardiology,* **47,** 157–170 (2009).
105. Verrier, R. L., Bonatti, R., Silva, A. F. G., Batatinha, J. A. P., Nearing, B. D., Liu, G., Rajamani, S., Zeng, D., and Belardinelli, L. I_f inhibition in the atrioventricular node by ivabradine causes rate-dependent slowing of conduction and reduces ventricular rate during atrial fibrillation. *Heart Rhythm*, *11*(12), 2288–2296.
106. Mesirca, P., Alig J., Torrente A. G., Müller J. C., Marger L., Rollin A., Marquilly C., Vincent A., Dübel S., Bidaud, I., Fernandez A., Seniuk A., Engeland B., Singh J., Miquerol L., Ehmke H., Eschenhagen T., Nargeot J., Wickman K., Isbrandt D., and Mangoni M. E. Cardiac arrhythmia induced by genetic silencing of 'funny' (f) channels is rescued by GIRK4 inactivation. *Nature Communications* **5,** 4664 (2014).
107. Rousseau, E., Smith, J. S. & Meissner, G. Ryanodine modifies conductance and gating behavior of single Ca2+ release channel. *American Journal of Physiology - Cell Physiology* **253,** C364–C368 (1987).
108. Ector, H., Vardas, P. (On behalf of the European Heart Rhythm Association, European Society of Cardiology). Current use of pacemakers, implantable cardioverter defibrillators, and resynchronization devices: data from the registry of the European Heart Rhythm Association. *European Heart Journal Supplements* **9,** I44–I49 (2007).
109. Puchtler, H., Waldrop, F. S. and Valentine, L. S. Polarization microscopic studies of connective tissue stained with picro-sirius red FBA. *Beitr Pathology,* **150,** 174–187 (1973).
110. Junqueira, L. C. U., Bignolas, G. and Brentani, R. R. Picrosirius staining plus polarization microscopy, a specific method for collagen detection in tissue sections. *Histochemical Journal* **11,** 447–455 (1979).
111. Whittaker, P., Kloner, R. A., Boughner, D. R. and Pickering, J. G. Quantitative assessment of myocardial collagen with picrosirius red staining and circularly polarized light. *Basic Research in Cardiology,* **89,** 397–410 (1994).
112. Bancroft, J. and Gamble, M. *Theory and practice of histological techniques (6th Ed.)*, (Baracourt Ltd, 2008).
113. Sandusky, G. E., Kerr, K. M. and Capen, C. C. Morphologic variations and aging in the

atrioventricular conduction system of large breed dogs. *The Anatomical Record*, **193,** 883–901 (1979).
114. Papadatos, G. A., Wallerstein, P. M. R., Head, C. E. G., Ratcliff, R., Brady, P. A., Benndorf, K., Saumarez, R. C., Trezise, A. E. O., Huang, Christopher L. J., Vandenberg, I., Colledge, W. H., and Grace A. A. Slowed conduction and ventricular tachycardia after targeted disruption of the cardiac sodium channel gene Scn5a. *Proceedings of National Acadmey of Science, USA*, *99* (9), 6210–6215 (2002).
115. Smith, A. and Bruton, J. *A colour atlas of histological staining techniques*. (1977).
116. Chandler, N. J., Greener, I. D., Tellez, J. O., Inada, S., Musa, H., Molenaar, P., DiFrancesco, D., Baruscotti, M., Longhi, R., Anderson, R. H., Billeter, R., Sharma, V., Sigg, D C., Boyett, M. R., and Dobrzynski, H. Molecular Architecture of the Human Sinus Node: Insights Into the Function of the Cardiac Pacemaker. *Circulation*, *119*(12), 1562–1575 (2009).
117. Morris, G. M., Boyett, M. R., Yanni, J., Billeter, R. and Dobrzynski, H. Detection and measurement of cardiac ion channels. *Methods and Models* 187–212 (Springer US, 2010).
118. Brown, H. F., DiFrancesco, D. and NOBLE, S. J. How does adrenaline accelerate the heart? *Nature,* **280,** 235–236 (1979).
119. Wahl-Schott, C. and Biel, M. HCN channels: Structure, cellular regulation and physiological function. *Cellular and Molecular Life Sciences,* **66,** 470–494 (2008).
120. Biel, M., Schneider, A. and Wahl, C. Cardiac HCN channels: structure, function, and modulation. *Trends in Cardiovascular Medicine,* **12,** 206–212 (2002).
121. Wainger, B. J., DeGennaro, M., Santoro, B., Siegelbaum, S. A. and Tibbs, G. R. Molecular mechanism of cAMP modulation of HCN pacemaker channels. *Nature,* **411,** 805–810 (2001).
122. Stieber, J., Herrmann, S., Feil, S., Löster, J., Feil, R., Biel, M., Hofmann, F., and Ludwig, A. The hyperpolarization-activated channel HCN4 is required for the generation of pacemaker action potentials in the embryonic heart. *Proceedings of the National Academy of Sciences of the United States of America*, *100* (25), 15235–15240. (2003).
123. Herrmann, S., Stieber, J., Stöckl, G., Hofmann, F. and Ludwig, A. HCN4 provides a 'depolarization reserve' and is not required for heart rate acceleration in mice. *The European Molecular Biology Organization Journal,* **26,** 4423–4432 (2007).
124. Meens, M. J., Pfenniger, A., Kwak, B. R. and Delmar, M. Regulation of cardiovascular connexins by mechanical forces and junctions. *Cardiovascular Research,* **99,** 304–314 (2013).
125. Saez, J. C., Berthoud, V. M., Branes, M. C., Martinez, A. D. and Beyer, E. C. Plasma membrane channels formed by connexins: their regulation and functions. *Physiology Reviews,* **83,** 1359–1400 (2003).
126. van Veen, T., van Rijen, H., Opthof., T. Cardiac gap junction channels: modulation of expression and channel properties. *Cardiovascular Research,* **51,** 217–229 (2001).
127. Kumar, N. M. and Gilula, N. B. The gap junction communication channel. *Cell* **84,** 381–388 (1996).
128. Sohl, G., and Willicke, K. Gap junctions and the connexin protein family. *Cardiovascular Research,* **62,** 228–232 (2004).
129. Boyett, M., Inada, S., Yoo, S., Li, J., Liu, J., Tellez, J., Greener, I., Honjo, H., Billeter, R., Lei, M., Zhang, H., Efimov, I., and Dobrzynski, H. Connexins in the sinoatrial and atrioventricular nodes. In S. Dhein, *Cardiovascular gap junctions* (Vol. 42, pp. 175–197). Karger Publishers (2006)
130. Francis, D., Stergiopoulos, K., Ek-Vitorín, J. F., Cao, F. L., Taffet, S. M., & Delmar, M. (1999). Connexin diversity and gap junction regulation by pHi. *Developmental Genetics*, *24*(1-2), 123–136 (1999).
131. L Harris, A. Emerging issues of connexin channels: biophysics fills the gap. *Quarterly Reviews of Biophysics,* **34,** (2002).
132. Ko, Y.S., Yeh, H. I., Ko, Y. L., Hsu, Y. C., Chen, C. F., Wu, S., Lee, Y. S., and Severs, N. J.Three-dimensional reconstruction of the rabbit atrioventricular conduction axis by combining histological, desmin, and connexin mapping data. *Circulation*, *109*(9), 1172–

1179 (2004).
133. Tellez, J. O., Dobrzynski, H., Greener, I. D., Graham, G. M., Laing, E., Honjo, H., Hubbard, S., Boyett, M. R., and Billeter, R. Differential expression of ion channel transcripts in atrial muscle and sinoatrial node in rabbit. *Circulation Research*, *99*(12), 1384–1393 (2006).
134. Gros, D. B. and Jongsma, H. J. Connexins in mammalian heart function. *Bioessays* **18,** 719–730 (1996).
135. Greener, I. D., Monfredi, O., Inada, S., Chandler, N. J., Tellez, J., Atkinson, A., Taube, M. A., Billeter, R., Anderson, R. H., Efimov, I. R., Molenaar, P., Sharma, S., Boyett, M. R., and Dobrzynski, H. Molecular architecture of the human specialised atrioventricular conduction axis. *Journal of Molecular and Cellular Cardiology*, *50*, 642–651 (2011).
136. Temple, I. P., Inada, S., Dobrzynski, H. and Boyett, M. R. Connexins and the atrioventricular node. *Heart Rhythm,* **10,** 297–304 (2013).
137. Coppen, S. R., Kodama, I., Boyett, M. R., Dobrzynski, H., Takagishi, Y., Honjo, H., Yeh, H. I., and Severs, N. J. Connexin45, a major connexin of the rabbit sinoatrial node, is co-expressed with connexin43 in a restricted zone at the nodal-crista terminalis border. *The Journal of Histochemistry and Cytochemistry : Official Journal of the Histochemistry Society*, *47*(7), 907–918 (1999).
138. Kreuzberg, M. M., Schrickel, J. W., Ghanem, A., Kim, J.-S., Degen, J., Janssen-Bienhold, U., Lewalter, T., Tiemann, K., and Willecke, K. Connexin30.2 containing gap junction channels decelerate impulse propagation through the atrioventricular node. *Proceedings of the National Academy of Sciences of the United States of America*, *103*(15), 5959–5964 (2006).
139. Reaume, A. G., de Sousa, P. A., Kulkarni, S., Langille, B. L., Zhu, D., Davies, T. C., Juneja, S. C., Kidder, G. M., and Rossant, J. Cardiac malformation in neonatal mice lacking connexin43. *Science (New York, N.Y.)*, *267*(5205), 1831–1834 (1995).
140. Krüger, O., Plum, A., Kim, J. S., Winterhager, E., Maxeiner, S., Hallas, G., Kirchhoff, S., Traub, O., Lamers, W. H., and Willecke, K. Defective vascular development in connexin 45-deficient mice. *Development*, *127*(19), 4179–4193. (2000).
141. Jansen, J. A., van Veen, T., de Bakker, J., and van Rijen, H. V. Cardiac connexins and impulse propagation. *Journal of Molecular and Cellular Cardiology*, *48*, 76–82 (2010).
142. Schrickel, J. W., Kreuzberg, M. M., Ghanem, A., Kim, J. S., Linhart, M., Andrie, R., Tiemann, K., Nikenig, G., Lewalter, T., and Willecke, K. Normal impulse propagation in the atrioventricular conduction system of Cx30.2/Cx40 double deficient mice. *Journal of Molecular and Cellular Cardiology*, *46*, 644–652 (2009).
143. Simon, A. M., Goodenough, D. A. and Paul, D. L. Mice lacking connexin40 have cardiac conduction abnormalities characteristic of atrioventricular block and bundle branch block. *Current Biology, 8, 295-298* (1998).
144. Gemel, J., Lin, X., Collins, R., Veenstra, R. D., and Beyer, E. C. Cx30.2 can form heteromeric gap junction channels with other cardiac connexins. *Biochemical and Biophysical Research Communication*, *369*, 388–394. (2008).
145. Jones, S. A., Lancaster, M. K. and Boyett, M. R. Ageing-related changes of connexins and conduction within the sinoatrial node. *Journal of Physiology (Lond.)* **560,** 429–437 (2004).
146. Boengler, K., Heusch, G. and Schulz, R. Connexin 43 and ischemic preconditioning: effects of age and disease. *Experimental gerontology, 41, 485-488* (2006).
147. Parton, R. G. and Simons, K. The multiple faces of caveolae. *Nature Reviews: Molecular Cell Biology,* **8,** 185–194 (2007).
148. Balijepalli, R. C. and Kamp, T. J. Caveolae, ion channels and cardiac arrhythmias. *Progress in Biophysics and Molecular Biology* **98,** 149–160 (2008).
149. Scherer, P. E. Expression of Caveolin-3 in Skeletal, Cardiac, and Smooth Muscle Cells. *Journal of Biological Chemistry* **271,** 15160–15165 (1996).
150. Minetti, C., Sotgia, F., Bruno, C., Scartezzini, P., Broda, P., Bado, M., Masetti, E., Mazzocco, M., Egeo, A., Donati, M. A., Volonté, D., Galbiati, F., Cordone, G., Bricarelli, F. D., Lisanti, M. P., and Federico Z. Mutations in the caveolin-3 gene cause autosomal dominant limb-girdle muscular dystrophy. *Nature Genetics*, *18*(4), 365–368 (1998).

151. Blanchard, A., Ohanian, V. and Critchley, D. The structure and function of α-actinin. *Journal of Muscle Research and Cell Motililty.* **10,** 280–289 (1989).
152. Gupta, V., Discenza, M., Guyon, J. R., Kunkel, L. M. and Beggs, A. H. α-Actinin-2 deficiency results in sarcomeric defects in zebrafish that cannot be rescued by α-actinin-3 revealing functional differences between sarcomeric isoforms. *The FASEB Journal.* **26,** 1892–1908 (2012).
153. Mohapatra, B., Jimenez, S., Lin, J. H., Bowles, K. R., Coveler, K. J., Marx, J. G., Chrisco M. A., Murphy, R. T., Lurie, P. R., Schwartz, R. J., Elliott, P., Vatta, M., McKenna, W., and Towbin, J. A. Mutations in the muscle LIM protein and α-actinin-2 genes in dilated cardiomyopathy and endocardial fibroelastosis. *Molecular Genetics and Metabolism*, *80*, 207–215 (2003).
154. North, K. N. and Beggs, A. H. Deficiency of a skeletal muscle isoform of α-actinin (α-actinin-3) in merosin-positive congenital muscular dystrophy. *Neuromuscular Disorders*, 6, 229-235 (1996).
155. Djinović-Carugo, K., Young, P., Gautel, M. and Saraste, M. Molecular basis for cross-linking of actin filaments: Structure of the α-actinin rod. *Cell*, 98, 537-546 (1999).
156. Wei, C. J., Xu, X., & Lo, C. W. Connexins and cell signaling in development and disease. *Annual Review of Cell and Developmental Biology*, *20*, 811–838 (2004).
157. Isom, L. L., De Jongh, K. S. and Catterall, W. A. Auxiliary subunits of voltage-gated ion channels. *Neuron* **12,** 1183–1194 (1994).
158. Van Veen, T. A. B., Stein, P. M., Royer, M. A., Le Quang, P. K., Charpentier, M. F., Colledge, P. W. H., Grace, A. A., Escande, D., de Bakker, J. M. T., and van Rijen, H. V. M. Impaired Impulse Propagation in Scn5a-Knockout Mice: Combined Contribution of Excitability, Connexin Expression, and Tissue Architecture in Relation to Aging. *Circulation*, *112*(13), 1927–1935 (2005).
159. Abriel, H. and Kass, R. S. Regulation of the Voltage-Gated Cardiac Sodium Channel Nav1.5 by Interacting Proteins. *Trends in Cardiovascular Medicine,* 15, 35-40 (2005).
160. Leoni, A.L., Gavillet, B., Rougier, J.-S., Marionneau, C., Probst, V., Le Scouarnec, S., et al. (2010). Variable $Na_v1.5$ Protein Expression from the Wild-Type Allele Correlates with the Penetrance of Cardiac Conduction Disease in the Scn5a+/− Mouse Model. *PloS One*, *5*(2), e9298 (2010).
161. Maltsev, V. A. and Lakatta, E. G. Normal heart rhythm is initiated and regulated by an intracellular calcium clock within pacemaker Cells. *Heart, Lung and Circulation* **16,** 335–348 (2007).
162. Tunwell, R., Wickenden, C., Bertrand, B., Shevchenko, V, Walsh, M Allen, P., and Lai, A. F. The human cardiac muscle ryanodine receptor-calcium release channel: identification, primary structure and topological analysis. *Biochemistry Journal*, *318*, 477–487 (1996).
163. Periasamy, M. and Kalyanasundaram, A. SERCA pump isoforms: Their role in calcium transport and disease. *Muscle Nerve* **35,** 430–442 (2007).
164. Catterall, W. A., Perez-Reyes, E., Snutch, T. P. and Striessnig, J. International Union of Pharmacology. XLVIII. Nomenclature and structure-function relationships of voltage-gated calcium channels. *Pharmacology Reviews,* **57,** 411–425 (2005).
165. Uslan, D. Z., Tleyjeh, I. M., Baddour, L. M., Friedman, P. A., Jenkins, S. M., St Sauver, J. L., and Hayes, D. L. Temporal trends in permanent pacemaker implantation: a population-based study. *American Heart Journal*, *155*(5), 896–903 (2008).
166. Aro, A. L., Anttonen, O., Kerola, T., Junttila, M. J., Tikkanen, J. T., Rissanen, H. A., and Huikuri, H. V. Prognostic significance of prolonged PR interval in the general population. *European Heart Journal*, 1–7 (2013).
167. Cheng, S., Keyes, M. J., Larson, M. G., McCabe, E. L., Newton-Cheh, C., Levy, D., Benjamin, E. J., Vasan, R. S., and Wang T. J. Long-term Outcomes in Individuals With Prolonged PR Interval or First-Degree Atrioventricular Block. *JAMA: The Journal of the American Medical Association* **301,** 2571–2577 (2009).
168. Savage, D. D., Corwin, L., Mcgee, D. L., Kannel, W. B. and Wolf, P. A. Epidemiologic Features of Isolated Syncope - the Framingham-Study. *Stroke* **16,** 626–629 (1985).
169. Ganzeboom, K. S., Mairuhu, G., Reitsma, J. B., Linzer, M., Wieling, W., and Van Dijk, N. Lifetime cumulative incidence of syncope in the general population: A study of 549

Dutch subjects aged 35-60 years. *Journal of Cardiovascular Electrophysiology*, *17*(11), 1172–1176 (2006).
170. Soteriades, E. S., Evans, J. C., Larson, M. G., Chen, M. H., Chen, L., Benjamin, E. J., and Levy, D. Incidence and Prognosis of Syncope. *New England Journal of Medicine*, *347*(12), 878–885 (2002).
171. Sun, B. C., Emond, J. A., and Camargo, C. A. Characteristics and admission patterns of patients presenting with syncope to US emergency departments, 1992-2000. *Academic Emergency Medicine* **11,** 1029–1034 (2004).
172. Blanc, J. J., L'Her, C., Touiza, A., Garo, B., L'Her, E., and Mansourati, J. Prospective evaluation and outcome of patients admitted for syncope over a 1 year period. *European Heart Journal*, *23*(10), 815–820 (2002).
173. Costantino, G., Perego, F., Dipaola, F., Borella, M., Galli, A., Cantoni, G., Dell'Orto, S., Dassi, S., Filardo, N., Duca, P. G., Montano, N., and Furlan, R. Short- and Long-Term Prognosis of Syncope, Risk Factors, and Role of Hospital Admission: Results From the STePS (Short-Term Prognosis of Syncope) Study. *Journal of American College of Cardiology*, *51*(3), 276–283 (2008).
174. Strickberger, S. A., Benson, W., Biaggioni, I., Callans, D. J., Cohen, M. I., Ellenbogen, K. A., Epstein, A. E., Friedman, P., Goldberger, J., Heidenreich, P. A., Klein, G. J., Knight, B. P., Morillo, C. A., Myerburg, R. J., and Sila, C. A. AHA/ACCF scientific statement on the evaluation of syncope - From the American Heart Association Councils on clinical cardiology, cardiovascular nursing, cardiovascular disease in the young, and stroke, and the quality of care and outcomes research interdisciplinary working group; and the American College of Cardiology Foundation in collaboration with the Heart Rhythm Society - Endorsed by the American Autonomic Society. *Circulation*, *113*(2), 316–327 (2006).
175. Ruwald, M. H., Hansen, M. L. and Lamberts, M. Comparison of Incidence, Predictors, and the Impact of Co-Morbidity and Polypharmacy on the Risk of Recurrent Syncope in Patients <85 Versus ≥85 Years of Age. *The American journal of Cardiology, 112, 1610-1615* (2013).
176. Brignole, M., Alboni, P., Benditt, D. G., Bergfeldt, L., Blanc, J. J., Bloch Thomsen, P. E., Fitzpatrick, A., and Hohnloser., S. Guidelines on management (diagnosis and treatment) of syncope. *European Heart Journal*, *25*(22), 2054–2072. (2004).
177. Crisel, R. K., Farzaneh-Far, R., Na, B. and Whooley, M. A. First-degree atrioventricular block is associated with heart failure and death in persons with stable coronary artery disease: data from the Heart and Soul Study. *European Heart Journal* **32,** 1875–1880 (2011).
178. Ahmed, N., Frontera, A., Carpenter, A., Cataldo, S., Connolly, G. M., Fasiolo, M., Cripps, T., Thomas, Glyn., Diab, I., and Duncan, E. R. Clinical Predictors of Pacemaker Implantation in Patients with Syncope Receiving Implantable Loop Recorder with or without ECG Conduction Abnormalities. *Pacing and Clinical Electrophysiology : PACE*, *38*(8), 934–941 (2015).
179. Petkar, S., Hamid, T., Iddon, P., Clifford, A., Rice, N., Claire, R., McKee, D., Curtis, N., Cooper, P. N., and Fitzpatrick, A P. Prolonged implantable electrocardiographic monitoring indicates a high rate of misdiagnosis of epilepsy--REVISE study. *Europace*, *14*(11), 1653–1660. (2012).
180. Pfeufer, A., van Noord, C., Marciante, K. D., Arking, D. E., Larson, M. G., Smith, A. V., et al. Genome-wide association study of PR interval. *Nature Genetics*, *42*(2), 153–159. (2010).

Appendix 1

Detailed Cryosection of each heart: 24 months old hearts (VO) 3 months old hearts (Y), Masson's Trichome stain (MT), Picrosirus red stain (PR), CCS (Cardiac Conduction system), INE (inferior nodal extension), CN (Compact node), PB (Penetrating bundle), His (Distal penetrating bundle/His Bundle)

HEART NO	TOTAL LEVELS	NO OF 20UM SECTION AT EACH LEVEL	DISTANCE IN BETWEEN EACH LEVEL	CCS STRUCTURE (EXTENSION ACROSS LEVELS)	MT SLIDES	PR SLIDES	HCN 4, CX 43 SLIDES
V01	L0 to L3 L5 to L9	24	500um	INE	L2 S12	L2 S10	L2 S9
	L4	40	500um	CN (L3 S2-L4)	L3 S2, 12	L3 S6, S 10	L3 S7
				PB	L4 S1,	L4 S2	L4 S3
				His	L4 S20	L4 S19	L4 S18
V02	L0 to L9	20-24	200um	INE	L3 S1	L3 S2	L3 S3
				CN	L3 S9	L3 S10	L3 S8
				PB	L4 S1	L4 S2	L4 S3
				His	L5 S1	L5 S2	L5 S3
V03	L0 to L9	20-24	200um	INE	L0 S5	L0 S4	L0 S3
				CN	L0 S10	L0 S9	L0 S8
				PB	L1 S1	L1 S2	L1 S3
				His	L1 S9	L1 S10	L1 S8
V05	L0 to L9	20-24	500um		Not suitable		
V06	L0 to L9	20-24	200um	INE	L1S1	L1 S2	L1 S3
				CN	L2 S1	L2 S2	L2 S3
				PB	L3 S9	L3 S10	L3 S8
				His	L4 S11	L4 S10	L4 S9
V07	L0 to L9	20-24	200um	INE	L2S1	L2 S2	L2 S3
				CN	L2 S9	L2 S9	L2 S8
				PB	L4 S11	L4 S10	L4 S9
				His	L5 S1	L5 S2	L5 S3
V08	L0 to L9	20-24	500um	INE	L1S1	L1 S2	L1 S3
				CN	L1 S6	L1 S5	L1 S4
				PB	L1 S12	L1 S11	L1 S9
				His	L2 S1	L2 S2	L2 S3
V09	L0 to L9	20-24	500um	INE	L1 S1	L1 S 2	L1 S3
				CN	L1 S12	L1 S10	L1 S9
				PB	L2 S7	L2 S6	L2 S5
				His/BB	L2 S12	L2 S10	L2 S9

Y01	L0 to L9	20-24	200um	INE	Not	Not	
				CN	Suitable	Suitable	
				PB			
				His/BB			
Y02	L0 to L9	20-24	200um	INE	L2 S6	L2 S5	L2 S4
				CN	L2 S12	L2 S11	L2 S10
				PB	L3 S1	L3 S2	L3 S3
				His/BB	L5 S10	L5 S9	L 5 S8
Y03	L0 to L9	20-24	200um	INE	Not suitable	Not suitable	
				CN			
				PB			
				His/BB			
Y04	L0 to L9	20-24	200um	INE	Not suitable	Not suitable	
				CN			
				PB			
				His/BB			
Y05	L0 to L9	20-24	200um	INE	L2 S10	L2 S9	L2 S8
				CN	L3 S7	L3 S6	L3 S5
				PB	L5 S7	L5 S6	L5 S5
				His/BB	L6 S1	L6 S2	L6 S3
Y06	L0 to L10	20-24	200um	INE	L10 S1	L10 S2	L10 S3
				CN (700um)	L9 S6,11	L9 S5, 10	L9 S9
				PB (1um)	L8 S12	L8 S11	L8 S9
				His/BB	L7 S1,12	L7 S2,11	L7 S9
Y07	L0 to L9	20-28	200um	INE	L2 S7	L2 S6	L2 S5
				CN (700um)	L2 S14 L3 S6	L2 S13 L3 S5	L2 S12
				PB (1 um)	L3 S12	L3 S11	L3 S10
				His/BB	L5 S6	L5 S5	L5 S4
Y08	L0 to L9	20-24	200um	INE	L3 S6	L3 S5	L3 S4
				CN	L3 S10	L3 S9	L3 S8
				PB (1 um)	L4 S1	L4 S2	L4 S3
				His/BB	L5 S1,10	L5 S2,9	L5 S8
Y09	L0 to L9	20-28	200um	INE	L1 S12	L1 S11	L1 S10
				CN (700um)	L2 S1,12	L2 S2,11	L2 S10
				PB (1um)	L3 S7	L3S6	L3 S5
				His/BB	L4 S5	L4 S4	L4 S3

Appendix 2

Comparison of individual old and young heart. Approximate three-dimensional size of the individual components of the AVJ**.** Also included is the number of nuclei seen per high power field (63X magnification) and collagen signal intensity. (V01, V03, V06, V07 are old hearts. Y06, Y07, Y08, Y09 are young hearts) CN (Compact node), PPB (Proximal penetrating bundle), DPB (Distal Penetrating bundle/His bundle).

HEART NO.	**CCS Structure**	**Length (Antero-posterior axis) um**	**Width (in 10X image) (horizontal axis) um**	**Height (10X) (Vertical axis)**	**Number of Nuclei seen per field (63X)**	**Collagen estimation Signal intensity arbitrary unit (Image J)**	**Collagen signal estimation (Polarized microscopy) Red and green (thin) Volocity**
V01	CN	660	587	194	120	183579	19.16/12.81
	PPB	320	406	450	141	304756	14.1/10.3
	DPB (His)	980	365	440	129	369553	12.33/10.62
V03	CN	400	468	636	151	270297	8.59/13.09
	PPB	280	444	836	158	451250	15.9/12.88
	DPB (His)	760	441	727	131	323498	15.24/12.34
V06	CN	520	662	269	89	436093	11.35/13.21
	PPB	360	532	474	138	454285	9.73/9.15
	DPB (His)	960	426	541	136	448084	8.03/9.23
V07	CN	600	681	725	82	295507	7.86/10.32
	PPB	400	423	892	129	441673	12.82/9.89
	DPB (His)	780	380	692	120	377875	9.62/9.39
Y06	CN	480	709	176	173	379611	9.8/10.77
	PPB	320	338	304	213	328231	9.07/8.31
	DPB (His)	920	269	302	182	372325	7.99/7.91
Y07	CN	640	560	188	210	312118	11.77/9.75
	PPB	280	440	260	232	323216	12.08/12.32
	DPB (His)	840	437	272	223	234217	11.71/8.87
Y08	CN	420	532	316	144	394832	9.91/8.63
	PPB	360	506	306	209	497831	13.63/10.37
	DPB (His)	880	526	308	163	354644	11.64/8.84
Y09	CN	680	434	115	201	219977	11.51/12.17
	PPB	320	489	484	182	491688	10.13/8.94
	DPB (His)	920	580	336	196	313802	9.56/9.03